# Title 40 CFR Part 191
# Subparts B and C
# Compliance Recertification Application 2014
# for the
# Waste Isolation Pilot Plant

# Appendix SOTERM-2014
# Actinide Chemistry Source Term



# United States Department of Energy
# Waste Isolation Pilot Plant

Carlsbad Field Office
Carlsbad, New Mexico

# Compliance Recertification Application 2014
# Appendix SOTERM-2014
# Actinide Chemistry Source Term

## Table of Contents

**List of Figures**

## List of Tables

## Acronyms and Abbreviations

| | |
|---|---|
| % | percent |
| $\alpha$ | alpha particle |
| $A_\gamma$ | Debye-Hückel parameter |
| $a_i$ | activity of a chemical species |
| $\mu$, or $\mu m$ | micrometer, micron |
| $\mu s$ | microsecond |
| am | amorphous |
| aq | aqueous |
| ASTP | Actinide Source Term Program |
| atm | atmosphere |
| $\beta$ | (apparent) stability constant, or beta particle |
| Bq | becquerel |
| BRAGFLO | Brine and Gas Flow code |
| C | Celsius; centigrade; concentration |
| CAPHUM | maximum (cap) actinide concentration associated with mobile humic colloids |
| CAPMIC | maximum actinide concentration that could be associated with microbes |
| CCA | Compliance Certification Application |
| CFR | Code of Federal Regulations |
| Ci | Curie |
| CMC | carboxymethylcellulose |
| CN | coordination number |
| coll | colloid |
| CONCINT | actinide concentration associated with mobile actinide intrinsic colloids |
| CONCMIN | actinide concentration associated with mobile mineral fragment colloids |
| CPR | cellulosic, plastic, and rubber materials |
| $C_{Pu}$ | maximum concentration of all combined isotopes of Pu |
| cr | crystalline phase |
| CRA | Compliance Recertification Application |
| DBR | direct brine release |
| D-H | Debye-Hückel theory |
| DNA | deoxyribonucleic acid |
| DOE | U.S. Department of Energy |
| DRZ | disturbed rock zone |
| $E_0$ or $E_h$ | potential |
| EDTA | ethylenediaminetetraacetic acid |
| EDS | energy dispersive x-ray spectroscopy |
| EPA | U.S. Environmental Protection Agency |
| ERDA | Energy Research and Development Administration |
| EQ3/6 | software program for geochemical modeling of aqueous systems |
| eV | electron volt |
| EXAFS | Extended X-Ray Absorption Fine Structure |
| F | Fahrenheit |
| $f_{CO_2}$ | fugacity of carbon dioxide |
| f(I) | Debye-Hückel function |

f'(I)  derivative of the Debye-Hückel function

FMT  Fracture-Matrix Transport

ft  foot/feet

$\gamma$  gamma radiation or activity coefficient

g  gaseous, or gram, or gravity of Earth

G  molecular yield in molecules/100 eV of absorbed ionizing radiation

g/L  gram per liter

g/mL  gram per milliliter

GBq  giga becquerel

GWB  Generic Weep Brine

h  hours

HEXS  high-energy X-ray scattering

hyd  hydrated

I  ionic strength

ICP-MS  inductively coupled plasma-mass spectrometry

ISA  isosaccharinic acid

K  degree Kelvin or stability constant

kDa  kilo Dalton

kg  kilogram

$K_d$  dissociation constant

km  kilometer

$K_s$  solubility constant$K_{sp}$ solubility product

$\lambda_{ij}$  second-order interaction coefficient

L  liter

LANL  Los Alamos National Laboratory

LANL-CO  Los Alamos National Laboratory – Carlsbad Operations

LET  Linear Energy Transfer

log  logarithm

$log_{10}$  logarithm base 10

LWB  land withdrawal boundary

$\mu_{ijk}$  third-order interaction coefficient

m  meter, molal

M  mole per liter

$m^2$  square meter

$m^3$  cubic meter

mg  milligram

mM  millimole per liter

mol  mole

molec  molecule

MPa  megapascal

mV  millivolt

n  neutron, or number

N  degree of polymerization number

nm  nanometer

NONLIN  Sandia code

$N_S$  Adsorption site density (sites/$nm^2$)

NUTS  Nuclide Transport System code
OXSTAT      oxidation state parameter
P      pressure
PA      performance assessment
PABC  Performance Assessment Baseline Calculation
PANEL      Program used in PA
PAVT  Performance Assessment Verification Test
$pC_{H+}$ or pcH  Negative logarithm of $H^+$ concentration in moles per liter
$pCO_2$  Partial pressure of carbon dioxide
pH      negative logarithm of $H^+$ activity
PHUMCIM      Proportionality constant for the actinide concentration associated with mobile humic colloids, in Castile brine
PHUMSIM      Proportionality constant for the actinide concentration associated with mobile humic colloids, in Salado brine
$pK_a$      negative logarithm of the dissociation constant of an acid
pm      picometer
pmH      negative logarithm of $H^+$ concentration in molal
ppm      parts per million
PROPMIC      proportionality constant describing the bioassociation of actinides with mobile microorganisms
ref      reference
RH      relative humidity
rpm      revolutions per minute
s      solid or second
SECOTP2D      computer program that simulates single or multiple component radionuclide transport in fractures or granular aquifers
SEM  scanning electron microscope
$S_{i,b}$      solubility calculated for oxidation state i in brine b
SIT      Specific Ion Interaction theory
SNL      Sandia National Laboratories
SOTERM      Actinide Chemistry Source Term (WIPP)
SPC      Salado Primary Constituents
SRB      sulfate-reducing bacteria
$SU_i$      solubility uncertainty sampled from a distribution unique to each oxidation state i
T      temperature
$t_{1/2}$      half-life
TDS      total dissolved solid
TR-LIF      Time-resolved laser induced fluorescence
TRU      transuranic
V      volt, or vanadium
w      with
WIPP  Waste Isolation Pilot Plant
WWIS  WIPP Waste Information System
XANES      X-Ray Absorption Near Edge Structure
XRD  X-Ray Diffraction
yr      year

$z_i$       charge of the specie "i"

**Elements and Chemical Compounds**

| | |
|---|---|
| Am | Americium |
| Am(II) | Americium in the +2 oxidation state |
| Am(III) | Americium in the +3 oxidation state |
| Am(IV) | Americium in the +4 oxidation state |
| Am(V) | Americium in the +5 oxidation state |
| Am(VI) | Americium in the +6 oxidation state |
| $Am^{2+}$ | Americium cation - Aqueous form of the americium in the +2 oxidation state that only exists as a transient |
| $Am^{3+}$ | Americium cation - Aqueous form of the americium in the +3 oxidation state |
| $Am^{4+}$ | Americium cation - Aqueous form of the americium in the +4 oxidation state |
| $Am(Cl)_n^{(3-n)}$ | Americium (III) chloride complex with n = 1 or 2 |
| $Am(CO_3)_n^{(3-2n)}$ | Americium (III) carbonate complex with n=1, 2, 3 or 4 |
| $Am\,OH\,CO_3$ | Americium (III) carbonato hydroxide |
| $AmO_2^+$ | Americium oxo-cation – Aqueous form of the americium in the +5 oxidation state |
| $AmO_2^{2+}$ | Americium oxo-cation – Aqueous form of the americium in the +6 oxidation state |
| $AmO_2OH$ | Americium (V) oxide hydroxide |
| $AmOH^{2+}$ | Americium (III) hydroxide cation – (1:1) complex |
| $Am(OH)_2^+$ | Americium (III) hydroxide cation – (1:2) complex |
| $Am(OH)_3$ | Americium hydroxide |
| $Am(OH)_4^-$ | Americium (III) hydroxide anion – (1:4) complex |
| $Am(OH)_n^{(3-n)}$ | Americium (III) hydroxide ion – (n:3-n) complex |
| $AmPO_4$ | Americium (III) phosphate |
| $Am(SO_4)_n^{(3-2n)}$ | Americium (III) sulfate complex with n = 1 or 2 |
| $[An]_p$ | Concentration of an adsorbed actinide element (mol/particle) |
| An | Actinide |
| An(III) | General actinide in the +3 oxidation state |
| An(IV) | General actinide in the +4 oxidation state |
| An(V) | General actinide in the +5 oxidation state |
| An(VI) | General actinide in the +6 oxidation state |

| | |
|---|---|
| $An^{3+}$ | Aqueous form of the actinide in the +3 oxidation state |
| $An^{4+}$ | Aqueous form of the actinide in the +4 oxidation state |
| $An^{n+}$ | Aqueous form of the actinide in the +n oxidation state |
| $An_2(CO_3)_3$ | Actinide (III) carbonate – (2:3) complex |
| $An_2(CO_3)_2^{2+}$ | Actinide (III) carbonate iaon – (2:2) complex |
| $AnB_4O_7^{+}$ | Actinide (III) tetraborate ion – (1:1) complex |
| $AnCl^{2+}$ | Actinide (III) chloride ion – (1:1) complex |
| $An(CO_3)^{+}$ | Actinide (III) carbonate ion – (1:1) complex |
| $An(CO_3)_2^{-}$ | Actinide (III) carbonate ion – (1:2) complex |
| $An(CO_3)_3^{3-}$ | Actinide (III) carbonate ion – (1:3) complex |
| $AnCO_3OH$ | Actinide (III) carbonate hydroxide |
| $AnL^{(n+m)}$ | Complex of an actinide with a charge n and an organic ligand L with a charge m |
| $An(V)O_2^{+}$ or $AnO_2^{+}$ | Aqueous form of the actinide in the +5 oxidation state |
| $An(VI)O_2^{2+}$ or $AnO_2^{2+}$ | Aqueous form of the actinide in the +6 oxidation state |
| $AnOH^{2+}$ | Actinide (III) hydroxide cation – (1:1) complex |
| $An(OH)_3$ | Hydroxide of the actinide (III) |
| $AnPO_4$ | Actinide (III) phosphate |
| $AnSO_4^{+}$ | Actinide (III) sulfate ion – (1:1) complex |
| $B_3O_3(OH)_4^{-}$ | Hydroxy polynuclear form of boric acid |
| $B_4O_7^{2-}$ | Tetraborate anion |
| $B(OH)_x^{3-x}$ | Hydroxyborate ions |
| $Br^{-}$ | Bromide anion |
| $[C]$ | Concentration of species $C$ in solution |
| $[C_\theta]$ | Concentration of a chosen standard state |
| C | Carbon or concentration |
| $C_6H_{10}O_5$ | Cellulose |
| $CH_4$ | Methane |
| $CH_3CO_2^{-}$ | Acetate anion |
| $(CH_2CO_2)_2C(OH)(CO_2)^{3-}$ | Citrate anion |
| $(CH_2CO_2)_2N(CH_2)_2N(CH_2CO_2)_2^{4-}$ | Ethylenediaminetetraacetate (EDTA) anion |
| $C_2O_4^{2-}$ | Oxalate anion |
| Ca | Calcium |

| | |
|---|---|
| $Ca^{2+}$ | Calcium cation |
| $CaCl_2$ | Calcium chloride |
| $CaCO_3$ | Calcium carbonate |
| $CaMg(CO_3)_2$ | Dolomite, calcium magnesium carbonate |
| $Ca[M(OH)_3]^{2+}$ | Calcium metal (III) hydroxide cation – (1:1:3) complex |
| $Ca_2[M(OH)_4]^{3+}$ | Calcium metal (III) hydroxide cation – (2:1:4) complex |
| $Ca_3[M(OH)_6]^{3+}$ | Calcium metal (III) hydroxide cation – (3:1:6) complex |
| $Ca_p[Cm(OH)_n]^{3+2p-n}$ | Calcium curium (III) hydroxide ion – (p:n:3+2p-n) complex |
| $Ca_4[Pu(OH)_8]^{4+}$ | Calcium plutonium (IV) hydroxide cation complex |
| $CaSO_4$ | Anhydrite, calcium sulfate |
| $CaSO_4 \cdot 2H_2O$ | Gypsum, hydrated calcium sulfate |
| $Ca_4[Th(OH)_8]^{4+}$ | Calcium thorium (IV) hydroxide cation complex |
| $Cl$ | Chlorine |
| $Cl^-$ | Chloride ion |
| $Cl_2$ | Chlorine |
| $Cl_2^-$ | Chlorine free radical |
| $Cl_3^-$ | Chlorine anion |
| $ClBr^-$ | Chloride bromide radical |
| $ClO^-$ | Hypochlorite anion |
| $ClO_2^-$ | Chlorite anion |
| $ClO_3^-$ | Chlorate anion |
| $ClO_4^-$ | Perchlorate anion |
| $Cm$ | Curium |
| $Cm(III)$ | Curium in the +3 oxidation state |
| $Cm(IV)$ | Curium in the +4 oxidation state |
| $Cm^{3+}$ | Curium cation – Aqueous form of the curium at the +3 oxidation state |
| $Cm_m(OH)_{3m}$ | Curium hydroxide polymer |
| $Cm(OH)_3$ | Curium hydroxide |
| $Cm(OH)_4^-$ | Curium (III) hydroxide anion – (1:4) complex |
| $CO_2$ | Carbon dioxide |
| $CO_3^{2-}$ | Carbonate anion |
| $Cr$ | Chromium |

| | |
|---|---|
| Cs | Cesium |
| $F^-$ | Fluoride |
| Fe | Iron |
| Fe(0), $Fe^0$ | Zero-valent iron, metallic iron |
| $FeCO_3$ | Iron (II) carbonate, ferrous carbonate |
| $Fe_2(OH)_3Cl$ | Iron -hibbingite, ferrous chloride trihydroxide |
| $Fe_3O_4$ | Magnetite, iron (II,III) oxide |
| $Fe^{2+}$ | Aqueous form of the iron in the +2 oxidation state, ferrous anion |
| $Fe^{3+}$ | Aqueous form of the iron in the +3 oxidation state, ferric anion |
| Fe(II) | Iron in the +2 oxidation state |
| $Fe(II)(OH)_2$ | Ferrous hydroxide |
| Fe(III) | Iron in the +3 oxidation state |
| $Fe(III)_2Fe(II)_4(OH)_{12}CO_3 \cdot 2H_2O$ | Green rust |
| $Fe(OH)_3$ | Ferric hydroxide |
| $Fe(OH)_2 \cdot (x-2)H_2O$ | Hydrated ferrous hydroxide |
| FeOOH | Goethite, iron oxide hydroxide |
| FeS | Iron (II) sulfideH    Hydrogen |
| $H^+$ | Hydrogen cation |
| $H_2$ | Hydrogen |
| $HPO_4^{2-}$ | Hydrogenphosphate anion |
| $HCO_3^-$ | Bicarbonate anion, hydrogen carbonate anion |
| $H_2O$ | Water |
| $H_2O_2$ | Hydrogen peroxide |
| HOBr | Hypobromous acid |
| HOCl | Hypochlorous acid |
| $H_2PO_4^-$ | Dihydrogen phosphate anion |
| $H_2S$ | Hydrogen sulfide |
| K | Potassium |
| $K^+$ | Potassium cation |
| KCl | Potassium chloride |
| $K_2MgCa_2(SO_4)_4 \cdot 2H_2O$ | Polyhalite |
| $KNpO_2CO_3 \cdot 2H_2O$ | Hydrated potassium neptunium (V) carbonate – (1:1:1) complex |

| | |
|---|---|
| $K_3NpO_2(CO_3)_2 \cdot 0.5H_2O$ | Hydrated potassium neptunium (V) carbonate – (3:1:2) complex |
| KOH | Potassium hydroxide |
| $K_2SO_4$ | Potassium sulfate |
| $K_2U_2O_7$ | Potassium diuranate |
| $Li^+$ | Lithium ion |
| M(III) | Metal in the +3 oxidation state |
| Mg | Magnesium |
| $Mg^{2+}$ | Magnesium cation |
| $MgCl_2$ | Magnesium chloride |
| $Mg_3(OH)_5Cl \cdot 4H_2O$ | Magnesium chloride hydroxide hydrate |
| $MgCO_3$ | Magnesite, magnesium carbonate |
| $Mg_5(CO_3)_4(OH)_2 \cdot 4H_2O$ | Hydromagnesite |
| $Mg_2(OH)_3Cl \cdot 4H_2O$ | Magnesium chloride hydroxide hydrate, magnesium oxychloride |
| MgO | Periclase, magnesium oxide |
| $Mg(OH)_2$ | Brucite, magnesium hydroxide |
| Mn | Manganese |
| $N_2$ | Nitrogen |
| Na | Sodium |
| $Na^+$ | Sodium cation |
| NaBr | Sodium bromide |
| NaCl | Sodium chloride |
| $NaClO_4$ | Sodium perchlorate |
| NaOH | Sodium hydroxide |
| $Na_2SO_4$ | Sodium sulfate |
| $Na_2S_2O_4$ | Sodium hydrosulfite |
| $NaAm(CO_3)_2$ | Sodium americium (III) carbonate |
| NaCl | Halite, sodium chloride |
| $NaHCO_3$ | Sodium bicarbonate |
| $NaNpO_2CO_3 \cdot 3.5H_2O$ | Hydrated sodium neptunium (V) carbonate – (1:1:1) complex |
| $Na_3NpO_2(CO_3)_2$ | Sodium neptunium (V) carbonate – (3:1:2) complex |
| NaOH | Sodium hydroxide |
| $Na_2U_2O_7 \cdot xH_2O$ | Sodium diuranate hydrate |

| | |
|---|---|
| Nd | Neodymium |
| Nd(III) | Neodymium in the +3 oxidation state |
| Nd(OH)$_3$ | Neodymium (III) hydroxide |
| Ni | Nickel |
| Ni$^{2+}$ | Nickel (II) cation |
| NO$_3^-$ | Nitrate anion |
| Np | Neptunium |
| Np(IV) | Neptunium in the +4 oxidation state |
| Np(V) | Neptunium in the +5 oxidation state |
| Np(VI) | Neptunium in the +6 oxidation state |
| Np$^{4+}$ | Neptunium cation – Aqueous form of the neptunium at the +4 oxidation state |
| NpO$_2$ | Neptunium (IV) oxide |
| NpO$_2^+$ or Np(V)O$_2^+$ | Neptunyl cation – Aqueous form of the neptunium at the +5 oxidation state |
| NpO$_2^{2+}$ or Np(VI)O$_2^{2+}$ | Neptunyl cation – Aqueous form of the neptunium at the +6 oxidation state |
| NpO$_5^{3-}$ | Neptunyl anion – Aqueous form of the neptunium at the +7 oxidation stateNpO$_2$CO$_3^-$   Neptunium (V) carbonate ion – (1:1) complex |
| NpO$_2$(CO$_3$)$_2^{3-}$ | Neptunium (V) carbonate ion – (1:2) complex |
| NpO$_2$(CO$_3$)$_3^{5-}$ | Neptunium (V) carbonate ion – (1:3) complex |
| Np(OH)$_3$ | Neptunium (III) hydroxide |
| Np(OH)$_4$ | Neptunium (IV) hydroxide |
| Np(OH)$_5^-$ | Neptunium (IV) hydroxide ion – (1:5) complex |
| NpO$_2$OH | Neptunium (V) hydroxide |
| NpO$_2$(OH)$_2$ | Neptunium (VI) hydroxide |
| NpO$_2$(OH)$_2^-$ | Neptunium (V) hydroxide ion – (1:2) complexO   Oxygen |
| O$_2$ | Molecular oxygen |
| OBr$^-$ | Hypobromite anion |
| OCl$^-$ | Hypochlorite anion |
| OH | Hydroxide |
| OH$^-$ | Hydroxide anion |
| OH· | Hydroxyl radical |
| Pb | Lead |

| | |
|---|---|
| $Pb^{2+}$ | Lead cation – Aqueous form of the lead at the +2 oxidation state |
| $Pb^{4+}$ | Lead cation – Aqueous form of the lead at the +4 oxidation state |
| $PbCl_2$ | Lead (II) chloride |
| $PbCO_3$ | Lead (II) carbonate |
| $[Pb_6O(OH)_6]^{4+}$ | Lead (II) polyoxyhydroxide cation |
| $PbO$ | Lead (II) oxide |
| $PO_4^{3-}$ | Phosphate anion |
| $(PbOH)_2CO_3$ | Lead (II) hydroxide carbonate |
| $PbS$ | Lead (II) sulfide |
| $PbSO_4$ | Lead (II) sulfate |
| $Pu$ | Plutonium |
| $Pu(III)$ | Plutonium in the +3 oxidation state |
| $Pu(IV)$ | Plutonium in the +4 oxidation state |
| $Pu(V)$ | Plutonium in the +5 oxidation state |
| $Pu(VI)$ | Plutonium in the +6 oxidation state |
| $Pu(VII)$ | Plutonium in the +7 oxidation state |
| $Pu^{3+}$ | Plutonium cation – Aqueous form of the plutonium at the +3 oxidation state |
| $Pu^{4+}$ | Plutonium cation – Aqueous form of the plutonium at the +4 oxidation state |
| $Pu(CO_3)^+$ | Plutonium (III) carbonate ion – (1:1) complex |
| $Pu(CO_3)_2^-$ | Plutonium (III) carbonate ion – (1:2) complex |
| $Pu(CO_3)_3^{3-}$ | Plutonium (III) carbonate ion – (1:3) complex |
| $PuF_2^{2+}$ | Plutonium (IV) fluoride cation |
| $PuO_2$ | Plutonium (IV) dioxide |
| $PuO_{2+x}$ | Oxidized plutonium (IV) dioxide |
| $PuO_2CO_3$ | Plutonium (VI) carbonate |
| $PuO_2CO_3^-$ | Plutonium (V) carbonate ion – (1:1) complex |
| $PuO_2(CO_3)_2^{3-}$ | Plutonium (V) carbonate ion – (1:2) complex |
| $PuO_2(CO_3)_2^{2-}$ | Plutonium (VI) carbonate ion – (1:2) complex |
| $PuO_2(CO_3)_3^{4-}$ | Plutonium (VI) carbonate ion – (1:3) complex |
| $PuO_2F^+$ | Plutonium (VI) oxofluoride cation |

| | |
|---|---|
| $PuO_2^+$ or $Pu(V)O_2^+$ | Plutonyl cation – Aqueous form of the plutonium at the +5 oxidation state |
| $PuO_2^{2+}$ or $Pu(VI)O_2^{2+}$ | Plutonyl cation – Aqueous form of the plutonium at the +6 oxidation state |
| $PuO_2(OH)_2$ | Plutonium (VI) hydroxide |
| $PuO_3 \cdot xH_2O$ | Plutonium (VI) trioxide-hydrate |
| $Pu(OH)_3$ | Plutonium (III) hydroxide |
| $Pu(OH)_3^+$ | Plutonium (IV) hydroxide cation – (1:3) complex |
| $Pu(OH)_4$ | Plutonium (IV) hydroxide |
| $[Pu(H_2O)_m]^{n+}$ | Hydrolysis complex of plutonium |
| $[Pu(O)Pu(O)Pu(O)...]_n$ | Plutonium polymer |
| $S^{2-}$ | Sulfide anion |
| $SO_4^{2-}$ | Sulfate anion |
| $Sr$ | Strontium |
| $Th$ | Thorium |
| $Th(IV)$ | Thorium in the +4 oxidation state |
| $Th^{3+}$ | Thorium cation – Aqueous form of the thorium at the +3 oxidation state |
| $Th^{4+}$ | Thorium cation – Aqueous form of the thorium at the +4 oxidation state |
| $Th(CO_3)_5^{6-}$ | Thorium (IV) pentacarbonyl ion complex |
| $ThISA_2^{2+}$ | Thorium (IV) isosaccharinic acid ion – (1:2) complex |
| $ThO_2$ | Thorium dioxide |
| $Th(OH)^{3+}$ | Thorium (IV) hydroxide ion – (1:1) complex |
| $Th(OH)_2^{2+}$ | Thorium (IV) hydroxide ion – (1:2) complex |
| $Th(OH)_3^+$ | Thorium (IV) hydroxide ion – (1:3) complex |
| $Th_4(OH)_{12}^{4+}$ | Thorium (IV) hydroxide ion – (4:12) complex |
| $Th_6(OH)_{15}^{9+}$ | Thorium (IV) hydroxide ion – (6:9) complex |
| $Th(OH)_4$ | Thorium hydroxide |
| $Th(OH)(CO_3)_4^{5-}$ | Thorium (IV) hydroxide carbonate ion – (1:1:4) complex |
| $Th(OH)_2(CO_3)_2^{2-}$ | Thorium (IV) hydroxide carbonate ion – (1:2:2) complex |
| $Th(OH)_3CO_3^-$ | Thorium (IV) hydroxide carbonate ion – (1:3:1) complex |
| $Th(OH)_2SO_4$ | Thorium (IV) hydroxide sulfate ion – (1:2:1) complex |
| $Th(OH)_4ISA_2^{2-}$ | Thorium (IV) hydroxide isosaccharinic acid ion – (1:4:2) complex |
| $Th(SO_4)_3^{2-}$ | Thorium (IV) sulfate ion – (1:3) complex |

$Th(SO_4)_2$      Thorium (IV) sulfate

$Th(SO_4)_2 \cdot K_2SO_4 \cdot 4H_2O$, $Th(SO_4)_2 \cdot 2K_2SO_4 \cdot 2H_2O$, $Th(SO_4)_2 \cdot 3.5K_2SO_4$      Hydrated potassium thorium (IV) sulfate complex

$Th(SO_4)_2 \cdot Na_2SO_4 \cdot 6H_2O$      Hydrated sodium thorium (IV) sulfate complex

U      Uranium

U(III)      Uranium in the +3 oxidation state

U(IV)      Uranium in the +4 oxidation state

U(V)      Uranium in the +5 oxidation state

U(VI)      Uranium in the +6 oxidation state

$U^{3+}$      Uranium cation – Aqueous form of the uranium at the +3 oxidation state

$U^{4+}$      Uranium cation – Aqueous form of the uranium at the +4 oxidation state

$UO_2$      Uraninite, uranium (IV) dioxide

$UO_2^{2+}$ or $U(VI)O_2^{2+}$      Uranyl cation – Aqueous form of the uranium at the +6 oxidation state

$UO_2CO_3$      Rutherfordine, uranium (VI) carbonate

$UO_2(CO_3)_2^{2-}$      Uranium (VI) carbonate ion – (1:2) complex

$UO_2(CO_3)_3^{4-}$      Uranium (VI) carbonate ion – (1:3) complex or triscarbonato complex

$(UO_2)_3(CO_3)_6^{6-}$      Uranium (VI) carbonate ion – (3:6) complex

$(UO_2)_2(CO_3)(OH)_3^{-}$      Uranium (VI) carbonate hydroxide ion – (2:1:3) complex

$(UO_2)_{11}(CO_3)_6(OH)_{12}^{2-}$      Uranium (VI) carbonate hydroxide ion – (11:6:12) complex

$UO_2(OH)_3^{-}$      Uranium (VI) hydroxide ion – (1:3) complex

$UO_2(OH)_4^{2-}$      Uranium (VI) hydroxide ion – (1:4) complex

$U(OH)_4$      Uranium (IV) hydroxide

$UO_2 . xH_2O$      Hydrous uranium (IV) dioxide

$(UO_2)(OH)_2 \cdot xH_2O$ or $UO_3 \cdot xH_2O$      Schoepite, hydrated uranium trioxide

V      Vanadium

$ZrO_2$      Zirconium dioxide

# SOTERM-1.0 Introduction

2  Appendix SOTERM-2014 (Actinide Chemistry Source Term) is a summary of the U.S.
3  Department of Energy's (DOE's) understanding of the Waste Isolation Pilot Plant (WIPP)
4  chemical conditions, assumptions, and processes; the underlying actinide chemistry; and the
5  resulting actinide concentrations that were calculated based on this repository chemistry. This
6  appendix supplements Appendix PA-2014 in the 2014 Compliance Recertification Application
7  (CRA-2014). The results summarized here are based, in part, on various assumptions about the
8  chemical conditions in the repository, and calculations, that were included in the formulation of
9  the baseline used for the CRA-2014 Performance Assessment (PA). The WIPP-related
10 geochemical experimental results obtained within and outside of the WIPP project since the
11 CRA-2009 was submitted are also summarized.

12 Actinide release from the WIPP is a critical performance measure for the WIPP as a transuranic
13 (TRU) waste repository. There are a number of potential pathways for actinide release
14 considered by the WIPP PA; these are discussed in detail in Appendix PA-2014. Quantifying the
15 impact of these releases contributes directly to assessing compliance with 40 CFR Part 191 (U.S.
16 EPA 1993).

17 In the undisturbed scenario for PA, actinide releases up the shafts or laterally through the marker
18 beds are insignificant in all realizations and have no impact on compliance (Appendix PA-2014,
19 Section 7). The self-sealing of the salt and the reducing anoxic environment in the repository
20 provide the primary mechanisms for geologic isolation of the TRU waste in the undisturbed
21 scenario. For the disturbed scenarios, actinide releases can occur as a result of inadvertent human
22 intrusions (i.e., boreholes drilled into or through the repository). For example, direct brine release
23 (DBR) to the accessible environment may occur during a drilling intrusion, or actinides may be
24 transported up a borehole to the Culebra Dolomite Member of the Rustler Formation and then
25 move laterally through the Culebra to the Land Withdrawal Boundary (LWB). The potential for
26 human intrusions makes it important to assess the range of possible repository conditions and
27 actinide concentrations associated with the disturbed scenarios.

28 This appendix focuses on the actinide source term used to calculate actinide release from the
29 WIPP for DBR and transport through the Salado Formation and Culebra. This actinide source
30 term is the sum of the soluble and colloidal species in brine. Direct release of actinide
31 particulates to the surface resulting from cuttings, cavings, and spallings is not considered part of
32 the actinide source term because these particulate releases do not depend on the mobilized
33 actinide concentrations in brine.

34 The relative importance of radioelements (Camphouse et al. 2013) that significantly contribute to
35 the actinide source term, and consequently impact the long-term performance of the WIPP,
36 which is unchanged since the CRA-2009 Performance Assessment Baseline Calculation (PABC)
37 (Clayton et al. 2010), is:

38 $$Pu \approx Am \gg U > Th \gg Np, Cm, \text{ and fission products} \quad \text{(SOTERM.1)}$$

39 The TRU components for this list of radionuclides are the alpha (α)-emitting isotopes of
40 plutonium (Pu), americium (Am), neptunium (Np), and curium (Cm) with half-lives greater than

1 20 years. These TRU actinides make up the waste unit factor used to calculate the normalized
2 release from the WIPP in U.S. Environmental Protection Agency (EPA) units, as required by 40
3 CFR Part 191. In SOTERM, the chemistry of thorium (Th) and uranium (U) is also discussed,
4 since these actinides are present in the WIPP waste and their chemistry is analogous to the TRU
5 components.

6 This appendix has the following overall organization:

7 − An overview of key near-field conditions and biogeochemical processes is presented in
8   Section SOTERM-2.0.

9 − An updated literature review and summary of WIPP-relevant results for the key actinides
10   is given in Section SOTERM-3.0.

11 − A summary of the WIPP actinide PA approach and assumptions, along with the
12   calculated actinide solution concentrations, is provided in Section SOTERM-4.0.

13 − The PA implementation of the dissolved and colloidal components of the source term is
14   described in Section SOTERM-5.0.

15 Each of these sections identifies important changes and/or new information since the CRA-2009
16 (U.S. DOE 2009) and the CRA-2009 PABC (Clayton et al. 2010).

17

# SOTERM-2.0 Expected WIPP Repository Conditions, Chemistry, and Processes

The pre-emplacement and post-emplacement near-field processes and conditions that could affect actinide concentrations in the WIPP are discussed in this section. An up-front summary of the current WIPP chemistry model assumptions and conditions is given in Table SOTERM-1. An up-front summary of the assumptions/role of the engineered barrier and key WIPP-relevant processes is given in Table SOTERM-2. The anticipated inventory of key waste, packaging and emplacement materials in the WIPP is summarized in Table SOTERM-3. All of these are discussed in more detail in the following sections. Emphasis in the detailed description is placed on how these processes and conditions in the repository could affect the concentrations of dissolved and colloidal actinide species in brine.

Overall, there are relatively few changes in the WIPP repository conditions, chemistry, and processes since the CRA-2009 and the CRA-2009 PABC. New data that support the current WIPP position in some areas were obtained. A preview of these data is given below.

***Changes in WIPP repository conditions, chemistry and processes since the CRA 2009 and CRA-2009 PABC:***

1) New inventory data, based on the 2012 annual inventory (Van Soest 2012) exist on the amounts of lead, iron and the cellulosic, plastic and rubber (CPR) material in the WIPP. This is summarized in Table SOTERM-3.

2) The minimum brine volume for DBR, which is unchanged at 17,400 $m^3$, is the basis of a variable brine volume PA implementation (Section SOTERM-2.2.4; Appendix PA-2014, Section 1.1.9).

3) Brine chemistry and actinide solubilities are now being calculated using EQ3/6 rather than the Fracture Matrix Transport (FMT) program, although the database is essentially the same. This is discussed in Section SOTERM-2.3.1.

4) Modeling and experimental studies to further evaluate the transitional brine chemistry between Generic Weep Brine (GWB) and Energy Research and Development Administration Well-6 (ERDA-6) brines were completed and are described in Section SOTERM-2.3.1. These data support past and ongoing WIPP specific research, but do not impact the WIPP PA.

5) The potential concentration of organic chelating agents has been updated based on new inventory data (Van Soest 2012; Brush and Domski 2013b). These new concentrations are discussed in section SOTERM-2.3.6.

6) Gas generation rates due to corrosion were recalculated based on the new WIPP relevant corrosion rates (Roselle 2013; Section SOTERM-2.3.4; Appendix PA-2014, Section 1.1.4).

7) A Significant amount of new data was obtained on the WIPP microbial ecology (Section SOTERM-2.4.1).  This new information is centered on indigenous microorganisms in salt from the WIPP and those present in briny groundwaters in the area of the WIPP.  Some progress was also made on the aerobic biodegradation of organic chelating agents and the bioassociation of WIPP specific isolates.  Although this has provided more insight to the nature of indigenous halophilic microorganisms, we do not have a complete understanding of this microbial ecology and these results have not led to a change in the WIPP microbial model.

**Table SOTERM-1.  Summary of Current WIPP Chemistry Model Assumptions and Conditions**

| Repository Condition or Parameter | CRA-2014 PA Assumptions | SOTERM-2014 Section |
|---|---|---|
| Ambient Geochemistry | Predominantly halite of the Salado Formation, with anhydrite interbeds and inclusions. | 2.1 |
| Temperature | Ambient temperature is 28 $^{o}$C (82 °F). An increase of up to 3 $^{o}$C (5.4 °F) is possible as a result of the emplacement of TRU waste. | 2.2.2 |
| Humidity | ~70 percent (%) relative humidity (RH) at the repository temperature. | 2.2.3 |
| Water Content | Host rock is groundwater-saturated with inclusions in the salt that range from 0.057% to 3% by mass. Repository is initially unsaturated until a borehole intrusion occurs.  Depending on pressure and intrusion scenarios, the first intrusion will occur between 100 and 1000 years (yrs). | 2.2.3 |
| Pressure | A maximum pressure in the repository of about 15 megapascals (MPa) (148 atmospheres [atm]), equivalent to the lithostatic stress at the repository level; a hydrostatic pressure of about 8 MPa (79.0 atm) at the bottom of an intrusion borehole at repository depth. | 2.2.1 |
| Gas Phase | Initially air/oxic at repository closure, but rapidly transitions to an anoxic atmosphere dominated by hydrogen with smaller amounts of methane and nitrogen. Trace amounts of carbon dioxide, hydrogen sulfide, and other microbial gases may be present. | 2.2.3 2.4.1 |
| Disturbed Rock Zone (DRZ) | Upper bound of 12 meters (m) above the repository and 2 m below the repository horizon. | 2.2.5 |
| Minimum Brine Volume for DBR | The calculated minimum volume of brine from any source needed for DBR release is 17,400 cubic meters (m$^3$).  This volume is the basis of the variable brine volume approach now used in PA. | 2.2.4 |
| WIPP Brine | High-ionic-strength brine that varies with pH and reaction with MgO but is bracketed by GWB and ERDA-6 brine formulations used in the WIPP project. | 2.3.1 |
| pH | The expected pH is about 9 (ionic-strength-corrected measured pH (pC$_{H+}$) of 9.5) and controlled by MgO.  The borate and carbonate present add to the brine buffer capacity. | 2.3.2 |

**Table SOTERM-2. Assumptions/Role of the Engineered Barrier, Emplaced Waste, and Key WIPP Subsurface Processes**

| Barrier or Process | CRA-2014 Assumptions and Role in PA | SOTERM-2014 Section |
|---|---|---|
| MgO | Engineered barrier for the WIPP that will sequester carbon dioxide ($CO_2$) and control increases and decreases in pH by the precipitation of brucite, hydromagnesite, and magnesite. | 2.3.3 |
| Corrosion | Container steel and metals in WIPP waste will react to remove oxygen and produce hydrogen. | 2.3.4 |
| Iron and Lead Chemistry | The chemistry of iron and lead, which are added to the repository, contributes to our overall understanding of the chemistry of actinides in brine, but this chemistry is selectively implemented in PA. | 2.3.4 and 2.3.5 |
| Organic Chelating Agents | The four organic chelating agents addressed by PA are acetate, oxalate, citrate and ethylenediaminetetraacetic acid (EDTA). These are assumed to not degrade under the expected WIPP conditions; their solubility is defined by their inventory (except for oxalate, which is solubility limited); these complex actinides and increase their solubility in the source term. | 2.3.6 |
| CPR | These materials are introduced to the WIPP as waste, packaging material and emplacement material. Their biodegradation leads to the formation of carbon dioxide that dissolves in brine to form bicarbonate/carbonate species that impact pH and complex actinides. | 2.3.7 |
| Microbial Effects | Gas generation, primarily carbon dioxide and hydrogen sulfide, resulting from the biodegradation of CPR materials and creation of reducing conditions, including bioreduction of actinide elements from higher oxidation states. Microbial processes are assumed to occur in all PA realizations. | 2.4.1 |
| Radiolysis | Localized oxidizing effects possible near high-activity actinides, but overall radiolytic processes are overwhelmed by the in-room chemistry. | 2.4.2 |

**Table SOTERM-3. Total Projected Waste, Packaging and Cement Material in the WIPP Repository (Van Soest 2012)**

| Material | Source/Type | *Amount (kg) | Total (kg) |
|---|---|---|---|
| Iron-based metals/alloys | Waste | $1.22 \times 10^7$ | $4.91 \times 10^7$ |
| | Packaging | $3.69 \times 10^7$ | |
| Aluminum-based metals/alloys | Waste | $4.57 \times 10^5$ | $4.57 \times 10^5$ |
| Lead | Packaging | $8.28 \times 10^3$ | $8.28 \times 10^3$ |
| Cellulosics | Waste | $3.66 \times 10^6$ | $4.65 \times 10^6$ |
| | Packaging | $7.23 \times 10^5$ | |
| | Emplacement | $2.6 \times 10^5$ | |
| Plastics | Waste | $5.50 \times 10^6$ | $9.51 \times 10^6$ |
| | Packaging | $2.77 \times 10^6$ | |
| | Emplacement | $1.25 \times 10^6$ | |
| Rubber | Waste | $1.18 \times 10^6$ | $1.25 \times 10^6$ |
| | Packaging | $7.33 \times 10^4$ | |
| CPR Total | Waste | $1.03 \times 10^7$ | $1.54 \times 10^7$ |
| | Packaging | $3.57 \times 10^6$ | |
| | Emplacement | $1.51 \times 10^6$ | |
| Cement | Reacted | $4.22 \times 10^6$ | $1.08 \times 10^7$ |
| | Combination | $6.55 \times 10^6$ | |
| MgO | Emplacement | N/A | 51,430 tons |
| Organic Ligands (all from waste) | Acetate | $9.96 \times 10^3$ | $2.41 \times 10^4$ |
| | Acetic Acid | $1.41 \times 10^4$ | |
| | Oxalate | $6.50 \times 10^2$ | $1.85 \times 10^4$ |
| | Oxalic Acid | $1.78 \times 10^4$ | |
| | Citrate | $2.55 \times 10^3$ | $7.78 \times 10^3$ |
| | Citric Acid | $5.23 \times 10^3$ | |
| | EDTA | $3.76 \times 10^2$ | $3.76 \times 10^2$ |
| *Includes remote-handled and contact-handled waste sources when applicable. | | | |

1  ## SOTERM-2.1 Ambient Geochemical Conditions

2  The ambient geochemical conditions are discussed in detail in the Compliance Certification
3  Application (CCA) (U.S. DOE 1996) and the CRA-2004, Chapter 2 and Chapter 6, Section 6.4.3
4  (U.S. DOE 2004). The Salado, which is the host formation, is predominantly pure halite (NaCl),
5  with interbeds (marker beds) consisting mainly of anhydrite ($CaSO_4$). The nearly pure halite
6  contains accessory evaporite minerals such as anhydrite ($CaSO_4$), gypsum ($CaSO_4 \cdot 2H_2O$),
7  polyhalite ($K_2MgCa_2(SO_4)_4 \cdot 2H_2O$), magnesite ($MgCO_3$), and clays. Small quantities of
8  intergranular (grain-boundary) brines and intragranular brines (fluid inclusions) are associated
9  with the salt at the repository horizon. These brines are highly concentrated solutions (ionic
10 strength up to 8 moles per liter [M]) of predominantly sodium ($Na^+$), magnesium ($Mg^{2+}$),
11 potassium ($K^+$), chloride ($Cl^-$), and sulfate ($SO_4^{2-}$), with smaller amounts of calcium ($Ca^{2+}$),
12 carbonate ($CO_3^{2-}$), and borate ($B(OH)_4^-$ and/or $B_4O_7^{2-}$). These brines have been in contact with
13 the Salado evaporite minerals since their deposition (estimated to be 250 million years) and are
14 saturated with respect to these minerals.

15 Underlying the Salado is the Castile Formation, composed of alternating units of interlaminated
16 carbonate, anhydrite, and nearly pure halite. The Castile in the vicinity of the WIPP site is known
17 to contain localized brine reservoirs with sufficient pressure to force brine to the surface if
18 penetrated by a borehole. Castile brines are predominantly saturated NaCl solutions containing
19 $Ca^{2+}$ and $SO_4^{2-}$, as well as small concentrations of other elements, and are about eight times more
20 concentrated than seawater. Overlying the Salado in the vicinity of the WIPP site is the Culebra
21 Dolomite Member of the Rustler Formation, a fractured dolomite ($CaMg(CO_3)_2$) layer.  It is
22 significant because it is expected to be the most transmissive geologic pathway to the accessible
23 environment. Culebra brines are generally more dilute than the Salado and Castile brines, and are
24 predominantly NaCl with $K^+$, $Mg^{2+}$, $Ca^{2+}$, $SO_4^{2-}$, and $CO_3^{2-}$. More detailed information on the
25 distribution of Culebra brine salinity in the WIPP site and vicinity can be found in Appendix
26 HYDRO-2014.

27 ## SOTERM-2.2 Repository Conditions

28 Repository conditions that could potentially affect actinide solubility are briefly summarized in
29 this section. These include repository pressure, repository temperature, water content and relative
30 humidity, the minimum free volume for actinide release (effective porosity), and the extent of the
31 DRZ.

32 ### SOTERM-2.2.1 Repository Pressure

33 The preexcavation lithostatic pressure (Stein 2005; Appendix PA-2014, Section 4.2.4) in the
34 WIPP at repository depth is about 15 MPa (148 atm). This pressure can be reestablished after
35 repository closure due to salt creep and gas generation, but there are a number of PA vectors that
36 predict pressure may not be fully restored even by the end of the 10,000-yr period of WIPP
37 performance, and final pressures may range from 6 to 15 MPa (in the undisturbed scenario) and
38 from 0.1 to 15 MPa (in the disturbed scenarios) considered in the CRA-2014 PA. In this context,
39 the pressure in the repository after closure cannot significantly exceed the far-field confining
40 stress of about 15 MPa.

1   DBR can occur when the pressure in the repository at the time of a drilling intrusion exceeds 8
2   MPa and a sufficient amount of brine has already flowed into the repository (see related
3   discussions in Section SOTERM-2.2.4, Stein (Stein 2005) and Clayton (Clayton 2008)). Eight
4   MPa is the pressure exerted by a column of brine-saturated drilling fluid at the depth of the
5   repository (Stoelzel and O'Brien 1996). For repository pressures less than 8 MPa, no DBRs are
6   assumed to occur because the fluid pressure in the repository cannot eject the drilling fluid from
7   the borehole. There is also no DBR until the brine volume exceeds the minimum brine volume
8   (see Section SOTERM-2.2.4) needed to fill the effective porosity present in the compacted TRU
9   waste.

10  The range of pressures expected in the WIPP will not likely have an impact on actinide
11  solubility.  The maximum pressure possible (~15 MPa) is well below pressures needed to affect
12  the solution chemistry, and is not expected to have a significant effect on actinide solubilities or
13  processes that lead to the association of actinides with colloidal particles.  For these reasons, the
14  effect of pressure on actinide solubility is not considered in the WIPP PA.

15  **SOTERM-2.2.2 Repository Temperature**

16  The ambient pre-emplacement temperature at the WIPP repository horizon is 27 degrees
17  centigrade (ºC) (80 degrees Farenheit (ºF)) (Bennett et al. 1996). The emplacement of TRU
18  waste in the WIPP introduces possible exothermic reactions:  MgO hydration, MgO carbonation,
19  microbial degradation, aluminum corrosion and cement hydration. The potential contributions of
20  each of these processes were re-evaluated for the CRA-2014 (see Appendix SCR-2014, Section
21  6.3.4.1.3) and leads to a maximum possible temperature increase of up to 39 ºC (12 ºC increase).
22  These elevated temperatures are expected to persist for a short period of time, perhaps a few
23  years or decades.  This is also discussed in Sanchez and Trellue (Sanchez and Trellue 1996) and
24  Wang and Brush (Wang and Brush 1996). For the purposes of PA, the temperature of the WIPP
25  underground repository is assumed to be constant with time at 300 Kelvin (K) (27 ºC [80 ºF])
26  (Appendix PA-2014, Section 4.2.2).

27  Actinide solubilities were calculated in the WIPP PA using thermodynamic and laboratory data
28  measured at 25 ºC [77 ºF]. The expected effect of the slightly elevated temperature in the WIPP
29  on actinide concentrations is relatively small, especially when compared to other uncertainties
30  inherent in the measurement and calculation of the actinide solubilities and colloidal
31  concentrations. For this reason, the very small effect of temperature on actinide solubility was
32  not considered in the WIPP PA calculations.

33  **SOTERM-2.2.3 Water Content and Relative Humidity**

34  A key argument for the WIPP as a TRU waste repository is that the self-sealing of the salt will
35  limit the availability and transport of water into and through the repository, and correspondingly
36  minimize the potential release of TRU nuclides from the repository. In all the undisturbed
37  repository scenarios considered by PA, no significant release of actinides from the WIPP is
38  predicted (Appendix PA-2014, Section 7). There is, however, groundwater in the WIPP, even in
39  undisturbed scenarios, that is potentially available to interact with the TRU waste. The salt
40  surrounding the waste is groundwater-saturated with both intergranular and intragranular water.
41  The amount of water present as inclusions in the salt is effectively used as an uncertain

1 parameter in PA calculations with a range of 0.057 to 3 weight % based on what was measured
2 in preexcavation salt (Skokan et al. 1987; Powers et al. 1978). In PA (Appendix PA-2014,
3 Section 4.2.4) this is done indirectly by sampling a range in the halite porosity for the intact and
4 DRZ salt (0.001 to 0.0519 and 0.0038 to 0.0548 respectively – see Ismail 2007). Available brine
5 can seep into the repository horizon and fill the pore volume of the transuranic (TRU) waste in
6 the excavated areas. The presence of some brine in the WIPP prior to brine saturation leads to an
7 environment that will contain an atmosphere of up to about 70% RH, defined by the vapor
8 pressure of saturated brine at the repository temperature. This water vapor pressure will be
9 present, at least in part, until brine saturation occurs as a result of some human intrusions or brine
10 seepage into the excavated area.

11 The presence of a humid environment in the WIPP prior to brine saturation may have a transitory
12 effect on actinide solubilities. These transitory/temporary phases are not considered in the WIPP
13 PA because they will be rapidly overwhelmed by the in-room chemistry and higher reactivity of
14 the waste components should brine inundation or saturation occur.

15 **SOTERM-2.2.4 Minimum Repository Brine Volume and Variable Brine Volume**
16 **Implementation**

17 The minimum brine volume is the lowest amount of brine needed for a DBR to occur during an
18 intrusion scenario.  Two criteria must be met:

19   1)  Volume-averaged pressure in the vicinity of the repository encounter by drilling must
20       exceed the drilling fluid hydrostatic pressure

21   2)  Brine saturation in the repository must exceed the residual saturation of the waste
22       material

23 The minimum brine volume is given by the following:

24       Minimum brine volume = (median sampled residual brine saturation)
25                                x (consolidated void volume)
26                          x (equivalent repository rooms)                         (SOTERM.2)

27 This was most recently recalculated by Clayton (Clayton 2008) to be 17,400 m$^3$. This 17,400 m$^3$
28 value corresponds to a consolidated void volume of 523.1 m$^3$, 120.3 equivalent rooms in the
29 repository, and a median value for the sampled residual brine saturation of 0.276.  These
30 parameters were calculated based on the method recommended by Stein (Stein 2005), except that
31 the drilling fluid hydrostatic pressure (8 MPa) was used rather than the lowest pressure
32 realization at 10,000 years.  This change makes the minimum volume calculation more
33 consistent with the DBR conceptual model.

34 The minimum repository brine volume has two important potential impacts on calculating
35 actinide concentrations in the WIPP. The first is that the predicted inventory of some actinides,
36 when fully dissolved in this brine volume, lead to concentrations that are below their predicted
37 solubility, most importantly Np and Cm. In this context, they are assumed to be fully dissolved
38 in the brine and since their inventory-limited concentration is small, the impact on the calculated
39 actinide release is insignificant. The second impact is on the predicted concentration of key

1  organic and inorganic complexants that coexist with the TRU species in WIPP waste. The
2  maximum concentrations of acetate, citrate, and EDTA (see Section SOTERM-2.3.6) are defined
3  by their fully dissolved concentration in this minimum brine volume.

4  **SOTERM-2.2.5 DRZ**

5  The DRZ is a zone immediately surrounding the excavated repository that has been altered by
6  the construction of the repository.  A more detailed discussion of the DRZ can be found in
7  Appendix PA-2014, Section 4.2.4. In the Brine and Gas Flow (BRAGFLO) code, the Upper
8  DRZ has a height of about 12 m (39 feet [ft]) and the Lower DRZ has a depth of about 2.2 m (7.2
9  ft). The creation of this DRZ disturbs the anhydrite layers and marker beds and alters the
10  permeability and effective porosity of the rock around the excavated areas, providing enhanced
11  pathways for the flow of gas and brine between the waste-filled rooms and the nearby interbeds.

12  The DRZ is important to the calculation of dissolved actinide concentrations because it
13  potentially makes the minerals in the interbeds "available" for reaction with the TRU and
14  emplaced waste components. The most important of these minerals is the calcium sulfate
15  (anhydrite) that could function as a source of sulfate for processes in the repository subsequent to
16  brine inundation. Currently, sulfate is assumed to be available from the DRZ into the waste area,
17  which prolongs microbial sulfate reduction processes in the WIPP.

18  # SOTERM-2.3 Repository Chemistry

19  Brine present in the WIPP will react with emplaced TRU waste, waste components, and the
20  engineered barrier material to establish the brine chemistry that will define actinide solubilities
21  and colloid formation. At the repository horizon, the brine composition will be defined by a
22  combination of factors that include the initial composition of the in-flow brine; reactions that
23  control pH; and the extent to which this brine is altered by equilibration with the waste
24  components, emplaced container materials, and the waste-derived organic chelating agents that
25  can dissolve in the brine.  An overview of this repository chemistry is given in this section.

26  **SOTERM-2.3.1 WIPP Brine**

27  Salado brine will enter the repository after closure, and can be supplemented by Castile brine in
28  some human intrusion scenarios. It is also possible that groundwater from the Rustler and Dewey
29  Lake Formation could flow down the borehole into the repository, mix with the waste, and then
30  be forced back up a borehole. The majority of WIPP-specific solubility studies since the CRA-
31  2004 were performed using brines that bracket the expected range in brine composition.
32  Including brine mixing in PA has been considered and rejected because using the end member
33  brines (i.e., GWB or ERDA-6 brines) brackets the median values and uncertainties for the
34  solubility calculations.

35  In addition to using these end-member brines in PA, other simplifying assumptions are also
36  made:

37      1.  Any brine present in the repository is well mixed with waste.

2.  Equilibria with halite and anhydrite, the most abundant Salado minerals at or near the stratigraphic horizon of the repository, are rapidly established.

3.  Oxidation-reduction (redox) equilibria with waste materials are not assumed.

4.  Brine compositions attained after equilibration of GWB or ERDA-6 with the MgO engineered barrier exist for the entire 10,000-year regulatory period.

The composition of brine in and around the WIPP site prior to waste emplacement was established by sampling the groundwater and intergranular inclusions in the Salado and Castile (Popielak et al. 1983; Snider 2003a). A number of synthetic brines that simulate these compositions were developed and have been used for WIPP laboratory studies (Lucchini et al. 2013c, Table 1). Currently, the two simulated brines that best represent these repository-relevant, end-member brines are: (1) GWB, which simulates intergranular (grain-boundary) brines from the Salado at or near the stratigraphic horizon of the repository (Snider 2003a); and (2) ERDA-6, which simulates brine from the ERDA-6 well, typical of fluids in Castile brine reservoirs (Popielak et al. 1983).

The reaction of GWB and ERDA-6 brines with MgO (brucite), halite, anyhydrite, and hydromagnesite leads to some potentially significant changes in the composition of the brine (Table SOTERM-4). These brines were reacted using EQ3/6 version 8.0a and database DATAA0.FMT.R2 (Brush and Domski 2013a). The most important of these changes for GWB brine is the lowering of the magnesium concentration from 1.02 to 0.330 M, a decrease in calcium concentration from 14 to 11.1 mM, and a pH of 8.82. For ERDA-6, there is a significant increase in the magnesium concentration from 19 to 136 millimoles per liter (mM), a decrease in total inorganic carbon from 16 to 0.455 mM, and an increase of the pH to 8.99 from 6.17. The pH associated with these MgO-reacted brines established the range of expected pH values in the WIPP for the calculation of actinide solubilities, and the composition of these reacted brines were used in PA to calculate actinide solubility in brine (Brush and Domski 2013a).

There are new data that validate the bracketing approach being used in the WIPP PA since the CRA-2009 submittal. Modeling (Brush et al. 2011) and experimental (Lucchini et al. 2013c) studies were conducted to investigate the pH dependency and the long-term stability of WIPP-specific brines. This was done to assess the validity of using the GWB and ERDA-6 formulations as bracketing brines in the solubility studies and establishes a broad-pH range comparison between modeling and experimental results.

The long-term stability of the unused GWB and ERDA-6 simulated brines (95% composition), used in actinide solubility studies showed no pattern of instability or precipitation. These results confirmed that the 95% formulations of the GWB and ERDA-6 brine were stable for up to six years and that the methods used for storage were appropriate and adequate during this time. The concentration of the brine components in the long-term uranium, neodymium and plutonium solubility and redox studies were also measured to determine their stability under the broader range of pH and experimental conditions used ($pC_{H+}$ of 6-12, presence of actinides/analogs, presence of carbonate, presence of iron). Under this broader set of interactions, the only changes noted were the precipitation of borate and magnesium salts in the higher-pH ERDA-6 experiments ($pC_{H+} > 10$).

1   The effect of $pC_{H+}$ on WIPP simulated brines was also investigated and modeled.   GWB (100%
2   formulation) was stepwise titrated up to $pC_{H+} \sim 13$, and the brine component concentrations were
3   determined after 3-week equilibrations. These experimental results were compared with the
4   predicted composition of the brine using the current WIPP brine model (Figures SOTERM-1 and
5   SOTERM-2).  Overall, there was good agreement between the experimental and the modeling
6   results at $pC_{H+} \leq 10.5$ (which includes the $pC_{H+}$ predicted for the expected conditions in the
7   WIPP).  The one exception to this is the decrease in tetraborate concentrations to $\sim 2 \times 10^{-3}$M
8   between $pC_{H+}$ of 10 and 10.5 (Figure SOTERM-1) since there are currently no Pitzer parameters
9   for tetraborate in the WIPP model.

10  At $pC_{H+} \geq 10.5$, there were a number of explainable discrepancies noted between the
11  experimental and modeling results for $Mg^{2+}$, $Ca^{2+}$ and tetraborate (Figures SOTERM-1 and
12  SOTERM-2). Specifically, calcium precipitation was only observed experimentally at $pC_{H+} >$
13  10.5; magnesium remains in solution above $pC_{H+}$ 10.5 in the experiments performed and does
14  not precipitate to the extent predicted by the model; and the tetraborate concentration goes
15  through a minimum at $pC_{H+}$ 9.75 that is also not captured in the modeling results. These results
16  are explained by precipitation of calcium carbonate, as it was observed in the experiments of
17  Kerber Schütz et al. (Kerber Schütz et al. 2011), and the resolubilization of magnesium due to a
18  change in the speciation of tetraborate at high $pC_{H+}$ (Schweitzer and Pesterfield 2010).

19  Overall, the modeling and experimental brine chemistry studies established a better
20  understanding of the actinide-relevant brine chemistry over a wider range of experimental
21  conditions than previously studied. GWB and ERDA-6 were confirmed as good "bracketing"
22  brines for WIPP-relevant studies, as GWB brine transitions into ERDA-6 at $pC_{H+} \sim 10.5$.
23  Relatively good agreement was found between the long-term experiments (using 95%
24  formulation brines) and the titration experiments (using the 100% formulation GWB).  All of
25  these results effectively increase the robustness of the current WIPP model and provide a better
26  foundation for future and ongoing WIPP-relevant actinide solubility studies.

**Table SOTERM-4. Composition of GWB and ERDA-6 Brine Before and After Reaction with Anhydrite, Brucite and Hydromagnesite. The reacted brine compositions were used to calculate actinide solubilities for the CRA-2014 PA.**

| Ion or property[a] | GWB Brine Composition[b] | GWB after reaction with MgO (phase 5), halite, and anhydrite[c] | ERDA-6 Brine Composition[d] | ERDA-6 after reaction with MgO (phase 5), halite, and anhydrite[c] |
|---|---|---|---|---|
| $B(OH)_x^{3-x}$ (see footnote e) | 158 mM | 186 mM | 63 mM | 62.3 mM |
| $Na^+$ | 3.53 M | 4.77 M | 4.87 M | 5.30 M |
| $Mg^{2+}$ | 1.02 M | 0.330 M | 19 mM | 136 mM |
| $K^+$ | 0.467 M | 0.550 M | 97 mM | 96.0 mM |
| $Ca^{2+}$ | 14 mM | 11.1 mM | 12 mM | 11.6 mM |
| $SO_4^{2-}$ | 177 mM | 216 mM | 170 mM | 182 mM |
| $Cl^-$ | 5.86 M | 5.36 M | 4.8 M | 5.24 M |
| $Br^-$ | 26.6 mM | 31.3 mM | 11 mM | 10.9 mM |
| Total Inorganic C (as $HCO_3^-$) | Not reported | 0.379 mM | 16 mM | 0.455 mM |
| pH | Not reported | 8.82 | 6.17 | 8.99 |
| Ionic Strength (M) | 7.44 | 6.44 | 5.32 | 5.99 |

a - ions listed represent the total of all species with this ion.
b – From Snider 2003a
c – From Brush, Domski and Xiong 2011
d – From Popielak et al. 1983
e – Boron species will be present in brine as boric acid, hydroxyl polynuclear forms ($B_3O_3(OH)_4^-$, and/or borate forms (e.g., $B_4O_7^-$)
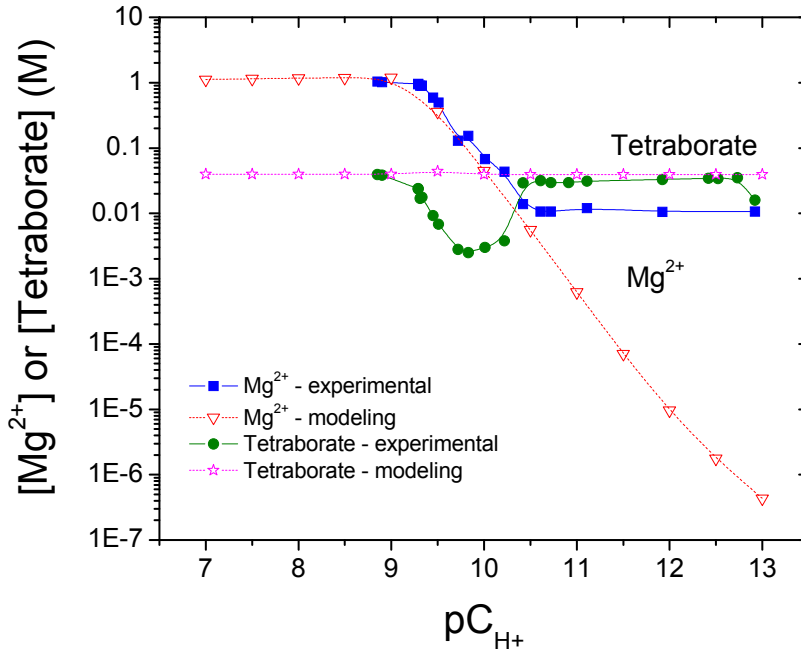
**Figure SOTERM-1.** **Comparison of Experimentally-measured (Lucchini et al. 2013c)**
**and Model-predicted (Brush et al. 2011) Concentrations of**
**Tetraborate and $Mg^{2+}$ in GWB 100% Saturated Brine as a**
**Function of $pC_{H+}$.**
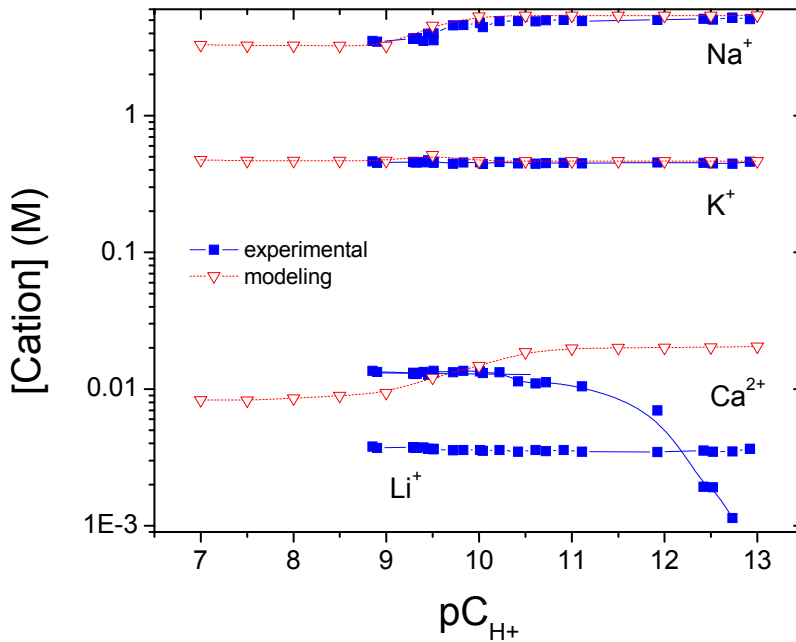


**Figure SOTERM-2.** **Comparison of Experimentally-measured (Lucchini et al. 2013c)**
**and Model-predicted (Brush et al. 2011) Concentrations of $Na^+$,**
**$K^+$, $Ca^{2+}$ and $Li^+$ in GWB 100% Saturated Brine as a Function of**
**$pC_{H+}$. $Li^+$ was not considered in the numerical simulation.**

1  **SOTERM-2.3.2 Brine pH and pH Buffering**

2   The brine pH is a very critical parameter in defining the solubility of actinides under conditions
3   where brine-mediated releases (DBR and transport through the Culebra) would be important in
4   the WIPP. There are a number of highly-coupled processes that can influence the pH when the
5   emplaced TRU waste is inundated with brine. The most important of these are the potential
6   buffering capacity of the brine coming into the WIPP, the reactions of this brine with emplaced
7   waste components (most notably reduced metals and organics), and microbial processes. The
8   reactions of the emplaced MgO barrier material are expected to sufficiently control and define
9   the pH when the repository is saturated with brine. Although there have been modeling and
10  experimental studies to investigate the pH of WIPP-specific brines, there is no significant change
11  in the key arguments for brine pH and pH buffering since the CRA-2009.

12  The range of brine composition that is likely to be present in the WIPP repository was discussed
13  in Section SOTERM-2.3.1 (see also Table SOTERM-4). These brines have an intrinsic buffering
14  capacity that is highest at pH 8.5-9. ERDA-6 brine, although it has an ambient pH of 6.2,
15  contains a number of constituents that, in the pH range of 8-10, add buffer capacity to the reacted
16  brine: carbonate/bicarbonate (16 mM), borate (63 mM), and divalent cations that tend to react
17  with hydroxide or carbonate to influence pH ($Ca^{2+}$ at 12 mM, and $Mg^{2+}$ at 19 mM). The $pK_a$ for
18  boric acid and dissolved carbonate/bicarbonate species are 9.0 and 9.67, respectively, which
19  explains the tendency of this brine to maintain the pH in the range of 8-10. Operationally, the
20  simulated ERDA-6 brines prepared in the laboratory have relatively high buffering capacity, and
21  significant changes in brine concentrations and pH are not routinely observed once the pH is
22  experimentally defined (Lucchini et al. 2013c). An operational pH range for ERDA-6 has been
23  defined as having an upper limit of pH ~10, which is the pH at which a cloud point (indicating
24  magnesium (Mg) precipitation) is observed. The pre-excavation ambient ERDA-6-like brine will
25  naturally add to the buffering capacity of the WIPP brine due to its acid-base components and
26  will establish a relatively high buffer capacity at the mildly alkaline conditions expected in the
27  WIPP.

28  The expected pH in the WIPP in the event of brine saturation, however, will be defined by the
29  reaction of the Castile ERDA-6-like brine with the waste components and barrier material. This
30  was re-evaluated as part of the documentation for the CRA-2014 PA (Brush et al. 2011; Table
31  SOTERM-4; Brush and Domski 2013a; Lucchini et al. 2013c). The hydration and carbonation
32  reactions of MgO are discussed extensively in Appendix MgO-2009. In PA, the following two
33  reactions combine to define $f_{CO_2}$ and the pH:

34  $$5Mg(OH)_2 + 4CO_2(aq\ or\ g) \leftrightarrows Mg_5(CO_3)_4(OH)_2 \cdot 4H_2O \qquad\qquad (SOTERM.3)$$

35  $$Mg(OH)_2 \leftrightarrows Mg^{2+} + 2OH^- \qquad\qquad (SOTERM.4)$$
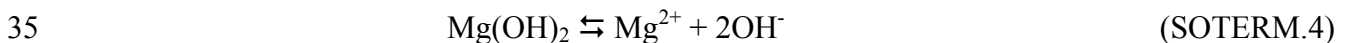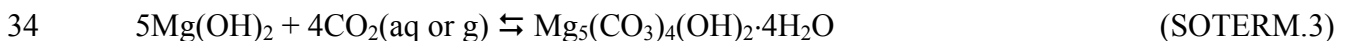
36  Calcite formation (see reaction SOTERM.5) may also occur (see Figure SOTERM-2). This
37  reaction is not considered in PA and remains a conservatism in the current PA model.

38  $$Mg(OH)_2 + Ca^{2+} + CO_2(aq\ or\ g) \leftrightarrows CaCO_3 + Mg^{2+} + H_2O(aq\ or\ g) \qquad\qquad (SOTERM.5)$$
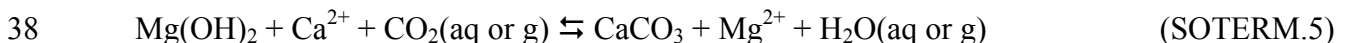
1    In PA, all vectors assume microbial activity consume organic material to produce $CO_2$ (see more
2    detailed discussion in Section SOTERM-2.4.1.1). Carbon dioxide production, if not for its
3    sequestration by MgO, would over time acidify any brine present in the repository and increase
4    the solubility of the actinides relative to that predicted for near-neutral and mildly basic
5    conditions. Current repository assumptions lead to a calculated $f_{CO2}$ of 3.14 x $10^{-6}$ atm ($10^{-5.50}$
6    atm) in both GWB and ERDA-6 and a predicted pH of 8.82 and 8.99 respectively. These $f_{CO2}$
7    and pH values were used in the actinide speciation and solubility calculations for all CRA-2014
8    PA vectors.

9    There are no new WIPP-specific results to report that explicitly address the MgO buffering of the
10   WIPP brine since the CRA-2009. The brine titration experiments and calculations that were
11   performed were described in section 2.3.1. These data are consistent with experimental results
12   published previously by the German program (Altmaier et al. 2003) that were discussed more
13   extensively in Appendix SOTERM-2009, section 2.3.2. All of these data suggest that MgO
14   controls the pH to a pH = $9 \pm 1$. In this context, it is predicted that brine pH will remain between
15   8 and 10 under the range of expected conditions in the WIPP.

16   **SOTERM-2.3.3 Selected MgO Chemistry and Reactions**

17   MgO is the bulk, granular material emplaced in the WIPP as an engineered barrier. The MgO
18   currently being placed in the WIPP contains $96 \pm 2$ mol % reactive constituents (i.e., periclase
19   and lime) (Deng et al. 2006; Reyes 2008). The amount of MgO emplaced in the WIPP is
20   currently calculated based on the estimated CPR content with an excess factor of 1.2, and it is
21   estimated that in excess of 50,000 metric tons will be emplaced in the WIPP by the time of
22   repository closure.

23   The chemistry of MgO is critical to the overall performance of the WIPP and is discussed in
24   detail in Appendix MgO-2009. The most recent data are described in Xiong and Lord (Xiong and
25   Lord 2008). The MgO, as the engineered barrier in the WIPP repository design, has two
26   important functions that directly support the PA calculation of actinide concentrations in brine:

27   1. Sequester the excess $CO_2$ produced by the microbial consumption of CPR material and
28      establish/maintain a low $f_{CO2}$ in the repository (see reaction SOTERM.3). This is currently
29      estimated to be $10^{-5.5}$ atm for GWB and ERDA-6 brine.

30   2. Establish and buffer the brine pH by maintaining a magnesium solution concentration that
31      reacts with hydroxide (see reaction SOTERM.4) to buffer the pH at about 9. This was part of
32      the pH discussion in Section SOTERM-2.3.2. This buffering removes uncertainty from the
33      actinide concentration calculations.

34   Initially, MgO will undergo hydration to generate brucite ($Mg(OH)_2$). In time, brucite will react
35   further to form magnesium chloride hydroxide hydrate (e.g., $Mg_3(OH)_5Cl \cdot 4H_2O$) in Salado brine
36   (Appendix MgO-2014, section MgO-4.1). These phases combine to control the concentration of
37   magnesium in high-magnesium brine (for example, GWB). The existence of magnesium as an
38   aqueous (aq) cation in equilibrium with excess magnesium minerals helps to establish the
39   solution pH.

1    For the reaction of MgO with GWB brine, PA uses a magnesium concentration of ~0.33 M
2    (Table SOTERM-4), which is supported by experimental results showing a magnesium
3    concentration ~0.3 M (Lucchini et al. 2013c). This reaction was also investigated by Altmaier et
4    al. (Altmaier et al. 2003) and Harvie, Møller, and Weare (Harvie, Møller, and Weare 1984).
5    Snider also noted that the rate of MgO hydration is most likely linked to mineral phase changes
6    between hydrated magnesium oxychloride and brucite (Snider 2003b). The existence of the
7    hydrated magnesium oxychloride phase was inferred from scanning electron microscope (SEM)
8    images, coupled with an energy dispersive x-ray spectroscopy system (EDS), to identify Mg–Cl
9    phases. The Altmaier and Harvie studies showed that the hydration reaction was a solid-phase
10   transformation between brucite and hydrated magnesium oxychloride that depends not on
11   magnesium concentration, but on chloride concentration, with an invariant point predicted at 1.8
12   m MgCl concentration and a $-\log m_{H+} = 8.95$.

13   The most important role of the MgO engineered barrier is to sequester carbon dioxide to
14   maintain a low $f_{CO_2}$ in the repository. Microbial consumption of CPR materials could produce
15   significant quantities of $CO_2$. Under these conditions, brucite and magnesium chloride hydrate
16   hydrate will react with the $CO_2$ generated. Both laboratory and modeling studies predict that the
17   following carbonation reaction will buffer $f_{CO_2}$ at a value of $10^{-5.50}$ atm in both GWB and
18   ERDA-6:

19       $5Mg(OH)_2 + 4CO_2(aq\ or\ g) \leftrightarrows Mg_5(CO_3)_4(OH)_2 \cdot 4H_2O$                     (SOTERM.6)
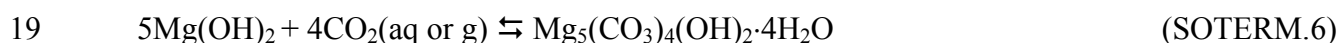
20   This reaction effectively removes excess $CO_2$ from the repository and bicarbonate/carbonate
21   from the brine. The initial product of MgO carbonation reaction is $Mg_5(CO_3)_4(OH)_2 \cdot 4H_2O$. This
22   is converted into $MgCO_3$, which is the expected stable mineral form of magnesium carbonate in
23   the WIPP, according to Reaction SOTERM.7:

24       $Mg_5(CO_3)_4(OH)_2 \cdot 4H_2O + CO_2(aq\ or\ g) + 10\ H_2O \leftrightarrows 5MgCO_3 \cdot 3H_2O$           (SOTERM.7)
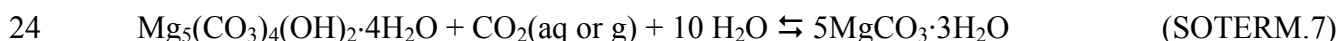
25   Reaction SOTERM.6 is slow and it is estimated that hundreds to thousands of years (Appendix
26   MgO-2009; Clayton 2013) are needed for the conversion of hydromagnesite to magnesite.
27   Consumption of $CO_2$ will prevent the brine acidification, and magnesium carbonate precipitation
28   will maintain low carbonate concentration in the WIPP brine to avoid the formation of highly
29   soluble actinide species with carbonate complexes. Although MgO will consume essentially all
30   $CO_2$, residual quantities in equilibrium with magnesite under the WIPP conditions will persist in
31   the aqueous and gaseous phases.

32   The importance of magnesium chemistry, and correspondingly the chemistry associated with the
33   emplaced MgO on the calculation of actinide concentrations in brine is clear. MgO sequesters
34   $CO_2$ and minimizes the buildup of carbonate in brine. At the expected pH, carbonate forms
35   strong complexes with the An(III), An(IV), and An(VI) oxidation states. An increased carbonate
36   concentration in brine would significantly increase actinide solubilities. Additionally, MgO helps
37   establish the pH in brine. The removal of $CO_2$ prevents a decrease in the pH that could also
38   significantly increase actinide solubility. An additional beneficial effect of MgO is to maintain a
39   solution concentration of $Mg^{2+}$ that will precipitate as brucite to keep the pH in the 8-10 range.
40   The presence of MgO leads to a more predictable chemistry that lowers the uncertainty when
41   calculating actinide concentrations in the WIPP brine.

1 **SOTERM-2.3.4 Iron Chemistry and Corrosion**

2 The WIPP repository will contain a large quantity of reduced iron due to the use of iron-based
3 containers for much of the emplaced TRU waste.  Currently, it is estimated that the WIPP will
4 contain over 49,000 metric tons of iron (Van Soest 2012) when all the waste is emplaced.  The
5 presence of this reduced metal will have an important role in the establishment of reducing
6 conditions in the WIPP by removing oxygen.  Reduced iron species (aqueous Fe(II) and Fe(0,
7 II)-valent minerals) are important because they will reduce higher-valent actinides in the WIPP,
8 leading to lower actinide solubilities (Section SOTERM-3.6; Reed et al. 2009; Reed et al. 2006).
9 The role of iron in the WIPP PA is unchanged since the CRA-2009, although new data on WIPP-
10 specific corrosion rates were obtained that are now the basis of gas generation rates due to
11 corrosion (Appendix PA-2014, Section1.1.4).

12 The chemistry of iron will have a pronounced effect on WIPP-relevant actinide chemistry in
13 many ways.  The linkages of iron chemistry to the redox chemistry are well established in the
14 literature (Farrell et al. 1999; Fredrickson et al. 2000; Qui et al. 2001; Nakata et al. 2004;
15 Behrends and Van Cappellen 2005).  Iron will establish reducing conditions conducive to the
16 overall reduction of higher-valent actinide species and precipitate an iron sulfide phase that
17 removes sulfide from solution.  Additionally, iron species could sequester carbon dioxide and
18 compete with actinides for organic and inorganic complexants, although there is no explicit
19 credit taken for this in the WIPP PA.

20 It is expected that oxic corrosion of steels and aerobic microbial consumption of CPR materials
21 will quickly consume the limited amount of oxygen ($O_2$) trapped within the repository at the time
22 of closure.  After $O_2$ is consumed, anoxic corrosion of metals will occur (Brush 1990; Brush
23 1995; Wang and Brush 1996; Roselle 2013).  In all of the vectors for the 2009 PA, the CRA-
24 2009 PABC, the 2004 PA, the CRA-2004 PABC, the CCA PA, and the EPA's CCA 1997
25 Performance Assessment Verification Test (PAVT), there were significant amounts of
26 uncorroded steels and other Fe-base alloys in the repository throughout the 10,000-yr regulatory
27 period.  The WIPP-specific experiments (Telander and Westerman 1993; Telander and
28 Westerman 1997) showed that steels and other Fe-based alloys will corrode by the following
29 reactions:

30 $$Fe + (x)H_2O \leftrightarrows Fe(OH)_2 \cdot (x-2)H_2O + H_2; \qquad (SOTERM.8)$$

31 $$3Fe + 4H_2O \leftrightarrows Fe_3O_4 + 4H_2; \qquad (SOTERM.9)$$

32 $$Fe + H_2O + CO_2 \leftrightarrows FeCO_3 + H_2; and \qquad (SOTERM.10)$$

33 $$Fe + H_2S \leftrightarrows FeS + H_2. \qquad (SOTERM.11)$$
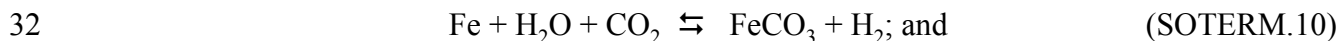
34 Since the experiments of Telander and Westerman (Telander and Westerman 1993; Telander and
35 Westerman 1997), a new series of steel and lead corrosion experiments has been conducted
36 (Roselle 2009, Roselle 2010, Roselle 2011a, Roselle 2011b, and Roselle 2013).  The object of
37 these experiments has been to determine steel and lead corrosion rates under WIPP-relevant
38 conditions.  Telander and Westerman (Telander and Westerman 1993; Telander and Westerman
39 1997) measured $H_2$ generation rates directly and from those measurements were then able to

1   calculate metal corrosion rates.  However, the new experiments directly measured metal
2   corrosion rates based on mass loss (Roselle 2013).  These new experiments showed that it is
3   possible for other corrosion products (e.g., green rust, hibbingite, etc.) to form (Roselle 2009,
4   2010, 2011a, 2011b, and 2013; Nemer et al. 2011).  In fact, Roselle (Roselle 2013) states that
5   green rust is the most likely corrosion product in experiments with low atmospheric $CO_2$
6   concentrations (<350 ppm).  At higher concentrations of $CO_2$ (>1500 ppm) iron carbonate was
7   seen as the major corrosion product (forming via SOTERM.10).  Assuming an idealized formula
8   for green rust as $[Fe(III)_2Fe(II)_4(OH)_{12}CO_3 \cdot 2H_2O]$, then the corrosion reaction would be written
9   as:

10      $$6\ Fe + CO_2 + 15\ H_2O \leftrightarrows Fe(III)_2Fe(II)_4(OH)_{12}CO_3 \cdot 2H_2O + 7\ H_2 \qquad \text{(SOTERM.12)}$$

11   Roselle (Roselle 2013) determined corrosion rates for steel inundated in brine in the absence of
12   $CO_2$.  Based on these rates, a new distribution was presented whose mean value is nearly an
13   order of magnitude less than the previous value determined by Wang and Brush (Wang and
14   Brush 1996).  Based on these new corrosion rates, there will still be significant amounts of
15   uncorroded steels and other Fe-base alloys in the repository throughout the 10,000-yr regulatory
16   period.

17   In reducing environments, reduced iron phases (Fe(II) oxides and zero valent iron) and aqueous
18   ferrous iron will be present.  These are all reducing agents towards key actinide species (Table
19   SOTERM-5) and will help establish the predominance of lower-valent actinides in the WIPP.
20   The concentration of ferrous iron could be relatively high in the WIPP brine, although its
21   solubility has not yet been explicitly determined.  There are also many potential reactions that
22   could control and/or define the iron chemistry.  The expectation is that ferrous hydroxide will
23   control the solubility of iron, leading to a predicted solubility in the range of $10^{-6}$ M to $10^{-4}$ M for
24   pH between 8.5 and 10.5 (Refait and Génin 1994).  A similar range of iron solubility in brines
25   was observed by Nemer et al. (Nemer et al. 2011) in experiments where Fe-hibbingite,
26   $Fe_2(OH)_3Cl$, was the solubility controlling phase.

1    **Table SOTERM-5.  Redox Half-Reaction Potentials for Key Fe, Pb, Pu, and U Reactions at**
2    **25 oC and I<1 (Morss, Edelstein, and Fuger 2006, Chapter 23)**

| Metal Species Reduced | $E_o$ (Acidic) (V) | $E_o$ at pH = 8 (V) |
|---|---|---|
| $Pb^{4+} \rightarrow Pb^{2+}$ | 1.69 | 2.47 |
| $PuO_2^+ \rightarrow Pu^{4+}$ | 1.170 | 0.70 |
| $PuO_2^{2+} \rightarrow PuO_2^+$ | 0.916 | 0.60 |
| $Fe(OH)_3(s) \rightarrow Fe^{2+}$ | Not Applicable | 0.1 |
| $FeOOH (s) \rightarrow FeCO_3(s)$ | Not Applicable | -0.05 |
| $UO_2^{2+} \rightarrow U^{4+}$ | 0.338 | -0.07 |
| $Pu^{4+} \rightarrow Pu^{3+}$ | 0.982 | -0.39 |
| $Pb^{2+} \rightarrow Pb$ | -0.1251 | -0.54 |
| $Fe^{3+} \rightarrow Fe^{2+}$ | 0.77 | -0.86 |
| $Fe(II)(OH)_2 \rightarrow Fe(0)$ | -0.44 | -0.89 |
| $U^{4+} \rightarrow U^{3+}$ | -0.607 | -1.95 |

3    Three important reactions of iron are considered.  The first is the reaction of metallic iron with
4    carbon dioxide to form strongly insoluble ferrous carbonate.  The solubility product of this salt is
5    log K = -10.8 at I = 0 (NIST 2004), and it is much smaller than magnesium carbonate.  This
6    suggests that the presence of iron will likely remove $CO_2$ from the repository more effectively
7    than MgO due to its lower solubility product.  This reaction is not included in the WIPP PA
8    because the $CO_2$ reacts sufficiently with MgO (so the Fe reaction is not needed) and the DOE
9    does not have sufficient data on the iron carbonation reaction.

10   The second is the reaction of iron and ferrous ions with the hydrogen sulfide that could be
11   generated in the repository by sulfate-reducing microbes.  This will lead to a very insoluble
12   ferrous sulfide precipitate with a solubility product of log $K_s$ = -17.2 (NIST 2004).  This helps
13   remove sulfide, which can complex actinides, from brine.  This reaction is assumed to occur
14   instantaneously in the PA.

15   Finally, iron species form strong complexes with organic ligands.  The strongest of these
16   complexes is with EDTA.  The net effect is that dissolved iron species will compete with
17   actinides for organic ligands, and in many cases out-compete the actinides to counteract the
18   potential enhancement of actinide solubility that would otherwise occur.  This reaction is not
19   currently included in the PA because the DOE does not have sufficient data on the reactions that
20   form iron EDTA complexes.  Work is currently underway to obtain the necessary
21   thermodynamic parameters for future input into the model.

22   **SOTERM-2.3.5 Chemistry of Lead in the WIPP**

23   Lead is present in the repository in the metallic form as part of the waste and waste packaging.
24   The currently anticipated inventory in waste packaging is approximately 8.3 metric tons (Van

1 Soest 2012). The reactivity of zero-valent lead is greatly mitigated by the formation of a thin,
2 coherent, protective oxide, oxycarbonate, chloride, or sulfate protective layer. Metallic lead also
3 reacts slowly with water at room temperature and undergoes corrosion to form oxides and
4 oxyhydroxides. Under slightly alkaline conditions, the hydrolysis of lead leads to formation of a
5 poly-oxyhydroxide cation, $[Pb_6O(OH)_6]^{4+}$. The following reactions are possible under WIPP-
6 relevant conditions:

7 $$2Pb + O_2 \leftrightarrows 2PbO \qquad\qquad (SOTERM.13)$$

8 $$2PbO + H_2O + CO_2 \leftrightarrows (PbOH)_2CO_3 \qquad\qquad (SOTERM.14)$$

9 $$Pb + H_2O + CO_2 \leftrightarrows PbCO_3 + H_2 \qquad\qquad (SOTERM.15)$$

10 $$Pb + H_2S \leftrightarrows PbS + H_2 \qquad\qquad (SOTERM.16)$$

11 $$Pb^{2+} + 2Cl^- \leftrightarrows PbCl_2 \qquad\qquad (SOTERM.17)$$

12 $$Pb^{2+} + SO_4^{2-} \leftrightarrows PbSO_4 \qquad\qquad (SOTERM.18)$$

13 $$5Pb^{2+} + PbO + 6OH^- \leftrightarrows [Pb_6O(OH)_6]^{4+} \qquad\qquad (SOTERM.19)$$
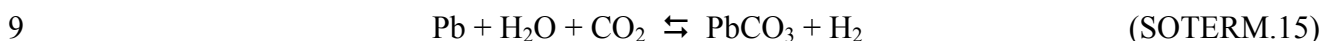
14 The corrosion of lead in WIPP-relevant conditions was studied extensively by Roselle (Roselle
15 2009, Roselle 2010, Roselle 2011a, Roselle 2011b, and Roselle 2013). In these experiments,
16 lead coupons were immersed in the WIPP brines (GWB and ERDA-6) under anoxic conditions
17 and a range of atmospheric $CO_2$ concentrations. Results from multiyear experiments show
18 formation of Pb-Ca carbonate phase at $CO_2 > 350$ ppm. No corrosion product buildup was
19 observed in the absence of $CO_2$; however, coupons were discolored due to the likely formation of
20 lead oxide. Corrosion rates for lead in the absence of $CO_2$ were similar to those measured for
21 steel (Roselle 2013).

22 The solubility of lead in the WIPP brine is expected to be low, due in part to the passivation
23 process, but also because of insoluble solids formation. Strong oxidants (e.g., radiolysis
24 products) may locally enhance the dissolution of lead, but alkaline brine, which contains
25 chlorides and carbonate/bicarbonate species, will overwhelm radiolytic effects to maintain a low
26 concentration of lead in the brine. In solution, lead will exist as $Pb^{2+}$ species that are redox-
27 active toward high-valent actinides (see Table SOTERM-5) and will help establish and maintain
28 reducing conditions in the brine.

29 Lead, as was the case with iron, can influence the redox chemistry (see Table SOTERM-5) and
30 precipitate carbonate and sulfide from the WIPP brine. This leads to a redox chemistry that will
31 help maintain reducing conditions and effectively lower carbonate concentration. Both of these
32 will potentially lower actinide solubility in the WIPP. These impacts are not considered in the
33 WIPP PA due to a lack of sufficient data, and this remains a conservatism in the WIPP model.

34 **SOTERM-2.3.6 Organic Chelating Agents**

35 Organic chelating agents are used in the processing and cleanup/decontamination of actinides
36 throughout the DOE complex. For this reason, they are often present as co-contaminants with the

1  TRU component in the WIPP waste. Some of these chelating agents strongly complex actinides
2  and have a significant effect on their solubility in brine. In this context, four organic chelating
3  agents–oxalate, acetate, citrate, and EDTA–are tracked as part of the WIPP inventory process,
4  and the potential effects of these complexants on the calculated actinide solubilities were
5  evaluated as part of the CRA-2014 WIPP PA (Brush and Domski 2013a and Brush and Domski
6  2013b).

7  The potential concentrations of the key organic ligands in the WIPP used in the CRA-2014 PA
8  were calculated by Brush and Domski (Brush and Domski 2013b) and are based on the 2012
9  WIPP inventory data (Van Soest 2012).  The organic concentrations for the minimum brine
10 volume used in the CRA-2009 PABC and CRA-2014 PA (see section SOTERM-2.2.4) are
11 summarized in Table SOTERM-6.  In the WIPP PA implementation, variable brine volume
12 concentrations will be used as described in Brush and Domski (Brush and Domski 2013a).

13 **Table SOTERM-6.  Comparison of the Concentrations of Organic Ligands in WIPP Brine**
14 **Used in the CRA-2009 PABC and the CRA-2014 PA**

| Organic Ligand | CRA-2009 PABC Maximum Anticipated Concentration (M)[b] | CRA-2014 PA Maximum Anticipated Concentration (M)[c] |
|---|---|---|
| Acetate | $1.94 \times 10^{-2}$ | $2.30 \times 10^{-2}$ |
| Oxalate[a] | $1.73 \times 10^{-2}$ | $1.18 \times 10^{-2}$ |
| Citrate | $2.38 \times 10^{-3}$ | $2.33 \times 10^{-3}$ |
| EDTA | $6.47 \times 10^{-5}$ | $7.40 \times 10^{-5}$ |
| a – the concentration of oxalate may be limited by its solubility, not inventory, in ERDA-6 brine. b – Brush and Xiong 2005a c – Brush and Domski 2013b | | |

15

16 Dissolved metals will compete with the actinides to form organic complexes. As the metals in
17 the repository corrode, additional transition metal ions will dissolve into the brine. These ionic
18 species include iron (Fe) and lead (Pb). Other steel constituents, such as nickel (Ni), chromium
19 (Cr), vanadium (V), and manganese (Mn), may also be present. Additionally, divalent cations in
20 the brine, most importantly $Mg^{2+}$ and $Ca^{2+}$, will also form complexes with these chelating agents
21 and compete with the actinide species. The stability constants for $Mg^{2+}$, $Ca^{2+}$, $Fe^{2+}$, $Pb^{2+}$, and
22 $Ni^{2+}$ and deprotonation constants for the organic acids are shown in Table SOTERM-7 (NIST
23 2004). These formation constants, in many respects, follow the same trends as the actinide
24 species with respect to the strength of the complexant (e.g., EDTA > citrate >> oxalate and
25 acetate).  When present in high enough concentrations, these metals will compete with the
26 actinide to form complexes and effectively lower the effect of organic complexation on actinide
27 solubility. However, this is not included in the PA and remains as a conservatism in the WIPP
28 actinide concentration model.

1  **Table SOTERM-7.  Apparent Stability Constants for Organic Ligands with Selected**
2  **Metals (NIST 2004)**

| Organic Ligand | $pK_a$ | Metal | Ionic Strength (m) | $\log_{10} \beta_1$ |
|---|---|---|---|---|
| EDTA | $k_1$ 8.86-9.05<br>$k_2$ 6.10-7.02<br>$k_3$ 2.79-2.54<br>$k_4$ 2.05-2.20 | $Fe^{2+}$<br>$Ni^{2+}$<br>$Pb^{2+}$<br>$Mg^{2+}$<br>$Ca^{2+}$ | 0.1<br>0.1<br>0.1<br>1<br>1 | 14.3<br>18.4<br>18<br>8.61<br>9.68 |
| Citrate | $k_1$ 5.58-5.30<br>$k_2$ 4.25-4.38<br>$k_3$ 2.85-3.06 | $Fe^{2+}$<br>$Ni^{2+}$<br>$Pb^{2+}$<br>$Mg^{2+}$<br>$Ca^{2+}$ | 0.1<br>0.1<br>1.0<br>0.1<br>0.1 | 4.4<br>5.18<br>4.44<br>3.43<br>3.48 |
| Oxalate | $k_1$ 3.74-4.23<br>$k_2$ 1.15-1.43 | $Fe^{2+}$<br>$Ni^{2+}$<br>$Pb^{2+}$<br>$Mg^{2+}$<br>$Ca^{2+}$ | 1.0<br>0.1<br>1.0<br>0.1<br>0.1 | 3.05<br>4.16<br>4.20<br>2.75<br>2.46 |
| Acetate | $k_1$ 4.52-4.99 | $Fe^{2+}$<br>$Ni^{2+}$<br>$Pb^{2+}$<br>$Mg^{2+}$<br>$Ca^{2+}$ | 3.0<br>0.1<br>0.1<br>0.1<br>0.1 | 0.54<br>0.88<br>2.15<br>0.51<br>0.55 |

3

4   There are two final, but important, observations about the organic chelating agents present in the
5   WIPP. First, they are expected to have very different tendencies toward biodegradation, based on
6   extensive experience with soil bacteria in the literature (Banaszak, Rittmann and Reed. 1998;
7   Reed, Deo and Rittmann 2010). Microbial activity, based on many general observations with soil
8   bacteria, will likely readily degrade citrate, oxalate, and acetate to very low (submicromolar)
9   steady-state concentrations. This important degradation pathway is not as certain for EDTA,
10  which tends to resist biodegradation in most groundwater. These degradation pathways have,
11  however, not been demonstrated for the halophiles typically present in the WIPP, and it is
12  currently assumed in the WIPP PA that no degradation pathways for these organic complexants,
13  microbiological or chemical, exist.

14  The second important observation is that these chelating agents, under WIPP-relevant conditions,
15  are expected to help establish reducing conditions in the WIPP because they tend to reduce
16  higher-valent actinides. This has been demonstrated in the WIPP brine for Np(V) and Pu(V/VI),
17  but was not observed for U(VI) (Reed et al. 1998). These chelating agents also tend to oxidize III
18  actinides to IV, which would have a beneficial effect on actinide solubility in the WIPP because
19  the actinides in the IV oxidation state are approximately 10 times less soluble than actinides in

1   the III oxidation state. These potentially beneficial effects of organic chelating agents on actinide
2   speciation are also currently not included in the WIPP PA and remain a conservatism in the
3   WIPP model.

4   **SOTERM-2.3.7 CPR in WIPP Waste**

5   The WIPP waste contains a relatively high amount of organic material, since much of the waste
6   is residue from laboratory operations where CPR materials were widely used. Current estimates
7   project over 14,000 metric tons of plastic and cellulosic materials with about 1,250 metric tons of
8   rubber material in the WIPP (Van Soest 2012; Table SOTERM-3). This organic material is
9   important from the perspective of repository performance in that it provides an organic
10  "feedstock" for microbial activity that could lead to gas generation (carbon dioxide, hydrogen,
11  hydrogen sulfide, and possibly methane), as well as degradation products that can complex
12  actinides or form pseudocolloids. CPR degradation is represented in the PA to evaluate these
13  potential impacts on the actinide concentrations and release.

# SOTERM-2.4 Important Post-emplacement Processes

15  There are three important post-emplacement processes that take place in the WIPP after
16  repository closure. These are metal corrosion, microbiological effects, and radiolysis. Metal
17  corrosion was already discussed as part of the iron chemistry section (Section SOTERM-2.3.4).
18  Microbiological effects and radiolysis are briefly discussed in this section.

19  **SOTERM-2.4.1 Microbial Effects in the WIPP**

20  Microbiological processes can have a significant effect on many aspects of subsurface chemical
21  and geochemical processes. This, particularly as it relates to contaminant transport and
22  remediation, has been well established for soil bacteria in low-ionic-strength and near-surface
23  groundwaters (Reed, Deo and Rittmann 2010; Banaszak, Rittmann and Reed 1998). In the
24  WIPP, as a result of the high-ionic-strength brines present, halophilic microorganisms will
25  predominate.  In prior recertifications, what was understood about halophilic organisms under
26  WIPP-relevant conditions was established through a series of long-term studies conducted as part
27  of the Actinide Source Term Program (ASTP) project by researchers at Brookhaven (Brush
28  1990; Francis and Gillow 1994; Brush 1995; Wang and Brush 1996).  This, since CRA-2009,
29  was significantly extended by newer studies (Swanson et al. 2012; Swanson et al. 2013a;
30  Swanson et al. 2013b; Swanson and Simmons 2013).  Although this new information has
31  increased our understanding of microbial processes in the WIPP, there are no changes to the
32  WIPP microbial model proposed for the CRA-2014.

33  The potential effects of microbial activity on the fate and transport of actinide metals from deep
34  geological waste repositories have been well described (McCabe 1990; Lloyd and Macaskie
35  2002; Pedersen 2002; Wang and Francis 2005) and may include 1) gas generation from the
36  degradation of organic waste components, 2) the creation of a reducing environment from
37  oxygen consumption, 3) redox reactions with metals and oxyanions, 4) the generation of organic
38  ligands from the incomplete degradation of organic waste components, and 5) the mobilization
39  of actinides adsorbed onto organism surfaces.

1    The WIPP PA considers gas generation, since it leads to $CO_2$ formation and increased dissolved
2    carbonate, and biocolloid formation to have the largest potential impact on the mobile
3    concentration of actinides in the source term.  Because of the scarcity of data during the time of
4    earlier certification efforts (Barnhart et al. 1978a, Barnhart et al. 1979b, Barnhart et al. 1979c and
5    Barnhart et al. 1979d), there are high levels of conservatism in the current WIPP microbial
6    model and there are no proposed changes to this model in the CRA-2014.  This conservatism is
7    attributed to the high uncertainty about microbial processes in hypersaline systems since these
8    are not well studied and because microbial processes attributed to low-ionic strength
9    environments were conferred upon the organisms that inhabit salt-based repositories.  In fact, we
10    are finding that organisms indigenous to hypersaline environments, such as the WIPP and its
11    environs, are not as metabolically diverse as is typically seen with their low ionic strength
12    counterparts and are, therefore, far less likely to play a large role in waste transformation.   There
13    is still uncertainty about what organisms may predominate should brine inundation occur, but it
14    is becoming clear that non-halophilic organisms introduced with emplaced waste are unlikely to
15    survive the near-field conditions. The microbial model assumptions that are used in the WIPP
16    PA are discussed extensively elsewhere (Appendix PA-2014, Sections 2.1.1 and 4.2.5; U.S. EPA
17    2006).  In this section we provide an updated view of the WIPP microbial ecology, present some
18    new experimental results and discuss these in the context of some of our current PA assumptions.
19    These results increase the DOE's overall understanding of the microbial ecology in the WIPP
20    and suggest that the current WIPP PA assumptions about microbial gas generation are
21    conservatively high.

22    **SOTERM-2.4.1.1 Microbial Ecology in the WIPP**

23    Hypersaline conditions result in a unique microbial ecology due to the thermodynamic
24    constraints imposed upon the organisms inhabiting such environments.  Survival in hypersaline
25    systems depends on an organism's ability to maintain osmotic balance with its external
26    environment (Oren 2006).

27    If the energetic cost of this maintenance exceeds the benefit of a given metabolic reaction, that
28    reaction will not proceed.  As a result, microbial metabolic processes are limited to the following
29    at salt concentrations greater than 2.5 M NaCl, the cut-off for extremely halophilic
30    microorganisms:  oxygenic and anoxygenic photosynthesis; aerobic respiration; denitrification;
31    fermentation; manganese, arsenite, and selenate reduction; dissimilatory sulfate reduction with
32    incomplete organic oxidation; methanogenesis from methylated amines; acetogenesis; and
33    chemolithotrophic oxidation of sulfur compounds (see Figure SOTERM-3; Oren 1999 and Oren
34    2011).  All of these processes are either energetically favorable or are performed by organisms
35    that maintain osmotic balance by a less costly strategy.
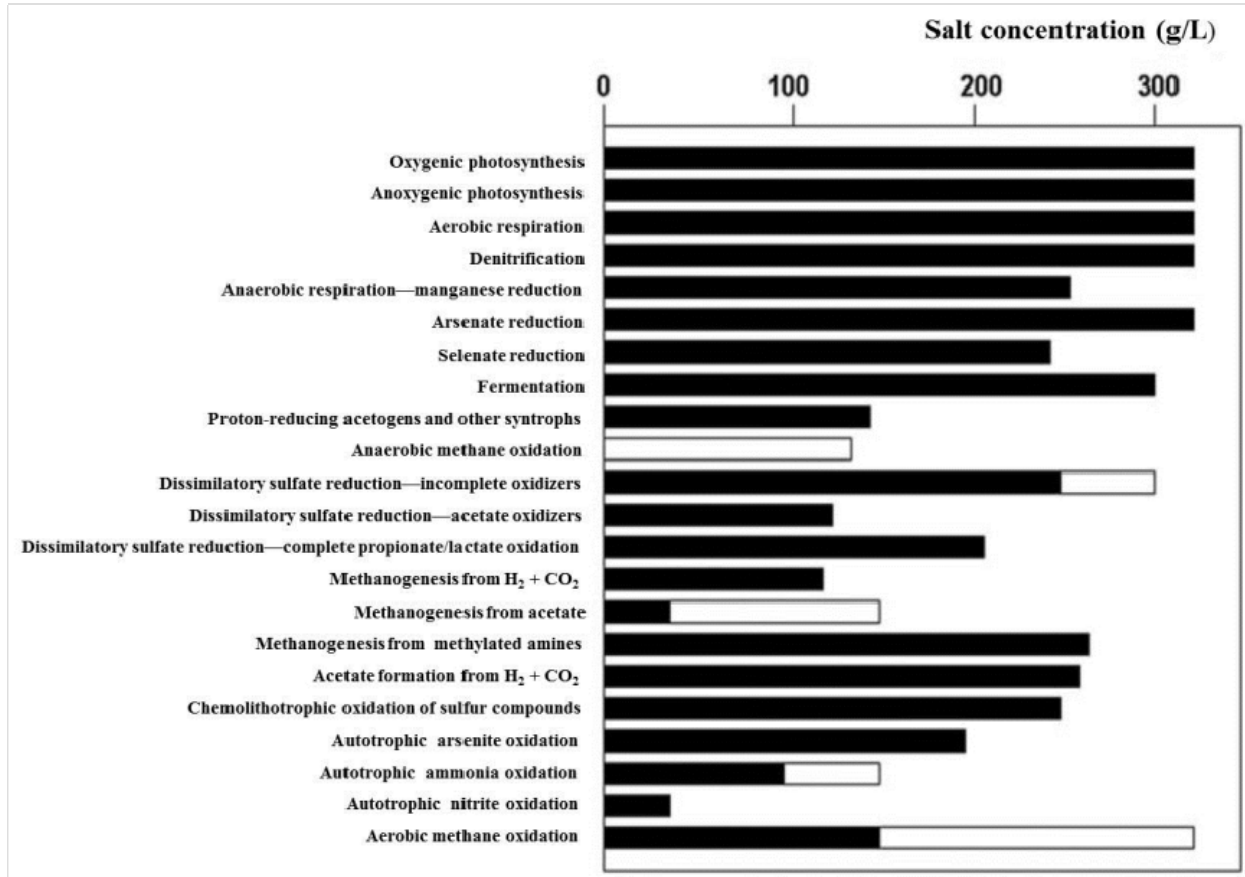
**Figure SOTERM-3. Approximate Upper Salt Concentration Limits for the Occurrence of Selected Microbial Processes (from Oren 2011). Solid bars are derived from laboratory experimental data using pure cultures; open bars are taken from in situ measurements of possible microbial activity.**

Apart from these thermodynamic constraints, the repertoire of potential microbial metabolic pathways within the WIPP is limited even further by 1) physical confinement of the repository without input of exogenous electron acceptors (especially oxygen), moisture (i.e., brine), or light; 2) high ionic strength; 3) high pH; and 4) nonideal substrates. These factors may restrict or effectively eliminate many capabilities.

Thus, microbial activity within the repository should be considered as varying in time and space (Swanson et al. 2012; Swanson and Simmons 2013). Obligate aerobic and extremely halophilic organisms may dominate the initial oxic environment, followed by the low-probability appearance of extremely halophilic anaerobes. In regard to space variation, extreme halophiles will dominate the near-field; while the salinity gradient will dictate the level of halophilism of organisms found within the far-field. Recent work on the characterization of microorganisms at the WIPP has supported these time and space assumptions and will be reviewed below (Swanson et al. 2012; Swanson and Simmons 2013).

1    *Variation in time*

2    Aerobic respiration by haloarchaea will be predominant immediately after repository closure and
3    will remain so until oxygen levels decrease from the corrosion of iron canisters and less
4    importantly, due to microbial activity.  Once oxygen has been depleted, nitrate, organic acids,
5    and sulfate will be present as potential electron acceptors.

6    While most haloarchaea are obligate aerobes, some are capable of nitrate reduction and
7    fermentation of small organics, such as amino acids.  However, once conditions become
8    anaerobic, haloarchaeal numbers will decrease and cells will become dormant.  The longevity of
9    these organisms entrapped in fluid inclusions or in interstitial brines is well documented; thus,
10   they will be present throughout repository history but are not likely to be active because of
11   unfavorable conditions (Norton and Grant 1988; Mormile et al. 2003; Schubert et al. 2009;
12   Schubert et al. 2010).

13   Halophilic, aerobic fungi and bacteria have also been isolated from WIPP halite (Swanson et al.,
14   2012; Swanson and Simmons 2013; Gunde-Cimermann et al. 2009).  These organisms may
15   survive the early oxic and moist conditions of the repository prior to inundation, but are unlikely
16   to survive in stringent WIPP brines that exceed either their sodium or magnesium tolerances.  In
17   anaerobic enrichments of WIPP halite, fungal hyphae did not elongate and spores did not grow,
18   and eventually the fungi died off (Swanson and Simmons 2013).

19   Bacteria have only been isolated from WIPP halite under aerobic, low-salt conditions, although
20   they may grow in up to 3.4 M NaCl (Swanson et al. 2012).  A halophilic denitrifier, *Halomonas*
21   sp. WIPP 1A, was isolated from previous studies, but its actual source is unknown (Francis et al.
22   2000).  Sulfate reducers (*Bacteria*) have thus far not been found in subsurface halite.  Gillow and
23   Francis (Gillow and Francis 2006) noted a sulfide precipitate in their long-term incubations,
24   which they attributed to the presence of sulfate-reducing bacteria (SRB); however, these
25   incubations were also inoculated with brine lake sediment, the most likely source of these
26   organisms.  SRBs have been found in other hypersaline environments (i.e., brine lakes, solar
27   salterns; Porter et al. 2007; Sørensen et al. 2009).  Their presence in seeps or in the underlying
28   Castile formation brines is unknown.  Sulfate is present in Castile brine and is also formed from
29   the dissolution of anhydrite present in the halite interbeds.

30   *Variation in space*

31   The variation of microbial communities in space concerns the near-field versus intermediate-
32   field versus far-field and reflects the variation in ionic strength in these spaces.  With differing
33   ionic strength comes differing community compositions and, hence, different metabolic
34   potential.

35   Extremely halophilic archaea and some few bacteria may survive at the NaCl concentrations
36   expected in the near-field.  Incubations of WIPP halite under high-salt conditions (4.7 M NaCl)
37   yielded only archaeal isolates (Swanson et al. 2012), and these survive in the WIPP brine.  The
38   intermediate-field, an area of hypothetical mixing of the repository soup and Culebra
39   groundwater, should support the growth of these same and other haloarchaea and also halophilic
40   bacteria and fungi.  The Culebra is considered to be the most likely pathway for actinide
41   migration from the repository, in the low-probability event of a breach into the WIPP horizon

1 (U.S. DOE 2011), and is therefore considered as the far-field. This space has been shown to be
2 dominated by a range of moderately halophilic and halotolerant bacteria, whose diversity
3 decreases as ionic strength increases (Swanson and Simmons 2013).

4 This distinction in space is important in that waste transformation will occur more readily in the
5 presence of bacteria than archaea. Metabolic activities shown to occur in the far-field include
6 aerobic respiration, fermentation, nitrate reduction, iron reduction, and sulfate reduction; while
7 still other processes are energetically feasible—reduction of other oxyanions, chemolithotrophy
8 (oxidation of ammonium, sulfide), methanogenesis at lower salt concentrations, and
9 methanotrophy (Oren 1999, Oren 2008, and Oren 2011; Swanson et al. 2012; Swanson and
10 Simmons 2013).

11 *Influence of Substrate*

12 Ideal substrates for haloarchaea include small organics, such as amino acids, acetate, glucose,
13 and often citrate (Oren 2006). Organic complexing agents—acetate, oxalate, citrate, and
14 EDTA—will be the predominant low-molecular-weight carbon substrates, but cellulosics may
15 contribute significantly to the carbon inventory. The availability of these substrates will depend
16 upon their dissolved concentrations in brine, which are expected to be at or below the current
17 inventory-predicted levels (Table SOTERM-6). The WIPP haloarchaea are capable of degrading
18 acetate, citrate, and oxalate in aerobic brines (Swanson et al. 2013a; Swanson et al. 2013b) but
19 there is as yet no evidence for anaerobic degradation. In the far-field, acetate and citrate
20 degraders are present, but the fates of oxalate and EDTA have not been studied (Swanson and
21 Simmons 2013).

22 *Organisms introduced in waste*

23 If soil has been introduced into waste containers, it may contain diverse microorganisms capable
24 of many different types of metabolism, and some may even be halotolerant. Spore-forming
25 organisms may survive in spore form for extremely long periods of time, but they will not likely
26 vegetate. Even a halophilic *Virgibacillus* sp. isolated from WIPP groundwater was unable to
27 grow at NaCl concentrations above 17.5%, at which point it sporulated (Swanson et al. 2012).
28 Although the survival of soil organisms at expected WIPP ionic strength has not been shown, gas
29 generation was reported in incubations of soil and TRU-simulated waste in brine (Caldwell et al.
30 1988); however, results were equivocal, and microbes were never looked for in the samples.

31 In spite of conditions inconducive to significant microbial activity, the theoretical possibility of
32 such an occurrence must be taken into consideration by PA, and the current knowledge of the
33 microbial ecology at the WIPP should not affect these assessments other than to underscore the
34 conservatism of the model.

35 **SOTERM-2.4.1.2 WIPP-related Microbial Degradation of CPR**

36 The generation of gas from the degradation of cellulose in waste repositories is an important
37 process that is difficult to reliably predict. The WIPP PA considers this process to be a
38 guaranteed occurrence, which is a very conservative approach, that proceeds completely to
39 carbon dioxide and water (Appendix PA-2014, Section 4.2.5) if the following conditions are met:
40 1) microorganisms capable of degrading cellulose are present at repository closure, 2) these

1    organisms can survive for a significant length of time, and 3) sufficient water, electron acceptors,
2    and nutrients are available to support their activity (Brush 1995).  The reality is that cellulose
3    degradation is a complex process requiring the concerted efforts of many different groups of
4    organisms, few of which are either found or would survive in the WIPP.  Additionally, the
5    degradation process differs between aerobic and anaerobic environments, as the organisms
6    within those spaces utilize different mechanisms for hydrolysis (Lynd et al. 2002; Wilson 2011).

7    Sources of cellulose in hypersaline habitats include dead algal biomass and halophytic debris.
8    Many halophilic microorganisms possessing cellulase activity or capable of growth on cellulosic
9    substrates have been reported.  Two fungi isolated from WIPP halite, one with documented
10   ligninolytic capability (*Cladosporium*; Cronin and Post 1977; Gunde-Cimerman et al. 2009),
11   were capable of growth on Kimwipes and using carboxymethylcellulose (CMC) as the sole
12   carbon source (Swanson and Simmons 2013).  Moderately halophilic bacteria, including
13   organisms similar to those isolated from the WIPP environs—e.g., *Halomonas* sp., *Virgibacillus*
14   sp., and *Salinicoccus* sp.—have also exhibited cellulase activity (Rohban et al. 2009), and an
15   extremely halophilic bacterium, *Marinimicrobium haloxylanilyticum*, was found to degrade
16   CMC in up to 22% NaCl.  A mixed culture, presumably archaea, enriched from WIPP halite
17   adhered to and altered Kimwipe fibers, as observed microscopically (Vreeland et al. 1998).

18   Of the above, the bacteria and fungi are unlikely to survive in the WIPP brines, and all are
19   obligately aerobic.  Only one anaerobic, cellulolytic microorganism has been isolated from a
20   hypersaline environment—*Halocella halocellulolytica* (Simankova and Zavarzin 1992;
21   Simankova et al. 1993).  This organism degrades cellulose (filter paper) in concentrations of
22   NaCl up to 20%.  Thus, it is unlikely that any significant anaerobic cellulose degradation will
23   occur in the WIPP near-field, but lower salinities may permit utilization in the far-field.

24   Early studies on gas generation were carried out as part of the Actinide Source Term Program
25   (ASTP) at Los Alamos National Laboratory, and later studies took place at Brookhaven National
26   Laboratory.  While inconclusive, these studies support the general opinion that organisms
27   introduced into the WIPP along with emplaced waste will not be able to survive in high ionic
28   strength media.

29   Later studies showed gas generation from cellulose degradation, and these were used as the basis
30   for the WIPP PA assumptions (Francis and Gillow 1993; Francis et al. 1997; Gillow and Francis
31   2006).  These studies used a mixed inoculum, including brine lake sediment and water,
32   underground brine seep, and halite.  Because of the relatively rich inoculum, the rates of gas
33   generation measured can be considered optimistic.  Sediments are rich in organisms, including
34   anaerobes, even in hypersaline systems.  Even so, these studies provide a more realistic scenario
35   than the earlier studies, especially since expected WIPP conditions were better known at the time
36   of design.

37   The presence of exogenous cellulolytic bacteria introduced in the waste drums themselves cannot
38   be ruled out and, in fact, these organisms have been detected in simulated waste pits (Field et al.
39   2010).  If any moisture were present in the drums, these organisms may have had a chance to
40   cause initial cellulose breakdown to products more easily metabolized by cellulase-producing
41   bacteria should they come into contact with these by-products during early oxic periods.  Again,

1  these organisms are unlikely to survive or be active in brine, although some are likely to be
2  halotolerant.

3  Cellulase-producing haloarchaea, including *Haloarcula*, *Halobacterium*, and *Halorubrum* spp.,
4  have been isolated previously from hypersaline salt lakes and salterns (Birbir et al. 2007).  While
5  these organisms are likely to thrive at high ionic strength, their use of cellulose by-products will
6  be limited, once again, to early oxic periods.

7  Still, complex organics may be more recalcitrant to degradation in anaerobic, hypersaline
8  systems.  Cellulose fibers have been preserved in fluid inclusions extracted from WIPP halite,
9  suggesting that this type of high-molecular weight organic is recalcitrant to degradation at high
10 salt concentrations, possibly owing to the lack of ionizing radiation, water available for
11 hydrolysis, and microbial activity (Griffith et al. 2008).

12 The current PA approach to account for CPR degradation, although there are many reasons that a
13 much lower extent of biodegradation should occur, remains conservative in that it assumes that
14 the biodegradation of all cellulosic and plastic material is guaranteed.  This adds to the overall
15 conservatism of the WIPP actinide source term model.

16 **SOTERM-2.4.1.3 Bioreduction of Multivalent Actinides**

17 The microbially induced reduction of higher-valent actinides would be an important beneficial
18 effect for the WIPP, in that lower-valent actinide species are less soluble.  This has recently been
19 the focus of much research due to its expected role in microbially mediated remediation and
20 containment of subsurface contaminants (Banaszak, Rittman, and Reed 1998; Banaszak et al.
21 1999; Lloyd, Young, and Macaskie 2000; Reed et al. 2007; Icopini, Boukhalfa, and Neu 2007;
22 Francis, Dodge, and Gillow 2008).  For soil bacteria, there is no question that biotic mechanisms
23 that lead to the reduction of actinides exist under a wide range of anaerobic subsurface
24 conditions.

25 There are, however, very few data concerning metal reduction in hypersaline environments
26 (Sorokin and Muyzer 2010; Emmerich et al. 2012).  This is likely due to the low solubility of
27 oxidized metal species in these systems; thus, the data are generally limited to lower ionic
28 strength systems, insoluble metal oxides in sediments, or metals associated with particulate
29 organic matter or associated with microbial mats.  The ability of WIPP-indigenous
30 microorganisms to reduce metals is again divided between near-field and far-field spaces.

31 Both *Clostridium* spp. and sulfate-reducing bacteria with metal-reducing capability have been
32 detected in the Culebra and could be capable of directly reducing higher-valent actinides in the
33 far-field (Swanson et al. 2012; Swanson and Simmons 2013).  Additionally, the indirect
34 reduction of iron by either fermenting *Halanaerobium* spp. or SRB was shown to precipitate
35 iron-sulfide complexes by lowering the redox potential or reducing sulfate, respectively, in iron-
36 amended enrichment incubations.  The reduction of iron by other SRB and fermenters has been
37 shown previously in hypersaline sediments (Emmerich et al. 2012).

38 In the near-field, however, it is less likely that direct biotic processes will cause actinide
39 reduction since haloarchaea have not been shown to directly reduce metals.

1 The potentially beneficial effects of bioreduction to lower the solubility of multivalent actinides
2 are not considered in the WIPP PA. There remains high uncertainty about this process for
3 halophilic microorganisms and there is not yet definitive WIPP-specific data to explain and
4 support this reduction pathway.

5 **SOTERM-2.4.1.4 Current WIPP PA Model for the Biodegradation of CPR**

6 There is no change from the CRA-2009 in the CPR microbial degradation model proposed in the
7 CRA-2014. There are no new gas generation rates, and the implementation and basis of the gas
8 generation rates has not changed (Appendix PA-2014, Section 4.2.5).

9 Currently, microbial activity is considered in all PA vectors. The presence of this microbial
10 activity means it is assumed that microbes may consume 100% of the cellulosic materials in the
11 repository, and that there is a probability of 0.25 that microbes may consume the plastic and
12 rubber materials. Thus, there is microbial consumption of cellulosic materials, but not of plastic
13 or rubber materials, in 75% of the PA realizations (vectors), and microbial consumption of CPR
14 materials in 25% of the vectors.

15 Microbial consumption of CPR materials could affect the actinide source term in four ways:

16    1) Production of significant quantities of $CO_2$, which could acidify the brine in the absence
17       of an MgO buffer or increase the solubility of actinides by increasing carbonate levels
18       that complex some actinides at the expected mildly alkaline pH

19    2) Bioreduction of higher-valent actinide species leading to lower-valent, less-soluble
20       actinide species

21    3) Degradation of solubilizing organic ligands, leading to lower actinide solubility

22    4) Increased biomass that may lead to the formation of microbial colloids that increase the
23       amount of actinide pseudocolloids in the brine

24 The effect of $CO_2$ production is discussed in this section. The remaining three effects are
25 implicitly considered in the analyses that address the oxidation-state distributions (Section
26 SOTERM-4.3), the effects of organic ligands (Section SOTERM-2.3.6), and the effects of
27 colloids (Section SOTERM-3.9). The simplifications used in the PA calculations for all four of
28 these effects are discussed at the end of this section.

29 Microbial activity, if it occurs to a significant extent in the WIPP, would consume CPR materials
30 by the following sequential reactions (Brush 1990; Francis and Gillow 1994; Brush 1995; Wang
31 and Brush 1996; Francis 1998):

32    $$C_6H_{10}O_5 + 4.8H^+ + 4.8NO_3^- \rightarrow 7.4H_2O + 6CO_2 + 2.4N_2; \qquad \text{(SOTERM.20)}$$

33    $$C_6H_{10}O_5 + 6H^+ + 3SO_4^{2-} \rightarrow 5H_2O + 6CO_2 + 3H_2S; \quad \text{(SOTERM.21)}$$

34    $$C_6H_{10}O_5 + H_2O \rightarrow 3CH_4 + 3CO_2. \qquad \text{(SOTERM.22)}$$
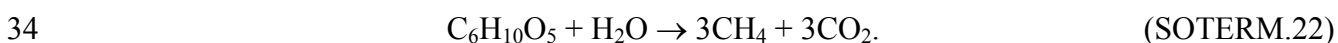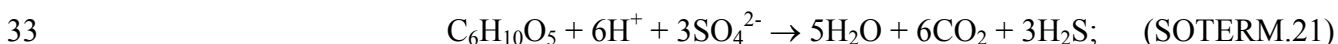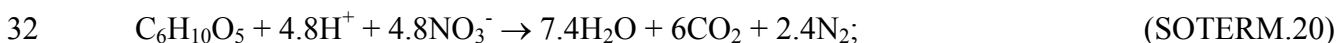
1    Methanogenesis, described by reaction SOTERM.22, is not included as a degradation pathway
2    because it is assumed that the sulfate present in the DRZ is always available.  This exclusion is
3    considered a conservative assumption relative to the amount of carbon dioxide that could be
4    produced.  In effect, the CRA-2014 PA assumes that an excess of sulfate is always available to
5    sustain sulfate-reduction as a mode of respiration.  When unlimited sulfate is available from
6    natural sources in the host rock, 4% of the gas generation occurs through denitrification and 96%
7    occurs by way of sulfate reduction.  The omission of methanogenesis is now further supported by
8    the fact that this process has been shown unfavorable at the ionic strengths expected in the WIPP
9    (Oren 2011, also see discussion in Section SOTERM-2.4.1.1).  Microbial consumption of CPR
10   materials, therefore, is assumed to produce significant quantities of $CO_2$, which could in turn
11   acidify any brine present in the repository and increase the solubilities of the actinides relative to
12   those predicted for neutral and mildly basic conditions.  Therefore, the DOE is emplacing MgO
13   in the repository to decrease actinide solubilities by consuming essentially all of the $CO_2$ that
14   could be produced by microbial consumption of CPR materials, and by buffering (controlling)
15   the $f_{CO_2}$ and pH within ranges that are favorable from the standpoint of actinide speciation and
16   solubility (see Section SOTERM-2.3.2).

17   Three effects of microbial consumption of CPR materials are recognized in the system
18   performance modeling.  A simplification has been made so the effects will be time-independent
19   after 100 years.  These effects are

20      1.   $CO_2$ production:  With the addition of excess MgO, the effects of $CO_2$ production are
21         minimized, and it is assumed that the system may be modeled using the brucite-
22         hydromagnesite $(Mg_5(CO_3)_4(OH)_2 \cdot 4H_2O)$ buffer.

23      2.   Redox effects: After 100 years, the repository will have a reducing environment.  This is,
24         in part, established by the postclosure microbial consumption of oxygen, but is also due
25         to the corrosion of steel.  This combined effect leads to the formation of an anoxic
26         reducing environment in the WIPP.

27      3.   Biocolloid formation:  Production of microbial colloids is possible and may contribute to
28         the formation of colloidal species that add to the actinide source-term concentration in
29         DBR release.

## 30   SOTERM-2.4.2 Radiolysis Effects in the WIPP

31   Radiolysis effects in the WIPP are caused by the interaction of ionizing radiation and particles
32   (neutrons, α, β, and γ) with the gases, brines, and materials present in the repository. These
33   effects have not been extensively studied under WIPP-related conditions, but there is a fairly
34   good general understanding of their extent and nature. For most conditions expected in the
35   WIPP, radiolytic effects are predicted to be transient and insignificant.  In this context, there is a
36   recognition that although radiolysis can lead to localized conditions and effects that could
37   oxidize multivalent actinides, the brine chemistry, metal corrosion, and microbiological activity
38   will combine to very rapidly overwhelm these effects.  For this reason, radiolysis effects on
39   actinide solubility are not explicitly included in the WIPP PA to calculate actinide
40   concentrations.  More specifics on the overall mechanisms, brine radiation chemistry, and
41   potential radiolytic effects on actinide speciation are given in this section.

1    There are no new data on the radiolysis of brine systems since the CRA-2009. Radiolytic effects
2    continue to be low in importance for transuranic waste under WIPP-relevant conditions and data
3    obtained (see section SOTERM-3.6) on Pu-Fe systems show that the iron chemistry and
4    expected reducing conditions prevail over radiolytic processes.

5    **SOTERM-2.4.2.1 Radiation Chemistry of Brine Systems**

6    The radiolysis of high-ionic-strength brine systems has not been extensively studied, but some
7    studies exist (Büppelman, Kim, and Lierse 1988; Kim et al. 1994; Kelm, Pashalidis, and Kim
8    1999; Ershov et al. 2002). The many components in the brine systems of interest to the WIPP
9    will lead to relatively complex radiation chemistry and the formation of numerous transients and
10    free radicals.

11    In contrast to this, the radiation chemistry of pure and dilute aqueous systems has been
12    extensively investigated, and detailed reviews of this research have been published (Draganic
13    and Draganic 1971; Spinks and Woods 1990). The irradiation of pure water leads to the
14    formation of molecular hydrogen peroxide ($H_2O_2$) and hydrogen ($H_2$). These molecular yields
15    are relatively insensitive to a wide range of conditions in dilute systems for a given type of
16    ionizing radiation. Molecular yields are $G_{H2} = 0.45$ molecule (molec)/100 electron-volt (eV) and
17    $G_{H2O2} = 0.7$ molec/100 eV for low Linear Energy Transfer (LET) ionizing radiation ($\beta$, and $\gamma$)
18    and $G_{H2} = 1.6$ molec/100 eV and $G_{H2O2} = 1.5$ molec/100 eV for high LET radiation ($\alpha$ and
19    neutrons). The radiolytic formation of hydrogen in the WIPP brine due to self-irradiation effects
20    of $^{239}$Pu was established and a molecular yield of $G_{H2} = 1.4$ molec/100 eV was measured (Reed
21    et al. 1993). This yield is consistent with the high LET literature, even though the irradiations
22    were performed in brine.

23    The high concentrations of electron and free radical scavengers present in the WIPP brine have a
24    pronounced effect on the radiation chemistry. Most importantly, halides react with the hydroxyl
25    radical (OH·) or act as scavengers (such as $Cl^-$ or $Br^-$) to gradually lower the molecular yield of
26    $H_2O_2$ as the concentration of the scavengers is increasing (Kelm, Pashalidis, and Kim 1999). In
27    this context, oxidizing transient species are "chemically" stored as oxychlorides and
28    oxybromides, leading to a shift towards more oxidizing conditions. Figure SOTERM-4 gives an
29    overview of the radiolytic pathways and mechanisms that are likely (Buppelmann, Kim, and
30    Lierse 1988). In NaCl brine, the formation of chloride species ($ClO^-$, HOCl, $Cl_2$, and $Cl_3^-$) is
31    favored, instead of $H_2O_2$ (Büppelmann, Kim, and Lierse 1988).

1   O$_2$
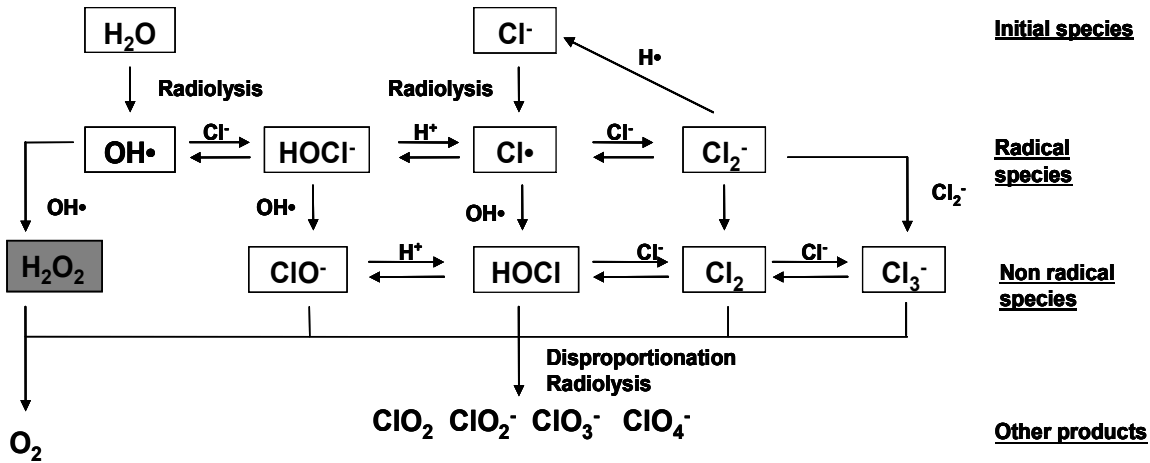
2   **Figure SOTERM-4.  NaCl Brine Radiolysis Species and Suggested Mechanism of**
3   **Production. The formation of chloride species (ClO$^-$, HOCl, Cl$_2$,**
4   **and Cl$_3^-$) is favored instead of H$_2$O$_2$ (based on data in**
5   **Büppelmann, Kim, and Lierse 1988).**

6   Kelm, Pashalidis, and Kim (Kelm, Pashalidis, and Kim 1999) showed that the formation of
7   hypochlorite ion increases with the chloride concentration and the dose (Figure SOTERM-5) in
8   NaCl brine. The authors found that in solutions containing 37 gigabecquerel (GBq)/liter (L) of
9   $^{238}$Pu, the hypochlorite concentration increases with time (dose) and appears to approach a steady
10  state (see Figure SOTERM-5). At a constant dose rate, the maximum hypochlorite concentration
11  depends on the chloride concentration. It was also observed that hypochlorite ion generation was
12  negligible when chloride concentrations were smaller than 2 M.
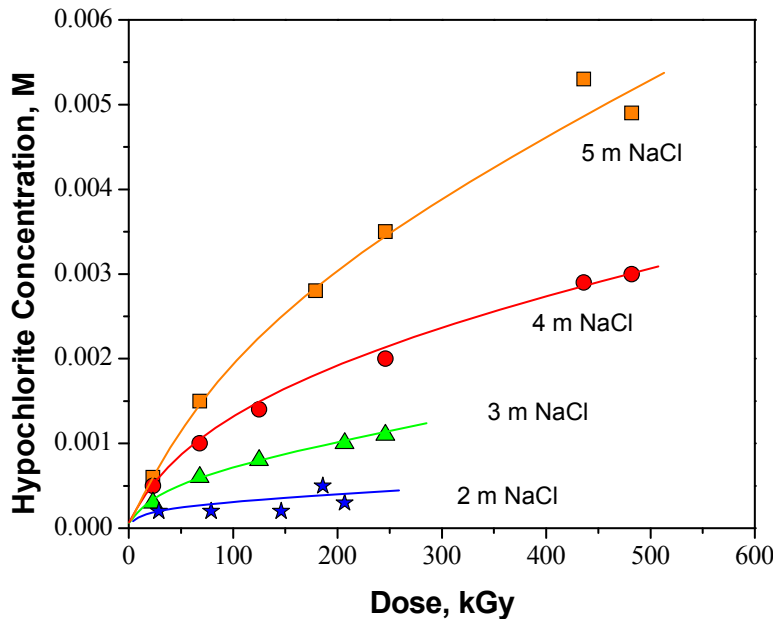


13

14  **Figure SOTERM-5.  Radiolytic Formation of Hypochlorite Ion in Solutions of Various**
15  **NaCl Concentrations at a Constant Alpha Activity of 37 GBq/L**
16  **at pH~12 (based on data in Kelm, Pashalidis, and Kim 1999)**

1 In the WIPP brine, however, some solutes other than chloride may play a role. Ershov et al.
2 (Ershov et al. 2002) showed that small amounts of bromide in natural brines under radiolysis can
3 give $Cl_2^-$, $ClBr^-$, and $Br^-$ radical anions at the radical step, and then mixed halogen molecules and
4 trihalide ions by radical recombination at the molecular step (Ershov et al. 2002). The hydrolysis
5 of mixed halogen molecules can then result in the formation of hypobromite ($OBr^-$) (acidic form:
6 hypobromous acid [HOBr]), a starting substance to more stable bromates of higher oxidation
7 state (Ershov et al. 2002).

8 Some WIPP-specific experiments were performed to establish the key radiolytic product in
9 GWB and ERDA-6 brine (Lucchini et al. 2010a). This study confirms that hydrogen peroxide
10 ($H_2O_2$) and hypochlorite ion ($OCl^-$) are unstable in these WIPP brines, due in part to metallic
11 impurities in the brine. There was, however, an accelerated decomposition of these species when
12 bromide ($Br^-$) was present, which is the case for both ERDA-6 and GWB brines. Here, $OCl^-$
13 readily and stoichiometricly reacted with $Br^-$ to form hypobromite ion ($OBr^-$), which appeared to
14 be the most important radiolytic transient observed under these conditions. $OBr^-$, like $OCl^-$, is
15 also an oxidizing species ($E°=0.76V$), that will likely lead to the oxidation of multivalent
16 actinides in the WIPP, but this reactivity has not been established experimentally under
17 representative WIPP conditions (Lucchini et al. 2010a).

18 In the WIPP, most of the brine radiolysis is caused by the deposition of alpha particles from the
19 TRU isotopes present in the WIPP waste. The range (distance traveled until the alpha particle's
20 energy is lost) of these alpha particles is very short (<40 microns) and radiolysis of the brine
21 solution will take place at the solid-liquid interface. Locally, the concentration of oxidative
22 radiolytic products of brine, such as hypochlorite, chlorite, chlorate, and products of their
23 reaction with brine components (e.g., hypobromite) may be high, and they may directly interact
24 with the radioactive surface. These "very-near" radiolytic effects, however, are expected to be
25 quickly mitigated by the bulk brine chemistry and the reaction of reducing agents (e.g., reduced
26 iron) with the oxidizing molecular products formed.

27 **SOTERM-2.4.2.2 Potential Radiolytic Effects on Actinide Speciation and Solubility**

28 A buildup of oxidizing radiolytic products in brine may increase the redox potential of the brine
29 (Büppelmann, Kim, and Lierse 1988), and consequently directly generate higher-valent actinide
30 species. Alternatively, these radiolytic products could be inserted into some solid actinide
31 phases. For example, Kim et al. (Kim et al. 1994) studied the solubility of schoepite,
32 $(UO_2)(OH)_2 \cdot xH_2O$, with hypochlorite ion in 0.1M NaCl at 25 °C (77 °F), in $CO_2$-free atmosphere
33 (Kim et al. 1994). Their X-Ray Diffraction (XRD) patterns of the residual precipitates showed
34 the introduction of the hypochlorite ion in precipitates. Kim et al. (Kim et al. 1994) observed that
35 the presence of hypochlorite ion in the initial schoepite structure enhanced the solubility of the
36 solid 10 to 100 times in the range of pH 6.0-9.8, compared with its solubility in the absence of
37 hypochlorite ion (Kim et al. 1994). However, this effect was reduced when the molar ratio [$ClO^-$
38 ]/[$UO_2^{2+}$] increased. This scenario is unlikely to occur in the WIPP because the potential buildup
39 of oxidizing radiolytic products generated in brine is readily overwhelmed by the overall
40 reducing capacity of the site (reduced metals and microbial processes).

41 The buildup of oxidizing radiolytic products due to brine radiolysis has also been shown to
42 significantly affect the solution chemistry of Am. For example, Am(III) was oxidized to the more

1 soluble forms of Am, namely $AmO_2^+$ and $AmO_2^{2+}$ (Magirius, Carnall, and Kim 1985; Katz,
2 Seaborg, and Morss 1986; Stadler and Kim 1988; and Meyer et al. 2002). Magirius, Carnall, and
3 Kim (Magirius, Carnall, and Kim 1985) reported on the radiation effects exerted upon a 5 M
4 NaCl solution at the pH 8 to 9 range using precipitated $Am(OH)_3$ at a concentration of $1.03 \times$
5 $10^{-3}$ M (1.07 curie [Ci]/L). They observed that the precipitate began to show discoloration,
6 changing from pink $Am^{3+}$ to brown $AmO_2^+$, within 24 hours (h), with quantitative oxidation of
7 all the Am to $AmO_2^+$ within 1 week. Because Pu is more readily oxidized than Am, the
8 expectation is that Pu could also be oxidized in irradiated brine. The metastability of Pu(VI) in
9 the WIPP brine when no reducing agents were present was established and attributed to self-
10 radiolysis effects of the $^{239}$Pu isotope used (Reed, Okajima, and Richmann 1994; Reed et al.
11 2006).

12 Stadler and Kim (Stadler and Kim 1988) also report the existence of higher oxidation states of
13 Am, due to self radiolysis. Solubility experiments on $Am(OH)_3$(solid[s]) in 3 M NaCl resulted in
14 much higher Am concentrations than was calculated from the solubility product. This difference
15 was assigned to the radiolytic oxidation of $Am^{3+}$ to $AmO_2^+$. Spectrophotometric evidence of
16 $AmO_2^+$ species in solution was reported. The authors report the value of $\log_{10}K_{S,0} = -9.3 \pm 0.5$ for
17 the reaction

18 $$AmO_2OH(s) \leftrightarrows AmO_2^+ + OH^- \hspace{3cm} (SOTERM.23)$$

19 The solubility product of $AmO_2OH(s)$ is in general agreement with other solubility studies on
20 different pentavalent actinides.

21 These results show there is clearly a potential for oxidized, higher-valent actinides to form in
22 brine when no reducing agents are present. This, however, needs to be interpreted in the context
23 of the strong reducing agents and processes that will predominate in the WIPP, such as
24 bioreduction (Section SOTERM-2.4.1.2), iron reduction (Section SOTERM-2.3.4), and
25 reduction by organic complexants (Section SOTERM-2.3.6).  The WIPP-specific data show that
26 the presence of reduced iron (Fe(II/0)) leads to a rapid reduction of Pu(VI) to Pu(IV) species
27 under a wide range of anoxic conditions (Reed et al. 2006; Reed et al. 2009; Section SOTERM-
28 3.6). These results are expected to extend to the Am(V) system, since this species is more readily
29 reduced than Pu(V/VI). Reduced iron will also react with radiolytically generated oxidizing
30 species, such as hypochlorite or hypobromite, to prevent their buildup in the brine solution with
31 time. In summary, these WIPP-specific results show that the reductants present in WIPP waste
32 (reduced metals and organics) will overwhelm potential radiolytic effects under the expected
33 conditions in the WIPP, and a significant and sustained radiolytic enhancement of actinide
34 solubilities is not predicted.

# SOTERM-3.0 WIPP-Relevant Actinide Chemistry

The speciation of actinides under WIPP-relevant conditions defines the source term for actinide release from the WIPP in release scenarios where dissolved actinide concentrations are important (e.g., DBR and transport through the Salado or Culebra). The key factors that establish the concentrations of dissolved actinides under subsurface conditions are known. The most important of these factors for the WIPP repository are:

1. Actinide redox chemistry is a critical factor in establishing the concentration of actinides in brine. The solubility of reduced actinides (III and IV oxidation states) is significantly lower than oxidized forms (V and/or VI). In this context, the reduced-metal chemistry and microbial processes that establish and maintain reducing conditions in the WIPP are important.

2. The complexation of each actinide species is a critical factor in defining its solubility. For a given oxidation state, the inorganic and organic complexes present will define the solubility of the actinide. These complexants are in the preemplacement environment, are part of the TRU waste that is emplaced, or are produced as a result of subsurface processes, most notably microbial and corrosion processes.

3. Intrinsic and pseudoactinide colloid formation is a critical factor in defining the overall solution concentration of each actinide. The contribution of actinide colloids to the concentration of actinides in the WIPP is predicted to be significant. Many of the key TRU species in their expected oxidation states tend to form colloids or strongly associate with the non-actinide colloids present (e.g., microbial, humic and mineral).

The WIPP PA approach that was established in the initial WIPP license application (U.S. DOE 1996), and continued through the CRA-2014 PA calculations (Camphouse et al. 2013), accounts for all three of these key factors.

The PA concept of actinide speciation in the WIPP is well grounded in what has been observed for actinide contaminants in near-surface groundwater. In natural systems, the following inorganic ligands are potentially important complexants of radionuclides in solution: $CO_3^{2-}/HCO_3^-$, $OH^-$, $Cl^-$, $SO_4^{2-}/S^{2-}$, fluoride ($F^-$), and phosphate. Additionally, anthropogenic and bioderived chelating agents can strongly bind actinide species and will compete with the inorganic complexants present. Lastly, the tendencies of actinides to form intrinsic colloids and strongly associate or bind with colloidal particles are also well established. The relative importance of these complexants and processes depends on the pH, radionuclide oxidation state present, the presence of other metals, and the relative ligand concentrations. There are a number of general reviews on various aspects of actinide environmental chemistry (Allard 1982; Choppin, Liljenzin, and Rydberg 2004 [pp. 94–112]; Clark, Hobart, and Neu 1995; Banaszak, Rittmann, and Reed 1998; Runde 2000; Nitsche et al. 1992; Reed, Deo and Rittmann 2010; Runde and Neu 2010).

For the anoxic, reducing, and mildly basic brine systems expected in the WIPP, the most important inorganic complexants are expected to be carbonate/bicarbonate and hydroxide. There are also important organic complexants that coexist in TRU waste with the potential to strongly

1   influence actinide solubility. In this context, the relative importance of actinides and overall
2   oxidation state with respect to their potential release from the WIPP is:

3   **Actinides:** $\qquad$ Pu $\approx$ Am $\gg$ U $>$ Th $\gg$ Np $\approx$ Cm $\qquad$ (SOTERM.24)

4   **Actinide Oxidation State:** An(III) $>$ An(IV) $\gg$ An(VI) $\gg$ An(V) $\qquad$ (SOTERM.25)

5   In the CRA-2014 PA (Appendix PA-2014, Section 8.4), the contribution of Pu, Am, U, Th, Cm,
6   and Np is expressly considered, although only Pu and Am contribute significantly to TRU
7   release from the WIPP. The III oxidation state is the most important oxidation state based on
8   current WIPP PA assumptions that Am always exists in the III state, Pu exists in the III state in
9   ~50% of the vectors, and the III oxidation state is more soluble than the IV (see Section
10  SOTERM-4.0 and Tables SOTERM-20 and SOTERM-24).

11  In this section, an update of the literature and a summary of new WIPP-specific data is provided
12  (when available) for all the actinides that contribute in one way or another to PA. Section
13  SOTERM-3.1 gives a summary of changes since the CRA-2009 and CRA-2009 PABC; Section
14  SOTERM-3.2 gives an overview of the projected and current inventory of actinides in the WIPP;
15  Section SOTERM-3.3, Section SOTERM-3.4, Section SOTERM-3.5, Section SOTERM-3.6 and
16  SOTERM-3.7 contain an overview of the relevant environmental chemistry and WIPP-specific
17  results for Th, U, Np, Pu, and Am/Cm, respectively; Section SOTERM-3.8 pertains to the
18  complexation of actinides by organic chelating agents in the WIPP; and Section SOTERM-3.9
19  provides an overview of the potential for the formation of actinide colloids in the WIPP. An up-
20  front overview of the current assumptions and understanding of WIPP actinide chemistry is
21  given in Table SOTERM-8. The PA implementation of this actinide environmental chemistry is
22  discussed in Section SOTERM-4.0 and Section SOTERM-5.0.

## SOTERM-3.1 Changes in Actinide Chemistry Information since the CRA-2009 and the CRA-2009 PABC

25  Overall, there are few significant changes in the CRA-2014 general approach and assumptions
26  used to understand and predict actinide behavior in the WIPP from a PA perspective. The
27  following key assumptions are continued:

28  • Oxidation state distributions for the TRU actinides, and correspondingly, assumptions
29    regarding their solubility calculations using redox-invariant analogs, have not changed.

30  • The approach used to calculate solubilities for Pu and Am oxidation states, which are the
31    key actinides from the perspective of PA, have not changed. EQ3/6, rather than FMT,
32    however, is now being used to calculate these solubilities with the WIPP actinide
33    database.

34  • Inventory assumptions regarding the amounts of organic chelating agents and actinides in
35    TRU waste are being updated annually.

36  • The WIPP colloidal model that accounts for intrinsic, mineral fragment, microbial and
37    humic colloidal enhancements has not changed.

**Table SOTERM-8. Overview of the WIPP PA View/Role and Relevant Environmental Chemistry of the Key Actinide Species in the WIPP (References for Each Actinide are Provided in the Following Sections)**

| Actinide | WIPP PA View/Role | Environmental Chemistry |
|---|---|---|
| Thorium | Not a TRU component. Currently included in PA calculations, but not a significant contributor to actinide release. Used as an oxidation-state invariant analog for the IV actinides. Th data are used in EQ3/6 to calculate the solubility of Pu(IV), Np(IV), and U(IV). | Exists as $Th^{4+}$ complexes and is sparingly soluble under a wide range of environmental conditions. Th has a high tendency towards intrinsic colloid formation. |
| Uranium | Not a TRU component. Potentially useful as a VI analog for Pu(VI) species. Currently, U is conservatively assumed to be U(VI) in 50% of the PA vectors (set at a 1 mM solubility) and U(IV) in 50% of the PA vectors. It is not predicted to be a significant contributor to actinide release (based on Ci). | Exists as $UO_2^{2+}$ and $U^{4+}$ species that are strongly correlated with redox conditions. Can form highly insoluble U(VI) and U(IV) phases. Can persist up to mM concentrations in near-surface groundwater. |
| Neptunium | TRU component. Currently included in the PA calculations, but not a significant contributor to actinide release. Assumed to be IV in 50% of the PA vectors and V in 50% of the PA vectors. Expected to predominate in the IV oxidation state under the conditions expected in the WIPP. | Mobile and relatively soluble as the $NpO_2^+$ species under oxidizing conditions. Is fairly insoluble and immobile as $Np^{4+}$ under reducing conditions. |
| Plutonium | TRU component. Major contributor to actinide release calculations. Assumed to be IV in 50% of PA vectors and III in the other 50% of PA vectors. | Relatively immobile and insoluble as a subsurface contaminant. Persists as $Pu^{4+}$ except under biomediated, strongly reducing conditions where $Pu^{3+}$ species may be formed. If transported, this will likey be primarily through colloidal mechanisms. |
| Americium | TRU component. Major contributor to actinide release calculations. Exists in the III oxidation state in all vectors and its thermodynamic data are used by EQ3/6 for all III oxidation state calculations. Significant colloidal contribution due to strong association as a pseudocolloid. | Relatively immobile and insoluble as a subsurface contaminant. Persists as $Am^{3+}$ complexes under a wide range of environmental conditions. |
| Curium | Small quantities of $^{243}Cm$, $^{245}Cm$, and $^{248}Cm$ are present in the WIPP. $^{244}Cm$, although present, is not a TRU waste component due to its <20 year half-life. These are very minor contributors to actinide release. Chemistry is analogous to Am(III). | Not a very significant concern as a subsurface contaminant. Has the same chemistry as Am, so it will persist as a $Cm^{3+}$ species. |
| Organic Chelating Agents | The effects of EDTA, citrate, oxalate, and acetate on actinide solubility are considered in the WIPP PA. These are present in the WIPP waste and it is assumed that they are neither destroyed nor created by WIPP-relevant subsurface processes. | EDTA can persist under a wide range of environmental conditions and strongly chelates actinides. Citrate, oxalate, and acetate will likely be degraded due to microbial activity. |
| Actinide Colloids | Intrinsic and pseudocolloids with actinides are formed. These are accounted for in the WIPP PA and add to the conservatism of the actinide concentrations calculated. | Importance and role of An colloid-facilitated transport are the subject of much ongoing debate. The key issue within the WIPP is the potential contribution of colloids to the actinide source term and not their ability to facilitate actinide transport. |

1　There are new data, within and outside the WIPP project, that continue to support and/or expand
2　the robustness of the current PA assumptions. The most important of these are:

3　　• New WIPP-specific data that confirm the predominance of lower-valent plutonium in
4　　　long-term, iron-dominated brine systems.

5　　• The solubility of An(IV) in simulated WIPP brines over a wide range of conditions was
6　　　experimentally determined using Th(IV) as an analog for Pu(IV). These data support
7　　　current PA solubilities for the IV actinides.

8　　• The effect of the complexation of organic chelating agents on actinide (III/IV) oxidation
9　　　states was experimentally determined. Relatively strong complexation effects are noted
10　　with An(III) that is consistent with current WIPP modeling.

11　　• The solubility of U(VI) as a function of carbonate was determined and shown to be well
12　　　below the current EPA-set limit of 1 mM.

13　　• The colloidal enhancement parameters were re-evaluated and new parameter
14　　　recommendations were made. Experiments specific to intrinsic, microbial, and to a lesser
15　　　extent mineral fragment colloids are reported. These data, although incomplete, provide
16　　　stronger supporting data for the current WIPP colloid model. The specific changes are
17　　　described in more detail in Section SOTERM-3.9.

18　　• A variable brine volume approach was implemented in PA to calculate actinide
19　　　solubility. This extends the minimum brine volume approach used in CRA-2009.

## 20　SOTERM-3.2 Actinide Inventory in the WIPP

21　The actinide inventory for the WIPP, based on the Performance Assessment Inventory Report –
22　2012 (Van Soest 2012), is given in Table SOTERM-9. This is the inventory used in CRA-2014.
23　Also included in this table is the calculated inventory-limited solubility of the various actinides
24　and radionuclides considered by the WIPP PA.

25　Over long time frames, only Pu and Am are expected to make a significant contribution to
26　releases from the WIPP (see time profile in Table SOTERM-10), although the relative
27　contribution of Am decreases significantly after 1000 years due to its half-life. Curium (Cm),
28　which is predominantly present as $^{244}$Cm, is well below the calculated solubility for III actinides
29　when fully dissolved and, with its very short half-life (18.11 years), will not be important beyond
30　the 100-year period of institutional control. Although some cesium (Cs) and strontium (Sr) is
31　initially present in the WIPP, these fission products can only contribute significantly to the
32　overall release from the WIPP for the first 100 years of repository history and are not significant
33　beyond the period of institutional control.

**Table SOTERM-9. WIPP Radionuclide Inventory (Van Soest 2012) Decay-Corrected to 2033. This Inventory was used in the CRA-2014 PA Calculations.**

| Selected Radionuclides | Activity (Ci) | Amount (kg) | Element-Specific Inventory (all reported isotopes) | Inventory-Defined Solubility Limit[a] (M) |
|---|---|---|---|---|
| **Actinides** | | | | |
| $^{229}$Th | 1.40 | $6.57\times10^{-3}$ | 7.04 Ci $1.35\times10^{4}$ Kg | >> Solubility |
| $^{230}$Th | 4.14 | 0.2 | | |
| $^{232}$Th | 1.50 | $1.35\times10^{4}$ | | |
| $^{233}$U | 139 | 14.2 | 528 Ci $2.26\times10^{5}$ Kg | >> Solubility |
| $^{234}$U | 242 | 38.3 | | |
| $^{235}$U | 76.4 | $3.49\times10^{4}$ | | |
| $^{236}$U | 5.44 | 83.2 | | |
| $^{238}$U | 64.8 | $1.91\times10^{5}$ | | |
| $^{237}$Np | 23.2 | 32.5 | 23.2 Ci 32.5 Kg | $8\times10^{-6}$ M ($\geq$ projected solubility) |
| $^{238}$Pu | $6.01\times10^{5}$ | 34.7 | $2.02\times10^{6}$ Ci $1.20\times10^{4}$ Kg | >> Solubility |
| $^{239}$Pu | $5.74\times10^{5}$ | $9.13\times10^{3}$ | | |
| $^{240}$Pu | $1.75\times10^{5}$ | 762 | | |
| $^{241}$Pu | $6.63\times10^{5}$ | 6.38 | | |
| $^{242}$Pu | $8.09\times10^{3}$ | $2.04\times10^{3}$ | | |
| $^{244}$Pu | 0.0101 | 0.567 | | |
| $^{241}$Am | $7.05\times10^{5}$ | 203 | $7.05\times10^{5}$ Ci 203 Kg | $5\times10^{-5}$ M ($\geq$ projected solubility) |
| $^{243}$Am | 51.2 | 0.254 | | |
| $^{244}$Cm | $9.97\times10^{3}$ | 0.122 | $9.97\times10^{3}$ Ci 0.122 Kg | ~ $3\times10^{-8}$ M |
| **Fission Products[b]** | | | | |
| $^{137}$Cs | $2.35\times10^{5}$ | 2.67 | $2.35\times10^{5}$ Ci 2.67 Kg | $1\times10^{-6}$ M |
| $^{90}$Sr | $2.09\times10^{5}$ | 1.51 | $2.09\times10^{5}$ Ci 1.51 Kg | $1\times10^{-6}$ M |

a Moles in the inventory divided by the minimum brine volume (17,400 m³)
b Fission products are not TRU, but are considered in the PA to calculate overall release

1    **Table SOTERM-10.  Time-dependence of Radionuclide Inventory (Van Soest 2012)**

| Element | 2033 (0 years) Ci (Kg) | 2133 (100 years) Ci (Kg) | 3033 (1000 years) Ci (Kg) | 12033 (10,000 years) Ci (Kg) |
|---|---|---|---|---|
| Th | 7.04 ($1.35 \times 10^4$) | 8.52 ($1.35 \times 10^4$) | 22.5 ($1.35 \times 10^4$) | 127 ($1.35 \times 10^4$) |
| U | 528 ($2.26 \times 10^5$) | 645 ($2.26 \times 10^5$) | 746 ($2.26 \times 10^5$) | 769 ($2.28 \times 10^5$) |
| Np | 23.2 (32.5) | 44.8 (62.9) | 140 (197) | 170 (238) |
| Pu | $2.02 \times 10^6$ ($1.20 \times 10^4$) | $1.03 \times 10^6$ ($1.19 \times 10^4$) | $7.24 \times 10^5$ (1.16E4) | $5.00 \times 10^5$ ($9.12 \times 10^3$) |
| Am | $7.05 \times 10^5$ (203) | $6.20 \times 10^5$ (179) | $1.47 \times 10^5$ (42.4) | 21.1 (0.0994) |
| Cm | $9.97 \times 10^3$ (0.122) | 216 ($2.65 \times 10^{-3}$) | $2.32 \times 10^{-13}$ ($2.84 \times 10^{-18}$) | 0.00 (0.00) |
| Cs | $2.35 \times 10^5$ (2.67) | $2.33 \times 10^4$ (0.265) | $2.17 \times 10^{-5}$ ($2.46 \times 10^{-10}$) | 0.00 (0.00) |
| Sr | $2.09 \times 10^5$ (1.51) | $1.78 \times 10^4$ (0.129) | $4.21 \times 10^{-6}$ ($3.05 \times 10^{-11}$) | 0.00 (0.00) |

2

3    # SOTERM-3.3 Thorium Chemistry

4    Th is not a TRU component, although an estimated 13.5 metric tons of Th will be in the WIPP.
5    The release of Th as the [230]Th isotope was calculated in the CRA-2014 PA and does not
6    significantly contribute to the overall release of activity from the WIPP.  Th is, however,
7    important for the WIPP in that it is used as a redox-invariant analog for the IV actinides (Pu(IV),
8    Np(IV), and U(IV)), and Th complexation data are used in the EQ3/6 code for the An(IV)
9    solubility calculations (Section SOTERM-4.1).

10    **SOTERM-3.3.1 Thorium Environmental Chemistry**

11    Th, under a wide range of conditions, has one stable oxidation state in aqueous solutions: the
12    $Th^{4+}$ tetravalent ion.  For this reason, the environmental chemistry of Th is understood from the
13    perspective of the solubility and complexation of this species, which is also the species expected
14    to be present in the WIPP environment when DBR and transport release scenarios are important.

15    Other oxidation states for Th in aqueous systems have been reported.  Klapötke and Schulz
16    (Klapötke and Schulz 1997) suggested a $Th^{3+}$ species as a somewhat stable species in slightly
17    acidic solution but this is not correct; it has been discounted because the proposed reaction for
18    the species' formation is shown to be thermodynamically impossible, and the azido-chloro $Th^{4+}$
19    complex was incorrectly assigned to the $Th^{3+}$ species (Ionova, Madic, and Guillaumont 1998).

1   The hydrolysis of $Th^{4+}$, as is true for all An(IV) species in the WIPP, is complex and a critically
2   important interaction in defining the overall solubility of Th.  This was recently investigated by
3   Ekberg et al. (Ekberg et al. 2000), Rai et al. (Rai et al. 2000), Moulin et al. (Moulin et al. 2001),
4   and Okamoto, Mochizuki, and Tsushim (Okamoto, Mochizuki, and Tsushim 2003), and was
5   critically reviewed by Neck and Kim (Neck and Kim 2001) and Moriyama et al. (Moriyama et
6   al. 2005). The authors have proposed a comprehensive set of thermodynamic constants that
7   extends to all tetravalent actinides.  The solubility products were determined for amorphous (am)
8   $Th(OH)_4$ (Neck et al. 2002; Altmaier et al. 2005 and Altmaier et al. 2006) and for crystalline
9   $ThO_2$ (Neck et al. 2003), as well as for specific ion interaction theory parameters (Neck,
10  Altmaier, and Fanghänel 2006).  The thermodynamic stability constants are listed in Table
11  SOTERM-11.

12  **Table SOTERM-11.  Thermodynamic Stability Constants for Key Th Hydrolytic Species**

| Hydrolytic Reaction/Species | Stability Constant |
|---|---|
| **Mononuclear Species** | |
| $Th(OH)_{4,\,am} \leftrightarrows Th^{4+} + 4OH^-$ <br> $Th(OH)_{4,\,cr} \leftrightarrows Th^{4+} + 4OH^-$ <br> $Th^{4+} + OH^- \leftrightarrows Th(OH)^{3+}$ <br> $Th^{4+} + 2OH^- \leftrightarrows Th(OH)_2^{2+}$ <br> $Th^{4+} + 3OH^- \leftrightarrows Th(OH)_3^{+}$ <br> $Th^{4+} + 4OH^- \leftrightarrows Th(OH)_{4,aq}$ | $\log K_{s,am} = -47.8 \pm 0.3$ <br> $\log K_{s,cr} = -53.2 \pm 0.4$ <br> $\log \beta^0_1 = 11.8 \pm 0.2$ <br> $\log \beta^0_2 = 22.0 \pm 0.6$ <br> $\log \beta^0_3 = 31 \pm 1$ <br> $\log \beta^0_4 = 38.5 \pm 1$ |
| **Polynuclear Species** | |
| $4Th^{4+} + 12OH^- \leftrightarrows Th_4(OH)_{12}^{4+}$ <br> $6Th^{4+} + 15OH^- \leftrightarrows Th_6(OH)_{15}^{9+}$ | $\log \beta^0_{4,12} = 141$ <br> $\log \beta^0_{6,15} = 176$ |

13

14  Discrepancies in the $ThO_2$(cr) solubility were recently studied (Vandenborre et al. 2010) and
15  assigned to the different forms of material present:  bulk $ThO_2$(cr) grains (80%) and
16  $ThO_x(OH)_y(H_2O)_z$(s) grain boundaries (20%). The hydrated material may originate from the
17  initial grain-boundary oxide materials, which are more sensitive to humidity than the bulk
18  materials. The solubilities of these two phases are quite different and together with the "local
19  solubility" (the most active sites) were used to explain the discrepancies noted.

20  The presence of carbonate in solution greatly increases the solubility of thorium dioxide ($ThO_2$).
21  An increase by one order of magnitude of the carbonate concentration in the range of $0.1 - 2$ M
22  leads to a five-order-of-magnitude increase in the Th(IV) solubility due to the formation of
23  mono- and penta-carbonate complexes.  Östhols, Bruno, and Grenthe (Östhols, Bruno, and
24  Grenthe 1994) proposed the following equilibrium reactions and the corresponding stability
25  constants:

26      $ThO_2 + H^+ + H_2O + CO_3^{2-} \leftrightarrows Th(OH)_3\,CO_3^-$      $\log K_{131} = 6.11 \pm 0.19$    (SOTERM.26)

27      $ThO_2 + 4H^+ + 5\,CO_3^{2-} \leftrightarrows Th(CO_3)_5^{6-} + 2H_2O$      $\log K_{105} = 42.12 \pm 0.32$   (SOTERM.27)

1   This speciation scheme, however, was criticized in recent work (Altmaier et al. 2005) because it
2   overpredicts the dependency of Th solubility on carbonate and underpredicts the effect of
3   hydrolysis at higher pH.  That hydrolysis prevails at pH >10 is supported by detailed
4   experimental results (Figure SOTERM-6).  These data are explained by the predominance in this
5   system of $Th(OH)(CO_3)_4^{5-}$ complex rather than $Th(CO_3)_5^{6-}$.  A greater role for other ternary
6   complexes of thorium (e.g., $Th(OH)_2(CO_3)_2^{2-}$), which are also likely to be present in the WIPP
7   conditions, is also proposed, and formation constants for these complexation reactions are
8   reported.  The use of the pentacarbonyl complex for the IV actinides in the WIPP PA, for these
9   reasons, is a conservative assumption that overpredicts the solubility of the IV oxidation state at
10  pH > 10.  A correction in the FMT database, now in the EQ3/6 database, to the value of the
11  $Th(OH)_4$(aqueous [aq]) to be consistent with Neck et al. (Neck et al. 2002) was incorporated into
12  the CRA-2004 PABC and there are no new changes in this speciation scheme in CRA-2014.

13  The dissolution of crystalline $ThO_2$ in low ionic strength media and the effect of carbonate and
14  calcium concentration on the solubility of thorium were investigated at alkaline pH (Kim et al.
15  2010). The observed thorium concentration in the groundwater was greater than predicted.   This
16  discrepancy was explained by the authors as the result of colloid formation.  Carbonate affected
17  the observed thorium solubility as expected.  There was no calcium enhancement of the thorium
18  solubility until a calcium concentration of 1.25 mM.

19  Oxyanions such as phosphate and, to a lesser extent, sulfate, also form $Th^{4+}$ complexes that can
20  precipitate at pH <5.  The effect of phosphate on solubility of microcrystalline $ThO_2$ is very
21  limited. The stability constants for $Th^{4+}/H_2PO_4^-$ and $Th^{4+}/HPO_4^{2-}$ were reported (Langmuir and
22  Herman 1980).  Overall, the role of these oxyanions is expected to be unimportant for the mildly
23  basic brines (pH ~8-10) present in the WIPP.

24  A new perturbation to the understanding of Th speciation, as well as other actinides in the IV
25  oxidation state, is the recent observation that Ca, and to a lesser extent, magnesium (Mg),
26  enhances Th solubility at pH >10 when carbonate is present (see Figure SOTERM-7).  In recent
27  publications, the formation of $Ca_4[Th(OH)_8]^{4+}$ and $Ca_4[Pu(OH)_8]^{4+}$ ion pairs in alkaline $CaCl_2$
28  solution is reported (Brendebach et al. 2007; Altmaier, Neck, and Fanghänel 2008).  These
29  species cause a rapid increase in the solubility of all tetravalent actinides at pH greater than 11.
30  This increased solubility is only observed at $CaCl_2$ concentrations above 0.5 M for Th(IV), and
31  correspondingly above 2 M for Pu(IV) species.  This effect can be discounted for the WIPP PA
32  because Ca concentrations in the WIPP are predicted to be approximately 14 mM or less with a
33  pH of approximately 8.7.  These are both well below the levels needed to see a significant effect
34  for both Th and Pu.

35  Actinides in the IV oxidation state, because of the complexity of their solution chemistry and
36  very high tendency towards hydrolysis, form colloidal species in groundwater.  The potential
37  effect of colloid formation on solubility of Th(IV) in concentrated NaCl and $MgCl_2$ solution was
38  recently published by Altmaier, Neck, and Fanghänel (Altmaier, Neck, and Fanghänel 2004) and
39  is shown in Figure SOTERM-8.  In neutral-to-alkaline solutions, colloids could be formed as Th
40  oxyhydroxide with log $[Th]_{(colloid\ [coll])} = -6.3 \pm 0.5$, independent of ionic strength.  In Mg
41  solutions, the formation of pseudocolloids (i.e., Th(IV)) sorbed onto $Mg_2(OH)_3Cl \cdot 4H_2O$(coll) led
42  to an apparent increase of the total Th concentration up to $10^{-5}$ M (Walther 2003; Degueldre and

1 Kline 2007; Bundschuh et al. 2000). For these reasons, colloid formation is addressed in the
2 WIPP PA.
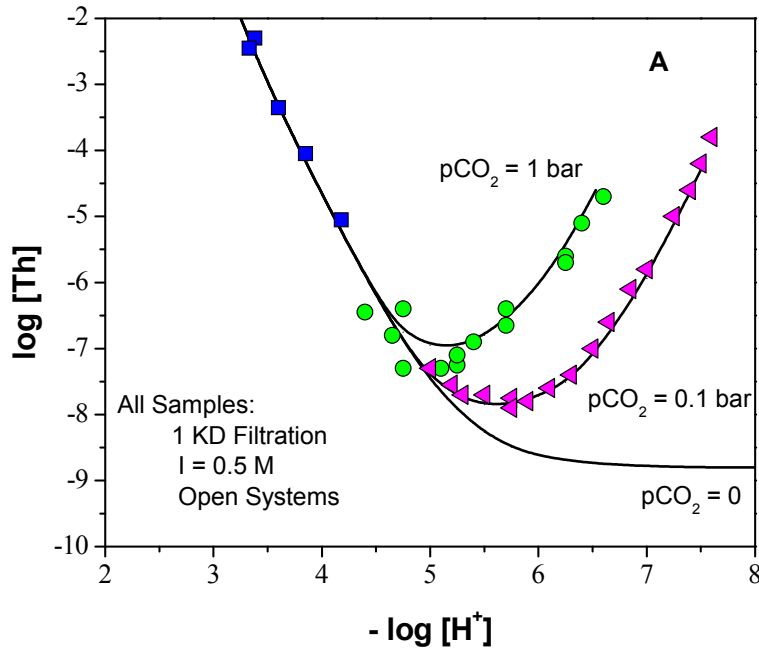
3
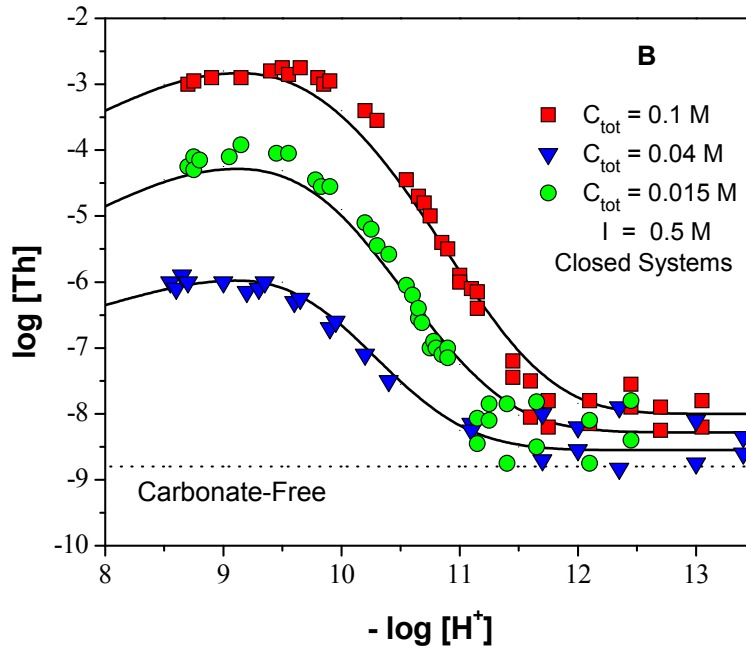


4

5 **Figure SOTERM-6. Solubility of Amorphous Th(IV) Oxyhydroxide as a Function of**
6 **Carbonate Concentration in 0.5 M for (A) pH = 2–8 and (B) pH**
7 **= 8–13.5. The solid lines are the calculated solubilities (based on**
8 **data in Altmaier et al. 2005).**
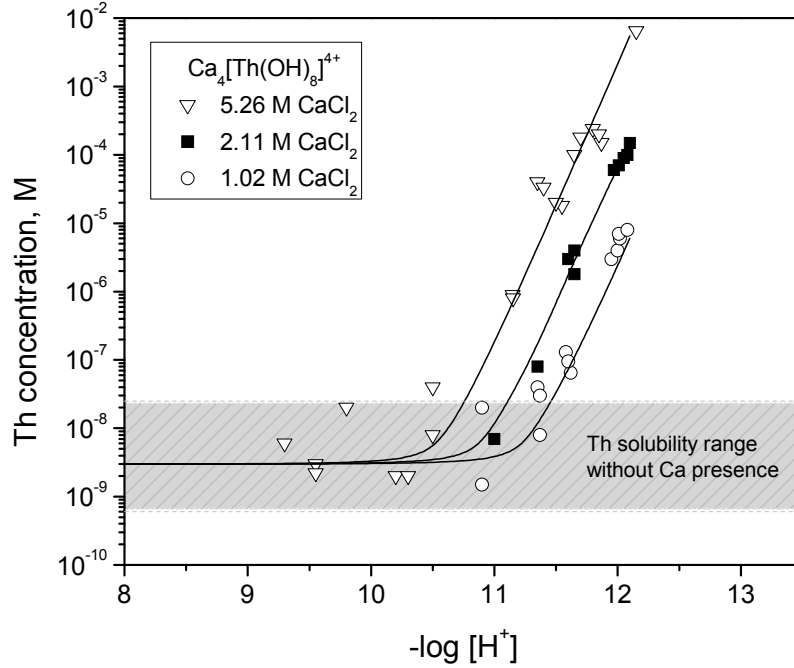
1
2    **Figure SOTERM-7.  Effect of Calcium-carbonate Ternary Complexes on the Solubility**
3    **of Th(IV) in Brine (Altmaier 2011).**
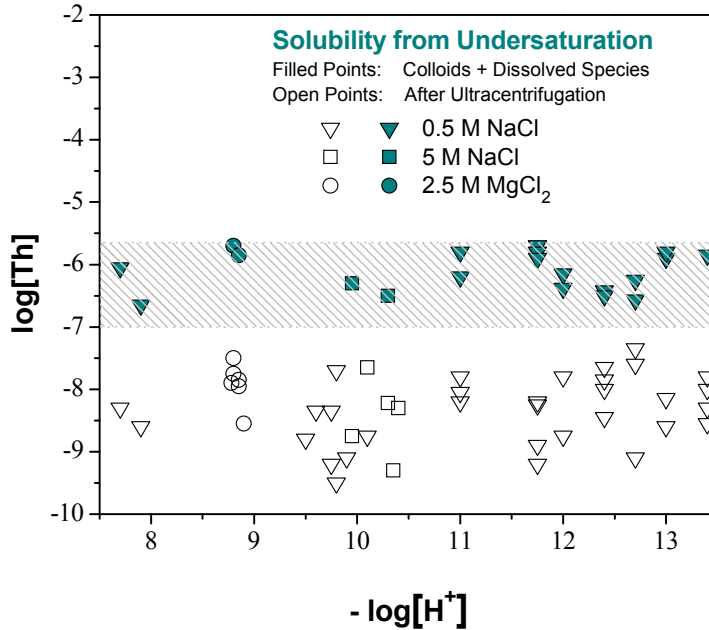


4
5    **Figure SOTERM-8.  Solubility of Th(OH)₄(am) Determined from Undersaturation in**
6    **0.5 NaCl, 5.0 M NaCl, and 2.5 M MgCl₂. Filled Points: Total Th**
7    **Concentrations (Including Colloids); Open Points: Th**
8    **Concentrations Measured after Ultracentrifugation at 90,000**
9    **Revolutions Per Minute ($5 \times 10^5$ g) (based on data in Altmaier,**
10   **Neck, and Fanghänel 2004).**

1    **SOTERM-3.3.2 WIPP-Specific Results since the CRA-2009 and the CRA-2009 PABC**

2    A study to establish the solubility of thorium under WIPP-specific conditions was completed
3    since CRA-2009.  These experiments were performed in carbonate-free and carbonate-
4    containing WIPP simulated brine to establish the effects of carbonate, $pC_{H+}$ and time on thorium
5    (IV) solubility and are published in a report entitled "Solubility of An(IV) in WIPP Brine,
6    Thorium Analog Studies in WIPP Simulated Brine" (Borkowski et al. 2012).

7    The results obtained are shown in Figure SOTERM-9.  After 2 years of equilibration in
8    carbonate-free brine, the measured solubility of thorium was $6\text{-}7\times10^{-7}$ M and was essentially
9    independent of pH and brine composition over the 6.5 to 11.5 $pC_{H+}$ range investigated.
10   Sequential filtration to ~ 10 nm pore size had little effect on the measured concentration.
11   Subsequent ultracentrifugation up to 1,000,000 g resulted in up to a 40% colloidal fraction (but
12   typically 20% or less), indicating that there was much less intrinsic colloid formation than
13   reported in Altmaier, Neck and Fanghänel (2004) - see Figure SOTERM-8.  The steady-state
14   thorium concentrations measured, however, are consistent with literature reports for simplified
15   brine systems (Altmaier, Neck and Fanghänel 2004) but show a significantly lower extent of
16   aggregation to form intrinsic colloids.
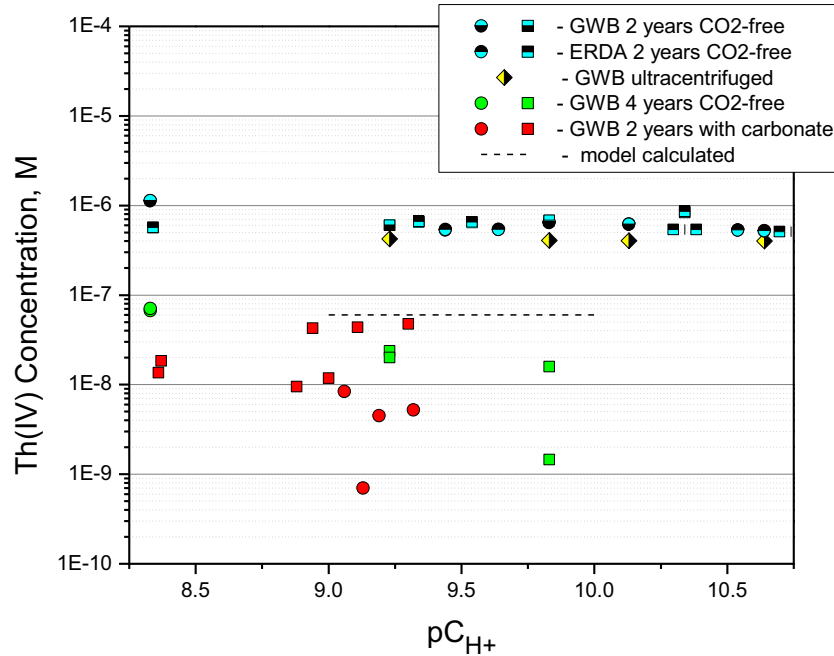
1
2       **Figure SOTERM-9.  The Concentration of Thorium Measured in WIPP Simulated**
3                               **Brine (GWB and ERDA-6) as a Function of Time, Filtration and**
4                               **the Presence of Carbonate.  Square symbols represent an**
5                               **undersaturation approach, whereas the circles represent the**
6                               **oversaturation approach.  Although high, but metastable,**
7                               **concentrations were initially present, in time the measured**
8                               **concentrations decreased and are at or below the WIPP model-**
9                               **predicted values (Borkowski et al. 2012).**

10      After an additional 2 years of equilibration, the thorium concentration in carbonate-free GWB
11      significantly decreased (green points in the figure).  For $pC_{H+}$ in the range of 7.5 to 8.3 (not all
12      data shown in Figure SOTERM-9), some samples did not show a change in the thorium
13      concentration, but others showed a decrease of over one order of magnitude and were similar to
14      the thorium concentrations measured in GWB containing $10^{-2}$ and $10^{-3}$ M carbonate.

15      The presence of carbonate, at a concentration that is ten-fold greater than expected in the WIPP,
16      had little/no effect on the measured thorium concentrations.  After two years of equilibration, the
17      thorium concentrations measured from under- and oversaturation in GWB did not depend on
18      carbonate concentration. Concentrations measured from oversaturation were 2.5 orders of
19      magnitude greater than those measured from undersaturation, indicating that metastable states
20      can persist for long periods of time. The trend in the oversaturation data (see Figure SOTERM-9)
21      is consistant with the literature data (Altmaier et al. 2005). In the undersaturation experiments,
22      which are more relevant to the WIPP situation, the average thorium concentration was $2 \times 10^{-8}$ M
23      and continued to decrease at $pC_{H+} > 9$. The oversaturation experiments showed a similar trend
24      and at $pC_{H+} > 9$ the thorium concentrations decreased to below $10^{-8}$ M. These results reproduce,
25      to some extent, the trends reported in the literature (Altmaier et al. 2005), but the much higher

1   ionic strength solutions used in our experiments shift our pH profile to a lower $pC_{H+}$ value by
2   approximately 1 pH unit.

3   At the expected WIPP repository $pC_{H+}$(~ 9.5), in the presence of carbonate, the thorium
4   concentrations in GWB brine were $2 \times 10^{-8}$ M or lower. This concentration trend suggests that at
5   repository conditions the mixed thorium hydroxy-carbonato complexes do not play any role in
6   the thorium solubility at $pC_{H+} > 9$.

7   The sequential filtration of thorium in the carbonate system (see Figure SOTERM-10) led to a
8   dissolved thorium concentration of $2\text{-}6 \times 10^{-8}$ M in GWB. In ERDA-6 brine, however, the
9   dissolved thorium concentration was about ten-fold greater and it is apparent that steady state
10  thorium concentration was not achieved. The colloidal thorium species appear to be very small,
11  less than 10 kDa (~5 nm). Overall, the truly dissolved thorium concentration was $3(\pm 2) \times 10^{-8}$ M.
12  The average total thorium concentration consisted of a dissolved fraction of 30 - 60% and a
13  colloidal fraction of 40 - 70%.

14  The WIPP-specific thorium solubility results just summarized support the ongoing WIPP
15  recertification effort in three important ways:  1) they provide empirical solubilities over a broad
16  range of conditions that improve the robustness of the WIPP PA model, 2) they resolve and
17  address published literature data in simplified brine systems that appeared to disagree with the
18  current WIPP PA approach, and 3) they provide an input that will help establish the intrinsic
19  colloidal enhancement factors for IV actinides.  There is general agreement between our data and
20  results reported in the literature for simplified brine systems, although we are seeing a far lower
21  colloidal fraction in the total concentrations measured.  After 4 years of equilibration, our
22  measured solubilities are slightly lower (by a factor of ~ 2) than the solubilities calculated in the
23  WIPP PA – this is well within the order of magnitude uncertainty typically observed between the
24  calculated and measured solubilities in complex brine systems.

25  A key motivation in the WIPP thorium solubility and speciation studies was to explain the
26  reports in the literature that very high colloidal fractions are present in high ionic-strength brine
27  systems (mainly Altmaier et al. 2004).  The WIPP-specific data show that there are colloids
28  present in these systems, but these are much less than what was reported.  The explanation for
29  this is a combination of the differences in brine composition (sodium chloride brine vs.
30  GWB/ERDA-6) between the two studies and the presence of MgO colloids in the Altmaier study
31  where mineral fragment colloids were likely formed (which is counted as part of their colloidal
32  fraction).  Perhaps a more important result in the WIPP-specific studies is the observation that
33  there is an equilibration between the intrinsic colloidal fraction and the dissolved species.  This
34  equilibrium shifts to a lower overall solubility with time that is now consistent with WIPP
35  modeling predictions.  This long-term shift defines these higher initial and essentially pH
36  independent values for thorium solubility (Figure SOTERM-9 and SOTERM-8) that were
37  obtained in both the German and WIPP data as metastable concentrations of thorium and
38  explains the apparent discrepancy between model-predictions and experimental results.  These
39  solubility data support the current WIPP PA assumptions on An(IV) solubility and extend
40  past project data to a broader range of pH and carbonate levels.  These results also note that Ca-
41  enhanced hydroxyl complexation can greatly increase the solubility of actinides (IV), something
42  that has only been understood in the last couple of years; however, this complexation requires
43  relatively high pH in combination with very high Ca levels, something that is not expected in the

1 WIPP. The expected pH and dissolved Ca levels in the WIPP predict no effect on An(IV)
2 dissolved concentration due to formation of this complex.
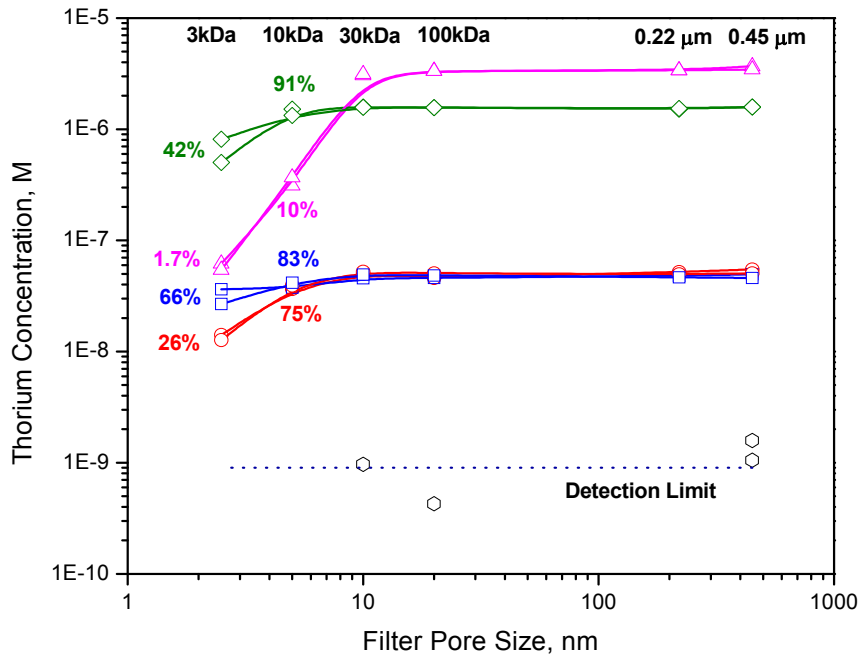
3



4 **Figure SOTERM-10. Thorium Concentration in Simulated WIPP Brine as a Function**
5 **of Pore Size. Ultrafilters used are given at the top of the figure**
6 **and correlate with the filter pore size on the x axis. The %**
7 **numbers shown correspond to the % of thorium that passed**
8 **through the filter for each data point.**

## SOTERM-3.4 Uranium Chemistry

10 Uranium is not a TRU component but is, by mass, the predominant actinide in the WIPP.
11 Current estimates predict that ~226 metric tons will be placed in the repository (Van Soest 2012),
12 but this is believed to be a high estimate since uranium content in waste is often indirectly
13 determined. By mass, approximately 85% of this will be the $^{238}$U isotope, with minor amounts
14 of $^{233}$U, $^{234}$U, $^{235}$U, and $^{236}$U. Uranium does not contribute significantly to actinide release
15 through cuttings/cavings and spallings because of its low specific activity ($1.22 \times 10^{4}$Bq.g$^{-1}$).
16 Uranium release can occur through the Culebra in very small amounts because of its potentially
17 high solubility and low partition coefficient ($K_d$) in the VI oxidation state.

18 Uranium release, as the $^{234}$U isotope, was calculated in the CRA-2014 PA. In the WIPP PA, the
19 oxidation state distribution assumption is that U speciates as U(IV) in the reduced PA vectors
20 and as U(VI) in the oxidized vectors (Section SOTERM-4.1). The concentration for U(VI) is
21 currently set at 1 mM (U.S. EPA 2005), since there is no An(VI) model in the WIPP. U(IV)
22 solubility is calculated using the Th(IV) speciation data in the WIPP model.

1  **SOTERM-3.4.1 Uranium Environmental Chemistry**

2  Uranium is by far the most studied of the actinides under environmentally relevant conditions.
3  An extensive review of this chemistry, as it relates to the WIPP case, was completed in 2009
4  (Lucchini et al 2010a; U.S DOE 2009), and is updated herein. More general reviews can be
5  found (Morss, Edelstein, and Fuger 2006; Guillaumont et al. 2003; Runde and Neu 2010). An
6  overview of U environmental chemistry is presented in this section.

7  **SOTERM-3.4.1.1 Uranium Subsurface Redox Chemistry**

8  Uranium can theoretically exist in aqueous solution in the III, IV, V, and VI oxidation states
9  (Hobart 1990; Keller 1971 [pp. 195–215]; Clark, Hobart and Neu 1995). In the environment,
10  however, only the IV and VI oxidation states, which exist as $U^{4+}$ and $UO_2^{2+}$ species, are present.
11  $U^{3+}$, should it be formed, is metastable and readily oxidized in aqueous solution, and U(V) only
12  exists as a very short-lived transient that instantaneously disproportionates to form U(IV) and
13  U(VI) species. The corresponding reduction potential diagram for U at pH = 0, 8, and 14 is
14  given in Figure SOTERM-11 (Morss, Edelstein, and Fuger 2006).

*pH*
0:  *+0.063 V*                    *+0.613 V*                    *-0.607 V*

U(VI) ⟶ U(V) ⟶ U(IV) ⟶ U(III)

8:  *-0.23 ± 0.05*          *+0.08 ± 0.12*          *-1.95 ± 0.17*
14: *-0.69 ± 0.24*          *-0.03 ± 0.24*          *-2.78 ± 0.35*

*+0.338 V*

*-0.07 ± 0.24*
*-0.36 ± 0.12*
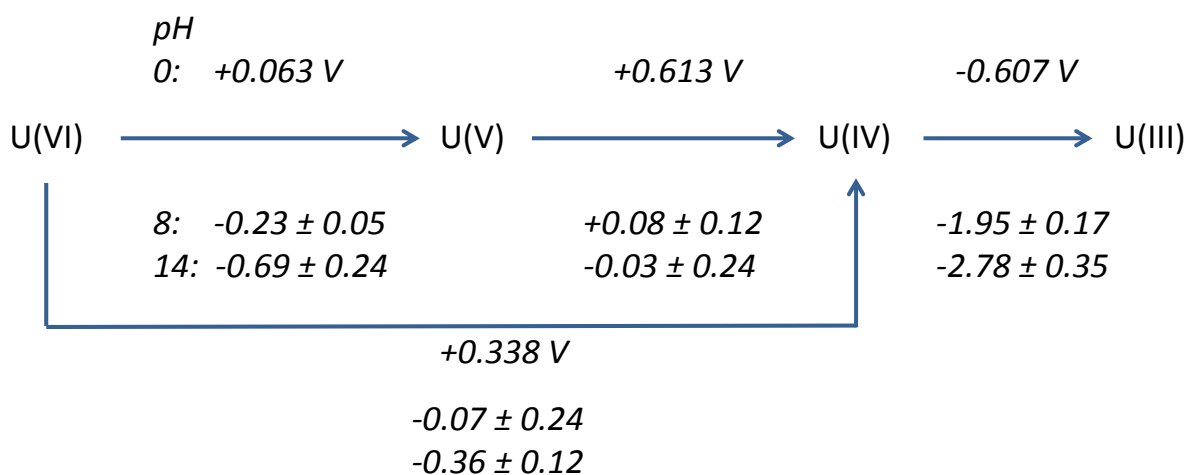
15

16  **Figure SOTERM-11. Reduction Potential Diagram for U at pH = 0, 8, and 14 (Based**
17  **on Data in Morss, Edelstein, and Fuger 2006). For the expected**
18  **reducing and mildly basic pH conditions in the WIPP, U(IV) is**
19  **predicted to be the predominant oxidation state.**

20  Under oxidizing subsurface conditions typical of most near-surface groundwater, U(VI) as $UO_2^{2+}$
21  uranyl complexes is the predominant oxidation state and is not easily reduced geochemically.
22  Thermodynamically, uranyl species are stable even under mildly reducing conditions and are not
23  reduced by some Fe(II) phases (see Table SOTERM-5). In anoxic WIPP brine experiments with
24  a hydrogen overpressure, uranyl persists as a stable hydrolytic or carbonate complex for over two
25  years (Reed and Wygmans 1997).

26  In the anoxic and strongly reducing environment expected in the WIPP, however, potential
27  reduction pathways exist. The two most important of these reduction pathways are reaction of
28  uranyl with reduced iron phases (Fe[0/II]), and bioreduction by anaerobic microorganisms (e.g.,

1   metal and sulfate reducers).  For these reasons, U(IV) is the oxidation state expected to
2   predominate in the WIPP when brine inundation occurs.

3   The use of iron barriers in the removal of uranyl from groundwater is well established and has
4   been reported for the removal of U(VI) from groundwater using zero-valent iron barriers (Gu et
5   al. 1998; Fiedor et al. 1998; Farrell et al. 1999) and iron corrosion products formed in saline
6   solution (Grambow et al. 1996).  However, in those studies, it was unclear whether the removal
7   of uranyl ($UO_2^{2+}$) resulted from reductive precipitation or from adsorption onto/incorporation
8   into the iron corrosion products (Gu et al. 1998).  In their experiments under saline conditions,
9   Grambow et al. (Grambow et al. 1996) found that a large percentage of U was rapidly adsorbed
10  onto the iron corrosion products consisting of over 97% hydrous Fe(II) oxide, and very little
11  U(IV) was found. Recently, Myllykylä and Ollila (Myllykylä and Ollila 2011) observed the
12  presence of U(IV) after adding an excess of Fe(II) to 0.01M NaCl and 0.002M $NaHCO_3$
13  solutions containing U(VI) inside an anaerobic glovebox.

14  Under anoxic conditions, Trolard et al. (Trolard et al. 1997) established that the corrosion of steel
15  and iron generates Fe(II)/Fe(III) hydroxide species known as green rusts.  Green rusts contain a
16  certain amount of nonhydroxyl anions (carbonate, halides, or sulfate); they have a high specific
17  surface area (Cui and Spahiu 2002) and a high cation sequestration capacity (O'Loughlin et al.
18  2003). They are considered metastable oxidation products of Fe(II) to magnetite $Fe_3O_4$ and
19  Fe(III) oxyhydroxides (e.g., goethite α-FeOOH) (O'Loughlin et al. 2003).  They could be
20  generated by iron corrosion in the WIPP brines (Wang et al. 2001). A few experimental studies
21  demonstrate that U(VI) is reduced to U(IV) by green rusts (Dodge et al. 2002; O'Loughlin et al.
22  2003).

23  Recent studies suggest that magnetite stoichiometry can significantly influence the extent of
24  U(VI) reduction (Latta et al. 2012). Latta et al. (Latta et al. 2012) demonstrated that
25  stoichiometric and partially oxidized magnetite ($Fe^{2+}/Fe^{3+} \geq 0.38$) reduce U(VI) to U(IV) in $UO_2$
26  nanoparticles in 2mM $NaHCO_3$ solution at pH 7.2, whereas with more oxidized magnetite
27  ($Fe^{2+}/Fe^{3+} < 0.38$), possibly sorbed U(VI) is the dominant phase observed. Atomistic simulations
28  conducted by Kerisit, Felmy and Ilton (Kerisit, Felmy and Ilton 2011), supported by existing
29  Extended X-Ray Absorption Fine Structure (EXAFS) data provide strong evidence for the
30  structural incorporation of U in Fe (hydro)oxides.  The complexity of the U-Fe-$H_2O$-$CO_2$ system
31  can explain the lack of a predominant mechanism (reduction-precipitation or
32  adsorption/incorporation) for the removal of U(VI) in the presence of iron phases (Du et al.
33  2011; Ilton et al. 2012; Singer et al. 2012a; Singer et al. 2012b).

34  Banaszak, Rittmann, and Reed (Banaszak, Rittmann, and Reed 1998) have reviewed the
35  important role of microbial processes in the reduction of multivalent metals under
36  anaerobic/reducing conditions. For uranyl in particular, several studies exist that show that U(VI)
37  is reduced to U(IV) species under a wide range of conditions (Lovley et al. 1991; Lovley et al.
38  1993; Barton et al. 1996; Huang et al. 1998; Abdelouas et al. 2000; Bender et al. 2000;
39  Fredrickson et al. 2000; Suzuki et al. 2003).  Most of this work pertains to groundwater bacteria,
40  and is not directly applicable to the WIPP.

41  There are relatively few studies that investigate the interaction of U with the halophiles that are
42  more typically present in the WIPP brine (Francis et al. 2004).  Some WIPP-relevant research

1   was done (Francis et al. 2000), but this work was mostly focused on gas generation, not actinide
2   interactions.  It remains to be demonstrated that the mechanisms leading to the bioreduction of
3   U(VI) also extend to the microbes present in the WIPP.

4   **SOTERM-3.4.1.2 Solubility of U(IV)**

5   Tetravalent U is expected to be the dominant oxidation state in the WIPP as a result of the
6   reducing conditions that will prevail.  The solubility of U(IV) under these conditions is
7   analogous to that observed for Th (see Section SOTERM-3.3) and is, in fact, calculated in the
8   WIPP PA with the Th(IV) database.

9   Experimentally, in solution, $U^{4+}$ is readily oxidized to $UO_2^{2+}$.  This occurs even when only trace
10  levels of oxygen exist that are often below the limit of detection by most laboratory
11  instrumentation.  This explains why there are relatively few studies of $U^{4+}$.  It is also problematic
12  because there are very large discrepancies in the literature as a result of experimental artifact.  In
13  particular, there are a number of published results (Rai, Felmy, and Ryan 1990; Gayer and Leider
14  1957; Ryan and Rai 1983; Tremain et al. 1981; Casas et al. 1998) that suggest amphotericity for
15  $U^{4+}$ at pH >10.  This, however, likely resulted from combined effects of two experimental
16  artifacts: (1) oxidation to $UO_2^{2+}$, which is much more soluble, and (2) the presence of carbonate,
17  which is a strong complexant of $U^{4+}$.

18  The solubility of U(IV) phases were also determined in simplified brines under conditions that
19  relate to the WIPP (Rai et al. 1997; Rai et al. 1998; Yajima, Kawamura, and Ueta 1995; Torrero
20  et al. 1994).  These data are shown in Figure SOTERM-12.  Rai et al. (Rai et al. 1997)
21  determined the solubility of freshly precipitated $UO_2 \cdot xH_2O$(am) in NaCl and $MgCl_2$ solutions of
22  various ionic strengths.  They estimate the concentration of $U(OH)_4$(aq) in equilibrium with
23  $UO_2 \cdot xH_2O$(am) to be about $10^{-8.0}$ M, and a number of data with greater concentrations in the
24  neutral and alkaline range are ascribed to the presence of U(VI) in solution.  This is in fair
25  agreement with the value of $10^{-(8.7 \pm 0.4)}$ M proposed by Yajima, Kawamura, and Ueta (Yajima,
26  Kawamura, and Ueta 1995).  It is important to note that U(IV) concentrations at pH >5 show no
27  significant dependence on the initial solid phase; both fresh precipitates in oversaturation
28  experiments or electrodeposited microcrystalline $UO_2$(s) in undersaturation experiments gave the
29  same results (Torrero et al. 1994).
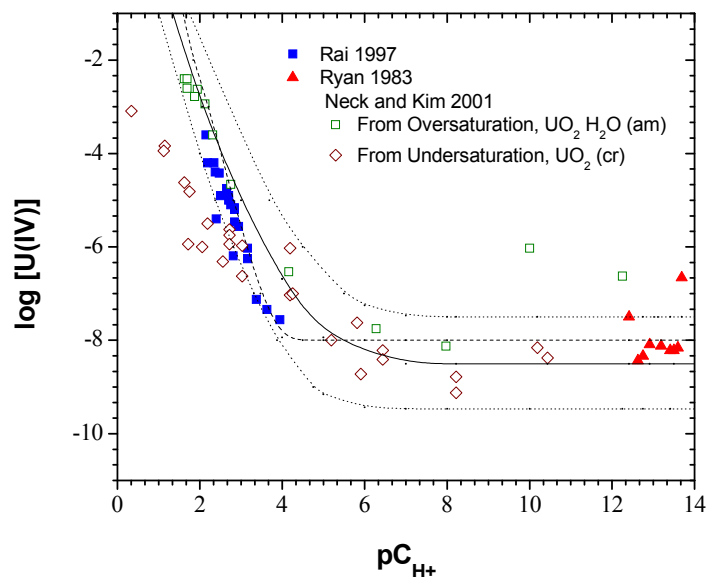
1

2      **Figure SOTERM-12. Solubility of UO$_2$(s) as a Function of pH at 20–25 ºC (68–77 °F) in**
3      **1M NaCl (based on Neck and Kim 2001). The experimental data**
4      **are from Ryan and Rai (1983), Rai et al. (1997), and Neck and**
5      **Kim (2001). The solid line is calculated by Neck with Log K$_{sp}$ =**
6      **(-54.5 ± 1.0) and the hydrolysis constants selected in Neck and**
7      **Kim (2001). The dotted lines show the range of uncertainty. The**
8      **dashed line is calculated with the model proposed by Rai et al.**
9      **(1997).**

10  **SOTERM-3.4.1.3 Speciation and Solubility of U(VI)**

11  U(VI) phases and aqueous species, although not expected to predominate in the WIPP, could be
12  present due to the localized effects of radiolysis (see Section SOTERM-2.4.2). The WIPP PA
13  currently makes the conservative assumption that U(VI) species predominate in 50% of the PA
14  vectors. The solubility of U(VI) is, however, not explicitly calculated in the WIPP PA, since
15  there is no model for actinides in the VI oxidation state. The potential contribution of U(VI)
16  species to the overall solubility of U in the WIPP is implicitly considered in the WIPP PA in the
17  1 mM value for U solubility (U.S. EPA 2005). Prior to this, the solubility of U was defined as
18  $1.2 \times 10^{-5}$ M based on an assessment of the literature and existing WIPP-relevant experimental
19  data by Hobart and Moore (Hobart and Moore 1996).

20  The solubility of U(VI) in the WIPP is expected to be defined by the combined contribution of
21  two processes: hydrolysis with oxyhydroxide phase formation, and carbonate complexation with
22  U carbonate phase formation. These are both very complex systems, and there are many
23  proposed speciation schemes. In carbonate-free or low-carbonate solutions, the speciation of
24  U(VI) is dominated by hydrolysis.

25  Yamazaki et al. (Yamazaki et al. 1992) conducted U(VI) solubility experiments from both
26  oversaturation and undersaturation in a synthetic brine at pC$_{H+}$ values ranging from 6.4 to 12.4.
27  The composition of this synthetic brine was close to the composition of the WIPP GWB brine,

1 with higher concentrations of NaCl, NaBr, KCl and $MgCl_2$ and ionic strength ~6 M. This
2 synthetic brine initially contained 0.11 mM of bicarbonate $HCO_3^-$, but the solution treatment
3 (continuous nitrogen gas flow above the solution) likely removed some of the carbonate from
4 solution before the later uranium additions and prevented any $CO_2$ uptake during the experiment.
5 The results obtained at the $pC_{H+}$ closest to WIPP repository conditions with no further carbonate
6 additions are listed in Table SOTERM-12. Uranium (VI) concentrations of approximately $10^{-7}$ M
7 were observed at $pC_{H+}$ = 10.4 and 12.4 when nitrogen gas was continuously passing over the
8 solutions to minimize $CO_2$ uptake. Despite extensive precipitation of brucite $Mg(OH)_2$ at these
9 high $pC_{H+}$ values, the solubility-controlling phase at $pC_{H+} \geq 9.3$ was found to be potassium
10 diuranate $K_2U_2O_7$.

11 Diaz-Arocas and Grambow (Diaz-Arocas and Grambow 1998) investigated uranium (VI)
12 solubility in NaCl solutions up to 5 M at 25 °C and different basic pH values, under an argon
13 atmosphere using an oversaturation approach. Their uranium concentration equilibria in 5 M
14 NaCl are presented in Table SOTERM-12. At pH $\geq$ 7.5, poorly crystalline sodium-uranates,
15 identified by XRD, were formed in solutions. Diaz-Arocas and Grambow indicated that the
16 solubility of this phase was about $3 \times 10^{-5}$ M at $pC_{H+}$ = 8.9 in 5 M sodium chloride in the absence
17 of carbonate.

18 Carbonate, as $CO_3^{2-}$, has a significant effect on the solubility of U(VI) (Clark, Hobart and Neu
19 1995; Guillaumont et al. 2003). In the absence of competing complexing ligands, carbonate
20 complexation will dominate the speciation of the uranyl ion under near-neutral pH conditions as
21 long as there is ample carbonate-bicarbonate available (Clark, Hobart and Neu 1995).
22 Complexation constants for binary U(VI) carbonate complexes at I = 0 M and 25 ºC (77 °F) are
23 listed in Table SOTERM-12 (Guillaumont et al. 2003).

1        **Table SOTERM-12.  Solubility of U(VI) in High-Ionic-Strength Media**

| U(VI) Concentration (M) | $pC_{H+}$ | Solution | Time (days) | Solid | Reference |
|---|---|---|---|---|---|
| $(2.8 \pm 1.8) \times 10^{-5}$ | 8.9 | 5M NaCl | $\approx 50$ | $Na_{0.68}UO_{3.34} \cdot (2.15\pm0.10)H_2O$ | Diaz-Arocas and Grambow 1998 |
| $(8.2 \pm 4.6) \times 10^{-5}$ | 7.6 | 5M NaCl | $\approx 110$ | $Na_{0.45}UO_{3.23} \cdot (4.5\pm0.1)H_2O$ | Diaz-Arocas and Grambow 1998 |
| $(4.2 \pm 1.9) \times 10^{-4}$ | 7.1 | 5M NaCl | $\approx 170$ | $Na_{0.29}UO_{3.15} \cdot (2.9\pm0.2)H_2O$ | Diaz-Arocas and Grambow 1998 |
| $(2.8 \pm 0.9) \times 10^{-6}$ | 6.5 | 5M NaCl | $\approx 170$ | $Na_{0.14}UO_{3.07} \cdot (2.5\pm0.1)H_2O$ | Diaz-Arocas and Grambow 1998 |
| $(1.82 \pm 0.01) \times 10^{-3}$ | 8.4 | Brine (air atmosphere) | 100 | α-schoepite (oversaturation) | Yamazaki et al. 1992 |
| $(1.81 \pm 0.01) \times 10^{-3}$ | 8.4 | Brine (air atmosphere) | 100 | α-schoepite (oversaturation) | Yamazaki et al. 1992 |
| $(1.40 \pm 0.05) \times 10^{-3}$ | 8.4 | Brine (air atmosphere) | 244 | α-schoepite (undersaturation) | Yamazaki et al. 1992 |
| $(1.80 \pm 0.05) \times 10^{-3}$ | 8.4 | Brine (air atmosphere) | 244 | α-schoepite (undersaturation) | Yamazaki et al. 1992 |
| $(3.8 \pm 0.4) \times 10^{-7}$ | 10.4 | Brine (initial 0.11mM $HCO_3^-$) | 150 | $Mg(OH)_2$ and $K_2U_2O_7$ (oversaturation) | Yamazaki et al. 1992 |
| $(3.1 \pm 0.3) \times 10^{-7}$ | 10.4 | Brine (initial 0.11mM $HCO_3^-$) | 150 | $Mg(OH)_2$ and $K_2U_2O_7$ (oversaturation) | Yamazaki et al. 1992 |
| $(1.7 \pm 1.4) \times 10^{-7}$ | 8.1 | ERDA-6 | 705 | To be determined (oversaturation) | Lucchini et al. 2013b |
| $(9.9 \pm 3.0) \times 10^{-8}$ | 9.6 | ERDA-6 | 705 | To be determined (oversaturation) | Lucchini et al. 2013b |
| $(3.1 \pm 1.3) \times 10^{-8}$ | 10.5 | ERDA-6 | 705 | To be determined (oversaturation) | Lucchini et al. 2013b |
| $(2.1 \pm 0.6) \times 10^{-6}$ | 7.4 | GWB | 705 | To be determined (oversaturation) | Lucchini et al. 2013b |
| $(4.3 \pm 1.3) \times 10^{-6}$ | 8.2 | GWB | 705 | To be determined (oversaturation) | Lucchini et al. 2013b |
| $(8.1 \pm 2.4) \times 10^{-7}$ | 9.2 | GWB | 705 | To be determined (oversaturation) | Lucchini et al. 2013b |
| $(2.7 \pm 0.5) \times 10^{-7}$ | 8.0 | ERDA-6 (initial 2mM carbonate) | 994 | To be determined (oversaturation) | Lucchini et al. 2013a |
| $(3.2 \pm 1.0) \times 10^{-5}$ | 8.8 | ERDA-6 (initial 2mM carbonate) | 994 | To be determined (oversaturation) | Lucchini et al. 2013a |
| $(3.5 \pm 2.8) \times 10^{-8}$ | 12.1 | ERDA-6 (initial 2mM carbonate) | 994 | To be determined (oversaturation) | Lucchini et al. 2013a |
| $(2.6 \pm 0.8) \times 10^{-6}$ | 7.6 | GWB (initial 2mM carbonate) | 994 | To be determined (oversaturation) | Lucchini et al. 2013a |
| $(7.1 \pm 1.4) \times 10^{-7}$ | 9.0 | GWB (initial 2mM carbonate) | 994 | To be determined (oversaturation) | Lucchini et al. 2013a |

1  **Table SOTERM-13.  Complexation Constants for Binary U(VI) Carbonate Complexes at I**
2  **= 0 M and 25 ºC (Guillaumont et al. 2003)**

| Reaction and Solubility Product for $UO_2CO_3$(crystalline [cr]) | |
|---|---|
| $UO_2CO_3(cr) \rightleftharpoons UO_2^{2+} + CO_3^{2-}$ | Log $K^0_{SP(cr)}$= -14.76 ± 0.02 |
| **Reactions and Formation Constants $\beta^0_{nq}$ for $(UO_2)_n(CO_3)_q^{2n-2q}$** | |
| $UO_2^{2+} + CO_3^{2-} \rightleftharpoons UO_2CO_3(aq)$ | Log $\beta^0_{11}$ = 9.94 ± 0.03 |
| $UO_2^{2+} + 2 CO_3^{2-} \rightleftharpoons UO_2(CO_3)_2^{2-}$ | Log $\beta^0_{12}$ = 16.61 ± 0.09 |
| $UO_2^{2+} + 3 CO_3^{2-} \rightleftharpoons UO_2(CO_3)_3^{4-}$ | Log $\beta^0_{13}$ = 21.84 ± 0.04 |
| $3 UO_2^{2+} + 6 CO_3^{2-} \rightleftharpoons (UO_2)_3(CO_3)_6^{6-}$ | Log $\beta^0_{36}$ = 55.6 ± 0.5 |

3

4   The three monomeric complexes of general formula $UO_2(CO_3)$, $UO_2(CO_3)_2^{2-}$, and $UO_2(CO_3)_3^{4-}$
5   are present under the appropriate conditions. There is also evidence from electrochemical,
6   solubility, and spectroscopy data that support the existence of $(UO_2)_3(CO_3)_6^{6-}$,
7   $(UO_2)_2(CO_3)(OH)_3^-$, and $(UO_2)_{11}(CO_3)_6(OH)_{12}^{2-}$ polynuclear species, which can only form under
8   the conditions of high-metal-ion concentration or high ionic strength (Clark, Hobart and Neu
9   1995).  At uranyl concentrations above $10^{-3}$ M, the trimeric cluster $(UO_2)_3(CO_3)_6^{6-}$ can also be
10  present in significant concentrations. When the uranyl ion concentration begins to exceed the
11  carbonate concentration, hydrolysis will play an increasingly important role (Clark, Hobart and
12  Neu 1995).

13  It is generally accepted that the major complex in solution at high carbonate concentrations is
14  $UO_2(CO_3)_3^{4-}$ (Kramer-Schnabel et al. 1992; Pepper et al. 2004).  However, at I = 0.5 M and I = 3
15  M, the polynuclear $(UO_2)_3(CO_3)_6^{6-}$ species becomes an important competitor of $UO_2(CO_3)_3^{4-}$.
16  Grenthe et al. (Grenthe et al. 1984) indicated that the formation of $(UO_2)_3(CO_3)_6^{6-}$ is favored at
17  high ionic strengths as a result of possible stabilization of the complex by ions of the background
18  electrolyte.

19  At high pH, Yamamura et al. (Yamamura et al. 1998) demonstrated that hydrolysis overwhelms
20  carbonate complexation. The solubility of U(VI) was measured in highly basic solutions (11≤ pH
21  ≤ 14) at an ionic strength of I = 0.5 – 2 M over a wide range of carbonate concentrations ($10^{-3}$ –
22  0.5 M) using both oversaturation and undersaturation approaches. In the oversaturation
23  experiments, the solubility of U(VI) decreased with increasing equilibration time from one week
24  to one year and was explained as an increase in the crystallinity of the solid phase with aging.
25  The solid phase was identified as $Na_2U_2O_7 \cdot xH_2O$ by XRD. The undersaturation experiments
26  conducted for one month with the solid phase indicated a rapid equilibrium. These data were
27  interpreted by considering the formation of $UO_2(OH)_3^-$, $UO_2(OH)_4^{2-}$, and $UO_2(CO_3)_3^{4-}$
28  (Yamamura et al. 1998).

29  A few experimental investigations were reported on the influence of carbonate on U(VI)
30  solubility in highly saline solutions (Yamazaki et al. 1992; Reed and Wygmans 1997; Lin et al.
31  1998; Fanghänel and Neck 2002).  Lin et al. (Lin et al. 1998) evaluated U(VI) solubilities with
32  up to 5M NaCl in a range of carbonate concentrations.  At carbonate-ion concentrations greater
33  than $10^{-7}$ M, $UO_2(CO_3)_3^{4-}$ was the dominant U(VI) complex in solution. At higher $CO_2$ partial

1  pressures, the solubility-controlling solid phase was found to be $UO_2CO_3(s)$, whereas at lower
2  partial pressures, sodium uranate was identified as the solid phase in NaCl-saturated solutions.
3  This study, although interesting, is of questionable use to the WIPP because the details were not
4  fully published.

5  Yamazaki et al. (Yamazaki et al. 1992) measured the solubility of U(VI) in synthetic brine and
6  an air atmosphere. The results obtained at $pC_{H+} = 8.4$ using both oversaturation and
7  undersaturation approaches are listed in Table SOTERM-12. At this $pC_{H+}$ value, millimole
8  concentrations of uranium were measured in solution. Solids obtained at $pC_{H+} = 8.4$ were
9  identified as poorly crystalline schoepite ($UO_3 \cdot xH_2O$) by X-Ray Diffraction (XRD). Yamazaki
10 carried out some calculations to model the competition between calcium and magnesium for
11 carbonate complexation in order to interpret his experimental solubility data. He concluded that
12 the uranium solubility decrease above $pC_{H+} = 8.4$ was related to a shift from the triscarbonato
13 uranyl complex $UO_2(CO_3)_3^{4-}$ to the uranyl hydroxide complexes $UO_2(OH)_n^{2-n}$, as precipitation of
14 calcium carbonate ($CaCO_3$) occurred, and to the conversion of schoepite to potassium diuranate.

15 The only U(VI) solubility values available in the literature that were obtained in the presence of
16 carbonate under WIPP-relevant conditions were featured in the fiscal year 1997 year-end report
17 by Reed and Wygmans (Reed and Wygmans 1997). The experiments were carried out in ERDA-
18 6 brine at pH 8 and 10, and in G-Seep brine at pH 5 and 7.  U(VI), Np(VI), and Pu(VI) were
19 added to the brine samples.  $CO_3^{2-}$ ($10^{-4}$ M) was also added to some of the samples. The
20 experiments were conducted under a hydrogen atmosphere at $25 \pm 5$ °C. Concentrations and
21 oxidation states of the actinides were monitored over time. The U(VI) concentration was stable
22 at approximately $1 \times 10^{-4}$ M when measured as a function of time in ERDA-6 brine at pH 10 in
23 the presence of $CO_3^{2-}$ (Reed and Wygmans 1997).

24 **SOTERM-3.4.2 WIPP-Specific Results since the CRA-2009 and the CRA-2009 PABC**

25 The solubility of U(VI) in the absence and the presence of carbonate was extensively studied
26 since the CRA-2009 in simulated GWB and ERDA-6 brine (Lucchini et al. 2010a, Lucchini et al.
27 2010b, 2013 and 2013a).  A summary of these results is shown in Figure SOTERM-13 and a
28 comparison of these results with other solubility data in the literature is given in Table
29 SOTERM-12.  No U(IV) solubility studies were conducted since Th(IV) is the analog for  the IV
30 actinides.

31 In the absence of carbonate, the measured U(VI) solubilities were about $10^{-6}$ M in GWB brine at
32 $pC_{H+} \geq 7$ and about $10^{-8}$ - $10^{-7}$ M in ERDA-6 at $pC_{H+} \geq 8$ (Lucchini et al. 2007, 2010a and
33 2010b).  These results put an upper bound of $\sim 10^{-6}$ M for the solubility of uranyl in the
34 carbonate-free WIPP brines for the investigated range of experimental conditions.  At the
35 expected $pC_{H+}$ in the WIPP ($\sim 9.5$), the measured uranium solubility was between $10^{-7}$ M and $10^{-6}$
36 M.  In the presence of carbonate, the highest uranium solubility obtained experimentally was $\sim$
37 $10^{-4}$ M, under WIPP-related conditions ($pC_{H+} \sim 9.5$).  It is important to note that this uranium
38 solubility, in the absence of carbonate, was 10-100 times lower than published results. The
39 uranium (VI) solubility experiments reported in two other relevant publications (Yamazaki et
40 al.1992; Diaz-Arocas and Grambow 1998) were performed in brines close to the WIPP brine
41 composition, but possibly with a less rigorous control of a carbon dioxide-free environment. The

1     impact of carbonate concentration on the solubility of uranium (VI) in the two simulated WIPP
2     brines can be explained in terms of three distinctive $pC_{H+}$ regions.
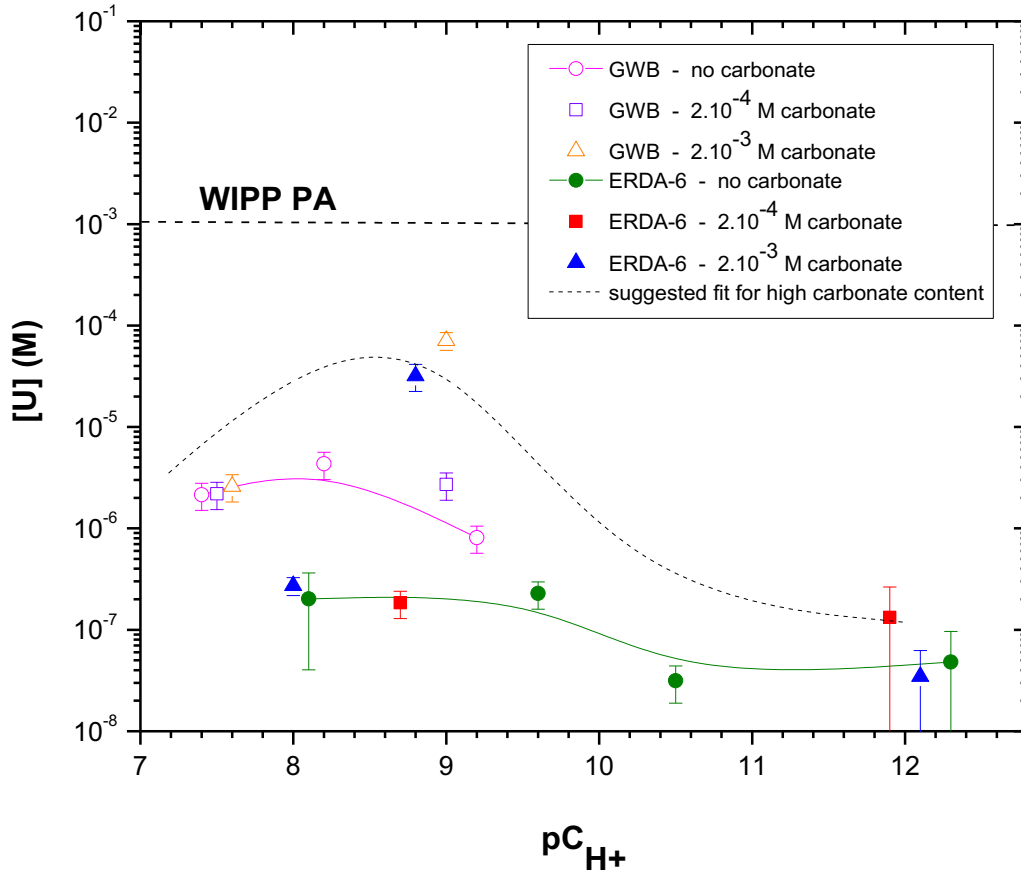


3

4     **Figure SOTERM-13.  Uranium Concentration in ERDA-6 (Open Symbols) and GWB**
5     **(filled symbols) versus $pC_{H+}$. in Nitrogen Controlled**
6     **Atmosphere, in the Absence of Carbonate or in the Presence of**
7     **Two Concentrations of Carbonate ($2\times10^{-4}$ M and $2\times10^{-3}$ M) at the**
8     **Beginning of the Experiments. The carbonate systems data**
9     **correspond to 17 samplings performed over 994 days.**

10     The first $pC_{H+}$ region is $7.5 \leq pC_{H+} \leq 8$.  In this $pC_{H+}$ region, the uranium concentration was
11     stable in both brines and independent of the carbonate concentration. However, there were small
12     differences in the uranium solubility due to differences in the composition of the brine: $\sim 10^{-6}$ M
13     in GWB, and $\sim 10^{-7}$ M in ERDA-6. These data indicated that there was no impact of carbonate in
14     this $pC_{H+}$ region ($7.5 \leq pC_{H+} \leq 8$), but there was certainly an effect due to one or more
15     components of the brines that were present in higher amounts in GWB than in ERDA-6. Based
16     on our investigation of neodymium solubility (Borkowski et al. 2010a), we postulated that borate
17     may also play a role in defining the uranium (VI) solubility in this $pC_{H+}$ region (see also
18     Borkowski et al. 2010b). This possibility was confirmed experimentally (Lucchini, Borkowski
19     and Richmann 2013; Lucchini et al. 2013a).

1   The second $pC_{H+}$ region of interest, $8 \le pC_{H+} \le 10$, is directly relevant to the WIPP. In this $pC_{H+}$
2   region, not only was there a compositional effect between the two brines studied (higher uranium
3   concentrations in GWB than in ERDA-6 for identical carbonate content), but there was also an
4   impact of carbonate on the observed uranium solubility in each brine.  At high carbonate content
5   ($2\times10^{-3}$ M in our experiments), the uranium concentrations reached $10^{-4}$ M, which was two or
6   more orders of magnitude higher than in the absence of carbonate. The low carbonate content
7   data ($2\times10^{-4}$ M) did not reflect a strong influence of carbonate on uranium solubility, since the
8   measured solubility was similar to the ones obtained in carbonate-free systems.

9   Lastly, the third $pC_{H+}$ region of interest is at $10 \le pC_{H+}$. In that $pC_{H+}$ region, the uranium
10  concentrations were stable around $10^{-7}$-$10^{-8}$ M. It is likely that hydrolysis overwhelmed any other
11  possible effects on uranium solubility.

12  These newly obtained solubility data for uranium (VI) in the WIPP brine accomplished the
13  following:

14      •   Provided the first WIPP-relevant data for the VI actinide oxidation state that
15          established the solubility of uranium (VI) over an extended $pC_{H+}$ range for GWB and
16          ERDA-6 brines in the absence or presence of carbonate

17      •   Established an upper limit of $\sim 10^{-6}$ M uranyl concentration at the reference $pC_{H+}$
18          WIPP case in the absence of carbonate, and an upper limit of $\sim 10^{-4}$ M uranyl
19          concentration at the reference $pC_{H+}$ WIPP case in the presence of 2 mM carbonate

20      •   Confirmed a lack of significant amphotericity in the WIPP simulated brines at high
21          pH values

22      •   Demonstrated a small effect of borate complexation in the $pC_{H+}$ range of 7.5 to 10

23      •   Supported the current assumption in PA that the solubility of U(VI), under the
24          expected range of conditions in the WIPP, will not exceed 1 mM

## SOTERM-3.5 Neptunium Chemistry

26  The WIPP repository is projected to contain ~32.5 kg of Np, primarily as the [237]Np isotope (see
27  Table SOTERM-8). Its inventory increases with time from the decay of [241]Am and the possibility
28  of [238]U (n, 2n) reactions to 223 Kg at 1000y after emplacement.  In the WIPP PA, Np speciates
29  as Np(IV) in 50% of the PA vectors and as Np(V) in the other 50% of the PA vectors. The
30  contribution of Np to actinide release from the WIPP was included in the CRA-2014 PA
31  calculation, but its effect on release was negligible. Arguments have already been made that it
32  should be excluded from consideration in the WIPP PA based on its low inventory (Brush and
33  Garner 2005).

### SOTERM-3.5.1 Neptunium Environmental Chemistry

35  The environmental chemistry of Np is somewhat unique in the actinide series as a result of the
36  relatively high stability of the $NpO_2^+$ species, which is in the V oxidation state, under a wide

1  range of conditions typically found in the subsurface. This oxidation state is prevalent when
2  oxidizing conditions predominate (Hobart 1990). It is mobile because it has a relatively high
3  solubility and it is not strongly sorbed or complexed. It does not hydrolyze strongly, with little or
4  no measurable hydrolysis until pH >9 (Neck, Kim, and Kanellakopulos 1992; Itagaki et al.
5  1992). Much of the complexation data for inorganic and organic complexes for Np pertains to
6  the V oxidation state for this reason (Lemire et al. 2001). The log $K_{sp}$ for $NpO_2OH$ (s) is 4.5 ±
7  0.06 (Neck, Kim, and Kanellakopulos 1992).

8  Np can, however, actually exist in up to five oxidation states in aqueous media. The redox
9  potentials under basic conditions are (Martinot and Fuger 1985):

10      + 0.58 V        + 0.6 V       + 0.3V    -2.1V
11      $NpO_5^{3-} \rightarrow NpO_2(OH)_2 \rightarrow NpO_2OH \rightarrow NpO_2 \rightarrow Np(OH)_3$ (SOTERM.28)
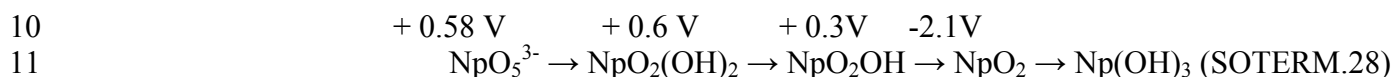
12  Only the Np(IV) and Np(VI) oxidation states, in addition to Np(V), can exist under the right
13  conditions in reducing or oxidizing groundwater (Hobart 1990; Keller 1971 [pp. 195–215];
14  Clark, Hobart and Neu 1995). These exist as $Np^{4+}$ complexes and $NpO_2^{2+}$ complexes.  Np(VI),
15  unlike Np(V), is strongly hydrolyzed at near-neutral pH and is readily reduced by many
16  constituents typically found in groundwater (e.g., organics and most reduced metals). For these
17  reasons, it does not tend to persist in groundwater under most conditions.

18  Under reducing anoxic conditions, $Np^{4+}$ species can predominate. These $Np^{4+}$ species readily
19  undergo hydrolysis and are comparable to $Pu^{4+}$ in this regard. This system is highly irreversible
20  and probably polymeric in nature, as is observed for $Pu^{4+}$. The measured solubility of $Np^{4+}$ is
21  $10^{-8.5}$ to $10^{-8.1}$ M with $Np(OH)_4$, not $Np(OH)_5^-$, as the predominant aqueous species (Rai and
22  Ryan 1985; Eriksen et al. 1993). The importance and predominance of the Np(IV) oxidation state
23  in reducing conditions is even more pronounced when anaerobic bacteria are present. Np(V) was
24  readily reduced by sulfate-reducing bacteria (Banaszak, Reed, and Rittmann 1998) and
25  methanogenic consortia (Banaszak et al. 1999), and precipitated as Np(IV) solids.

26  In WIPP-specific experiments (Reed and Wygmans1997), spectroscopic evidence for the
27  reduction of Np(VI) to Np(V) in ERDA-6 (Castile) brine at pH 10 was observed along with
28  complete reduction of Np(VI) to Np(V) in G-Seep (Salado) brine at pH 7 when no iron or
29  microbial activity were present. In the presence of oxalate, citrate, and EDTA, rapid and
30  complete reduction of Np(VI) to Np(V) coupled with a slower formation of Np(IV) species was
31  observed. The stability of Np(V) under these conditions is further confirmed by Neck, Runde,
32  and Kim (Neck, Runde, and Kim 1995), who showed that Np(V) carbonate complexes are stable
33  in 5M NaCl.

34  In the expected WIPP environment, however, where anoxic and reducing conditions with
35  microbial activity and reduced iron are expected to be present, Np(IV) is expected to be the
36  predominant oxidation state (Rai and Ryan 1985; Rai, Strickert, and McVay 1982; Kim et al.
37  1985; Pryke and Rees 1986). This is based on studies of the solubility of $NpO_2OH$ in 1 M and 5
38  M NaCl solutions at pH 6.5, where the reduction of Np(V) to Np(IV) was observed (Kim et al.
39  1985; Neck, Kim, and Kanellakopulos 1992).

1  **SOTERM-3.5.2 WIPP-Specific Results since the CRA-2009 and the CRA-2009 PABC**

2  There are no new WIPP-relevant results on the chemistry and speciation of Np since CRA-2009
3  and the CRA-2009 PABC.  Neptunium is not a key contributor to release from the WIPP.

4  # SOTERM-3.6 Plutonium Chemistry

5  Plutonium is a key TRU component that contributes significantly to the potential for TRU
6  release from the WIPP under all release mechanisms considered by PA.  Pu isotopes, estimated
7  to be ~12 metric tons at the time of closure, represent approximately 77% of the Ci content for
8  actinides in TRU waste (see Table SOTERM-8) at emplacement. This changes with time to 62%,
9  83% and >99% at 100, 1000 and 10,000 years after emplacement due to radioactive decay and
10  the relatively long half-life of $^{239}$Pu.  There are five isotopes of Pu that make a significant
11  contribution to the Pu inventory, but $^{239}$Pu, $^{238}$Pu, and $^{241}$Pu are the major contributors to the Ci
12  content. Under the conditions expected in the WIPP, Pu(IV) is expected to be the predominant
13  oxidation state (Weiner 1996). A more extensive review of Pu subsurface speciation issues as
14  they pertain to the WIPP case was completed (Reed et al. 2009).

15  In the WIPP PA, all of the Pu is assumed to be reduced and present in the III or IV oxidation
16  state.  Half of the PA vectors contain 100% Pu(III), with the other half of the vectors containing
17  100% Pu(IV) species. Because the solubility of Pu(III) is roughly 10 times higher, the
18  assumption that it is present is a conservatism built into the WIPP PA.  The two higher-valent Pu
19  oxidation states, Pu(V) and Pu(VI), are not considered in the PA because they cannot persist
20  under the expected reducing and anoxic conditions in the WIPP.

21  **SOTERM-3.6.1 Plutonium Environmental Chemistry**

22  Generally, Pu can exist in oxidation states III, IV, V, VI, and VII (Katz, Seaborg, and Morss
23  1986, p. 781). Of these, only Pu(V), Pu(IV), and Pu(III) are expected to be important under
24  environmentally relevant oxidizing and reducing conditions.  Pu(VII) is very unstable and exists
25  only in extremely basic solutions (for example, 7 M NaOH) that are not expected in the WIPP.
26  Pu(VI) and Pu(V) can persist in the WIPP in the absence of reductants, but they are readily
27  reduced in the presence of Fe(II/0) species, reduced by many organic chelators (Reed et al.
28  1998), and possibly reduced in anaerobic, biologically active systems (Reed et al. 2007; Icopini,
29  Boukhalfa, and Neu 2007). The reduction of Pu(VI/V), under WIPP-relevant conditions, was
30  shown by Clark and Tait (Clark and Tait 1996), Reed and Wygmans (1997), and Reed et al.
31  (Reed et al. 2007).  In this context, only Pu(III) and Pu(IV) oxidation state species are expected
32  to be present under WIPP-related conditions.

33  **SOTERM-3.6.1.1 Importance of Redox for Plutonium Speciation**

34  The role and importance of redox reactions in determining actinide mobility and solubility are
35  beyond question (Van Luik et al. 1987; Allard 1982; Choppin and Rao 1992). The redox
36  potentials for the various oxidation states at pH 7 are (Cleveland 1979, pp. 11–46)

$$\text{PuO}_2(\text{OH})_2 \text{ (aq)} \quad \overset{+0.77 \text{ V}}{\rightarrow} \quad \text{PuO}_2^+ \quad \overset{+1.11 \text{ V}}{\rightarrow} \quad \text{PuO}_2 \cdot \text{H}_2\text{O (s)} \quad \overset{-0.63 \text{ V}}{\rightarrow} \quad \text{Pu}^{3+}$$

$$+0.94 \text{ V}$$
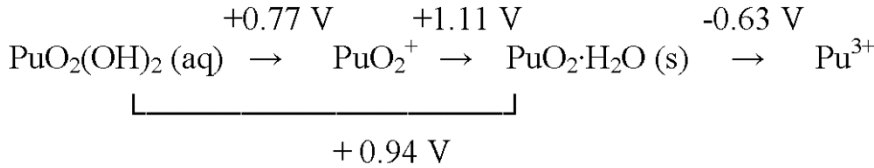
1                                                                                          (SOTERM.29)

2    A typical phase diagram for Pu in groundwater that illustrates the importance of redox is shown
3    in Figure SOTERM-14.
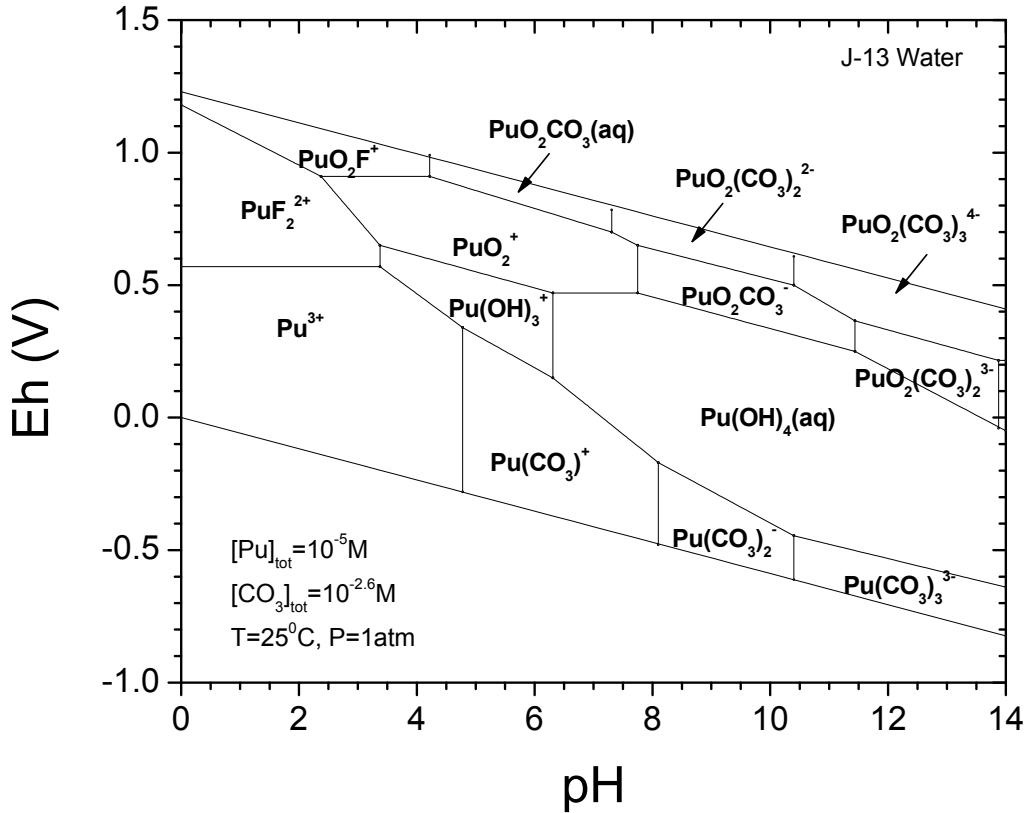


4
5    **Figure SOTERM-14.  Speciation Diagram for Plutonium in Carbonated Low-Ionic-**
6                              **Strength Groundwater (Based on Data Presented in Runde et al.**
7                              **2002). This illustrates the expected lower solubility of reduced**
8                              **Pu(III) and Pu(IV) phases, and suggests that the dominant Pu**
9                              **species in the pH 8-9 range are hydrolytic species with lesser**
10                             **contributions from carbonate.**

11   Higher-valent Pu, specifically Pu(V) and Pu(VI), can be present in near-surface oxidizing
12   groundwaters (Orlandini, Penrose, and Nelson 1986). The association of Pu(V) with organic
13   colloidal material was proposed as the mechanism by which subsurface migration occurred.
14   Pu(VI), in near-neutral systems, is strongly and irreversibly hydrolyzed (Okajima and Reed
15   1993). It is also readily reduced by organics and reduced metal species even when oxygen is
16   present to form Pu(V), and is not generally stable under most groundwater-relevant conditions.

1   Pu(V), by analogy with Np(V), does not undergo hydrolysis until pH >7 and tends to form weak
2   complexes. It readily disproportionates to form Pu(IV) and Pu(VI) at high concentrations and is
3   relatively easy to reduce in the environment under anoxic conditions. $Fe^{2+}$(aq), Fe(II) minerals,
4   and metallic iron reduce Pu(V) to Pu(IV).

5   In geochemical systems, redox control is often interpreted in terms of the iron, and in a broader
6   sense, reduced metal, mineralogy, and associated aqueous chemistry (Sanchez, Murray, and
7   Sibley 1985; White, Yee, and Flexser 1985). In the WIPP case, iron will undergo anoxic
8   corrosion, producing $Fe^{2+}$. Both metallic iron ($Fe^0$) and $Fe^{2+}$ have been shown to quantitatively
9   reduce Pu(VI) in the WIPP brines to either Pu(IV) or Pu(III). Clark and Tait (Clark and Tait
10  1996) and Felmy et al. (Felmy et al. 1996) have experimentally observed the reduction of Pu(VI)
11  carbonates by either $Fe^0$ or $Fe^{2+}$ to Pu(IV). In the absence of carbonates, a quantitative reduction
12  of Pu(VI) is also observed, but the oxidation state of the resulting species cannot be definitively
13  determined because its concentration is below the lower detection limit of the oxidation state
14  analytical process (about $10^{-9}$ M). However, since this concentration is well below the expected
15  solubility of Pu(V) species, it was reasonably assumed that the Pu must have been reduced to
16  either the IV or III oxidation state. Neretnieks (Neretnieks 1982) has shown that when dissolved
17  actinides in moving groundwater came in contact with Fe(II), the actinides were reduced to a
18  much-less-soluble oxidation state and precipitated.

19  Pu(III) is not predicted to be stable under the expected WIPP conditions. There are, however,
20  some mechanisms identified in which Pu(III) species can be formed. Felmy et al. (Felmy et al.
21  1989) observed some Pu(III) in the WIPP brines at neutral and slightly basic conditions. PA
22  conservatively takes account of these minor mechanisms by assuming that Pu is speciated as
23  Pu(III) in 50% of the PA vectors.

24  General studies of Pu in brine have been done by a number of investigators (Büppelmann et al.
25  1986; Büppelmann, Kim, and Lierse 1988; Clark, Hobart, and Neu 1995; Nitsche et al. 1992;
26  Nitsche et al. 1994; Pashalidis et al. 1993; Villareal, Bergquist, and Leonard 2001; Reed et al.
27  1993; Reed, Okajima, and Richmann 1994; Reed and Wygmans 1997). There has also been an
28  assessment of the actinide chemistry in the WIPP CCA (Oversby 2000; Brush, Moore, and Wall
29  2001; U.S. EPA 2006). These studies confirm reduction of higher-valent Pu under the expected
30  WIPP conditions and establish the key speciation trends for Pu in the WIPP (see Figure
31  SOTERM-15). These trends are captured in the WIPP PA through analogy with Am(III) for
32  Pu(III) and with Th(IV) for Pu(IV).
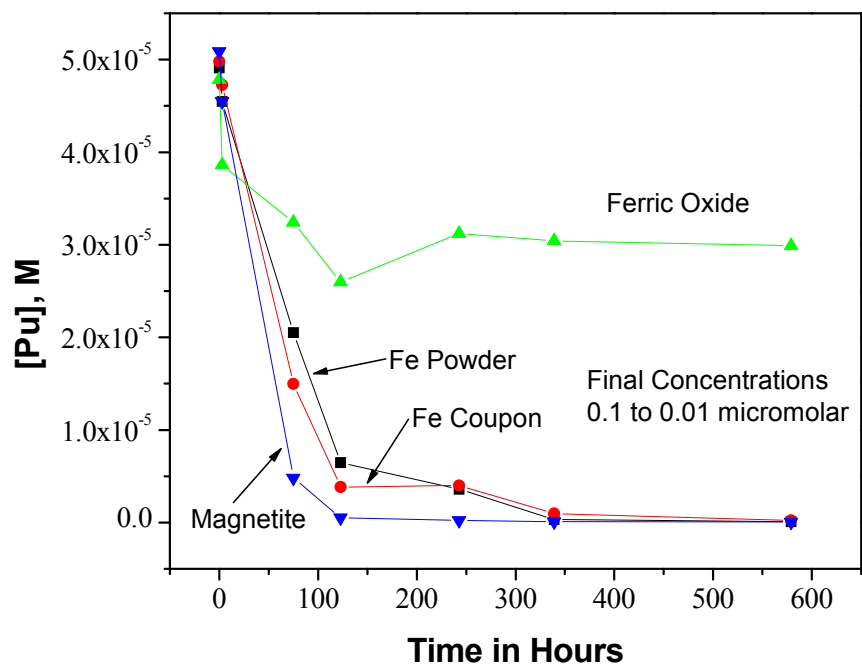
1
2    **Figure SOTERM-15.  The Concentration of Pu as a Function of Time in the Presence of**
3                              **Iron Powder, Iron Coupon, Ferric Oxide, and Magnetite (Mixed**
4                              **Iron Oxide) (Reed et al. 2009)**

5    **SOTERM-3.6.1.2 Bioreduction of Higher-Valent Plutonium**

6    Comprehensive and critical reviews of how actinide species and microorganisms interact have
7    been published (Banaszak, Rittmann, and Reed 1998; Neu, Ruggiero, and Francis 2002; Reed et
8    al. 2010). The likelihood that this could occur and recent results with Fe(III) reduction were
9    discussed in Section SOTERM-2.4.1.4. Additionally, the important role of microbial activity
10   through biotic transformations (Zitomer and Speece 1993; Banaszak, Rittmann, and Reed 1998;
11   Rittmann, Banaszak, and Reed 2002; Reed et al. 2007) in defining oxidation state distribution of
12   multivalent metals and actinides has been recognized.

13   Although the bioreduction of uranyl and neptunyl species is well established, there are relatively
14   few studies of the bioreduction of plutonyl species. Reed et al. (Reed et al. 2007) demonstrate
15   that *Shewanella alga*, a ubiquitous metal-reducing soil bacterium, reduces Pu(V) to Pu(III/IV)
16   species. Icopini, Boukhalfa, and Neu (Icopini, Boukhalfa, and Neu 2007) have shown that
17   *Geobacter* and *Shewanella oneidensis* also reduce higher-valent Pu to Pu(III/IV) species.

18   These Pu data are consistent with the oxidation state predictions in microbially active systems. It
19   is particularly important to note that Pu(IV) is the expected oxidation state under a wide range of
20   anoxic subsurface conditions, with no Pu(V) or Pu(VI) species expected. The recent Pu
21   bioreduction results confirm that highly reducing conditions are being generated by metal-
22   reducing bacteria under anaerobic growth conditions and support the current WIPP PA
23   assumption that higher-valent actinides cannot persist when the concentration of dissolved
24   actinides is important and microbial activity is prevalent.

1  There are no studies on the bioreduction of Pu(V/VI) under WIPP-relevant conditions (note
2  discussion in Section SOTERM-2.4.1.4. Halophilic microorganisms (Gillow et al. 2000;
3  Swanson and Simmons 2013; Swanson et al. 2012) typically found and expected to predominate
4  in the WIPP environment have not been studied for their ability to reduce higher-valent
5  actinides, although they will contribute to the establishment of reducing conditions in the WIPP.

6  **SOTERM-3.6.1.3 Thermodynamic Stability of Higher-Valent Plutonium: $PuO_{2+x}$**

7  It has long been held that Pu oxide, as $PuO_2$, is the thermodynamically favored form of Pu oxide.
8  This oxide is likely the predominant form of Pu in TRU waste and is believed to be the most
9  important phase under WIPP-related conditions. In the last few years, however, there have been
10  a number of studies that question this key and fundamental assumption.

11  Haschke, Allen, and Morales (Haschke, Allen, and Morales 2000) report that near-stoichiometric
12  plutonium dioxide reacts with water vapor at temperatures between 25 °C and 350 °C (77 °F and
13  662 °F) according to the following reaction:

14  $$PuO_2(s) + xH_2O(g) \rightarrow PuO_{2+x}(s) + xH_2(g) \qquad \text{(SOTERM.30)}$$
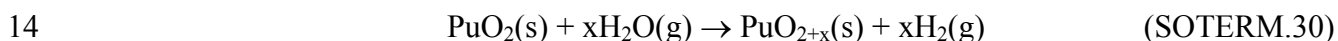
15  Here, water vapor is reduced by polycrystalline $PuO_2$ to produce hydrogen (H) and a previously
16  unknown higher-oxide $PuO_{2+x}$ with $x$ as large as 0.27. If only Pu(IV) and Pu(V) are present in
17  $PuO_{2.27}$, this oxide has 46% Pu(IV) and 54% Pu(V). Once formed, the $PuO_{2+x}$ may dissolve in
18  contact with groundwater to form aqueous $PuO_2^+$ or $PuO_2^{2+}$ species (Haschke and Ricketts
19  1995).

20  There remains some controversy about the mechanisms that led to the observation of higher-
21  valent Pu in the $PuO_{2+x}$. This process only occurs under unsaturated conditions at high relative
22  humidities. Haschke, Allen, and Morales (Haschke, Allen, and Morales 2000) argue that this
23  conversion is due to a chemical reaction (that is, the above reaction has a Gibbs energy less than
24  zero) rather than a radiolysis-induced reaction because the reaction rate is temperature
25  dependent. However, there seems to be some contribution from radiolysis in this process and this
26  may be the dominant mechanism (LaVerne and Tandon 2002). Neither of these mechanisms are
27  expected to impact WIPP repository performance.

28  The behavior of $PuO_2$ in contact with water was studied as a function of time by means of the
29  short-lived isotope [238]Pu, as well as the longer-lived [239]Pu (Rai and Ryan 1982). This study
30  concluded that crystalline $PuO_2$, amorphous $PuO_2$, and amorphous $PuO_3 \cdot xH_2O$ all convert to a
31  material intermediate between crystalline $PuO_2$ and a hydrated amorphous material that contains
32  both Pu(IV) and Pu(VI). These authors hypothesized that alpha particles generated by [238]Pu or
33  [239]Pu irradiated water to generate OH radicals that reacted to form Pu(V) and/or Pu(VI) on the
34  oxide surface. These observations are why the formation of localized oxidizing zones, where
35  some higher-valent Pu can persist, is recognized in the WIPP PA. Reduction of these species,
36  however, leads to a reformation of Pu(IV) hydrous oxide precipitates.

37  The overall issue of a thermodynamic driver for higher-valent Pu oxides, although it has received
38  much recent attention in the literature, is not yet resolved, but has a relatively insignificant
39  impact on the WIPP regardless of the mechanisms at work. A prolonged unsaturated phase in the

1    WIPP could lead to the formation of some $PuO_{2+x}$, but this will be quickly overwhelmed in an
2    aqueous environment and the higher-valent Pu will be reduced to Pu(III/IV) species, as described
3    in Section SOTERM-3.5.1.1 and Section SOTERM-3.5.1.2. Both DBR and transport-release
4    scenarios assume brine inundation and, correspondingly, the rapid introduction of reducing
5    conditions.

6    **SOTERM-3.6.2 WIPP-Specific Results since the CRA-2009 and the CRA-2009 PABC**

7    Since the CRA-2009 and CRA-2009 PABC, the WIPP-specific Pu-Fe interaction studies (Reed
8    et al. 2010) were extended in time to almost 6 years to establish the long-term oxidation state
9    distribution of plutonium in these iron-dominated brine systems.  In these investigations [242]Pu,
10   initially as $PuO_2^{2+}$, was used to minimize radiolytic effects.  Additionally these were done in two
11   WIPP-relevant brines (see Table SOTERM-4): GWB as a high magnesium brine typical of
12   MgO-reacted brine, and ERDA-6 as a high sodium chloride brine typical of brine found in the
13   far field.  The initial oxidation state was established using absorption spectrometry (Varian
14   CARY 5000) and solids were prepared from these brines using established methods.  Initially,
15   only Pu(IV) was evident in the XANES analysis (see Figure SOTERM-16).  This correlated with
16   a plutonium concentration that was in the range of $2 \times 10^{-9}$ M to as high as $1.5 \times 10^{-7}$ M at the
17   lower end of the pH range (pH = 7).  These data agreed with the results obtained in a prior study
18   after approximately two years when Pu-239 was the plutonium isotope (Reed et al. 2007).  After
19   ~5.8 years, these same solid samples were re-analyzed and found to be mostly Pu(III) with a
20   small amount of Pu(IV) in a few samples (see Figure SOTERM-17 and Table SOTERM-14).
21   The observation of Pu(III) in the solid phase correlated with an increase in the plutonium
22   solution concentrations from $1 \times 10^{-8}$ M to $3 \times 10^{-7}$ M (see Figure SOTERM-18).  This is a slight
23   elevation in concentration, by a factor of ~ 2 to 5, when compared to the earlier Pu(IV)-relevant
24   data.  This increased solubility is also consistent with the phase transformation to Pu(III) since
25   the solubility of Pu(III) is expected to be somewhat higher than Pu(IV).

26   The plutonium (III/IV) solids data show a qualitative correlation with the Fe(II)/Fe(III) ratio and
27   measured redox potential ($E_h$). Experiments with less negative $E_h$ also had a greater amount of
28   Fe(III) and Pu(IV) species present in the system.  This adds to the linkages seen by others
29   between the iron and plutonium chemistry in subsurface conditions.  Although these specific
30   experiments were performed in brine, they are consistent with the correlation between iron
31   chemistry and other metals observed in low ionic strength groundwater (Masue-Slowey et al.
32   2011; Holm and Curtiss 1989; Christensen et al. 2000).  The overall reaction sequence is given
33   by:

$$Pu(V/VI) \xrightarrow{\text{Rapid}} Pu(IV) \xrightarrow{\text{Slow}} Pu(III/IV) \qquad \text{(SOTERM.31)}$$

34   The predominance of Pu(III) at long times provides a strong data point on the reducing
35   conditions that iron creates under WIPP-relevant conditions, but does not account for radiolytic
36   impacts on $E_h$, and the effects of organic complexation which will stabilize Pu(IV) relative to
37   Pu(III).  These data, taken in context, strongly support the current WIPP PA assumption that
38   Pu(III) and Pu(IV) will be prevalent in the WIPP and both oxidation states will contribute to the
39   actinide source term.
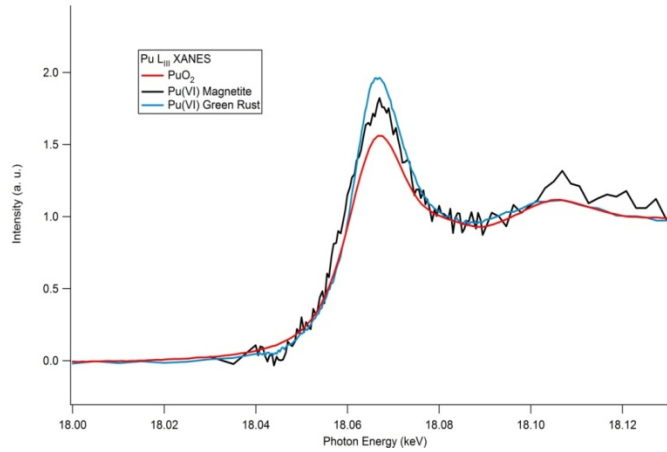
**Figure SOTERM-16. XANES Analysis of Plutonium Precipitates in the Magnetite and Iron Reduction Experiments at 3 Months. Pu(IV) phases were predominantly noted.**
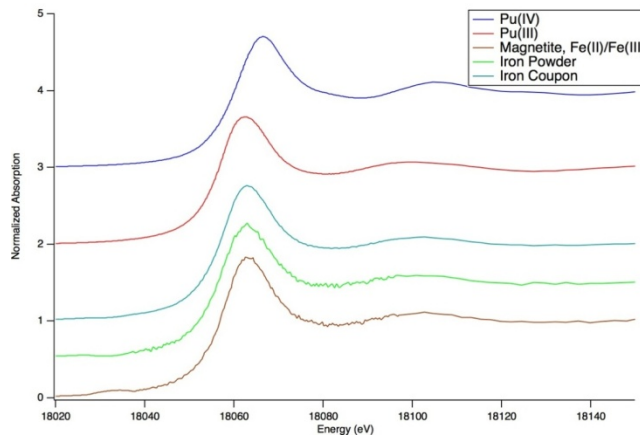


**Figure SOTERM-17. XANES Analysis of Solid Samples from the Pu-Fe Interactions Studies after ~ 6 Years. Pu(III) was the predominant oxidation state noted.**
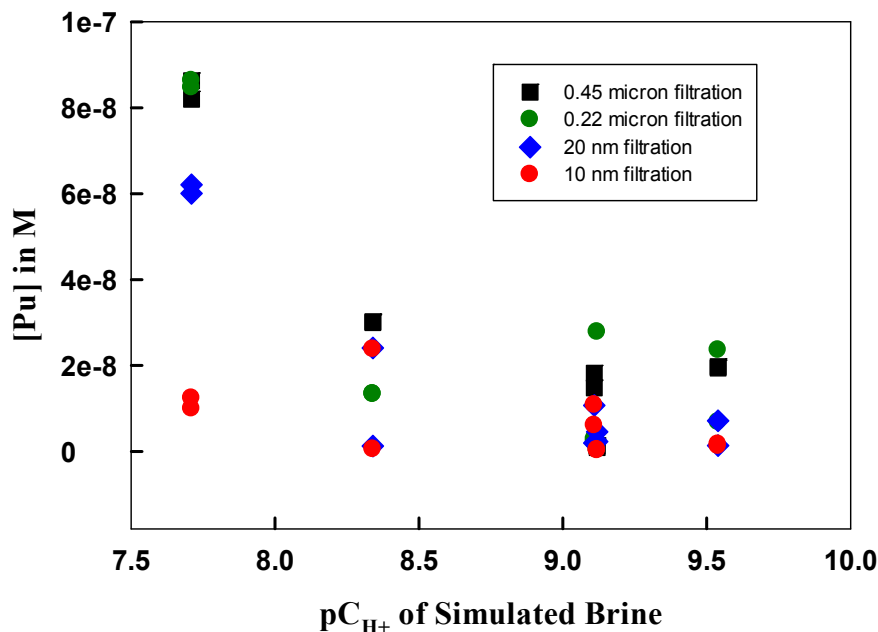
1

2    **Figure SOTERM-18. Effect of Filtration on the Measured Concentration of Plutonium**
3    **as a Function of $pC_{H+}$. Data shown are 0.45 μ (black squares),**
4    **0.22μ (green circles), 20 nm (blue diamonds) and 10 nm (red**
5    **circles) filtrations. Uncertainty in the filtration data, based on**
6    **ICP-MS analyses, is estimated to be ± 20%. The concentration**
7    **of 10 nm-filtered plutonium at $pC_{H+}$ ~ 9.5 is 3 x $10^{-7}$ M.**

8    **Table SOTERM-14. Qualitative Redox Indicators for Iron Interactions with Plutonium**
9    **under Anoxic Conditions**

| Experiment | Description | [a] Oxidation State of Pu Solid | [b] $[Fe]_{total}$ in mM (%$Fe^{2+}$ in solution) | [c] $E_h$ Measured (± 3 mV) |
|---|---|---|---|---|
| PuFe23OX | ERDA-6 brine at pH ~9 with excess magnetite | ~87% Pu(III), rest Pu(IV) | 0.12 (25%) | -122 mV |
| PuFeCE8 | ERDA-6 brine at pH ~8 with Fe coupon | ~100% Pu(III) | ND | ND |
| PuFeCE10 | ERDA-6 brine at pH ~ 9.6 with Fe coupon | ~100% Pu(III) | 0.27 (100%) | ND |
| PuFeP | ERDA-6 brine at pH~9 with excess Fe powder | ~100% Pu(III) | 0.18 (100%) | -175 mV |
| PuFeC | ERDA-6 brine at pH ~ 9 with Fe coupon | ~90% Pu(III), rest Pu(IV) | 0.18 (58%) | -110 mV |
| PuFeG7 | GWB brine at pH ~6.7 with Fe coupon | ~ 100% Pu(III) | 12.62 (97%) | -210 mV |
| a. Pu(III) content established by XANES analysis of solids b. Fe(II) content established by analysis using FerroZene® c. Eh measurement made using an Orion combination ORP electrode   ND – not determined | | | | |

1  # SOTERM-3.7 Americium and Curium Chemistry

2  There are relatively small quantities of Am in TRU waste (see Table SOTERM-9), and this is
3  anticipated to be ~ 0.203 metic tons at emplacement.  The high activity of $^{241}$Am (t$_{1/2}$ = 432 years,
4  3.443 Ci/g) makes Am a key contributor to potential actinide release from the WIPP at earlier
5  times in repository history (~26% initially, decreasing to 17% and ~0% at 1000 and 10,000 years
6  after emplacement). In the WIPP PA, Am is in the trivalent state in all vectors and the aqueous
7  concentration consists of Am$^{3+}$ complexes and colloidal species.

8  Cm is also present in very small quantities in the WIPP (Table SOTERM-9) and exists primarily
9  as the $^{244}$Cm isotope. The high activity of this isotope (t$_{1/2}$ = 18.11 years) makes Cm an important
10  species in the WIPP at the very early stages of repository history. It is essentially unimportant for
11  the PA because it has decayed away by the end of the 100-year period for active institutional
12  controls. However, other Cm isotopes with longer half-lives are present in the inventory and are
13  considered by the WIPP PA. The environmental chemistry of Am and Cm are very similar, and
14  most of what is said in this section about the environmental chemistry of Am also applies to Cm.

15  A more detailed review of the literature for Am can be found as part of a WIPP report
16  (Borkowski et al. 2008). The solubility of An(III) was measured in the WIPP brine over a wide
17  range of conditions using Nd(III) as a redox-invariant analog. These data support current WIPP
18  PA calculations for the solubility of Pu(III) and Am(III) in the WIPP brine and are also
19  summarized in Borkowski et al. (Borkowski et al. 2008).

20  ## SOTERM-3.7.1 Americium and Curium Environmental Chemistry

21  Am is a 5f electron element and, like other elements of the actinide group, can exist in aqueous
22  solution in several oxidation states. The electrode potentials for some Am couples are presented
23  in Figure SOTERM-19.  The trivalent state of Am is the most stable aqueous oxidation state
24  (Katz, Seaborg, and Morss 1986, p. 912), and it is quite difficult to oxidize in aqueous solution
25  (Hobart, Samhoun, and Peterson 1982). The trivalent Am ion has an ionic radius of 97.5
26  picometers (pm) (coordination number [CN]=6) and its chemical properties can be used as an
27  analog for Pu(III), which has a similar ionic radius (100 pm at CN=6) and charge density, as well
28  as for Cm(III) (97 pm at CN=6).
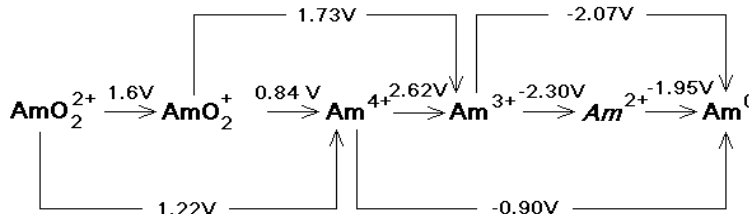


29

30  **Figure SOTERM-19.  Redox Potential for Some Am Redox Couples (Silva et al. 1995,**
31  **p. 74)**

32

1 The *Am(II)* species is italicized to stress that it is only a transient species. As discussed by
2 Martinot and Fuger (Martinot and Fuger 1985), there is evidence for the formation of *Am(II)* in
3 aqueous perchlorate solution in the pulse radiolysis experiment. The half-life of this species was
4 estimated to be approximately 5 μs. This species is not observed during the electroreduction of
5 Am(III) to the metal in noncomplexing media (David, Maslennikov, and Peretrukhin 1990).
6 Cm is also distinguished by the relatively great stability of the III oxidation state with respect to
7 oxidation or reduction (Katz, Seaborg, and Morss 1986, p. 970). The stability of Cm(III) may be
8 attributed to the half-filled f-shell electronic configuration ($5f^7$). The oxidation of Cm(III) is
9 achieved only with the strongest oxidizing agents, and only one report claims evidence for an
10 oxidation state higher than IV (Korpusov, Patrusheva, and Dolidze 1975). The Cm(III) to
11 Cm(IV) transition has not been successfully induced by ozone or electrochemically, and the
12 Cm(IV) phosphotungstate produced by oxidizing with peroxysulfate is considerably less stable
13 than the Am(IV) analog (Katz, Seaborg, and Morss 1986, p. 971). In the reducing environment
14 of the WIPP repository, any higher-valent Cm produced radiolytically would be unstable. For all
15 these reasons, the predominant oxidation state for Cm in the WIPP environment is Cm(III).

16 Higher-valent Am species have also been noted. Am(IV) species, with an ionic radius estimated
17 by Shannon (Shannon 1976) to be 85 pm, is only stable in the presence of strongly complexing
18 anions such as carbonate, fluoride, phosphate, or phosphotungstate, and was never found in any
19 appreciable amount in trivalent Am solutions.

20 The pentavalent and hexavalent dioxoamericium ions $AmO_2^+$ and $AmO_2^{2+}$ can be generated
21 under strongly oxidizing conditions. Free radicals produced from α particles in water readily
22 reduce these dioxoamericium ions back to $Am^{3+}$. In concentrated NaCl solution, in which the
23 radiolysis products are strong oxidants, pentavalent and hexavalent Am are the predominant
24 species (Büppelmann et al. 1986). Without an oxidant, the pentavalent dioxoamericium ion
25 slowly disproportionates to $AmO_2^{2+}$ and $Am^{3+}$. These higher oxidation states are not stable in
26 natural waters and can be readily reduced by action of reductants naturally present in those
27 waters.

28 The speciation of Am in groundwater under mildly alkaline conditions is primarily defined by
29 hydrolysis and carbonate complexation. Hydrolysis is generally represented by the following
30 reaction:

31 $$Am^{3+} + nH_2O \;\leftrightharpoons\; Am(OH)_n^{(3-n)} + nH^+ \qquad\qquad (SOTERM.32)$$
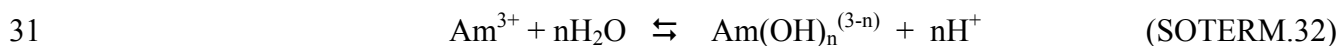
32 Silva measured the $^{243}$Am(OH)$_3$(crystalline [cr]) and Nd(OH)$_3$(cr) solubilities in 0.1 M NaClO$_4$
33 solution at $25 \pm 1$ $^{\circ}$C within the pH range 6 to 10 (Silva et al. 1995, p. 79-97). This is the only
34 study with Am hydroxide using an x-ray-characterized crystalline solid. The solid phase was
35 prepared by rigorously controlled, high-temperature transformation of Am(OH)$_3$(am). Optical
36 viewing by SEM of the solid samples at the end of the solubility experiments showed no changes
37 in the crystal. The use of the $^{243}$Am isotope diminished α-particle damage of the crystal as a
38 result of the 17-times-lower specific activity compared to $^{241}$Am. The weakness of this
39 experiment was the relatively short equilibration time of only 48 days. A log ($K_{sp}$) of $16.6 \pm 0.4$
40 was obtained for the Am(OH)$_3$ phase. The corresponding hydrolysis constants are listed in Table
41 SOTERM-15. Similar values for Nd(III) hydrolysis were derived from the Nd(OH)$_3$(cr)
42 solubility measurements.

1  Stadler and Kim (Stadler and Kim 1988) investigate the pH dependence of $Am(OH)_3(s)$
2  solubility in 0.1 M $NaClO_4$ and more concentrated Na chloride and perchlorate solutions at $25 \pm$
3  0.5 $^{\circ}C$. The effect of $\alpha$-induced radiolysis on solubility was also studied using different total
4  concentrations of [241]Am. The solid phase was not characterized in this work. Although the solid
5  used in this work was different than that used by Silva et al. (Silva et al. 1995, pp. 275–76), the
6  reported solubility products are in agreement. It is unclear, however, if the same phase controls
7  the Am solubility in these two cases, because of markedly different preparation conditions of the
8  starting solids.

9  Kim et al. (Kim et al. 1984) measured the solubility of $Am(OH)_3(s)$ at I = 0.1 and 0.3 M $NaClO_4$,
10 in the absence of $CO_2$ and at $pCO_2 = 10^{-3.5}$ atm, and attributed the solubility measured in terms of
11 contributions from the hydroxy, carbonato- and mixed Am hydroxy-carbonato complexes.  No
12 characterization of the solid was reported in this work, so it was assumed to be $AmCO_3OH(s)$.
13 Several investigators found that changes in the solid phase in aqueous suspensions of Am(III)
14 hydroxide due to aging conditions become evident in hours and continue for weeks. Similar
15 results were reported by Felmy, Rai, and Fulton (Felmy, Rai, and Fulton 1990). These authors
16 measured the solubility of $AmCO_3OH(cr)$ at $pCO_2 = 10^{-3}$ atm.  The change in total Am
17 concentration measured in this work as a function of pH was similar to that reported by Kim et
18 al. (Kim et al. 1984).  Similar plots for the solubility of Nd in 5 M NaCl were measured by
19 Borkowski et al. (Borkowski et al. 2008); however, the Nd concentrations obtained for the
20 comparable $pC_{H+}$ values were two to three orders of magnitude greater as a result of the higher
21 ionic strength present.

22 **Table SOTERM-15.  Hydrolysis Constants of Am(III) (in Logarithmic Units)**
23 **Corresponding to Equation SOTERM.32**

| $AmOH^{2+}$ | $Am(OH)_2^+$ | $Am(OH)_3(aq)$ | Medium | Reference |
|---|---|---|---|---|
| $-7.93 \pm 0.35$ | $-14.77 \pm 0.25$ | $-24.71 \pm 0.11$ | 0.1 M $NaClO_4$ | Kim et al. 1984 |
| $-7.5 \pm 0.3$ | $-15.4 \pm 0.4$ | $-26.9 \pm 0.5$ | 0.1 M $NaClO_4$ | Stadler and Kim 1988 |
| $-7.8 \pm 0.4$ | $-15.4 \pm 0.5$ | $-26.9 \pm 0.5$ | 0.1 M NaCl | Stadler and Kim 1988 |
| $-8.1 \pm 0.3$ | $-15.8 \pm 0.4$ | $-27.0 \pm 0.5$ | 0.6 M NaCl | Stadler and Kim 1988 |
| $-7.7 \pm 0.3$ | $-16.7 \pm 0.7$ | $-25.0 \pm 0.3$ | 0.1 M $NaClO_4$ | Silva et al. 1995, p. 81 |
| $-6.9 \pm 0.2$ | | $-23.8 \pm 0.9$ | 0.1 M $NaClO_4$ | Rösch et al. 1989 |
| $<-8.2$ | $-17.1 \pm 0.7$ | $<-27.0$ | $I \rightarrow 0$ | Rai et al. 1983 |
| $-6.40 \pm 0.11$ | $-13.40 \pm 0.16$ | $-20.31 \pm 0.17$ | 3 M $NaClO_4$ | Pazukhin and Kochergin 1989 |
| $-7.0 \pm 0.4$ | $-15.1 \pm 0.4$ | $-26.4 \pm 0.5$ | 0.1 M $NaClO_4$ | Silva et al. 1995, p. 294 |
| $-7.2 \pm 0.5$ | $-15.1 \pm 0.7$ | $-26.2 \pm 0.5$ | I = 0.1 M | Neck et al. 2009, p. 1557 |

24

1   Am complexation by carbonate was extensively investigated by solvent extraction,
2   spectrophotometry, electromigration, and solubility (Kim et al. 1984; Rösch et al. 1989; Felmy,
3   Rai, and Fulton 1990; Meinrath and Kim 1991; Nitsche et al. 1995; Torretto et al. 1995).  Many
4   different soluble species have been proposed for the Am-water-carbonate system: pure
5   carbonate, bicarbonate, and/or mixed hydroxy-carbonate complexes. Silva et al. (Silva et al.
6   1995) carefully studied and reinterpreted the literature data.  It is the consensus in these studies
7   that $Am(CO_3)_n^{(3-2n)}$, with n = 1, 2 and 3, are the predominant carbonate complexes.  According to
8   Silva et al. (Silva et al. 1995), there is no experimental evidence for the existence of a complex
9   with n = 4 even at the highest carbonate concentrations.  The report also suggests that there is no
10  evidence for the formation of Am(III)-bicarbonate or hydroxy-carbonate complexes in solution.
11  These data are, however, in disagreement with the more recent work done by Fanghänel and Kim
12  (Fanghänel and Kim 1998), which reports spectroscopic evidence for the formation of the n = 4
13  species.

14  Data reported by Kim et al. (Kim et al. 1984) indicate that up to $pC_{H+}$ = ~8.0, the carbonate
15  complexation does not affect the solubility of Am(III).  Analysis of Yuci groundwaters by Chen
16  et al. (Chen et al. 2010), with a composition and $E_h$ intermediate to the Yucca Mountain J-13 and
17  UE-25 well compositions, demonstrates an americium carbonate solubility of $1.8 \times 10^{-9}$ M at pH =
18  7.0 and $1.2 \times 10^{-9}$ M at pH = 8.5 when equilibrated against solid $AmOH(CO)_3$.  The presence of
19  $10^{-4} – 10^{-2}$ M carbonate was shown not to influence amercium solubility in the pH range of 8-10.
20  For the higher $pC_{H+}$, the presence of carbonate in 0.1-0.3 M $NaClO_4$ increases solubility of
21  Am(III) in relation to carbonate-free systems, and at $pC_{H+}$ = 10 this difference is almost 4 orders
22  of magnitude.  The predominance of carbonate complexation is observed in the $pC_{H+}$ range from
23  7.5 to 10.  At higher $pC_{H+}$, hydrolysis predominates over carbonate complexation.

24  Neck et al. (Neck et al. 2009) used known data on the solubility of $Am(OH)_3$, the hydrolysis of
25  Am(III) and Cm(III), additional data from an extensive solubility study of $Nd(OH)_3$(s) in NaCl,
26  $MgCl_2$ and $CaCl_2$ media of various ionic strength media and time resolved laser induced
27  fluorescence (TR-LIF) data for Cm(III) in alkaline $CaCl_2$ to evaluate a comprehensive set of
28  standard-state equilibrium constants and ion interaction parameters for the specific ion
29  interaction theory SIT and Pitzer equations at 25 $^oC$ in the M(III) - $H^+$ - $Na^+$ - $Mg^{2+}$ - $Ca^{2+}$ - $Cl^-$ -
30  $OH^-$ - $H_2O$ system.  The solubility and hydrolysis behavior of Am(III), Cm(III) and Nd(III) in
31  both calcium-free and calcium-containing solutions is consistently described using a model that
32  includes the ternary Ca-M(III)-OH complexes $Ca[M(OH)_3]^{2+}$, $Ca_2[M(OH)_4]^{3+}$ and
33  $Ca_3[M(OH)_6]^{3+}$.   Data are presented in Neck Tables 1, 2 and 3 for the SIT and Pitzer parameters
34  for this system.  Solubility studies in NaCl – NaOH, $NaClO_4$ – NaOH, pure NaOH and KOH
35  solutions up to pH = 14 showed no evidence for the formation of $Am(OH)_4^-$, which would
36  increase the americium solubility at high pH.  Study of the TR-LIF behavior of curium in
37  alkaline solutions of various media at pH > 10 showed that $Cm(OH)_3$(aq), which would be
38  expected to dominate the speciation at pH = 11-14, nor the complex $Cm(OH)_4^-$, could be
39  detected, primarily due to low curium solubility.  Almost all of the curium is present as
40  $Cm_m(OH)_{3m}$ polymers or colloidal $Cm(OH)_3$(am).  In alkaline $CaCl_2$ solutions at I = 0.1 – 3M
41  and pH ~ 10.5, as opposed to the sodium-based media above, the behavior of curium is strikingly
42  different.  Cm(III) emission bands were observed caused by complexes with three, four and six
43  $OH^-$ ligands.  These complexes, not found in NaCl – NaOH media, are stabilized by the
44  association of $Ca^{2+}$ ions, e.g., the ternary complexes $Ca_p[Cm(OH)_n]^{3+2p-n}$.  Stability constants for
45  the complexation reaction:

1
$$pCa^{2+} + Cm^{3+} + nH_2O = Ca_p[Cm(OH)_n]^{3+2p-n} + nH^+ \quad \text{(SOTERM.33)}$$

2   are log $^*\beta^o_{1,1,3}$ = -26.3 ± 0.5, log $^*\beta^o_{2,1,4}$ = -37.2 ± 0.6 and log $^*\beta^o_{3,1,6}$ = -60.7 ± 0.5.  These
3   reactions do not affect the WIPP case under current conditions.

4   An extensive series of experiments, reported for CRA-2009, were performed to determine the
5   solubility of Nd(III) as an analog for Pu(III) and Am(III) solubility in the brine (Borkowski et al.
6   2008). In this study, the solubility was determined in GWB and ERDA-6 brine, over a pH range
7   of 6-12, and as a function of carbonate concentration. These solubility data extended earlier
8   studies in simplified brines to simulated WIPP brine compositions and cover a broader range of
9   experimental conditions.  A composite of literature and WIPP-specific data is shown in Figure
10  SOTERM-20.



11
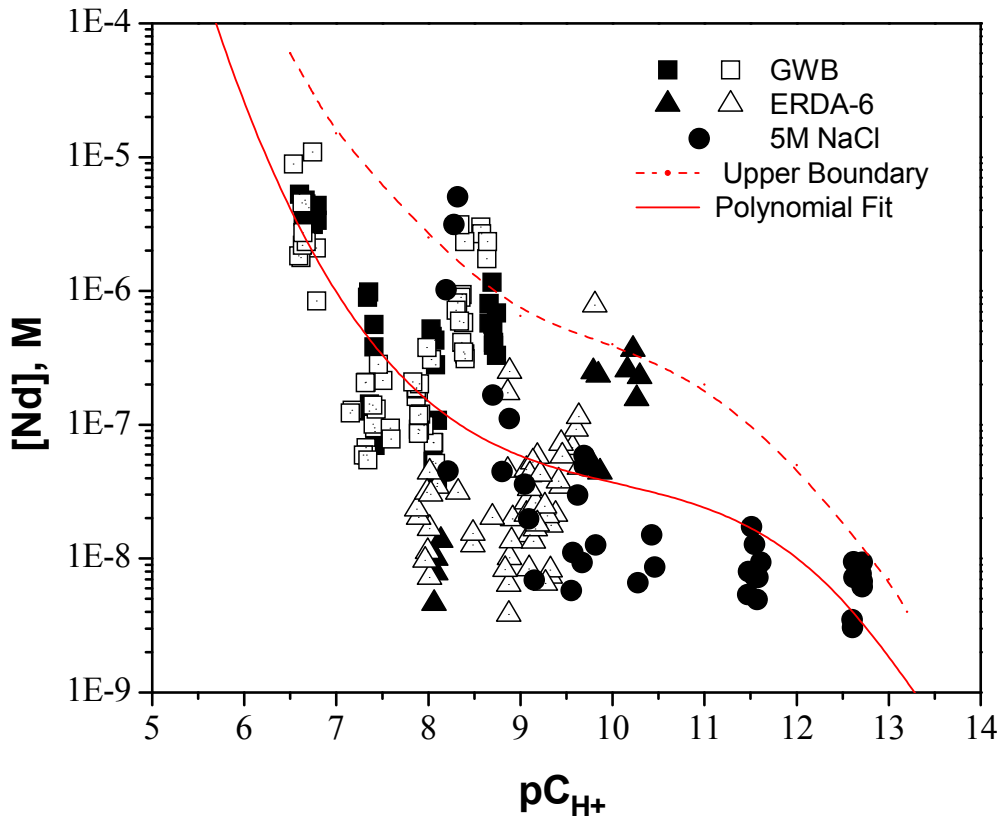
**Figure SOTERM-20.  Composite of Nd Solubility Trends Under All Conditions**
**Investigated (Borkowski et al. 2008). Open symbols correspond**
**to undersaturation experiments and closed symbols correspond**
**to oversaturation experiments.**

16  **SOTERM-3.7.2 WIPP-Specific Results since the CRA-2009 and the CRA-2009 PABC**

17  There are no new WIPP-specific data since CRA-2009 and CRA-2009 PABC that is centered on
18  the solubility of An(III) in brine.  New data showing the impacts of organic complexation are
19  summarized in section 3.8.

1    # SOTERM-3.8 Complexation of Actinides by Organic Chelating Agents

2    The complexation of chelating agents with actinides has a significant impact on the
3    concentrations of actinides in brine.  At the pH of interest to the WIPP PA, only EDTA and
4    citrate complex strongly enough to impact observed concentrations and this impact is mostly
5    centered on the An(III) oxidation state.

6    **SOTERM-3.8.1 Stability Constants for Organic Complexation with Actinides**

7    The stability constants for organic ligand-actinide complexation were determined as part of the
8    WIPP ASTP at Florida State University (Choppin et al. 1999). These data are summarized in
9    Table SOTERM-16 and demonstrate some key trends in actinide complexation. For acetate,
10   oxalate, and citrate, the strength of the complex formed is in the same order: IV > VI > III > V.
11   For EDTA, the VI and III are switched. For the most part, the III and IV actinides, which are the
12   two most important oxidation states in the WIPP, are strongly affected by organic complexation
13   and thus can out-compete carbonate and hydrolysis if the organic concentrations are high
14   enough. Of the four organic chelating agents considered, only citrate and EDTA are expected to
15   form strong enough complexes to influence the speciation of actinides and potentially increase
16   actinide concentrations under the expected conditions in the WIPP.

17   **Table SOTERM-16.  Apparent Stability Constants for the Complexation of Organic**
18   **Ligands with Actinides in NaCl Media (Choppin et al. 1999)**

| Organic Ligand | Actinide Ion | NaCl (molality) | $\log_{10} \beta_1$ |
|---|---|---|---|
| Acetate | $Am^{3+}$ | 0.3 to 5 | 1.44 - 2.2 |
|  | $Th^{4+}$ | 0.3 to 5 | 3.68 - 4.18 |
|  | $NpO_2^+$ | 0.3 to 5 | 1.05 - 1.8 |
|  | $UO_2^{2+}$ | 0.3 to 4 | 2.23 - 3.09 |
| Oxalate | $Am^{3+}$ | 0.3 to 5 | 4.17 - 4.63 |
|  | $Th^{4+}$ | 0.3 to 5 | 7.04 - 7.47 |
|  | $NpO_2^+$ | 1.0 to 5.0 | 3.62 - 4.63 |
|  | $UO_2^{2+}$ | 0.3 to 5 | 5.82 - 6.7 |
| Citrate | $Am^{3+}$ | 0.3 to 5 | 4.84 - 5.9 |
|  | $Th^{4+}$ | 0.1 to 5 | 9.31 - 10.18 |
|  | $NpO_2^+$ | 0.1 to 5 | 2.39 - 2.56 |
|  | $UO_2^{2+}$ | 0.3 to 5 | 7.07 - 7.32 |
| EDTA | $Am^{3+}$ | 0.3 to 5 | 13.76 - 15.1 |
|  | $Th^{4+}$ | 0.3 to 5 | 15.56 - 16.94 |
|  | $NpO_2^+$ | 0.3 to 5 | 5.45 - 6.7 |
|  | $UO_2^{2+}$ | 0.3 to 4 | 10.75 - 12.16 |

19

20   The possible impact of isosaccharinic acid (ISA) on thorium speciation was also considered.
21   ISA is a chemical breakdown product of cellulosic material that has been shown to occur at
22   pH>12.  The two diastereoisomers, α- and β-isosaccharinic acids, are the products of chemical
23   degradation of cellulosic materials in alkaline solutions. The alkaline degradation of different
24   cellulosic materials was studied for the alkaline conditions that may exist in the initial stages of a
25   cementitious repository (pH ~ 13.3). ISA is expected to be present in cement pore water, but it is

1  strongly adsorbed to the cement surface. In the pore water, the concentration of ISA is expected
2  to reach $10^{-4}$ M (Van Loon et al. 1997). The complexation data for ISA is very limited and there
3  are no literature references for the tetravalent cations such as thorium. ISA is structurally a 2-
4  hydroxycarboxylic acid; therefore, by analogy we can relate the complexation of thorium by ISA
5  to the stability constants for Th(IV) with glycolic acid, lactic acid and 2-hydroxybutanoic acid
6  (log K of 4.3, 4.2 and 3.8 respectively). Ligands with such low stability constants cannot
7  outcompete An(IV) hydrolysis.

8  Rai et al. (Rai et al. 2000) developed a model for Th(IV) complexation with ISA. The major
9  feature of their model is the predominance of thorium ternary complexes, e.g., $Th(OH)_4ISA_2^{2-}$ ,
10 not $ThISA_2^{2+}$ complexes, as was proposed by Allard and Ekberg (Allard and Ekberg 2006a and
11 Allard and Ekberg 2006b). According to Rai's model, mM ISA concentrations will not affect
12 solubility of thorium. Data for higher ISA concentrations might be questionable, because Rai's
13 model is based on 15 and 69 days equilibration times for $\sim10^{-6}$ M thorium concentrations. On the
14 basis of our experiments and those published by German researchers, µM thorium concentrations
15 can persist for years as a metastable state without ISA present. Complexes with a similar
16 stoichiometry were also observed for uranium (VI) and the authors did not observe any enhanced
17 solubility caused by ISA for pH in the range of 9.0 to 13.5 (Warwick et al. 2006).

18 For WIPP-related conditions, the occurrence of cellulosic chemical degradation pathways have a
19 very low probability and, even if degradation occurs, the ISA formed will likely have a
20 negligible effect on An(IV) solubility.

## SOTERM-3.8.2 WIPP-specific Data on Organic Complexation Effects Since CRA-2009 and CRA-2009 PABC

23 The effect of organic complexation on the An(III) and An(IV) oxidation state were evaluated
24 under WIPP-relevant conditions.  EDTA and citrate had a strong effect on the An(III) solubility,
25 but had essentially no impact on An(IV).

26 The effect of organic complexation on the solubility of Th(IV), as the An(IV) actinide analog,
27 was determined in GWB brine in the presence of inventory-predicted organic concentration.  The
28 simultaneous presence of four organic chelating agents ($2.42 \times 10^{-3}$ M acetate, $3.02 \times 10^{-2}$
29 oxalate, $3.62 \times 10^{-3}$ citrate and $9.28 \times 10^{-5}$ EDTA) led to a measured thorium solubility of $7.34 \times$
30 $10^{-7}$ M in GWB brine at $pC_{H+} = 9.3$.  This is in agreement with the 2-year solubility data
31 (Borkowski et al., 2012) of $5 \times 10^{-7}$ M and there is an order of magnitude agreement with the
32 recently calculated thorium solubility for CRA-2014 (Brush and Domski 2013a).  These
33 experimental data confirm that there is no significant effect on the measured thorium solubility
34 due to the presence of the organic chelators at or near their inventory-predicted limits.

35 The effect of organic complexation on the concentration of neodymium, as the An(III) analog,
36 was also evaluated for each key chelating agent.  These data are shown in Figure SOTERM-21.
37 These data show a strong effect of citrate and EDTA where a 1:1 complex with the neodymium
38 is being formed and the concentration of the neodymium is approximately the concentration of
39 EDTA  in ERDA-6 brine and ~ 50% of the concentration of EDTA in GWB brine.
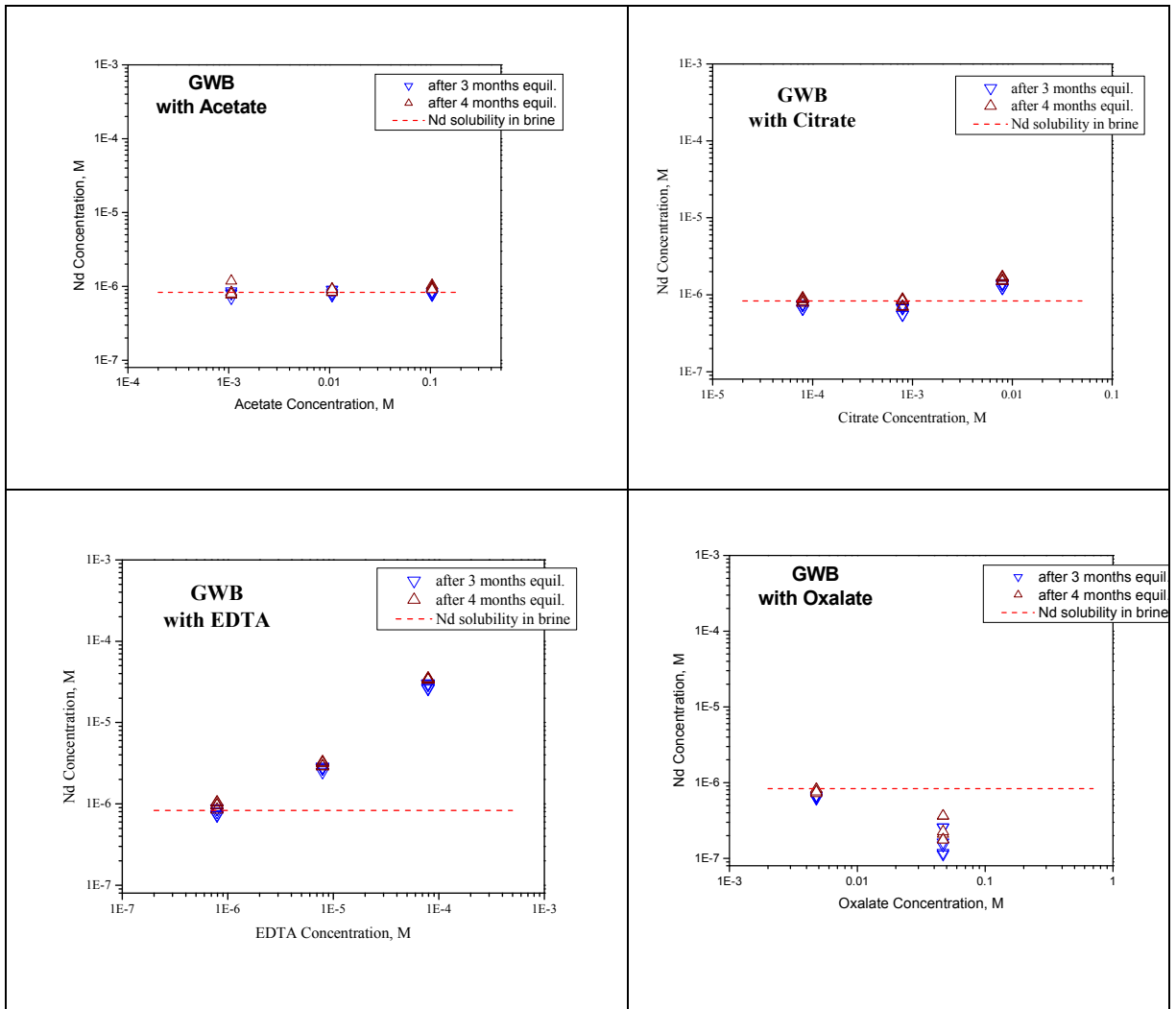
1  **Figure SOTERM-21.  Effect of EDTA, Citrate, Oxalate and Acetate on the Solubility of**
2  **Nd$^{3+}$ in GWB Brine.**

3  ## SOTERM-3.9 Actinide Colloids

4  The potential for colloidal species to have a role in defining the solution concentration and
5  mobility of actinides in the WIPP was recognized early in the WIPP licensing process.  This led
6  to the development of a colloid model that accounts for these colloidal species.  This model was
7  based on an extensive literature review, some WIPP-specific experimental data, and some
8  conservative simplifications that were extensively peer reviewed prior to the first license
9  application (CCA).  In this model, four types of colloids that could contribute to the actinide
10  source term are identified:  intrinsic, mineral, microbial and humic.  The EPA found this model
11  and approach to be satisfactory in the WIPP certification and subsequently in the CRA-2004 and
12  CRA-2009 recertification.  There has been essentially no change in this model since its initial
13  certification by the EPA.

14  Actinide colloids in the WIPP are potentially important since the actinide source term is defined
15  by the WIPP PA as the sum of contributions from dissolved actinide species and mobile colloidal

1 actinide species (see U.S. DOE 2004, Appendix SOTERM-2004, and Reed et al. 2013) for a
2 more detailed discussion of WIPP-relevant colloids). The importance of colloids in the migration
3 and transport of actinide contaminants, although it continues to receive attention in the literature,
4 remains somewhat controversial and difficult to prove. In this context, the consideration of
5 colloidal enhancement of actinide concentrations by the WIPP PA is, at least in part, a
6 conservatism that is built into the overall PA approach. In this context, the sorption of colloidal
7 actinides onto fixed substrates and their filtration in low-porosity media will also reduce the
8 mobile colloidal actinide source term, but no credit is currently being taken for this potentially
9 significant reduction in colloidal concentrations.

10 Actinide colloids or pseudocolloids may be generated in the WIPP repository as a result of

11 1. Hydrolysis (intrinsic chemistry).

12 2. The interactions of dissolved actinide species with microbially derived colloids or colloids
13    formed due to the corrosion of steel and waste constituents.

14 3. The hydrodynamic entrainment of colloidal-sized mineral fragments, as well as several other
15    mechanisms.

16 The formation of colloids could enhance actinide release in two ways. First, increased actinide
17 concentration will increase the magnitude of DBR release and the effective actinide source term
18 concentration for transport through the Culebra. Second, colloids have very different transport
19 properties than dissolved species, and are predicted to migrate more rapidly in the subsurface.
20 This transport mechanism could enhance the overall actinide release in the WIPP through
21 migration pathways in the Culebra member and the Salado.

22 The current WIPP colloidal model defines four potential colloidal contributions to the mobile
23 actinide concentration that comprises the actinide source term:

24 Four potential types of colloids are recognized in the CCA and these definitions have not
25 changed since then.

26 *1. Mineral fragments are hydrophobic, hard-sphere particles that are kinetically stabilized or*
27    *destabilized by electrostatic forces, and may consist of crystalline or amorphous solids.*
28    *Mineral fragments may be made kinetically stable by coatings with steric stabilizers that*
29    *prevent close contact. Mineral fragments may act as substrates for sorption of actinides or*
30    *they may consist of precipitated or coprecipitated actinide solids.*

31 *2. Actinide intrinsic colloids are macromolecules of actinides that, at least in some cases, may*
32    *mature into a mineral-fragment-type of colloidal particle. When immature, they are*
33    *hydrophilic; when mature, they become hydrophobic.*

34 *3. Humic substances are hydrophilic, soft-sphere particles that are stabilized by salvation*
35    *forces. They are often powerful substrates for uptake of metal cations and are relatively*
36    *small (less than 100,000 atomic mass units).*

4.  *Microbes are relatively large colloidal particles that are stabilized by hydrophilic coatings on their surfaces, which behave as steric stabilizing compounds.  They may act as substrates for extracellular actinide sorption or they may actively bioaccumulate actinides intracellularly.*

In this section, the general environmental aspects of colloid-enhanced transport in the subsurface are discussed, along with an update of relevant WIPP-specific results since the CRA-2009 PABC.

**SOTERM-3.9.1 Actinide Colloids in the Environment**

The extent and potential formation of actinide colloids continues to be debated by researchers in the field.  Since the CCA, there have been over 100 publications on actinide colloid chemistry that range in topics from real-system transport studies to the structure and inherent stability of actinide colloids.  These remain largely focused on plutonium and its associated and very complex subsurface chemistry, but there are also studies on neptunium, americium, thorium and curium reported in the literature.  It is also important to note that relatively few of these studies specifically address ionic-strength effects on colloid formation, stability and mobility.  In this context, there are very few studies that in high ionic-strength systems (I > 5 M) and only a small fraction of these studies have direct application to the WIPP repository safety case.

A more extensive literature review is provided elsewhere (Reed et al. 2013).  Key observations from the literature that impact the WIPP colloid model parameters are:

- A wide variety of actinide colloids are now noted to form in natural systems (see for example Khasanova et al. 2007).  This differs somewhat from the conclusion made at the time of the CCA that only Pu colloids could form.

- Colloids that form in nature tend to be associated with iron colloidal species and tend to help immobilize rather than mobilize actinides.  This is consistent with the WIPP model assumptions that only iron mineral colloids seem to form (see also new WIPP-specific date in section SOTERM-3.9.2).  Colloidal species in the WIPP conceptualization primarily add to the source term concentration with only a small contribution to transport pathways through the Culebra.

- There are new data showing the existence of nanoclusters as an integral part of the aqueous speciation of some actinides.  These are also seen in WIPP-specific brine systems (Reed et al. 2013; Section SOTERM-3.9.2).

- Bioassociation of actinides is observed in the literature and we have shown that this also extends to halophilic microorganisms (Figure SOTERM-22; Ams et al. 2013; Reed et al. 2013; Section SOTERM-3.9.2).
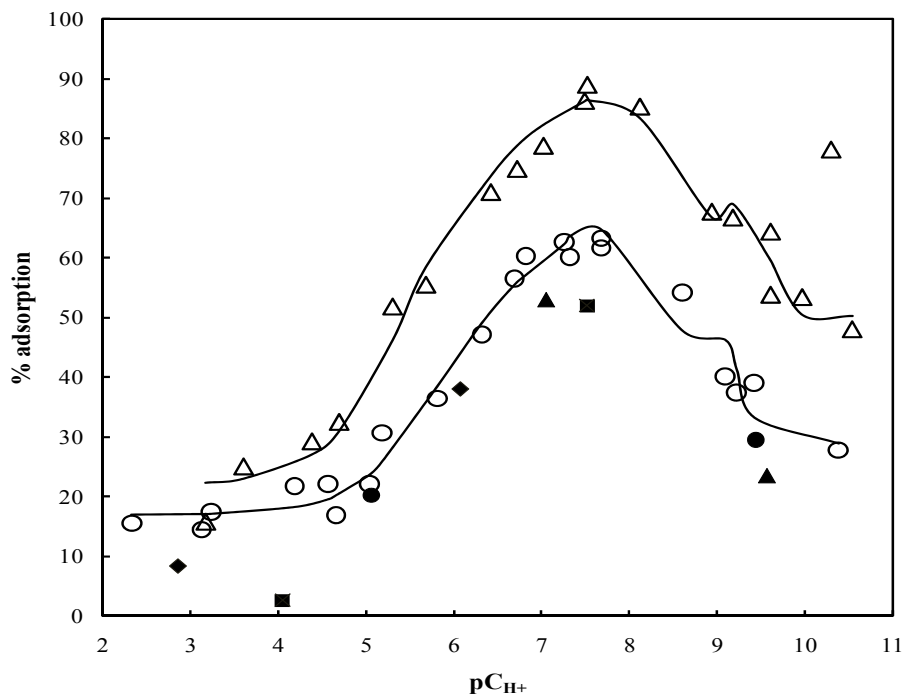
1

2  **Figure SOTERM-22.   Experimental Data for Neptunium (V) Adsorption onto**
3  **Chromohalobacter sp. as a Function of pH in 2 (Open Circles)**
4  **and 4 (Open Triangles) M NaClO$_4$.  Adsorption experiments**
5  **were performed with 5 x 10$^{-6}$ M total neptunium (V) and 5 grams**
6  **per liter (g/L) (wet weight) bacteria (Ams et al. 2013).  Solid**
7  **curves represent best-fit calculated surface complexation models.**
8  **Solid diamonds, squares, triangles, and circles represent the**
9  **results of desorption experiments performed with 5 x 10$^{-6}$ M total**
10  **neptunium (V) and 5 g/L (wet weight) bacteria in 2 M NaClO$_4$.**

11  *Overall Impact of literature publications on the WIPP Colloid Model*

12  Although there continues to be some progress made in the assessment of the colloidal issue as it
13  applies to the potential subsurface migration of actinide species, there remains a great deal that is
14  not well understood and substantive progress in this area is not likely in the very near future.
15  The following general recommendations remain:

16  • It remains critical that the WIPP model continue to address the colloid issue.

17  • There is no literature evidence that the current four-colloid type model is inadequate; if
18  anything it continues to be a conservative assumption built into the model.

19  • Current literature shows that colloidal species, intrinsic and mineral, of a number of
20  actinides, not just plutonium, is observed – this is somewhat of a departure from the
21  initial CCA literature survey conducted.  These literature data, however, still do not
22  explicitly address high ionic-strength systems.

1 • The structural data point towards intrinsic colloids that persist as very small (typically <
2   10nm) species.

3 • Biosorption data show that increased ionic-strength increased the extent of sorption and
4   the overall trend with pH was to go through a maximum at about pH 8 and then decrease
5   with increasing pH. At the predicted $pC_{H+}$ of ~ 9.4 in the WIPP site, biosorption is in the
6   range of ~ 40-65%.

**SOTERM-3.9.2 WIPP-Specific Results since the CRA-2009 and CRA-2009 PABC**

8  The mineral, intrinsic and microbial contribution to the WIPP mobile colloidal actinide source
9  term model was re-examined in light of recent literature results and new WIPP-specific data
10 (Reed et al. 2013). An extensive amount of work under WIPP-specific conditions was
11 completed to re-assess the microbial colloid enhancement parameters. There were some
12 discrepancies in the model in this area due to the lack of extensive WIPP-specific data at the time
13 of the CCA. These experiments build on the more extensive understanding that we now have
14 about the microbial ecology in the WIPP. Microbial colloid enhancement parameters based on
15 these new data are recommended and these are, in general, more realistic and lead to a lower
16 overall contribution of microorganisms to the actinide source term.

17 As a whole, the WIPP-specific data obtained since CRA-2009 provide the first WIPP-specific
18 data on colloids since the time of the CCA. These data, although not complete, provide
19 significant improvement in our understanding of the potential contribution of colloidal species to
20 the actinide source term. Additionally, some inconsistencies between the known solution
21 chemistry and literature observation are addressed. Updated parameters (see discussion in
22 Section SOTERM-4.0) for the intrinsic, mineral and microbial colloid enhancement parameters
23 are recommended.

**SOTERM-3.9.2.1 Intrinsic and Mineral Colloids**

25 The intrinsic and mineral colloidal fraction of the actinides and analogs investigated as part of
26 the long-term solubility studies was determined to provide WIPP-specific data. The size
27 fractionation was determined using ultrafiltration and, in some cases, ultracentrifugation methods
28 down to ~ 2.5 nm. In almost all cases, <10 nm size nanospecies were observed and assigned to
29 the intrinsic colloidal fraction. The >10 nm size fraction was also established and used to
30 evaluate the existence of mineral colloids.

31 The size distribution of aqueous species was shown for thorium and plutonium(III) in Figures
32 SOTERM-10 and SOTERM-18 respectively. Additionally, results were obtained for
33 neodymium (Figure SOTERM-23), uranium (Figure SOTERM-24) and plutonium in more detail
34 (Figure SOTERM-25). In most cases, there was no filtration effect above 10 nm with the
35 notable exception of plutonium where iron was also present in solution. There was no evidence
36 for Mg-derived colloidal contributions.
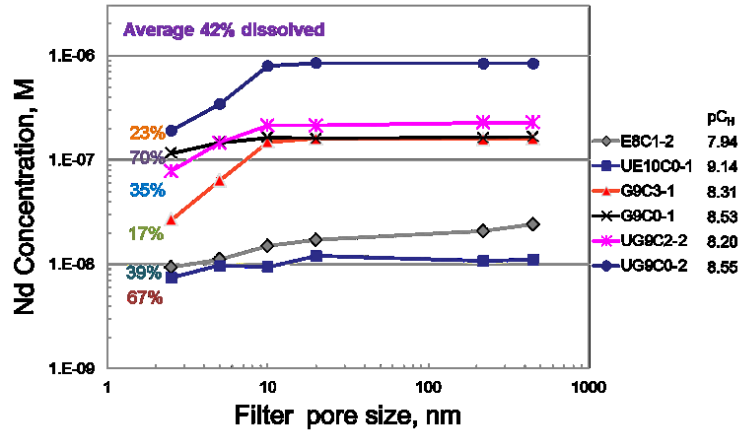
1
2       **Figure SOTERM-23.  Sequential Filtration Results for the Long-term Neodymium**
3                        **Solubility Studies in Brine (E = ERDA-6; G = GWB) as a**
4               **Function of Filter Pore Size for Different pC$_{H+}$ and Brines.**
5           **Significant filtration effects are only noted for filters that are 10**
6                                   **nm or smaller in size.**



7
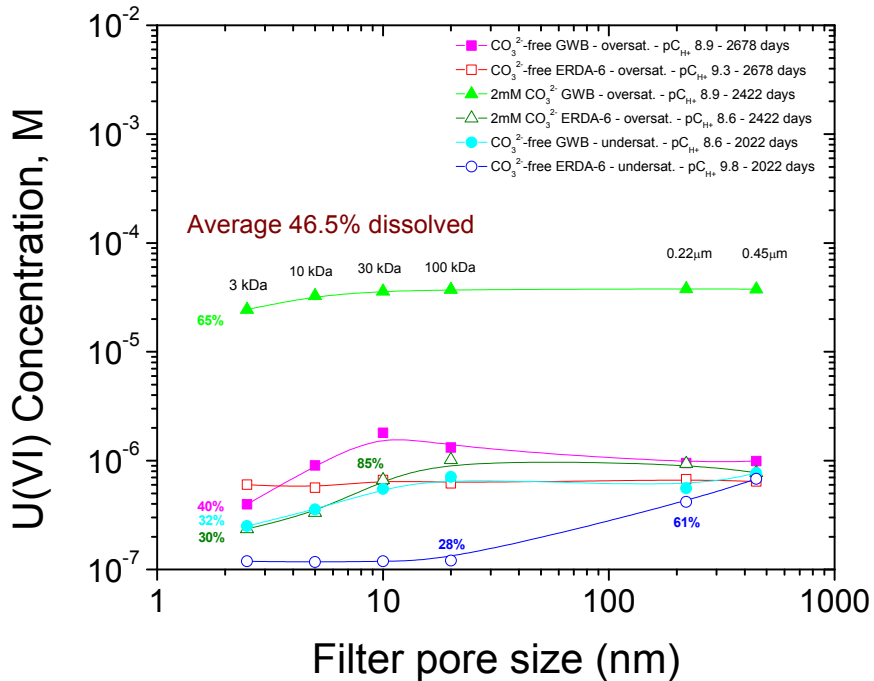
8       **Figure SOTERM-24.  Concentration of Uranium Measured during Sequential**
9                        **Filtration as a Function of Different Pore Size Filters for**
10              **Different Brine Solutions at Different pC$_{H+}$.  Little/no filtration**
11                       **effect noted in all but one case above 10 nm filtration size.**
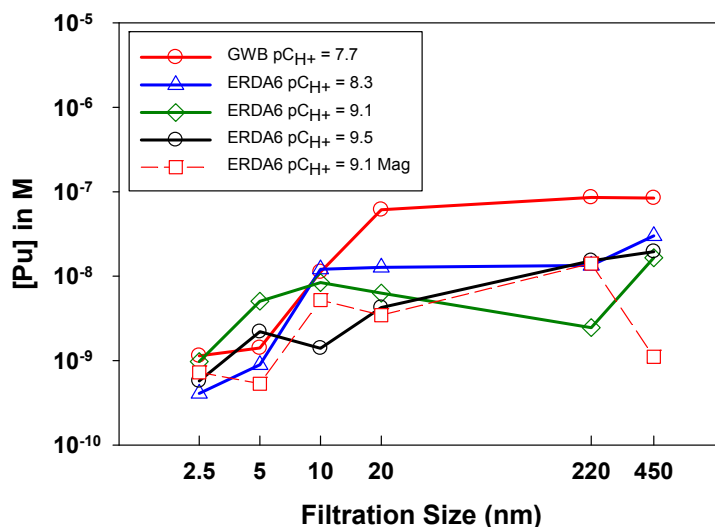
**Figure SOTERM-25.  Sequential Filtration Data for the Pu-Fe Experiments as a Function of Filtration at Different $pC_{H+}$ and Brine Composition. GWB and ERDA-6 brine experiments contained excess iron powder with the exception of the "mag" designated experiment in ERDA-6 that contained excess magnetite.**

**SOTERM-3.9.2.2 Humic Colloids**

The stability of humic and fulvic acid in the WIPP brine was investigated (Wall et al. 2005) and found to be unstable in the presence of MgO.  These results add to the conservatism of the WIPP colloid model in that it shows that humic colloids are not likely in the WIPP.  There is, however, no change in the model parameter assumptions for this colloidal species.

**SOTERM-3.9.2.3 Microbial colloids**

Experiments to measure the bioassociation of the An(III) and An(IV) actinides with WIPP-relevant microorganisms were performed.  These experiments were focused on the biosorption of the two most important actinide oxidation states, Nd(III) for An (III) and Th(IV) for An(IV), towards  a representative halophilic bacteria and archaea.  Redox-invariant analogs were used so that there was no question about the oxidation state being sorbed.  These biosorption data are used to recalculate the PROPMIC microbial colloid enhancement parameter and, when combined with laboratory observations of microbial growth under WIPP-relevant conditions, a biomass-based CAPMIC value (see Section SOTERM-5.4).

The microorganisms used in the biosorption experiments are indigenous to the WIPP area.  The bacterium used, *Chromohalobacter* sp., was isolated from brine retrieved from a shallow subsurface monitoring well incubated under aerobic conditions (Swanson et al. 2012; Ams et al. 2013).  Although these are incubated aerobically, from the point of view of biosorption, the DOE expects these to be representative of anaerobically derived species.  The origins of this water are believed to be a mixture of seepage from an above-ground, but now capped, mine tailings salt pile and actual groundwater flow through the Santa Rosa and Dewey Lake contact (U.S. DOE 2011).  Since then, this bacterium has also been isolated from incubations of WIPP halite at

1 lower salt concentrations, and a Culebra groundwater incubated under aerobic, transitional, and
2 nitrate-reducing conditions.   The archaea utilized in these studies was *Halobacterium noricense*.
3 This was isolated from incubations of halite in generic media and in the WIPP brines, detected in
4 other subterranean salts worldwide (including Germany), requires 2.5-5 M NaCl, tolerates pH 6-
5 10, and is 0.3-1.5 μm in size.

6 The biosorption experiments are described in detail elsewhere (Reed et al. 2013).   The
7 biosorption of actinides towards microorganisms should correlate with their aqueous speciation.
8 For this reason, it would be expected that similar oxidation states would exhibit similar
9 biosorption behavior, at least to the extent that their aqueous speciation is similar.

10 Example biosorption data are shown for thorium in Figure SOTERM-26.  It is notable that the
11 biosorption data are different for bacteria and archaea and EDTA complexation can reduce the
12 extent of biosorption noted.  In both +3 and +4 cases and in both Francis' and LANL-CO work,
13 the PROPMIC values obtained for *Archaea* are less than those for *Bacteria*.

14 ### *Changes in approach for An(III/IV) Biosorption Enhancement Parameters*

15 Based on the current understanding of halophilism and microbial ecology at the WIPP site,
16 microbial enhancement parameters were determined based on five observations made in the
17 biosorption and microbial growth-related experiments.

18 • First, an emphasis on the archaeal data for the near field was used since this presented the
19   most realistic scenario of which organisms will be present.  In PA, however, bacterial
20   values were used.

21 • Second, the biosorption data obtained at the lowest pH values investigated ($\sim$ $pC_{H+}$ = 8.5)
22   are most reliable and should be the basis of the PROPMIC calculation.  These have well
23   correlated biomass dependencies (so sorption is the predominant process) and overall
24   concentration stability.  The higher pH data for both thorium and neodymium appear to
25   have significant contributions from precipitation pathways, although this is clearly more
26   evident in the thorium data.

27 • Third, it is more consistent with the overall WIPP actinide model to use actinide
28   oxidation state rather than element to assign biosorption enhancement parameters –
29   although element-specific values are also provided.  In the PA implementation, the
30   element-specific values were used.

31 • Fourth, CAPMIC values were changed for all elements to a concentration based on
32   microbial biomass and sorption capacity.  This adds more realism to the model and
33   accounts for variability in the toxicity data – which was used in prior CRAs to determine
34   this value.

35 • Fifth, a biomass-based number was used for CAPMIC.  The new biomass-based
36   CAPMICs are less than the total mobile values in the case of the +3 oxidation state.
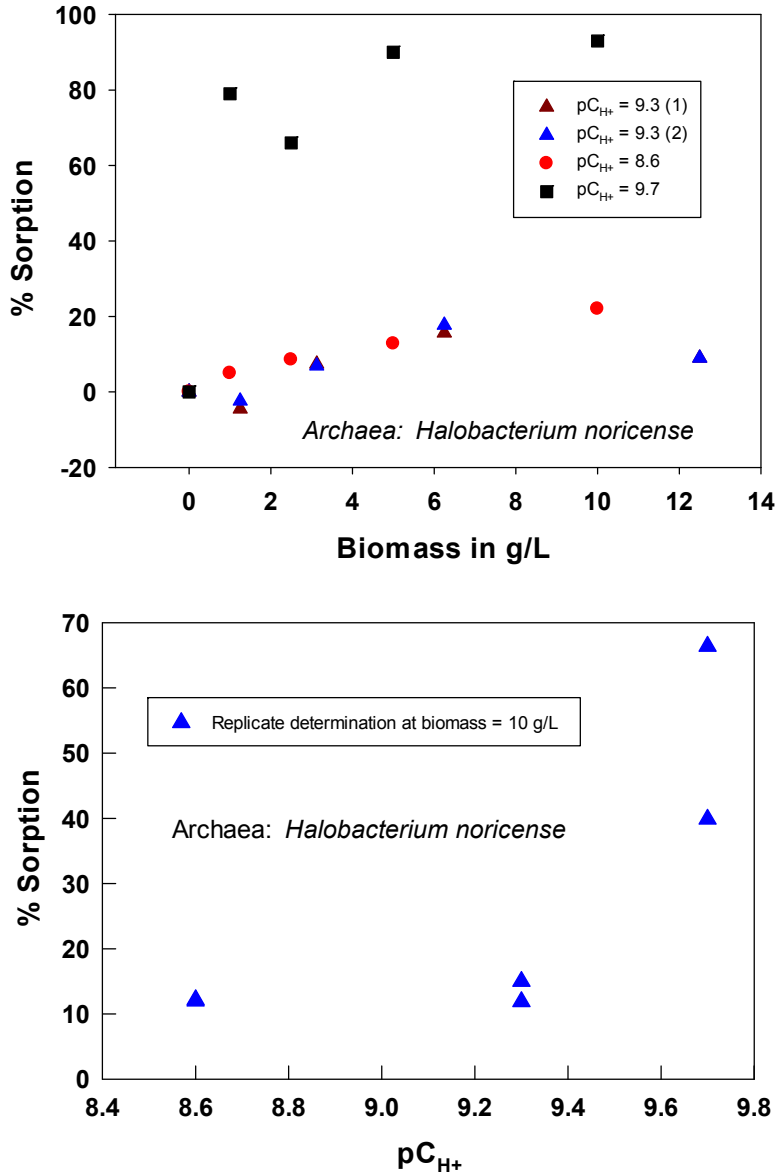
1  **Figure SOTERM-26.  Biomass Dependency (top) and % Sorption (Bottom) of Thorium**
2  **as a Function of pC$_{H+}$ in pH-specific WIPP Brine.  Reliance on**
3  **lower-pH data was necessary due to the coupling of precipitation**
4  **at the higher pHs investigated.**

5

6

# SOTERM-4.0 Calculation of the WIPP Actinide Source Term

The calculation of the WIPP dissolved-actinide source term was performed for the CRA-2014 PA (Brush and Domski 2013a) using the computer code EQ3/6 (Wolery 1992; Wolery and Daveler 1992; Wolery 2008; Wolery, Xiong and Long 2010) version 8.0a and the database DATA0.FMT.R2 (Xiong 2011a). A general description of the modeling approach to establish the actinide source term for the WIPP PA is described in this section.

***Changes since the CRA-2009 and CRA-2009 PABC***

There are essentially no significant changes in the approach and overall conceptual model used to determine the solubility of actinides in the WIPP since CRA-2009.  There are some changes in the mechanics of this process that are noted here:

- FMT is no longer used.  All solubility calculations are done with EQ3/6.  The qualification of EQ3/6 was done as a precursor to this transition (Wolery 2008; Wolery, Xiong and Long 2010; Xiong 2011b). The Pitzer data set of chemical equations has not changed.

- The colloid enhancement parameters for the actinides were updated based on new WIPP-specific data and published literature (see Section SOTERM-3.9).

- Variable brine volume is now being implemented in PA (see SOTERM-5.1.4 and Brush and Domski 2013a).

## SOTERM-4.1 Overview of WIPP Approach to Calculate Actinide Solubilities

The overall approach used to establish the actinides important in WIPP releases and calculate their solubilities for use in the WIPP PA is summarized in this section. This approach consists of the following:

- Assess the WIPP inventory and regulations that govern the application of the WIPP certification to determine the likely actinides of interest and, correspondingly, the key waste components that may affect their solubility.

- Establish a conceptual model for the key subsurface interactions and release mechanisms and using a combination of literature review and WIPP-specific experimental results to establish the likely oxidation state distribution, the species that affect actinide solubility and the parameters required to model the system at high ionic strength. This approach featured the following:

  - Conservative assumptions, within the bounds of the conditions expected, for the oxidation state distribution.

  - Use of redox-invariant analogs for multivalent actinides to determine formation constants and establish oxidation-specific solubilities.

1  – Use of the Pitzer activity-coefficient model and associated parameters to model
2  solubilities at the high ionic strengths present. The Pitzer approach is recognized as
3  the best approach for I > 0.3 M in brine systems.

4  – Calculate the solubility of the key actinides in the WIPP using the EQ3/6 code. The
5  solubilities are modeled in reacted GWB and ERDA-6 brines and include the effects
6  of organic complexation.  This is expected to bracket the range in the composition of
7  the brine expected.

8  • Establish the effects of colloids on the solubilities calculated.

9   • Tabulate and assign uncertainty distributions in the range of expected conditions and
10  brine compositions to these solubility data.  A new method for this is used in CRA-2014
11  (see Brush and Domski 2013c).

12  This range of possible solubilities for a wide range of possible conditions defines the actinide
13  source term provided to the WIPP PA for the calculation of TRU release from the WIPP.

## SOTERM-4.2 Use of Oxidation-State-Invariant Analogs

14

15  The solubility and speciation of multivalent actinides are often investigated with lanthanide and
16  actinide analogs that mimic the property of interest but, for varying reasons, provide an
17  advantage to the experimenter. The best example of this, used extensively in the WIPP modeling
18  approach, is the use of redox-invariant analogs for the multivalent actinides, most notably Pu, to
19  determine oxidation-state-specific properties (e.g., solubility or complexation). The advantage of
20  these types of analogs is that they remove the uncertainty of oxidation-state change from the
21  experiment, which is a complexity that can often lead to uncertain or incorrect interpretations of
22  the results obtained.

23  For the TRU actinides, the redox-invariant analogs used are lanthanides or other actinides.
24  Lanthanides, as 4f-electron elements, possess physical and chemical characteristics that make
25  them good analogs for the actinides when they are redox-invariant under the conditions of the
26  experiment. Correspondingly, actinides with their 5f-electron character also have good physical
27  and chemical properties to be analogs for other actinides if they also have redox stability under
28  WIPP-relevant conditions. This analog approach, although sometimes criticized in the literature,
29  considerably simplifies experimental design and consequently improves the reliability of the
30  experimental data (Choppin 1999).

31  A key argument for the use of analogs in WIPP-related experiments is that key complexants that
32  define actinide solubility in the WIPP are hard-donor complexants (e.g., hydroxide, carbonate,
33  borate, chloride, and/or sulfate). The use of lanthanides as analogs for actinides is based on
34  observations in many extraction systems, along with the associated crystallographic data
35  (Siekierski 1988) that show they are good analogs for compounds containing hard donor ligands
36  (oxygen) where the cation-anion interactions are primarily electrostatic in nature. In this context,
37  Nd(III) is a good analog for the chemical behavior of Am(III) and Pu(III) under most
38  circumstances in the WIPP. Not only do these species have the same 3+ charge, they also have
39  similar ionic radii for coordination number 6 (CN=6): 97.5 pm for $Am^{3+}$, 98.3 pm for $Nd^{3+}$, and

1    100 pm for $Pu^{3+}$ (Shannon 1976). In this context, the magnitudes of electrostatic attractions

2    between these metal ions and corresponding ligands will be similar, yielding comparable

3    thermodynamic stabilities.

4    Th is used by the WIPP as a redox-invariant analog for Pu(IV), U(IV), and Np(IV). The use of

5    the $Th^{4+}$ stability constants to represent the other An(IV) species is conservative. $Th^{4+}$ is the

6    largest of the tetravalent actinide ions. It therefore has the lowest charge density and,

7    correspondingly, relatively weaker ionic interactions when compared to the other tetravalent

8    actinides. This is best exhibited by its lower tendency towards hydrolysis and intrinsic polymer

9    formation relative to the other actinides (see Section SOTERM-3.2). For these reasons, the use of

10   $Th^{4+}$ as an analog is conservative, as Th will likely be the most soluble of the actinides in the

11   tetravalent state under comparable WIPP-relevant conditions.

12   To a lesser extent, actinides are analogs for each other, depending on the oxidation state. Np(V),

13   which has much greater redox stability than Pu(V) and much more favorable spectroscopy, is

14   often used as an analog for Pu(V). U(VI), which is much more redox stable than Pu(VI) and

15   Np(VI), is also used as an analog for these TRU actinides, although U(VI) is in fact a poor

16   analog for Pu(VI) solubility. Am(III) and Cm(III) are also excellent analogs for Pu(III) as a result

17   of their much greater redox stability and comparable ionic radii.

## 18   SOTERM-4.3 Actinide Inventory and Oxidation State Distribution in the
## 19   WIPP

20   The actinide inventory used in CRA-2014 PA was the 2012 inventory that was summarized in

21   Van Soest (Van Soest 2012). Key aspects of this were provided in Tables SOTERM-10 and

22   SOTERM-11.

23   The oxidation states used by the WIPP PA to model actinide solubility are tabulated in Table

24   SOTERM-17. Also included are the assumed abundance percent of each oxidation state and the

25   speciation data set used in EQ3/6 for each oxidation state. This table is based on a general

26   understanding of the corresponding actinide chemistry summarized in Section SOTERM-3.0.

27

1    **Table SOTERM-17.  Oxidation States of the Actinides in the WIPP as Used in the CRA-**
2    **2014 PA**

| Actinide Element | Oxidation States, Abundance (%), and Analog Used (If Any) | | | | |
|---|---|---|---|---|---|
| | Oxidation State[a,b] | | | | EQ3/6 Speciation Data Used |
| | III | IV | V | VI | |
| Thorium | — | 100 % | — | — | Thorium |
| Uranium | — | 50 % | — | 50 % | 1 mM assumed for VI, Th for IV |
| Neptunium | — | 50% | 50 % | — | Np for V Th for IV |
| Plutonium | 50 % | 50 % | — | — | Am for III Th for IV |
| Americium | 100 % | — | — | — | Americium |
| Curium | 100 % | — | — | — | Americium |

a Oxidation state distributions (percentages) refer to the percent of PA vectors that have 100% of the specified oxidation state.
**b** In PA calculations the distribution of oxidation states is correlated for U, Np, and Pu such that the states for all three elements are simultaneously either in the lower oxidation state (U(IV), Np(IV), and Pu(III)) or in the higher oxidation state (U(VI), Np(V), and Pu(IV)).

3

4    A number of conservative assumptions are reflected in this table:

5    1.  Use of 1 mM concentration for the solubility of U(VI). The actual solubility of U(VI) in the
6         WIPP under the expected range of conditions is estimated to be <0.1 mM.

7    2.  Use of Th as an analog for the IV actinides (see Section SOTERM-4.1 and Section
8         SOTERM-3.2).

9    3.  The assumption of a probability that 50% of the vectors have Pu(III) and 50% of the vectors
10        have Pu(IV). The predominant Pu species expected is Pu(IV), although some Pu(III) is
11        possible as a transient (see discussion in Section SOTERM-3.6).   This is conservative
12        because Pu(III) is approximately 6 to 10 times more soluble than corresponding Pu(IV)
13        phases.

14   4.  The assumption of a probability that 50% of the vectors have U(IV) and 50% of the vectors
15        have U(VI). The predominant uranium species expected is U(IV), which is approximately
16        four orders of magnitude less soluble than U(VI), based on current assumptions.

17   **SOTERM-4.4 Actinide Speciation Reactions Used in EQ3/6**

18   The version of the database used with the EQ3/6 code for the CRA-2014 PA was
19   DATA0.FMT.R2 (Xiong 2011a). This was a conversion of the FMT database used in CRA-2009
20   into the EQ3/6 format and was extensively qualified (Wolery, Xiong and Long 2010).   There
21   were no significant changes to the speciation reactions and data used.  For these reactions (see
22   Wolery 1992 for a detailed discussion), log K is the log of the product of the activity of each
23   reaction product (to the power of its coefficient) divided by the product of the activity of each
24   reactant (to the power of its coefficient).

1 **SOTERM-4.4.1 The III Actinides: Pu(III), Am(III), Cm(III)**

2 The thermodynamic database for the III actinides currently used in EQ3/6 was described by
3 Giambalvo (Giambalvo 2002a) and updated by Wolery (Wolery, Xiong and Long 2010). Nd,
4 Am, and Cm are generally used to establish solubility of An(III) because, unlike plutonium, they
5 have redox-stable trivalent oxidation states. Speciation and solubility data for the III actinides
6 were parameterized for use in the Pitzer activity-coefficient model by Felmy et al. (Felmy et al.
7 1989) for the $Na^+$- $Pu^{3+}$-$Cl^-$-$H_2O$ system; by Felmy, Rai, and Fulton (Felmy, Rai, and Fulton
8 1990) for the $Na^+$-$Am^{3+}$-$OH^-$-$HCO_3^-$-$H_2O$ system; by Rai, Felmy, and Fulton (Rai, Felmy, and
9 Fulton 1995) for the $Na^+$-$Am^{3+}$-$PO_4^{3-}$-$SO_4^{2-}$-$H_2O$ system; and by Rao et al. (Rao et al. 1996) for
10 the $Na^+$-$Nd^{3+}$-$CO_3^{2-}$-$HCO_3^-$-$H_2O$ system. EQ3/6 uses the Am(III) data to calculate the solubility
11 for all the III actinides. A diagram of the predominant species for Am is shown in Figure
12 SOTERM-27.

13 The inorganic aqueous and solubility-limiting species featured in the model for Am(III) are

| Am(III) Reactions | log K | |
|---|---|---|
| $Am3+ + CO32- \leftrightarrows AmCO3+$ | 8.1 | (SOTERM.34) |
| $Am^{3+} + 2CO_3^{2-} \leftrightarrows Am(CO_3)_2^-$ | 13.0 | (SOTERM.35) |
| $Am^{3+} + 3CO_3^{2-} \leftrightarrows Am(CO_3)_3^{3-}$ | 15.2 | (SOTERM.36) |
| $Am^{3+} + 4CO_3^{2-} \leftrightarrows Am(CO_3)_4^{5-}$ | 13.0 | (SOTERM.37) |
| $Am^{3+} + OH^- \leftrightarrows AmOH^{2+}$ | 6.4 | (SOTERM.38) |
| $Am^{3+} + 2OH^- \leftrightarrows Am(OH)_2^+$ | 12.3 | (SOTERM.39) |
| $Am^{3+} + 3OH^- \leftrightarrows Am(OH)_3(aq)$ | 16.3 | (SOTERM.40) |
| $Am^{3+} + Cl^- \leftrightarrows AmCl^{2+}$ | 0.24 | (SOTERM.41) |
| $Am^{3+} + 2Cl^- \leftrightarrows AmCl_2^+$ | -0.74 | (SOTERM.42) |
| $Am^{3+} + SO_4^{2-} \leftrightarrows Am(SO_4)^+$ | 3.25 | (SOTERM.43) |
| $Am^{3+} + 2SO_4^{2-} \leftrightarrows Am(SO_4)_2^-$ | 3.7 | (SOTERM.44) |
| $Am^{3+} + OH^- + CO_3^{2-} \leftrightarrows AmOHCO_3(s)$ | 22.7 | (SOTERM.45) |
| $Na^+ + Am^{3+} + 2CO_3^{2-} + 6H_2O \leftrightarrows NaAm(CO_3)_2 \cdot 6H_2O(s)$ | 21.4 | (SOTERM.46) |
| $Am^{3+} + PO_4^{3-} \leftrightarrows AmPO_4(cr)$ | 24.8 | (SOTERM.47) |

14 In these reactions, "aq," "cr," and "s" are the abbreviations for aqueous, crystalline, and solid,
15 respectively. The An(III) database was extended to mixed $Na^+$-$CO_3^{2-}$-$Cl^-$ media, and was shown

1 to reproduce the independently measured solubility of $NaAm(CO_3)_2(s)$ in 5.6 M NaCl (Runde
2 and Kim 1994) and the measured Nd(III) solubility in the WIPP brine (Borkowski et al. 2008).
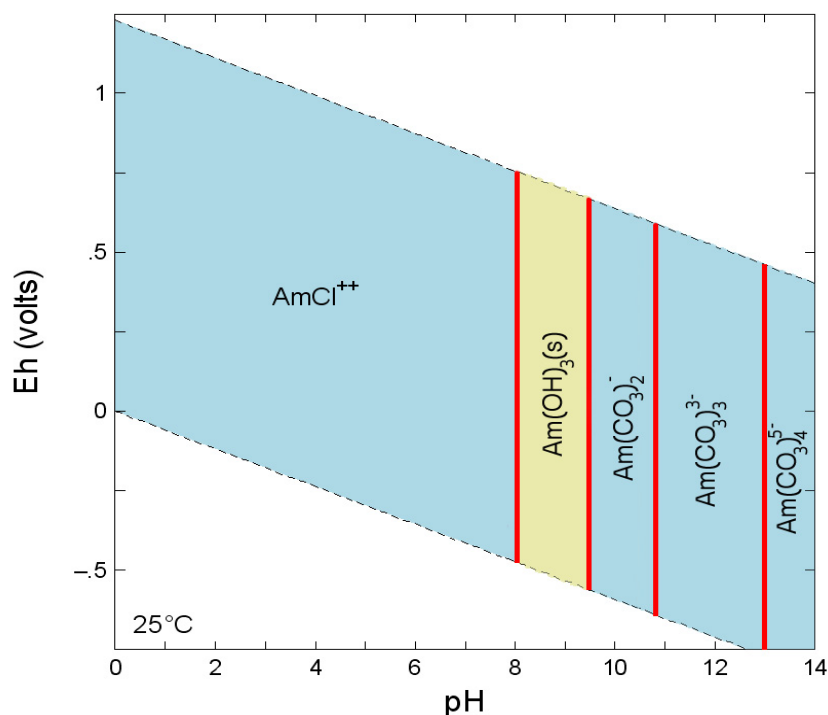


3

4 **Figure SOTERM-27. Predominant Am Species as a Function of pH and $E_h$ Based on**
5 **the Speciation Reactions 34 to 47 (Richmann 2008)**

6 **SOTERM-4.4.2 The IV Actinides: Th(IV), U(IV), Pu(IV), Np(IV)**

7 The IV actinides addressed by the WIPP PA are Th(IV), U(IV), Pu(IV), and Np(IV). The
8 variation in charge-to-radius ratio for the tetravalent actinides is greater than for actinides in
9 other oxidation states (Cotton and Wilkinson 1988, pp. 11–46), and larger differences in the
10 chemical behavior among the IV actinides is expected. The application of the Th(IV) model to
11 the other IV species (U(IV), Np(IV), and Pu(IV)) is more uncertain, yet still conservative
12 because Th(IV) is the most soluble of these elements under WIPP conditions. The model was
13 evaluated against data for Pu(IV) and Np(IV) solubility and demonstrated to predict the chemical
14 behavior of these actinides conservatively.

15 The thermodynamic database for the IV actinides currently used in EQ3/6 was described by
16 Giambalvo (Giambalvo 2002b). Speciation and solubility data for Th(IV) were parameterized for
17 the Pitzer activity-coefficient model for the $Na^+$-$K^+$-$Mg^{2+}$-$Cl^-$- $SO_4^{2-}$-$CO_3^{2-}$-$HCO_3^-$ -$OH^-$-$H_2O$
18 system. This model requires the species $Th^{4+}$, $Th(OH)_2SO_4$ (s), $Th(SO_4)_3^{2-}$, $Th(SO_4)_2$ (aq), $ThO_2$,
19 $Th(OH)_4(aq)$, $Th(OH)_3CO_3^-$, and $Th(CO_3)_5^{6-}$ to describe the data pertinent to the WIPP (Felmy,
20 Mason, and Rai 1991; Rabindra et al. 1992; Felmy et al. 1996). A diagram of the predominant
21 Th speciation, based on Reactions SOTERM.48 to 59, is shown in Figure SOTERM-28.
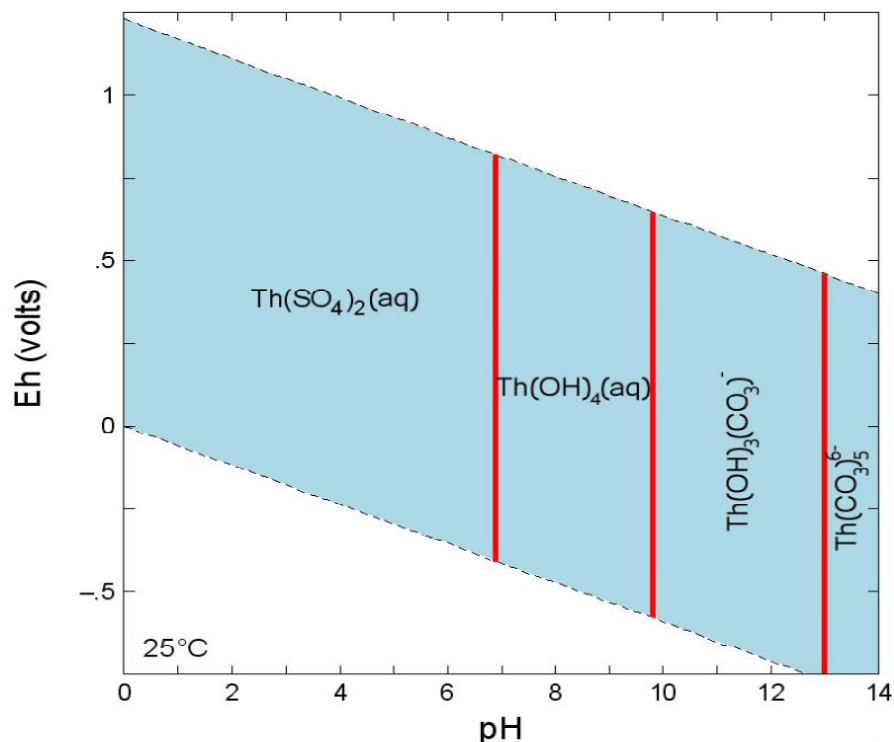
1

2　**Figure SOTERM-28.　Predominant Species of Th as a Function of pH and Redox**
3　**Conditions (Richmann 2008). Thorianite is predicted to**
4　**predominate at the conditions expected in the WIPP repository.**

5　The inorganic aqueous and solubility-limiting species featured in the IV model are:

| Th(IV) Reactions | log K | |
|---|---|---|
| $ThO_2(am) + 2H_2O \leftrightarrows Th(OH)_4(aq)$ | -7.0 | (SOTERM.48) |
| $Th^{4+} + 4OH^- \leftrightarrows Th(OH)_4(aq)$ | 38.5 | (SOTERM.49) |
| $Th^{4+} + 3OH^- + CO_3^{2-} \leftrightarrows Th(OH)_3CO_3^-$ | 38.3 | (SOTERM.50) |
| $Th^{4+} + 5CO_3^{2-} \leftrightarrows Th(CO_3)_5^{6-}$ | 27.1 | (SOTERM.51) |
| $Th^{4+} + 2SO_4^{2-} \leftrightarrows Th(SO_4)_2(aq);$ | 11.6 | (SOTERM.52) |
| $Th^{4+} + 3SO_4^{2-} \leftrightarrows Th(SO_4)_3^{2-};$ | 12.4 | (SOTERM.53) |
| $Th^{4+} + 2SO_4^{2-} + 9H_2O \leftrightarrows Th(SO_4)_2 \cdot 9H_2O(s);$ | 13.0 | (SOTERM.54) |
| $Th^{4+} + 2SO_4^{2-} + 8H_2O \leftrightarrows Th(SO_4)_2 \cdot 8H_2O(s)$ | 12.9 | (SOTERM.55) |
| $Th^{4+} + 2Na^+ + 3SO_4^{2-} + 6H_2O \leftrightarrows$ $Th(SO_4)_2 \cdot Na_2SO_4 \cdot 6H_2O(s)$ | 17.6 | (SOTERM.56) |

**Th(IV) Reactions**                                 **log K**

$$Th^{4+} + 2K^+ + 3SO_4^{2-} + 4H_2O \leftrightarrows$$
$$Th(SO_4)_2 \cdot K_2SO_4 \cdot 4H_2O(s) \qquad 18.1 \qquad (SOTERM.57)$$

$$Th^{4+} + 4K^+ + 4SO_4^{2-} + 2H_2O \leftrightarrows$$
$$Th(SO_4)_2 \cdot 2K_2SO_4 \cdot 2H_2O \ (s) \qquad 21.2 \qquad (SOTERM.58)$$

$$Th^{4+} + 7K^+ + 5.5SO_4^{2-} \leftrightarrows Th(SO_4)_2 \cdot 3.5K_2SO_4(s). \qquad 24.7 \qquad (SOTERM.59)$$

1 **SOTERM-4.4.3 The V Actinides: Np(V)**

2 The only V actinide of interest to the WIPP is Np(V), which exists as the neptunyl ion, $NpO_2^+$.
3 Pu(V), which can be formed under some conditions, is transitory and not expected to persist in
4 significant quantities in the WIPP. The base model for Np(V) comes from Fanghänel, Neck, and
5 Kim (Fanghänel, Neck, and Kim 1995), constructed for the German repository program.

6 The thermodynamic database for the V actinides currently used in EQ3/6 is described by
7 Giambalvo (Giambalvo 2002c). Np(V) speciation and solubility were parameterized in the Pitzer
8 activity-coefficient model for the $Na^+$-$K^+$-$Mg^{2+}$-$Cl^-$- $SO_4^{2-}$-$CO_3^{2-}$-$HCO_3^-$ -$OH^-$-$H_2O$ system. The
9 model requires the aqueous species $NpO_2^+$, $NpO_2OH(aq)$, $NpO_2(OH)_2^-$, $NpO_2CO_3^-$,
10 $NpO_2(CO_3)_2^{3-}$, and $NpO_2(CO_3)_3^{5-}$, and the solid species $NpO_2OH(am)$, $NpO_2OH(aged)$,
11 $Na_3NpO_2(CO_3)_2(s)$, $KNpO_2CO_3 \cdot 2H_2O(s)$, $K_3NpO_2(CO_3)_2 \cdot 0.5H_2O(s)$, and $NaNpO_2CO_3 \cdot 3.5H_2O(s)$
12 to explain the available data. The predominant species for Np(V) are shown in Figure SOTERM-
13 29.

14 The inorganic aqueous and solubility-limiting species used are:

**Np(V) Reactions**                                 **log K**

$$NpO_2^+ + OH^- \leftrightarrows NpO_2OH(aq) \qquad 2.7 \qquad (SOTERM.60)$$

$$NpO_2^+ + OH^- \leftrightarrows NpO_2OH(s, am) \qquad 8.8 \qquad (SOTERM.61)$$

$$NpO_2^+ + OH^- \leftrightarrows NpO_2OH(s, aged) \qquad 9.5 \qquad (SOTERM.62)$$

$$NpO_2^+ + 2OH^- \leftrightarrows NpO_2(OH)_2^- \qquad 4.5 \qquad (SOTERM.63)$$

$$NpO_2^+ + CO_3^{2-} \leftrightarrows NpO_2CO_3^- \qquad 5.0 \qquad (SOTERM.64)$$

$$NpO_2^+ + 2CO_3^{2-} \leftrightarrows NpO_2(CO_3)_2^{3-} \qquad 6.4 \qquad (SOTERM.65)$$

$$NpO_2^+ + 3CO_3^{2-} \leftrightarrows NpO_2(CO_3)_3^{5-} \qquad 5.3 \qquad (SOTERM.66)$$

$$Na^+ + NpO_2^+ + CO_3^{2-} + 3.5H_2O \leftrightarrows$$
$$NaNpO_2(CO_3) \cdot 3.5H_2O(s) \qquad 11.1 \qquad (SOTERM.67)$$

**Np(V) Reactions**                                                     **log K**

$$3Na^+ + NpO_2^+ + 2CO_3^{2-} \leftrightarrows Na_3NpO_2(CO_3)_2(s)$$     14.2     (SOTERM.68)

$$K^+ + NpO_2^+ + CO_3^{2-} \leftrightarrows KNpO_2(CO_3)(s)$$     13.6     (SOTERM.69)

$$3K^+ + NpO_2^+ + 2CO_3^{2-} + 0.5H_2O \leftrightarrows$$

$$K_3NpO_2(CO_3)_2 \cdot 0.5H_2O(s)$$     -4.8     (SOTERM.70)

1
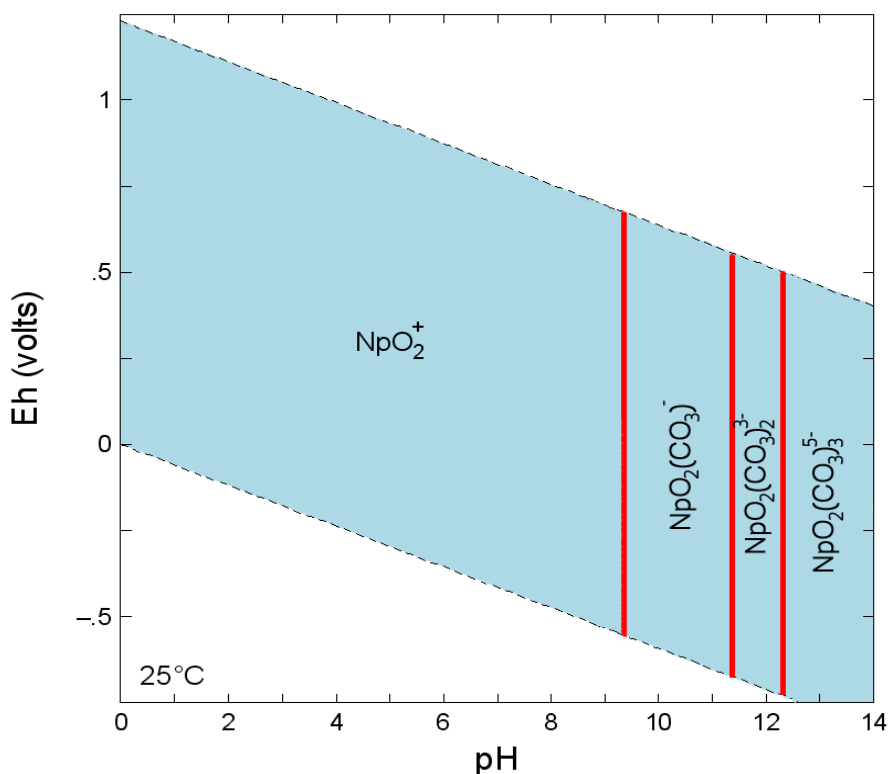


2

3  **Figure SOTERM-29.  Predominant Species Diagram for Np as a Function of pH and $E_h$**
4  **Based on the Np Speciation Data Reactions 60 to 70 (Richmann**
5  **2008)**

6  **SOTERM-4.4.4 The VI Actinides: U(VI)**

7  The An(VI) EQ3/6 model has not been developed sufficiently for reliable use in predicting
8  concentrations of this oxidation state in the WIPP brines under various solution conditions.
9  Although uranyl carbonate can be successfully modeled, the hydrolysis behavior of U(VI) is
10  quite complicated and no satisfactory predictive models applicable to WIPP-like conditions are
11  yet available. Because the implementation of an MgO backfill limits the pmH and $f_{CO_2}$ to
12  discrete values, empirical measurement of the solubility of U(VI) in WIPP and/or WIPP–like
13  brines became practical. As documented in Hobart and Moore (Hobart and Moore 1996) and

1 used in prior PA calculations, the solubility of U(VI) at pH 10, in the absence of carbonate, was
2 determined to be $8.8 \times 10^{-6}$ m. This is augmented by additional data from U(VI) solubility studies
3 in WIPP-relevant carbonate-free brines reported in Section SOTERM-3.3.2 (Lucchini et al.
4 2010a; Lucchini et al. 2013a; Lucchini et al. 2013b). Here, the measured U(VI) solubility was
5 $10^{-7}$ M to $10^{-6}$ M for GWB and ERDA-6 brine, respectively. The solubility of U(VI) currently
6 used in the WIPP PA was established through discussions with the EPA to be 1 mM (U.S. EPA
7 2005) to account for the potential and expected effects of carbonate.

## SOTERM-4.5 Calculations of Actinide Solubility Using the EQ3/6 Computer Code

10 Details of the implementation of EQ3/6 are described in more detail elsewhere (Wolery 2008;
11 Wolery and Jarek 2003; Wolery, Xiong and Long 2010; Brush and Domski 2013a). EQ3/6
12 calculates chemical equilibrium for user-specified total element amounts in aqueous or
13 aqueous/mineral geochemical systems. The EQ3/6 calculations of actinide solubility in the WIPP
14 system performed for the WIPP PA included preequilibration with halite, anhydrite, brucite, and
15 hydromagnesite (Brush and Domski 2013a), which are the minerals present in large quantities in
16 the repository. The effects of the MgO backfill are realized by equilibrating brine with brucite,
17 magnesite, and hydromagnesite.

### SOTERM-4.5.1 Pitzer Approach for High-Ionic-Strength Brines

19 The Pitzer activity-coefficient model is substantially different in approach from the classic
20 Debye-Hückel (D-H) theory of the behavior of ionic solutions. The latter is a theoretical
21 approach to describing the behavior of dilute solutions; more importantly, because many ionic
22 solutes do not behave ideally even at very low concentrations, D-H provides a means to calculate
23 the activity, $a_i$, of a desired species. This is of great importance, as the Gibbs free energies of the
24 various species in solution can be used to calculate solution equilibria if one knows the effective
25 concentration of those species, i.e., their "activity" in solution. The activity of a given species $i$ is
26 tied to the molality of that species as $a_i = \gamma_i m_i$. Since the molality of species $i$ is known, the
27 unknown that must be calculated to determine $a_i$ is, therefore, $\gamma_i$. The simplest form relating
28 activity to molality from the D-H law is

29
$$\log \gamma_i = -A_\gamma z_i^2 \left( \frac{\sqrt{I}}{1+\sqrt{I}} \right)$$
(SOTERM.71)

30 where $A\gamma$ is the Debye-Hückel parameter, $z_i$ is the charge of the $i$th species and $I$ is the overall
31 solution ionic strength. The fundamental difficulty with the D-H formalism is that even with
32 extensions (Davies equation, B-dot equation)(Wolery 2008), the D-H law begins to deviate
33 significantly from real solution behavior somewhere in the general region of I = 0.3 molal. As
34 the WIPP brines (and many other highly concentrated ionic species of interest) are well above
35 this level of ionic strength, many times with $I > 5$, another description is required to properly
36 describe the activities of the ionic species.

37 In 1973, Pitzer proposed a set of semiempirical equations to describe $a_i$. Pitzer (Pitzer 1973)
38 wrote the Gibbs excess energy of a solution as a virial expansion, where a portion of the overall

1    expansion can be tied down to a formalism similar to the D-H law and the majority of the
2    remaining constants are empirically determined from measurements of the desired ions. The
3    most general form of the equation is

4
$$\ln \gamma_i = \left(\frac{z_i^2}{2}\right) f'(I) + 2\sum_i \lambda_{ij}(I)m_j + \sum_{ik}\left(\left(\frac{z_i^2}{2}\right)\lambda'_{jk}(I) + 3\mu_{ijk}\right)m_j m_k ,$$    (SOTERM.72)

5    where $f(I)$ is a Debye-Hückel function, $f'(I)$ is its derivative df/dI, the $\lambda_{ij}$ are second-order
6    interaction coefficients, $\lambda'_{ij}(I)$ is the derivative $d\lambda_{ij}/dI$, and the $\mu_{ijk}$ are third-order interaction
7    coefficients. The experimentally observable values $\beta^{(0)}$, $\beta^{(1)}$, $\beta^{(2)}$, $\alpha_1$, $\alpha_2$, $C^\varphi$, and so forth are used
8    to calculate the $\lambda_{ij}$ and $\mu_{ijk}$ values needed to calculate $\gamma_i$ (for more detail, see Wolery and Daveler
9    1992).

10   This approach has proven highly effective and has successfully described the behavior of
11   solutions at high ionic strength. The disadvantage of this technique is that binary and ternary
12   coefficients for the expansion are normally needed to completely describe all the activities of the
13   different species; in addition, if the number of species in solution grows, the number of
14   calculations grows that much faster, i.e., on the order of the cube of the number of species. This
15   problem would be even worse, except that many of the terms describing neutral species can be
16   legitimately neglected in geochemical systems.

17   This parameter-determination problem is of particular interest in the description of actinide
18   behavior in the WIPP, since the GWB and ERDA-6 brines of interest contain a wide variety of
19   ions in and of themselves, in addition to the actinides introduced into the repository. As a result
20   of this, it was necessary to constrain the total number of possible species in solution, aqueous,
21   solid or gas, and in addition, to determine Pitzer parameters for many species by analogy to
22   others rather than by experimental measurement. This is the basis of the parameter and species
23   selection in the current database, DATA0.FMT.R2, which contains the parameters for those
24   species incorporated into the limited species set description. In practice, this has worked well to
25   describe solution behavior in the WIPP within a limited set of pH values at 25 $^o$C.

26   **SOTERM-4.5.2 Calculated Actinide Solubilities**

27   The oxidation-state-specific actinide solubilities calculated for the CRA-2014 PA with EQ3/6 are
28   summarized in Table SOTERM-18. For historical perspective, the calculated solubilities from
29   prior PA analyses are also tabulated. In the CRA-2014 PA, the data are shown for two brines in
30   the presence of organics, and as a function of equilibration with hydromagnesite. The
31   hydromagnesite case is recognized by the project as the most relevant to the WIPP. It is
32   important to note that, overall, the calculated solubilities have not changed much over time
33   except for the effects of increased complexation of the An(III) actinides with organics as this
34   inventory has increased.

35   As shown in Table SOTERM-18, the calculated solubility of the III actinides was $2.59 \times 10^{-6}$ M
36   to $1.48 \times 10^{-6}$ M in the CRA-2014 PA (Brush and Domski 2013a). These data are also fairly
37   consistent with recently measured results for Nd(III) solubility in brine (Borkowski et al. 2008).
38   A somewhat broader range was noted historically: $2.88 \times 10^{-7}$ M to $2.59 \times 10^{-6}$ M. The expected

1  solubility of the IV actinides ranges between $6.05 \times 10^{-8}$ M and $7.02 \times 10^{-8}$ M. This is also
2  somewhat consistent with prior calculations and has increased slightly. Overall the solubility of
3  the IV actinides is four to eight times lower than that predicted for the III actinides. The main
4  reason for increases noted in CRA-2014 PA was the presence of organics in the brines.

5  Uncertainties in the solubility data and uncertainty in the NONLIN least-squares refinement, for
6  Pitzer parameter determination, result in uncertainty in the model predictions. This distribution
7  was sampled and used in PA as discussed in Section SOTERM-5.0 (Brush and Domski 2013c).

8  Four organic ligands are included in EQ3/6 calculations of actinide solubilities. These are acetate
9  $(CH_3CO_2^-)$, citrate $[(CH_2CO_2)_2C(OH)(CO_2)^{3-}]$, EDTA $[(CH_2CO_2)_2N(CH_2)_2N(CH_2CO_2)_2^{4-}]$, and
10  oxalate $(C_2O_4^{2-})$. The current anticipated inventory of these complexing agents, with their
11  inventory-limited solubilities in the WIPP, were summarized in Tables SOTERM-3 and
12  SOTERM-7. These ligands are included in the solubility calculations because (1) approximately
13  60 organic compounds were identified among the nonradioactive constituents of the TRU waste
14  to be emplaced in the WIPP (Brush 1990; Drez 1991; U.S. DOE 1996); (2) 10 of these 60
15  organic compounds could, if present in the WIPP, increase actinide solubilities because they are
16  soluble in aqueous solutions such as the WIPP brines, and because they form complexes with
17  dissolved actinides (Choppin 1988); and (3) of these 10 water-soluble organic ligands that form
18  complexes with actinides, 4 (acetate, citrate, EDTA, and oxalate) are included in PA and tracked
19  in the WIPP inventory (see the CCA, Appendix SOTERM, p. 96).

20  **Table SOTERM-18.  Historical Actinide Solubilities Calculated for the CRA-2004 PABC,**
21  **the CRA-2009 PABC and CRA-2014 PA (Brush and Domski 2013a, Table 13).**

| Actinide Oxidation State, and Brine | CRA-2004 PABC (M) | CRA-2009 PABC (M) | CRA-2014PA, 1× Minimum Brine Volume (M) | CRA-2014 PA, 5× Minimum Brine Volume  (M) |
|---|---|---|---|---|
| III, GWB | $3.87 \times 10^{-7}$ | $1.66 \times 10^{-6}$ | $2.59 \times 10^{-6}$ | $6.47 \times 10^{-7}$ |
| III, ERDA-6 | $2.88 \times 10^{-7}$ | $1.51 \times 10^{-6}$ | $1.48 \times 10^{-6}$ | $3.92 \times 10^{-7}$ |
| IV, GWB | $5.64 \times 10^{-8}$ | $5.63 \times 10^{-8}$ | $6.05 \times 10^{-8}$ | $6.07 \times 10^{-8}$ |
| IV, ERDA-6 | $6.79 \times 10^{-8}$ | $6.98 \times 10^{-8}$ | $7.02 \times 10^{-8}$ | $7.20 \times 10^{-8}$ |
| V, GWB | $3.55 \times 10^{-7}$ | $3.90 \times 10^{-7}$ | $2.77 \times 10^{-7}$ | $1.82 \times 10^{-7}$ |
| V, ERDA-6 | $8.24 \times 10^{-7}$ | $8.75 \times 10^{-7}$ | $8.76 \times 10^{-7}$ | $6.44 \times 10^{-7}$ |

22

## SOTERM-4.6 Calculation of Colloidal Contribution to Actinide Solution Concentrations

25  The importance and role of colloids in defining the concentration of actinides in the WIPP was
26  discussed in Section SOTERM-3.9, and more extensive discussions of WIPP-related results are
27  available (Reed et al. 2013; CCA Appendix SOTERM, Section 6). The PA conceptual approach
28  used to account for colloidal enhancement of actinide concentrations was developed as part of
29  the CCA and has not changed since this initial implementation. The four types of colloids
30  identified as relevant to the WIPP are listed and described in Table SOTERM-19.

1   Three types of parameter values were determined: (1) constant concentration values, (2)
2   concentration values proportional to the dissolved actinide concentration, and (3) maximum
3   concentration values. These parameter types are summarized Table SOTERM-20 and were
4   initially described in parameter record packages (Papenguth and Behl 1996; Papenguth 1996a;
5   Papenguth 1996b; Papenguth 1996c).

6   For microbes, the proportionality relationship was made by element. For humic actinides,
7   however, the relationship was made by oxidation state, rather than by element. For microbes and
8   humic substances, the experiments described in the parameter record packages noted above also
9   provided a basis to define upper limits of the actinide concentration that could be associated with
10   each of those colloid types. For both humic and microbial actinides, the upper limit parameter
11   was defined by element, rather than oxidation state, and is in units of molality. The use of the
12   two upper limit parameters is slightly different, and is described in the sections below discussing
13   humic substances and microbes.

14   **Table SOTERM-19.  Classification of Four Colloid Types Considered by the WIPP PA**

| | |
|---|---|
| Mineral Fragment Colloids | Hydrophobic, hard-sphere particles that are kinetically stabilized or destabilized by electrostatic forces and may consist of crystalline or amorphous solids. Mineral fragments may be made kinetically stable by coatings with steric stabilizers that prevent close contact. Mineral fragments may act as substrates for sorption of actinides, or they may consist of precipitated or coprecipitated actinide solids. |
| Intrinsic Actinide Colloids | Intrinsic actinide colloids (also known as true colloids, real colloids, Type I colloids, and Eigenkolloide) are macromolecules of actinides that, at least in some cases, may mature into a mineral-fragment type of colloidal particle. When immature, they are hydrophilic; when mature, they become hydrophobic. |
| Humic Colloids | Humic substances are hydrophilic, soft-sphere particles that are stabilized by solvation forces. They are often powerful substrates for uptake of metal cations and are relatively small (less than 100,000 atomic mass units). |
| Microbial Colloids | Microbes are relatively large colloidal particles stabilized by hydrophilic coatings on their surfaces, which behave as steric stabilizing compounds. They may act as substrates for extracellular actinide sorption or actively bioaccumulate actinides intracellularly. |

15

1 **Table SOTERM-20. Material and Property Names for Colloidal Parameters**

| Material | Property | Brief Description of Parameter |
|---|---|---|
| Th, U, Np, Pu, Am | CONCMIN | Concentration of actinide associated with mobile mineral fragment colloids |
| Th, U, Np, Pu, Am | CONCINT | Concentration of actinide associated with mobile intrinsic actinide colloids |
| Th, U, Np, Pu, Am | PROPMIC | Proportionality constant for concentration of actinides associated with mobile microbes |
| PHUMOX3 [a] PHUMOX4 PHUMOX5 PHUMOX6 | PHUMCIM | Proportionality constant for concentration of actinides associated with mobile humic colloids; in Castile brine; actinide solubilities include organics (complexes with man-made organic ligands); solubilities were calculated assuming equilibrium with Mg-bearing minerals (brucite and hydromagnesite) |
| PHUMOX3 [a] PHUMOX4 PHUMOX5 PHUMOX6 | PHUMSIM | Proportionality constant for concentration of actinides associated with mobile humic colloids; in Salado brine; actinide solubilities include organics (complexes with man-made organic ligands); solubilities were calculated assuming equilibrium with Mg-bearing minerals (brucite and hydromagnesite) |
| Th, U, Np, Pu, Am | CAPMIC | Maximum (cap) concentration of actinide associated with mobile microbes |
| Th, U, Np, Pu, Am | CAPHUM | Maximum (cap) concentration of actinide associated with mobile humic colloids |

a   Proportionality constant for actinide concentrations associated with mobile humic substances for PHUMOX3, for actinide elements with oxidation state *III* (that is, Pu(III) and Am(III)); PHUMOX4, oxidation state IV (Th(IV), U(IV), Np(IV), and Pu(IV)); PHUMOX5, oxidation state V (Np(V)); and PHUMOX6, oxidation state VI (U(VI)).

2

3   The colloid concentration factors used in the CRA-2014 PA are summarized in Table SOTERM-
4   21. The general approach used to account for colloidal enhancement of actinide solubilities is
5   described in detail in Appendix SOTERM-2014, Section 5.2 and Appendix PA-2014, Section
6   4.3.  There were essentially no changes in the approach used from the CRA-2009 PABC
7   although all the parameters were re-assessed.

1    **Table SOTERM-21.  Colloid enhancement parameters used in CRA-2009 and CRA-2014 (Appendix SOTERM-2009; Reed et**
2                                                    **al. 2013)**

| Actinide | CONCMIN (Concentration on Mineral Fragments [a]) | CONCINT (Concentration as Intrinsic Colloid [a]) (M) | | PROPMIC (Proportion Sorbed on Microbes [b]) | | CAPMIC (Maximum Sorbed on Microbes[c]) (M) | | Proportion Sorbed on Humics [b] | | CAPHUM[d] (Maximum Sorbed on Humics [a]) |
| | | | | | | | | PHUMSIM (Salado) [d] | PHUMCIM (Castile) [d] | |
| CRA | 2009 and 2014 | 2009 | 2014 | 2009 | 2014 | 2009 | 2014 | 2009 and 2014 | 2009 and 2014 | 2009 and 2014 |
|---|---|---|---|---|---|---|---|---|---|---|
| Th(IV) | $2.6 \times 10^{-8}$ | 0 | $2 \times 10^{-8}$ | 3.1 | 1.76 | 0.0019 | $2.3 \times 10^{-6}$ | 6.3 | 6.3 | $1.1 \times 10^{-5}$ |
| U(IV) | $2.6 \times 10^{-8}$ | 0 | $2 \times 10^{-8}$ | 0.0021 | 1.76 | 0.0021 | $2.3 \times 10^{-6}$ | 6.3 | 6.3 | $1.1 \times 10^{-5}$ |
| U(VI) | $2.6 \times 10^{-8}$ | 0 | $3 \times 10^{-8}$ | 0.0021 | 1.76 | 0.0021 | $2.3 \times 10^{-6}$ | 0.12 | 0.51 | $1.1 \times 10^{-5}$ |
| Np(IV) | $2.6 \times 10^{-8}$ | 0 | $2 \times 10^{-8}$ | 12.0 | 1.76 | 0.0027 | $2.3 \times 10^{-6}$ | 6.3 | 6.3 | $1.1 \times 10^{-5}$ |
| Np(V) | $2.6 \times 10^{-8}$ | 0 | ND | 12.0 | 1.76 | 0.0027 | $2.3 \times 10^{-6}$ | $9.1 \times 10^{-4}$ | $7.4 \times 10^{-3}$ | $1.1 \times 10^{-5}$ |
| Pu(III) | $2.6 \times 10^{-8}$ | $1 \times 10^{-9}$ | $2 \times 10^{-8}$ | 0.3 | 1.76 | $6.8 \times 10^{-5}$ | $2.3 \times 10^{-6}$ | 0.19 | 1.37[e] | $1.1 \times 10^{-5}$ |
| Pu(IV) | $2.6 \times 10^{-8}$ | $1 \times 10^{-9}$ | $2 \times 10^{-8}$ | 0.3 | 1.76 | $6.8 \times 10^{-5}$ | $2.3 \times 10^{-6}$ | 6.3 | 6.3 | $1.1 \times 10^{-5}$ |
| Am(III) | $2.6 \times 10^{-8}$ | 0 | $4 \times 10^{-9}$ | 3.6 | 0.32 | 1.0 | $3.1 \times 10^{-8}$ | 0.19 | 1.37[e] | $1.1 \times 10^{-5}$ |

a    In units of moles colloidal actinide per liter – 2009 and 2014 parameters are the same
b    In units of moles colloidal actinide per mole dissolved actinide
c    In units of moles total mobile actinide per liter
d    Humic colloid parameters for CRA-2009 and CRA-2014 are unchanged
e    At 0.5 probability
NOTE:    The colloidal source term is added to the dissolved source term to arrive at a total source term. Mineral fragments were provided with distributions, but the maximum was used as described in Appendix PA-2014, Section 8.4

3

# 1    SOTERM-5.0 Use of the Actinide Source Term in PA

2    The WIPP ASTP provided the parameters to construct the maximum dissolved and suspended
3    colloidal actinide concentrations for use in modeling the mobilization and transport of actinides
4    in the disposal system. In the WIPP PA, mobilization of radionuclides is represented by the
5    PANEL code and transport of radionuclides within the repository and the Salado is represented
6    by the Nuclide Transport System (NUTS) code (Appendix PA-2014, Section 6.7.3 and Section
7    PA-6.7.2, respectively). A description of the simplifications, manipulations, and approach used
8    in the PA to perform this modeling is discussed in this section.

## 9    SOTERM-5.1 Simplifications

10    The DOE has concentrated on those processes most likely to have a significant impact on system
11    performance. Therefore, several simplifications were used in the modeling of radionuclide
12    mobilization and transport in the CCA PA, the CCA PAVT, the CRA-2004 PA, the CRA-2004
13    PABC, the CRA-2009 PA, the CRA-2009 PABC and the CRA-2014 PA calculations. These
14    include

15    •   Using constant solubility parameters and constant colloidal parameters throughout the
16        repository and regulatory period for a given realization

17    •   Modeling only the isotopes most important to compliance

18    •   Using the compositions of Castile and Salado brines (the end-member brines) to bracket the
19        behavior of mixtures of these brines within the repository

20    •   Sampling only the uncertain parameters with the most significant effect on repository
21        performance

22    •   Combining dissolved and colloidal species for transport within the disposal system, as
23        modeled by NUTS and PANEL

### 24    SOTERM-5.1.1 Elements and Isotopes Modeled

25    Selection of isotopes for modeling mobilization and transport in the disposal system with NUTS
26    and PANEL is described in Appendix PA-2014, Section PA-8.4. Runs of PANEL, the PA code
27    that computes total mobilized radionuclide concentrations, include 29 radionuclides in the decay
28    calculations (Kim 2013b, Table 3 and Table 11). Runs of NUTS, the PA code that computes
29    radionuclide transport within the Salado, are based on five radionuclides ($^{230}$Th, $^{234}$U, $^{238}$Pu,
30    $^{239}$Pu, and $^{241}$Am) that represent groupings of radionuclides with similar decay and transport
31    properties (Kim 2013a; Appendix PA-2014, Section PA-4.3.2). The number of radionuclides for
32    transport calculations in NUTS has been reduced because calculations for the full WIPP
33    inventory and decay chains would be very time consuming and because accurate results can be
34    achieved with this limited set of radionuclides (Kicker and Zeitler 2013, Section 4).

35    Transport calculations in the Culebra use a reduced set of four radionuclides ($^{230}$Th, $^{234}$U, $^{239}$Pu,
36    and $^{241}$Am) for computational efficiency (Garner 1996). $^{238}$Pu has been omitted from transport in

1     the Culebra because its short half-life (87.7 years) means that little $^{238}$Pu will enter the Culebra
2     via brine flows up a borehole.

3     **SOTERM-5.1.2 Use of Brine End Members**

4     The general scenarios described in Appendix PA-2014, Section PA-2.3.2.2 and Section PA-8.3
5     and considered in the source term calculations may be categorized into three groups: (1)
6     undisturbed performance (BRAGFLO S1 scenario); (2) intrusion through the repository and into
7     the Castile, intersecting a pressurized brine reservoir (BRAGFLO S2, S3, and S6 scenarios); and
8     (3) intrusion through the repository, but not into a pressurized brine reservoir (BRAGFLO S4
9     and S5 scenarios). The specific scenarios and the associated type of borehole intrusion
10     considered by the WIPP PA are listed in Table SOTERM-22.

11     **Table SOTERM-22. WIPP PA Modeling Scenarios for the CRA-2014 PA (Garner and**
12     **Leigh 2005; Leigh et al. 2005; Kim 2013a)**

| BRAGFLO Scenario | Description | Brine Used in PA |
|---|---|---|
| S1 | E0 (Undisturbed Repository) | Salado (GWB) |
| S2 | E1 intrusion at 350 years penetrates the repository and a brine pocket | Castile (ERDA-6) |
| S3 | E1 intrusion at 1000 years penetrates the repository and a brine pocket | Castile (ERDA-6) |
| S4 | E2 intrusion at 350 years penetrates the repository (only) | Salado (GWB) |
| S5 | E2 intrusion at 1000 years penetrates the repository (only) | Salado (GWB) |
| S6 | E2 intrusion at 1000 years penetrates the repository (only); E1 intrusion at 2000 years penetrates the repository and a brine pocket | Castile (ERDA-6) |

13

14     Brine may enter the repository from three sources, depending on the nature of the borehole
15     intrusion. Under all scenarios, brine may flow from the surrounding Salado through the DRZ
16     and into the repository in response to the difference between the hydraulic head in the repository
17     and in the surrounding formation. For the BRAGFLO S2 through S6 scenarios, in which a
18     borehole is drilled into the repository, brine may flow down the borehole from the Rustler and/or
19     the Dewey Lake. For the BRAGFLO S2, S3, and S6 scenarios, in which a pressurized Castile
20     brine reservoir is intercepted, brine from the Castile may flow up the borehole into the
21     repository.

22     As mentioned in Section SOTERM-2.3.1, the brines in the Salado and Castile have different
23     compositions and the actinide solubilities are somewhat different in each of these end-member
24     compositions.

25     The composition of the more dilute groundwaters from the Rustler and Dewey Lake are expected
26     to change rapidly upon entering the repository as a result of fast dissolution of host Salado
27     minerals from the walls and floor of the repository. These minerals comprise about 90-95%
28     halite and about 1-2% each of polyhalite, gypsum, anhydrite, and magnesite (Brush 1990).
29     Calculations titrating Salado rock into dilute brines using EQ3/6 (Wolery 1992; Wolery and
30     Daveler 1992) show that gypsum, anhydrite, and magnesite saturate before halite. When halite
31     saturates, the brine composition is very similar to that of Castile brine. One hundred times as
32     much polyhalite must be added to the system before the resulting brine has a composition similar
33     to Salado brines. These calculations indicate that if dilute brines dissolve away only the surfaces

1 of the repository, they will obtain Castile-like compositions, but if they circulate through the
2 Salado after saturating with halite, they may obtain compositions similar to Salado brine.
3 Similarly, if Castile brine circulates through enough host rock, it may also approach Salado brine
4 composition. In either case, the actual brine within the repository may be described as a mixture
5 of the two concentrated-brine end members: Salado and Castile. This mixture, however, is very
6 hard to quantify, because it is both temporally and spatially variable. Only in the undisturbed
7 scenario is the mixture well defined as 100% Salado brine over the 10,000-year regulatory
8 period. In this context, the Salado (GWB) and Castile (ERDA-6) brines bracket the range of
9 expected brine compositions.

10 For a panel intersected by a borehole, the BRAGFLO calculations show that in the 10% of the
11 repository represented by the BRAGFLO panel computational cells, the ratio of brine inflow that
12 enters through the borehole versus through inflow from the host rock varies in time and depends
13 on the sampled parameter values and scenario considered. This ratio was the only measure of
14 brine mixing available to the source term runs in the CCA PA, the CCA PAVT, the CRA-2004
15 PA, the CRA-2004 PABC, the CRA-2009 PA, the CRA-2009 PABC, and the CRA-2014 PA
16 calculations. As an estimate, this ratio (1) does not account for compositional changes that occur
17 when H$_2$O is consumed by corrosion reactions or MgO hydration reactions; (2) does not resolve
18 the details of flow, diffusion, and brine interaction with internal pillars and the DRZ; and (3) is
19 an average over one-tenth of the repository. It is expected that the fraction of Salado brine will
20 be quite high in areas of the repository distant from the borehole and much lower near the
21 borehole. Because radionuclide travel up the borehole can lead to significant release, the
22 solubility of radionuclides near the borehole is important. Given these uncertainties, the DOE
23 decided to use the Castile end-member composition to calculate radionuclide solubilities for
24 scenarios where a borehole penetrates a brine reservoir, and to use the Salado end-member
25 composition for scenarios where it does not (see Table SOTERM-22).

26 **SOTERM-5.1.3 Sampling of Uncertain Parameters**

27 The uncertain parameters to be sampled for the PA were selected based on the expected
28 significance of their effect on repository performance. The following four parameters are
29 sampled independently (Kim 2013a):

30 • The solubility uncertainty for oxidation state III (see discussion below and Figure SOTERM-
31    30).

32 • The solubility uncertainty for oxidation state IV (see discussion below and Figure SOTERM-
33    31).

34 • The oxidation state for Pu, Np, and U. The sampled value is a flag that is "low" 50% of the
35    time and "high" 50% of the time. If the flag is set to "high," Pu is assumed to be in the IV
36    oxidation state, Np is assumed to be in the V oxidation state, and U is assumed to be in the
37    VI oxidation state. If the flag is set to "low," Pu is assumed to be in the III oxidation state
38    and Np and U are assumed to be in the IV oxidation state.

39 • The humic acid proportionality constant for the III oxidation state in Castile brine (see Table
40    SOTERM-21 and Figure SOTERM-32).

1
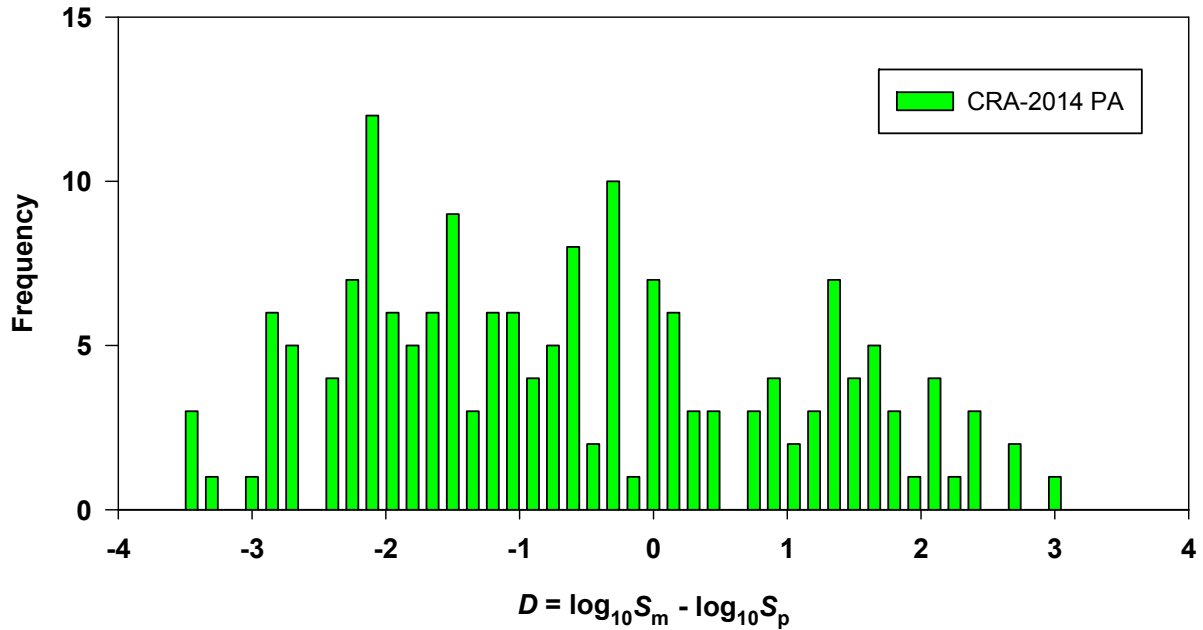
**Figure SOTERM-30.  Frequency Distribution of the Difference of Experimental log Solubility ($\log_{10}S_m$) from Model-Predicted Value ($\log_{10}S_p$) for Nd(III) and Am(III).  A total of 243 measured and predicted solubilities were compared (Brush and Domski 2013c).**

6   As discussed by Garner and Leigh (Garner and Leigh 2005, Section 2.3), the solubility
7   uncertainty for oxidation state V is zero.  There is no uncertainty assigned to the solubility for
8   oxidation state VI because the EPA specified a fixed, maximum solubility of $1 \times 10^{-3}$ mol/L for
9   U(VI).

10  Actinide solubilities for a single realization in the PA depend on (1) the oxidation state; (2) the
11  brine for that realization (see Table SOTERM-22); and (3) the solution concentration
12  uncertainty, as shown in Equation (SOTERM.73).
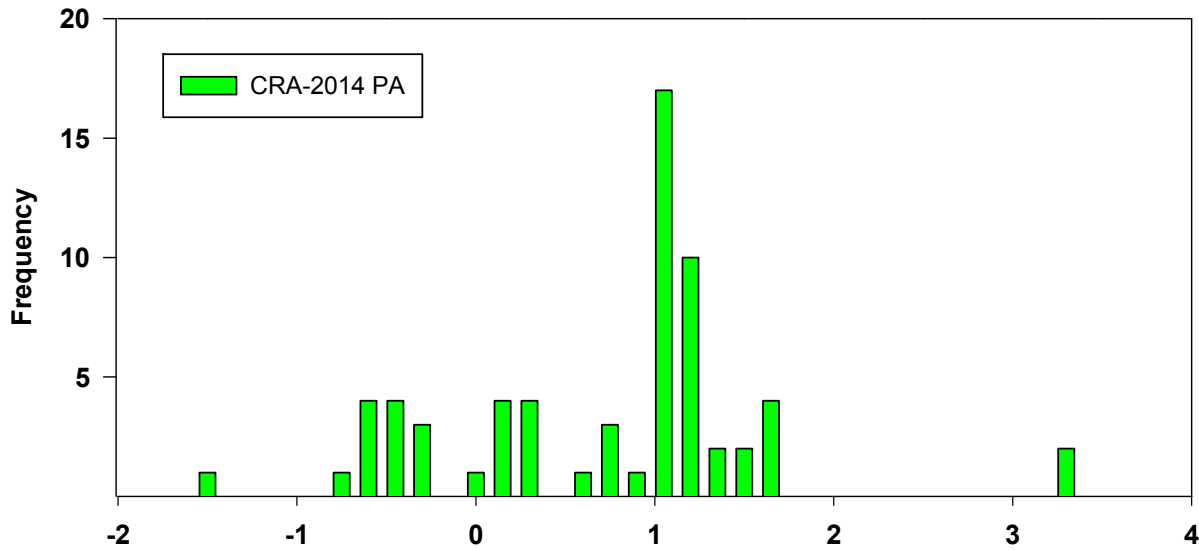
1

2 **Figure SOTERM-31. Frequency Distribution of the Deviation of Experimental log**
3 **Solubility from Model-Predicted Value for all An(IV)**
4 **Comparisons. A total of 45 measured and predicted solubilities**
5 **were compared (Brush and Domski 2013c).**

6 $$C_{i,b} = (S_{i,b}) \times (10^{SU_i}) \hspace{2cm} \text{(SOTERM.73)}$$

7 $C_{i,b}$, used for every element in oxidation state $i$, is the concentration of oxidation state $i$ and brine
8 $b$. $S_{i,b}$ is the solubility calculated for oxidation state $i$ in brine $b$ with EQ3/6 (see Table
9 SOTERM-18). $SU_i$ is the solubility uncertainty sampled from a distribution unique to each
10 oxidation state. Figure SOTERM-30 shows the distribution of SU values for oxidation state III.
11 Figure SOTERM-31 shows the distribution of SU values for oxidation state IV. These
12 distributions are calculated and documented in Brush and Domski (Brush and Domski 2013c).

13 Figure SOTERM-32 shows the cumulative distribution function for the humic-acid
14 proportionality constant. All other humic-acid proportionality constants are constant values for
15 both Castile and Salado brines, as shown in Table SOTERM-21.

16 **SOTERM-5.1.4 Multiple Brine Volumes**

17 Variable brine volume in the calculation of radionuclide concentrations in brine was
18 implemented in the CRA-2014 PA. Radionuclide solubilities were calculated in terms of 1×, 2×,
19 3×, 4×, and 5× the minimum repository brine volume necessary for a DBR. Implementation of
20 multiple brine volumes in PANEL calculations needs actinide solubilities that were calculated
21 over multiple brine volumes by Brush and Domski (Brush and Domski 2013a). The calculated
22 baseline actinide solubilities at 1× and 5× minimum brine volume are listed in Table SOTERM-
23 19. A more detailed discussion of these results and the effects of variable brine volumes can be
24 found in Brush and Domski (Brush and Domski 2013a).

1   **SOTERM-5.1.5 Combining the Transport of Dissolved and Colloidal Species in the Salado**

2   Dissolved and colloidal species may transport differently because of different diffusion rates,
3   sorption onto stationary materials, and size-exclusion effects (filtration and hydrodynamic
4   chromatography).  With maximum molecular diffusion coefficients of about $4 \times 10^{-10}$ m$^2$/s,
5   actinides are estimated to diffuse about 10 m in 10,000 years, a negligible distance.  Sorption and
6   filtration have beneficial but unquantified effects on performance.  Hydrodynamic
7   chromatography may increase colloidal transport over dissolved transport by, at most, a factor of
8   two for theoretically perfect colloidal-transport conditions.  In the WIPP, the expected increase is
9   much lower.  Given the small or beneficial nature of these effects, they were not included in the
10  CCA PA, the CCA PAVT, the CRA-2004 PA, the CRA-2004 PABC, the CRA-2009 PA, the
11  CRA-2009 PABC, or the CRA-2014 PA calculations of radionuclide transport in the repository.
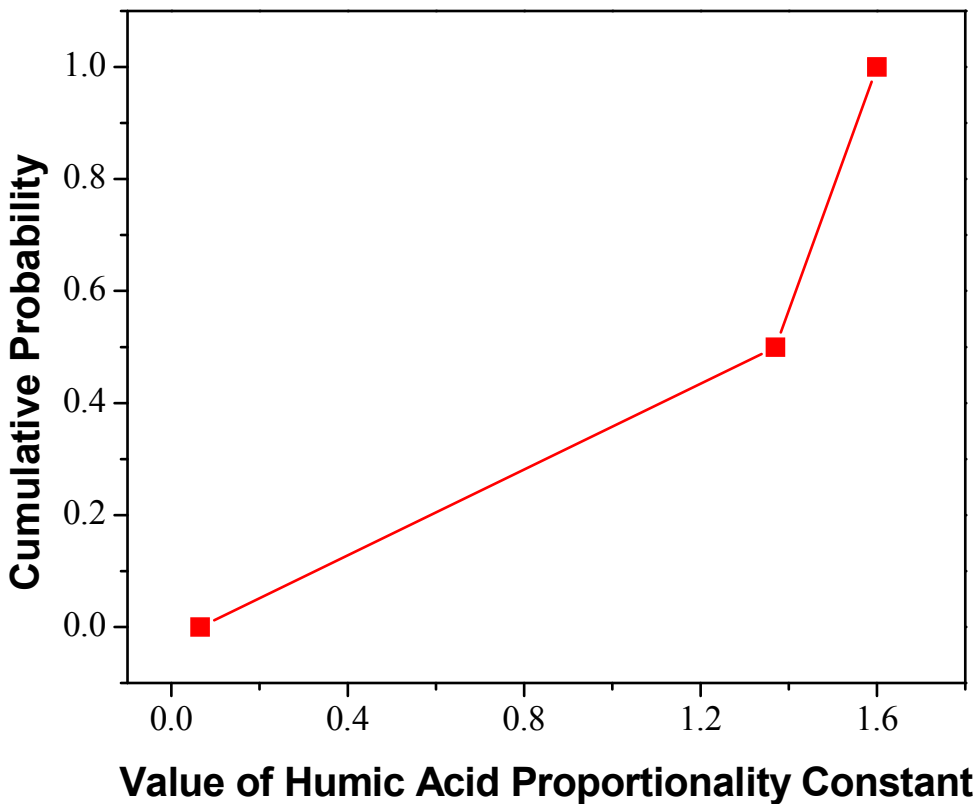


12

13   **Figure SOTERM-32.  Cumulative Distribution Function for the Humic-Acid**
14   **Proportionality Constant for the III Oxidation State in Castile**
15   **Brine**

16   **SOTERM-5.2 Construction of the Source Term**

17   Because PA does not differentiate dissolved from colloidal species for transport in the Salado,
18   the total source term in the Salado is the sum of both components..  To model transport within
19   the Culebra, however, this simplification was replaced by separating the mobilized actinides
20   delivered to the Culebra by Salado transport codes into five components (dissolved, humic,

1 microbial, mineral-fragment, and intrinsic colloids) to account for differences in their transport
2 behavior. This is important because transport within the repository occurs through, at most,
3 hundreds of meters of poorly defined waste undergoing decomposition, whereas transport
4 through the Culebra occurs over kilometers in a relatively homogeneous (compared to waste)
5 fractured dolomite.

6 The parameters required to construct the source term were as follows:

1. Solubilities for four oxidation states in Salado and Castile brines, the two brine end
   members.

2. Uncertainty distributions to be applied to the median solubilities for oxidation states III
   and IV.

3. A scheme for assigning sampled oxidation states ("low" or "high").

4. Colloidal concentrations or proportionality constants for each actinide (Th, U, Np, Pu,
   and Am) and an associated oxidation state for each of four colloid types.

5. Caps on the actinide concentrations that may be applied to two types of colloids
   (microbial and humic).

6. Cm is assigned the source term calculated for Am (i.e., it has the same
   solubility/speciation as Am up to its inventory limit).

18 Cm and Np are not explicitly transported in NUTS, although they are implicitly lumped with
19 other modeled isotopes. They are, however, included in the PANEL calculations for use with the
20 DBR calculations in PA.

21 These parameters are combined into a single maximum concentration for each modeled actinide
22 in the PA calculations. The term "total mobilized concentration" is used for the combined
23 concentrations of dissolved and colloidal species. The combined concentrations are not
24 necessarily the actual concentrations, because the concentration may be lower as a result of
25 inventory limits. Both NUTS and PANEL assume that the actinide concentrations specified by
26 the total mobilized concentrations are attained instantaneously as long as sufficient inventory is
27 available. When the inventory is insufficient, the actual mobilized concentration will be lower
28 and is said to be inventory limited. The calculation of the total mobilized concentration is
29 performed by PANEL for each of 100 sampled vectors in a replicate. A similar methodology to
30 generate the combined maximum concentrations was used for the CCA PA, the CCA PAVT, the
31 CRA-2004 PA, the CRA-2004 PABC, the CRA-2009 PA, the CRA-2009 PABC and the CRA-
32 2014 PA.

33 All of the source term parameters and their associated distributions are entered into the PA
34 parameter database. For each sampled parameter, the Latin Hypercube Sampling code uses the
35 distribution from the PA parameter database to create 100 sampled values. These values are
36 combined with the parameters that have constant values and stored in computational databases
37 for each of the 100 vectors (i.e., 100 realizations), which constitute one replicate. For each
38 realization, PANEL uses both the constant and sampled values for all of the source term

1  parameters, and constructs the source term for NUTS and PANEL, as shown below.  This
2  process is repeated for scenarios using the Salado end-member total mobilized concentration and
3  for scenarios using the Castile end-member total mobilized concentration.

4  $\qquad$ Dissolved = Baseline Solubility $\times 10^{\text{Sampled from Solubility Uncertainty Distribution}}$ $\qquad$ (SOTERM.74)

5  IF (Dissolved × Proportionality Constant of Humic Colloids < Humic Cap),
6  $\qquad$ THEN Humic = Dissolved × Proportionality Constant of Humic Colloid, $\quad$ (SOTERM.75)

7  $\qquad$ ELSE  Humic = Humic Cap

8  $\qquad$ Mineral = Database Concentration (a constant value) $\qquad$ (SOTERM.76)

9  $\qquad$ Intrinsic = Database Concentration (a constant value) $\qquad$ (SOTERM.77)

10 Microbial_temp = Dissolved × Proportionality Constant of Microbial Colloids,
11 Total Mobile_temp = Dissolved + Humic + Microbial_temp + Mineral + Intrinsic

12 IF (Total Mobile_temp < Microbial Cap),
13 $\qquad$ THEN Microbial = Microbial_temp, $\qquad$ (SOTERM.78)

14 $\qquad$ ELSE  IF( (Dissolved + Humic + Mineral + Intrinsic) > Microbial Cap ),
15 $\qquad$ THEN Microbial = 0
16 $\qquad$ ELSE  Microbial = Microbial Cap – (Dissolved + Humic + Mineral + Intrinsic)

17 $\qquad$ Total Mobile = Dissolved + Humic + Microbial + Mineral + Intrinsic $\qquad$ (SOTERM.79)

18 For actinides with more than one oxidation state, the oxidation state is specified by the oxidation-
19 state parameter

20 IF (OXSTAT ≤ 0.5); THEN Lower Oxidation State,
21 $\qquad$ ELSE  Higher Oxidation State $\qquad$ (SOTERM.80)

22 $\qquad$ where OXSTAT is the oxidation-state parameter sampled from a uniform distribution
23 $\qquad$ between 0 and 1.

24 Solubility calculations are performed for Am(III), Th(IV), and Np(V) and the oxidation-state
25 analogy is used to apply the values calculated for these elements/oxidation states to other
26 actinide elements in the same oxidation states (if any). The total mobilized concentration and
27 mobile fractions for Cm are set equal to the values for Am.  In addition, the PA groups
28 radioisotopes with similar decay and transport properties for the NUTS and SECOTP2D
29 (component radionuclide transport in fractures or granular acquifers) transport calculations, as
30 explained in Section SOTERM-5.1.5.  For example, the U solubility is decreased to account for
31 the shared solubility with the low-activity $^{238}$U, which is not explicitly modeled, enabling NUTS
32 to properly represent the effect of the U isotopes on compliance using the single lumped isotope
33 $^{234}$U (Appendix PA-2014, Section PA-4.3.2).

1  PANEL also calculates the fraction of each actinide mobilized by the five different mechanisms,
2  as follows:

3      Fraction dissolved = Dissolved/Total Mobile                              (SOTERM.81)

4      Fraction on humics = Humic/Total Mobile                                  (SOTERM.82)

5      Fraction in/on microbes = Microbial/Total Mobile                         (SOTERM.83)

6      Fraction on mineral fragments = Mineral/Total Mobile                      (SOTERM.84)

7      Fraction as intrinsic colloid = Intrinsic/Total Mobile                    (SOTERM.85)

## 8  SOTERM-5.3 Example Calculation of Actinide Solubility

9   As an example, for one realization in Salado brine, the sampled value for OXSTAT was 0.9, so
10  Pu would be present in the IV state.  The sampled value of the solubility uncertainty distribution
11  was 0.09 for the IV state, which has a median brine solubility of $6.05 \times 10^{-8}$ M.  The humic
12  proportionality constant for the IV oxidation state in Salado brine is 6.3, the microbial
13  proportionality constant for Pu is 1.76, the humic cap is $1.1 \times 10^{-5}$ M, the microbe cap for Pu is
14  $2.3 \times 10^{-6}$ M, the concentration of the actinide on mineral fragments is $2.6 \times 10^{-8}$ M, and the Pu
15  intrinsic-colloid concentration is $2 \times 10^{-8}$ M.

16  For this realization, the maximum dissolved concentration of Pu(IV) used by the PA would be

17                $C_{Pu} = (6.05 \times 10^{-8}) \times (10^{0.09}) = 7.44 \times 10^{-8}$ M.          (SOTERM.86)

18  (The calculations for this example have been rounded to two significant figures, although the PA
19  would not round the intermediate or final values.)  $C_{Pu}$ is the maximum dissolved concentration
20  of all combined isotopes of Pu.

21  The maximum humic-complexed Pu would be

22      $(7.44 \times 10^{-8}$ M$)(6.3$ mol adsorbed per mol$) = 4.69 \times 10^{-7}$ M.          (SOTERM.87)

23  This value, however, does not exceed the cap for humic-mobilized Pu, $1.1 \times 10^{-5}$ M.  Therefore,
24  in this case, the cap would not be used for the maximum humic-mobilized actinide concentration.
25  Note that the humic-mobilized concentration of Pu exceeds the maximum dissolved
26  concentration of Pu, which is usually the case.

27  The maximum microbial-mobilized Pu would be

28      $(7.44 \times 10^{-8}$ M$)(1.76$ mol bioaccumulated per mol$) = 1.31 \times 10^{-7}$ M.          (SOTERM.88)

29  This value is less than the cap, $2.3 \times 10^{-6}$ M, so the cap does not affect microbial-mobilized Pu
30  for this realization.

1  The total mobilized concentration of Pu(IV) for this realization would then be the sum of the
2  dissolved and colloidal contributions (see Equation [SOTERM.79]):

3  Total Mobile = Dissolved + Humic + Microbial + Mineral + Intrinsic,     (SOTERM.89)
4  $= 7.44 \times 10^{-8} + 4.69 \times 10^{-7} + 1.31 \times 10^{-7} + 2.6 \times 10^{-8} + 2.0 \times 10^{-8}$,
5  $= 7.20 \times 10^{-7}$ M.

## 6  SOTERM-5.4 Calculated Dissolved, Colloidal, and Total Actinide Solubilities

7  The output of the PANEL calculations is a computational database containing the source term
8  and effective inventories.  NUTS and PANEL both assume instantaneous dissolution and
9  colloidal mobilization up to the solubility limits when sufficient inventory is present, as
10  discussed in Appendix PA-2014, Section PA-4.3.4.  Table SOTERM-23 shows the dissolved and
11  colloidal components of the source term and the total mobile actinide concentrations obtained
12  when median parameter values are used. For conservatism, 1× minimum brine volume was used
13  because total mobilized concentration for a radionuclide decreases as the brine volume increases
14  (Kim 2013a).

15  **Table SOTERM-23.  Concentrations (M) of Dissolved, Colloidal, and Total Mobile**
16  **Actinides Obtained Using Median Parameter Values for the CCA PAVT, CRA-2004**
17  **PABC, CRA-2009 PABC and CRA-2014 PAa**

| Actinide Oxidation State and Brine | PAVT | CRA-2004 PABC | CRA-2009 PABC | CRA-2014 PA |
|---|---|---|---|---|
| Pu(III), dissolved, Salado brine | $9.75 \times 10^{-8}$ | $3.61 \times 10^{-7}$ | $1.96 \times 10^{-6}$ | $3.46 \times 10^{-7}$ |
| Pu(III), colloidal, Salado brine | $7.48 \times 10^{-8}$ | $2.04 \times 10^{-7}$ | $9.87 \times 10^{-7}$ | $7.21 \times 10^{-7}$ |
| Pu(III), total mobile, Salado brine | $1.72 \times 10^{-7}$ | $5.64 \times 10^{-7}$ | $2.95 \times 10^{-6}$ | $1.07 \times 10^{-6}$ |
| Pu(III), dissolved, Castile brine | $1.06 \times 10^{-8}$ | $2.68 \times 10^{-7}$ | $1.78 \times 10^{-6}$ | $1.98 \times 10^{-7}$ |
| Pu(III), colloidal, Castile brine | $4.46 \times 10^{-8}$ | $4.75 \times 10^{-7}$ | $3.00 \times 10^{-6}$ | $6.65 \times 10^{-7}$ |
| Pu(III), total mobile, Castile brine | $5.52 \times 10^{-8}$ | $7.44 \times 10^{-7}$ | $4.79 \times 10^{-6}$ | $8.62 \times 10^{-7}$ |
| Am(III), dissolved, Salado brine | $9.75 \times 10^{-8}$ | $3.61 \times 10^{-7}$ | $1.96 \times 10^{-6}$ | $3.46 \times 10^{-7}$ |
| Am(III), colloidal, Salado brine | $3.96 \times 10^{-7}$ | $1.39 \times 10^{-6}$ | $7.45 \times 10^{-6}$ | $9.57 \times 10^{-8}$ |
| Am(III), total mobile, Salado brine | $4.93 \times 10^{-7}$ | $1.75 \times 10^{-6}$ | $9.41 \times 10^{-6}$ | $4.42 \times 10^{-7}$ |
| Am(III), dissolved, Castile brine | $1.06 \times 10^{-8}$ | $2.68 \times 10^{-7}$ | $1.78 \times 10^{-6}$ | $1.98 \times 10^{-7}$ |
| Am(III), colloidal, Castile brine | $7.78 \times 10^{-8}$ | $1.34 \times 10^{-6}$ | $8.88 \times 10^{-6}$ | $3.01 \times 10^{-7}$ |
| Am(III), total mobile, Castile brine | $8.83 \times 10^{-8}$ | $1.61 \times 10^{-6}$ | $1.07 \times 10^{-5}$ | $4.98 \times 10^{-7}$ |
| Th(IV), dissolved, Salado brine | $1.06 \times 10^{-8}$ | $6.70 \times 10^{-8}$ | $1.70 \times 10^{-8}$ | $6.46 \times 10^{-7}$ |
| Th(IV), colloidal, Salado brine | $1.25 \times 10^{-7}$ | $6.56 \times 10^{-7}$ | $1.86 \times 10^{-7}$ | $4.12 \times 10^{-6}$ |
| Th(IV), total mobile, Salado brine | $1.36 \times 10^{-7}$ | $7.23 \times 10^{-7}$ | $2.03 \times 10^{-7}$ | $4.76 \times 10^{-6}$ |
| Th(IV), dissolved, Castile brine | $3.33 \times 10^{-8}$ | $8.07 \times 10^{-8}$ | $2.11 \times 10^{-8}$ | $7.50 \times 10^{-7}$ |
| Th(IV), colloidal, Castile brine | $3.39 \times 10^{-7}$ | $7.85 \times 10^{-7}$ | $2.24 \times 10^{-7}$ | $4.77 \times 10^{-6}$ |
| Th(IV), total mobile, Castile brine | $3.73 \times 10^{-7}$ | $8.65 \times 10^{-7}$ | $2.45 \times 10^{-7}$ | $5.52 \times 10^{-6}$ |

[a.] Values are calculated using data retrieved from the WIPP PA Database http://tgw.sandia.gov/ and equations SOTERM.74 through SOTERM.79.

**Table SOTERM-23.  Concentrations (M) of Dissolved, Colloidal, and Total Mobile Actinides Obtained Using Median Parameter Values for the CCA PAVT, CRA-2004 PABC, CRA-2009 PABC and CRA-2014 PA[a] (*Continued*)**

| Actinide Oxidation State and Brine | PAVT | CRA-2004 PABC | CRA-2009 PABC | CRA-2014 PA |
|---|---|---|---|---|
| U(IV), dissolved, Salado brine | $1.06 \times 10^{-8}$ | $6.70 \times 10^{-8}$ | $1.70 \times 10^{-8}$ | $6.46 \times 10^{-7}$ |
| U(IV), colloidal, Salado brine | $9.26 \times 10^{-8}$ | $4.48 \times 10^{-7}$ | $1.33 \times 10^{-7}$ | $4.13 \times 10^{-6}$ |
| U(IV), total mobile, Salado brine | $1.03 \times 10^{-7}$ | $5.15 \times 10^{-7}$ | $1.50 \times 10^{-7}$ | $4.77 \times 10^{-6}$ |
| U(IV), dissolved, Castile brine | $3.33 \times 10^{-8}$ | $8.07 \times 10^{-8}$ | $2.11 \times 10^{-8}$ | $7.50 \times 10^{-7}$ |
| U(IV), colloidal, Castile brine | $2.36 \times 10^{-7}$ | $5.35 \times 10^{-7}$ | $1.59 \times 10^{-7}$ | $4.78 \times 10^{-6}$ |
| U(IV), total mobile, Castile brine | $2.69 \times 10^{-7}$ | $6.15 \times 10^{-7}$ | $1.80 \times 10^{-7}$ | $5.53 \times 10^{-6}$ |
| Pu(IV), dissolved, Salado brine | $1.06 \times 10^{-8}$ | $6.70 \times 10^{-8}$ | $1.70 \times 10^{-8}$ | $6.46 \times 10^{-7}$ |
| Pu(IV), colloidal, Salado brine | $9.67 \times 10^{-8}$ | $4.69 \times 10^{-7}$ | $1.39 \times 10^{-7}$ | $4.12 \times 10^{-6}$ |
| Pu(IV), total mobile, Salado brine | $1.07 \times 10^{-7}$ | $5.36 \times 10^{-7}$ | $1.56 \times 10^{-7}$ | $4.76 \times 10^{-6}$ |
| Pu(IV), dissolved, Castile brine | $3.33 \times 10^{-8}$ | $8.07 \times 10^{-8}$ | $2.11 \times 10^{-8}$ | $7.50 \times 10^{-7}$ |
| Pu(IV), colloidal, Castile brine | $2.47 \times 10^{-7}$ | $5.60 \times 10^{-7}$ | $1.66 \times 10^{-7}$ | $4.77 \times 10^{-6}$ |
| Pu(IV), total mobile, Castile brine | $2.80 \times 10^{-7}$ | $6.40 \times 10^{-7}$ | $1.87 \times 10^{-7}$ | $5.52 \times 10^{-6}$ |
| U(VI), dissolved, Salado brine | $7.07 \times 10^{-6}$ | $1.00 \times 10^{-3}$ | $1.00 \times 10^{-3}$ | $1.00 \times 10^{-3}$ |
| U(VI), colloidal, Salado brine | $8.89 \times 10^{-7}$ | $1.31 \times 10^{-5}$ | $1.31 \times 10^{-5}$ | $1.11 \times 10^{-5}$ |
| U(VI), total mobile, Salado brine | $7.96 \times 10^{-6}$ | $1.01 \times 10^{-3}$ | $1.01 \times 10^{-3}$ | $1.01 \times 10^{-3}$ |
| U(VI), dissolved, Castile brine | $7.15 \times 10^{-6}$ | $1.00 \times 10^{-3}$ | $1.00 \times 10^{-3}$ | $1.00 \times 10^{-3}$ |
| U(VI), colloidal, Castile brine | $3.69 \times 10^{-6}$ | $1.31 \times 10^{-5}$ | $1.31 \times 10^{-5}$ | $1.11 \times 10^{-5}$ |
| U(VI), total mobile, Castile brine | $1.08 \times 10^{-5}$ | $1.01 \times 10^{-3}$ | $1.01 \times 10^{-3}$ | $1.01 \times 10^{-3}$ |

b. Values are calculated using data retrieved from the WIPP PA Database http://tgw.sandia.gov/ and equations SOTERM.74 through SOTERM.79.

# SOTERM-6.0 References

(*Indicates a reference that has not been previously submitted.)

Abdelouas, A., W. Lutze, W. Gong, E.H. Nuttall, B.A. Strietelmeier, and B.J. Travis. 2000. "Biological Reduction of Uranium in Groundwater and Subsurface Soil." *The Science of the Total Environment*, vol. 250: 21.

Allard, B. 1982. *Solubilities of Actinides in Neutral or Basic Solutions*. Actinides in Perspective. N. Edelstein, ed. New York: Pergamon. pp. 553–80.

Allard, S., and C. Ekberg. 2006a. "Complexing properties of a α-isosaccharinate: thorium." *Radiochimica Acta* 94, 537–540.*

Allard, S., and C. Ekberg. 2006b. "Complexing properties of α-isosaccharinate: stability constants, enthalpies and entropies of Th-complexation with uncertainty analysis." *J. Solution Chem*. 35, 1173–1186.*

Altmaier, M., V. Metz, V. Neck, R. Muller, and T. Fanghänel. 2003. "Solid-Liquid Equilibria of $Mg(OH)_2$(cr) and $Mg_2(OH)_3Cl_4H_2O$(cr) in the System Mg-Na-H-OH-Cl-$H_2O$ at 25ºC." *Geochimica et Cosmochimica Acta*, vol. 67: 3595–3601.

Altmaier, M., V. Neck, and Th. Fanghänel. 2004. "Solubility and Colloid formation of Th(IV) in concentrated NaCl and $MgCl_2$ Solutions." *Radiochimica Acta*, vol. 92: 537–43.

Altmaier, M., V. Neck, and Th. Fanghänel. 2008. "Solubility of Zr(IV), Th(IV) and Pu(IV) hydrous oxides in $CaCl_2$ solutions and the formation of ternary Ca-M(IV)-OH complexes." *Radiochimica Acta* vol. 96: (9-11) 541-550.*

Altmaier, M., V. Neck, M.A. Denecke, R. Yin, and Th. Fanghänel. 2006. "Solubility of $ThO_2$ $\cdot xH_2O$(am) and the Formation of Ternary Th(IV) Hydroxide-Carbonate Complexes in $NaHCO_3$-$Na_2CO_3$ Solutions Containing 0–4M NaCl." *Radiochimica Acta*, vol. 94: 495–500.

Altmaier, M., V. Neck, R. Müller, and Th. Fanghänel. 2005. "Solubility of $ThO_2$ $xH_2O$(am) in Carbonate Solution and the Formation of Ternary Th(IV) Hydroxide-carbonate Complexes." *Radiochimica Acta*, vol. 93: 83–92.

Ams, D.A., J.S. Swanson, J. Szymanowski, J.B. Fein, M. Richmann, and D.T. Reed. 2013. "The Effect of High Ionic Strength on Neptunium (V) Adsorption to a halophilic bacterium." *Geochimica et Comoschimica Acta*, vol.: 110: 45-57.*

Banaszak, J.E., D.T. Reed, and B.E. Rittmann. 1998a. "Speciation-Dependent Toxicity of Neptunium(V) Towards Chelatobacter heintzii." *Environmental Science and Technology*, vol. 32: 1085–91.

Banaszak, J.E., B.E. Rittmann, and D.T. Reed. 1998b. *Subsurface Interactions of Actinide Species and Microorganisms: Implications for the Bioremediation of Actinide-Organic Mixtures*. ANL-98/26. Argonne, IL: Argonne National Laboratory.

1  Banaszak, J.E., S.M. Webb, B.E. Rittmann, J.-F. Gaillard, and D.T. Reed.  1999.  "Fate of
2  Neptunium in Anaerobic, Methanogenic Microcosm." *Scientific Basis for Nuclear Waste
3  Management XXII*, vol. 556: 1141–49.

4  Barnhart, B.J., E.W. Campbell, J.M. Hardin, E. Martinez, D.E. Caldwell, and R. Hallett.  1978a.
5  *Potential microbial impact on transuranic wastes under conditions expected in the Waste
6  Isolation Pilot Plant (WIPP)*.  LA-7788-PR Progress Report, October-December 15, 1978.  Los
7  Alamos, NM: Los Alamos Scientific Laboratory.*

8  Barnhart, B.J., E.W. Campbell, J.M. Hardin, E. Martinez, D.E. Caldwell, and R. Hallett.  1979b.
9  *Potential microbial impact on transuranic wastes under conditions expected in the Waste
10  Isolation Pilot Plant (WIPP)*.  LA-7839-PR Progress Report, December 15, 1978-March 15,
11  1979.  Los Alamos, NM: Los Alamos Scientific Laboratory.*

12  Barnhart, B.J., E.W. Campbell, E. Martinez, D.E. Caldwell, and R. Hallett.  1979c.  *Potential
13  microbial impact on transuranic wastes under conditions expected in the Waste Isolation Pilot
14  Plant (WIPP)*.  LA-7918-PR Progress Report, March 15-June 15, 1979.  Los Alamos, NM: Los
15  Alamos Scientific Laboratory.*

16  Barnhart, B.J., E.W. Campbell, J.M. Hardin, E. Martinez, D.E. Caldwell, and R. Hallett.  1979d.
17  *Potential microbial impact on transuranic wastes under conditions expected in the Waste
18  Isolation Pilot Plant (WIPP)*.  LA-8297-PR Progress Report, October 1, 1978-September 30,
19  1979.  Los Alamos, NM: Los Alamos Scientific Laboratory.*

20  Barton, L.L., K. Choudhury, B.M. Thomson, K. Steenhoudt, and A.R. Groffman.  1996.
21  "Bacterial Reduction of Soluble Uranium: The First Step of In Situ Immobilization of Uranium."
22  *Radioactive Waste Management and Environmental Restoration*, vol. 20: 141–51.

23  Behrends, T., and P. Van Cappellen.  2005.  "Competition Between Enzymatic and Abiotic
24  Reduction of Uranium(VI) under Iron Reducing Conditions." *Chemical Geology*, vol. 220: 315–
25  27.

26  Bender, J., M.C. Duff, P. Phillips, and M. Hill.  2000.  "Bioremediation and Bioreduction of
27  Dissolved U(VI) by Microbial Mat Consortium Supported on Silica Gel Particles."
28  *Environmental Science and Technology*, vol. 34: 3235–41.

29  Bennett, D., Y. Wang, and T. Hicks.  1996.  Memorandum to Distribution (Subject: *An
30  Evaluation of Heat Generation Processes for the WIPP*).  20 August 1996.  ERMS 240635.
31  Albuquerque, NM: Sandia National Laboratories.*

32  Birbir, M., B. Calli, B. Mertoglu, R. Bardavid, A. Oren, M. Ogmen and A. Ogan.  2007.
33  "Extremely Halophilic Archaea from Tuz Lake, Turkey, and the Adjacent Kaldirim and Kayacik
34  Salterns." *World J. Microbiol Biotechnol*, 23:309-316.*

35  Borkowski, M., J.-F. Lucchini, M.K. Richmann, and D.T. Reed.  2008.  *Actinide (III) Solubility
36  in WIPP Brine: Data Summary and Recommendations*.  LCO-ACP-08, LANL\ACRSP Report,
37  LA-14360.  Los Alamos, NM: Los Alamos National Laboratory.

Borkowski, M. J-F. Lucchini, M.K. Richmann, and D.T. Reed.  2010a.  *Actinide (III) Solubility in WIPP Brine: Data Summary and Recommendations*.  Report LA-14360.  Los Alamos, NM: Los Alamos National Laboratory.*

Borkowski, M., M.K. Richmann, D.T. Reed, and Y.-L. Xiong.  2010b.  "Complexation of Nd(III) with Tetraborate Ion and Its Effect on Actinide(III) Solubility in WIPP Brine." *Radiochimica Acta*, vol.: 98.9-11 (2010):  577–582.*

Borkowski, M., M.K. Richmann, and J-F. Lucchini.  2012.  *Solubility of An(IV) in WIPP Brine: Thorium Analog Studies in WIPP Simulated Brine*.  Los Alamos Report LCO-ACP-17, LA-UR 12-24417.  Carlsbad, NM: Los Alamos National Laboratory.*

Brendebach, B., M. Altmaier, J. Rothe, V. Neck, and M.A. Denecke.  2007.  EXAFS Study of Aqueous Zr(IV) and Th(IV) Complexes in Alkaline $CaCl_2$ Solutions: $Ca_3[Zr(OH)_6]^{4+}$ and $Ca_4[Th(OH)_8]^{4+}$."  *Inorganic Chemistry*, vol. 46: 6804–10.

Brush, L.H.  1990.  *Test Plan for Laboratory and Modeling Studies of Repository and Radionuclide Chemistry for the Waste Isolation Pilot Plant*.  SAND90-0266.  ERMS 226015.  Albuquerque, NM: Sandia National Laboratories.

Brush, L.H.  1995.  *Systems Prioritization Method—Iteration 2 Baseline Position Paper: Gas Generation in the Waste Isolation Pilot Plant* (March 17).  ERMS 228740.  Albuquerque, NM: Sandia National Laboratories.

Brush, L.H., and J. Garner.  2005.  Letter to D. Kessel (Subject: *Additional Justification for the Insignificant Effect of Np on the Long-Term Performance of the WIPP*).  21 February 2005.  ERMS 538533.  Albuquerque, NM: Sandia National Laboratories.

Brush, L.H., and P.S. Domski.  2013a.  *Prediction of Baseline Actinide Solubilities for the WIPP CRA-2014 PA*.  Analysis report, January 21, 2013.  ERMS 559138.  Carlsbad, NM: Sandia National Laboratories.*

Brush, L.H., and P.S. Domski.  2013b.  *Calculation of Organic-Ligand Concentrations for the WIPP CRA-2014 PA*.  Analysis report, January 14, 2013.  ERMS 559005.  Carlsbad, NM: Sandia National Laboratories.*

Brush, L.H., and P.S. Domski.  2013c.  *Uncertainty Analysis of Actinide Solubilities for the WIPP CRA-2014 PA, Rev. 1 Supercedes ERMS 559278*.  ERMS 559712.  Albuquerque, NM: Sandia National Laboratories.*

Brush, L.H., and Y. Xiong.  2005a.  *Calculation of Organic-Ligand Concentrations for the WIPP Performance Assessment Baseline Calculations* (May 4).  ERMS 539635.  Carlsbad, NM: Sandia National Laboratories.

Brush, L.H., and Y. Xiong.  2005b.  *Calculation of Actinide Solubilities for the WIPP Performance Assessment Baseline Calculations, Analysis AP-120, Rev. 0* (Rev. 0).  AP-120.  ERMS 539255.  Carlsbad, NM: Sandia National Laboratories.

1   Brush, L.H., P.S. Domski, and Y.-L. Xiong. 2011 *Predictions of the Compositions of Standard*
2   *WIPP Brines as a Function of pcH for Laboratory Studies of the Speciation and Solubilities of*
3   *Actinides*. Analysis report, June 23, 2011. ERMS 555727 Carlsbad, NM: Sandia National
4   Laboratories.*

5   Brush, L.H., R.C. Moore, and N.A. Wall. 2001. *Response to EEG-77, Plutonium Chemistry*
6   *under Conditions Relevant for WIPP Performance Assessment: Review of Experimental Results*
7   *and Recommendations for Future Work, by V. Oversby*. ERMS 517373. Carlsbad, NM: Sandia
8   National Laboratories.

9   Bundschuh, T., R. Knopp, R. Müller, J.I. Kim, V. Neck, and Th. Fanghänel. 2000. "Application
10  of LIBD to the Determination of the Solubility Product of Thorium(IV)-Colloids."
11  *Radiochimica Acta*, vol. 88: 625–629.

12  Büppelmann, K., J.I. Kim, and Ch. Lierse. 1988. "The Redox Behavior of Pu in Saline
13  Solutions under Radiolysis Effects." *Radiochimica Acta*, vol. 44/45: 65–70.

14  Büppelmann, K., S. Magirius, Ch. Lierse, and J.I. Kim. 1986. "Radiolytic Oxidation of Am (III)
15  to Am (V) and Pu(IV) to Pu (VI) in Saline Solution." *Journal of Less- Common Metals*, vol.
16  122: 329–36.

17  Caldwell, D., R. Hallet, M. Molecke, E. Martinez, and B. Barnhart. 1988. *Rates of CO$_2$*
18  *Production From the Microbial Degradation of Transuranic Wastes Under Simulated Geologic*
19  *Isolation Conditions*. Report SAND87-7170. Carlsbad NM: Sandia National Laboratories.*

20  Camphouse, R.C., D.C. Kicker, S. Kim, T. Kirchner, J. Long, B. Malama, and T. Zeitler. 2013.
21  *Summary Report for the 2014 WIPP Compliance Recertification Application Performance*
22  *Assessment*. ERMS 560252. Carlsbad, NM: Sandia National Laboratories.*

23  Casas, I., J. De Pablo, J. Gimenez, M.E. Torrero, J. Bruno, E. Cera, R.J. Finch, and R.C. Ewing.
24  1998. "The Role of pe, pH, and Carbonate on the Solubility of UO2 and Uraninite under
25  Nominally Reducing Conditions." *Geochimica et Cosmochimica Acta*, vol. 62: 2223–31.

26  Chen, T., Wang, X., Tian, W., Sun, M., Li, C., Liu, X., Wang, L., and C. Liu. 2010. "Solubility
27  Analysis of Americium in Yuci Groundwater." *Acta Physico-Chimica Sinica*, vol. 26(4), 811-
28  816.*

29  Choppin, G.R. 1988. Letter to L.H. Brush (Subject: *Chemicals Listed Could Interact with*
30  *Actinides*). 29 December 1988. Tallahassee, FL: WIPP Central Files.

31  Choppin, G.R. 1999. "Utility of Oxidation State Analogs in the Study of Plutonium Behavior."
32  *Radiochimica Acta*, vol. 85: 89–95.

33  Choppin, G.R., A.H. Bond, M. Borkowski, M.G. Bronikowski, J.G. Chen, S. Lis, J. Mizera, O.
34  Pokrovski, N.A. Wall, Y.X. Xia, and R.C. Moore. 1999. *WIPP Actinide Source Term Test*
35  *Program: Solubility Studies and Development of Modeling Parameters*. SAND 99-0943.
36  Albuquerque, NM: Sandia National Laboratories.

Choppin, G.R., and L.F. Rao. 1992. *Reduction of Neptunium(VI) by Organic Compounds*. *Transuranium Elements: A Half Century* (pp. 262–75). L.R. Morss and J. Fuger, eds. Washington, DC: American Chemical Society.

Choppin, G.R., J. Liljenzin, and J.O. Rydberg. 2004. *Radiochemistry and Nuclear Chemistry*. 3$^{rd}$ ed. Woburn, MA: Butterworth-Heinenmann.

Christensen, T.H., P.L. Bjerg, S.A. Banwart, R. Jakobsen, G. Heron, and H-J. Albrechtsen. 2000. "Characterization of Redox Conditions in Groundwater Contaminant Plumes." *Journal of Contaminant Hydrology*, vol. 45: 165-241.

Clark, D.L., and C.D. Tait. 1996. Memorandum to Sandia WIPP Records Center (Subject: *SWCF-A: 1.1.10.1.1: NQ: Actinide Source Term: LANL Monthly Reports*). Sandia WIPP Central File A: WBS 1.1.10.1.1. WPO 31106. Albuquerque, NM: Sandia National Laboratories.

Clark, D.L., D.E. Hobart, and M.P. Neu. 1995. "Actinide Carbonate Complexes and Their Importance in Actinide Environmental Chemistry." *Chemical Reviews*, vol. 95: 25.*

Clayton, D.J. 2008. Memorandum to Larry Brush (Subject: *Update to the Calculation of the Minimum Brine Volume for a Direct Brine Release*). 2 April 2008. ERMS 548522. Carlsbad, NM: Sandia National Laboratories.*

Clayton, D.J. 2013. *Justification of Chemistry Parameters for Use in BRAGFLO for AP-164, Revision 1*. ERMS 559466. Carlsbad, NM: Sandia National Laboratories.*

Clayton, D.J., R.C. Camphouse, J.W. Garner, A.E. Ismail, T.B. Kirchner, K.L. Kuhlman, and M.B. Nemer. 2010. *Summary Report of the CRA-2009 Performance Assessment Baseline Calculation*. ERMS 553039. Carlsbad, NM: Sandia National Laboratories.*

Cleveland, J.M. 1979. *The Chemistry of Plutonium*. La Grange Park, IL: American Nuclear Society.

Cotton, F.A., and G. Wilkinson. 1988. *Advanced Inorganic Chemistry*. 5th ed. New York: Wiley.

Cronin, E., and F. Post. 1977. "Report of a Dematiaceous Hyphomycete From the Great Salt lake, Utah." *Mycologia*, 69: 846-847.*

Cui, D., and K. Spahiu. 2002. "The Reduction of U(VI) on Corroded Iron under Anoxic Conditions." *Radiochimica Acta*, vol. 90: 623–28.

David, F., A.G. Maslennikov, and V.P. Peretrukhin. 1990. "Electrochemical Reduction of Actinides ions in Aqueous solution: Application to Separations and Some Intermetallic Compound Synthesis." *Journal of Radioanalytical Nuclear Chemistry*, vol. 143: 415–26.

Degueldre, C., and A. Kline. 2007. "Study of Thorium Association and Surface Precipitation on Colloids." *Earth and Planetary Science Letters*, vol. 264: 104–13.

Deng, H., S. Johnson, Y. Xiong, G.T. Roselle, and M. Nemer. 2006. *Analysis of Martin Marietta MagChem 10 WTS-60 MgO*. ERMS 544712. Carlsbad, NM: Sandia National Laboratories.

Diaz-Arocas, P., and B. Grambow. 1998. "Solid-liquid Phase Equilibria of U(VI) in NaCl Solutions." *Geochimica et Cosmochimica Acta*, vol. 62: 245–63.

Dodge, C.J., A.J. Francis, J.B. Gillow, G.P. Halada, C. Eng, and C.R. Clayton. 2002. "Association of Uranium with Iron Oxides Typically Formed on Corroding Steel Surfaces." *Environmental Science and Technology*, vol. 36: 3504–11.

Draganic, I.G., and Z.D. Draganic. 1971. *Primary Products of Water Radiolysis: Oxidizing Species–the Hydroxyl Radical and Hydrogen Peroxide*. The Radiation Chemistry of Water (pp. 91–121). New York: Academic.

Drez, P.E. 1991. *Preliminary Nonradionuclide Inventory of CH-TRU Waste, Preliminary Comparison with 40 CFR Part 191, Subpart B for the Waste Isolation Pilot Plant, December 1991. Volume 3: Reference Data* (pp. A-43 through A-53). Eds. R.P. Rechard, A.C. Peterson, J.D. Schreiber, H.J. Iuzzolino, M.S. Tierney, and J.S. Sandha. SAND91-0893/3. Albuquerque, NM: Sandia National Laboratories.

Du, X., B. Boonchayaanant, W.-M. Wu, S. Fendorf, J. Bargar, and C.S. Criddle. 2011. "Reduction of Uranium(VI) by Soluble Iron(II) Conforms with Thermodynamic Predictions." *Environmental Science & Technology*, vol.45: 4718-25.*

Ekberg, C., Y. Albinsson, M.J. Comarmond, and P.L. Brown. 2000. "Studies on the Behavior of Thorium(IV)." *Journal of Solution Chemistry*, vol. 29, no. 1: 63–86.

Emmerich, M., A Bhansali, T. Lösekann-Behrens, C. Schröder, A. Kappler, and S. Behrens. 2012. "Abundance, Distribution, and Activity of Fe(II)-Oxidizing and Fe(III)-Reducing Microorginaism in Hypersaline Sediments of Lake Kasin, Sourthern Russia." *Appl. Environ. Microbiol*, 78(12): 4386-4399.*

Eriksen, T.E., P. Ndamamba, D. Cui, J. Bruno, M. Caceci, and K. Spahiu. 1993. *SKB Technical Report 93-18*. Stockholm: Svensk Kärnbränsleforsorjning AB.

Ershov, B.G., M. Kelm, E. Janata, A.V. Gordeev, and E. Bohnert. 2002. "Radiation-Chemical Effects in the Near-Field of a Final Disposal Site: Role of Bromine on the Radiolytic Processes in NaCl-Solutions." *Radiochimica Acta*, vol. 90: 617.

Fanghänel, Th., and J.I. Kim. 1998. "Spectoscopic Evaluation of Thermodynamics of Trivalent Actinides in Brines." *Journal of Alloys and Compounds*, vol. 271–273: 728–737.

Fanghänel, Th., and V. Neck. 2002. "Aquatic Chemistry and Solubility Phenomena of Actinide Oxides/hydroxides." *Pure Applied Chemistry*, vol. 74: 1895–1907.

Fanghänel, Th., V. Neck, and J.I. Kim. 1995. "Thermodynamics of Neptunium(V) in Concentrated Salt Solutions: II. Ion Interaction (Pitzer) Parameters for Np(V) Hydrolysis Species and Carbonate Complexes." *Radiochimica Acta*, vol. 69: 169–76.

Farrell, J., W.D. Bostick, R.J. Jarabeck, and J.N. Fiedor. 1999. "Uranium Removal from Ground Water Using Zero Valent Iron Media." *Ground Water*, vol. 37: 618–24.

Felmy, A.R., D. Rai, and R.W. Fulton. 1990. "The Solubility of AmOHCO3(cr) and the Aqueous Thermodynamics of the System Na+-Am3+-HCO3--CO32--OH—H2O." *Radiochimica Acta*, vol. 50: 193–204.

Felmy, A.R., D. Rai, J.AS. Schramke, and J.L. Ryan. 1989. "The Solubility of Plutonium Hydroxide in Dilute Solution and in High-Ionic Strength Chloride Brines." *Radiochimica Acta*, vol. 48: 29–35.

Felmy, A.R., D. Rai, S.M. Sterner, M.J. Mason, N.J. Hess, and S.D. Conradson. 1996. *Thermodynamic Models for Highly Charged Aqueous Species: The Solubility of Th(IV) Hydrous Oxide in Concentrated NaHCO$_3$ and Na$_2$CO$_3$ Solutions* (August 14). ERMS 240226. Carlsbad, NM: Sandia National Laboratories.

Felmy, A.R., M.J. Mason, and D. Rai. 1991. "The Solubility of Hydrous Thorium(IV) Oxide in Chloride Media: Development of an Aqueous Ion-Interaction Model." *Radiochimica Acta*, vol. 55: 177–85.

Fiedor, J.N., W.D. Bostick, R.J. Jarabek, and J. Farrell. 1998. "Understanding the Mechanism of Uranium Removal from Groundwater by Zero-Valent Iron Using X-Ray Photoelectron Spectroscopy." *Environmental Science and Technology*, vol. 32: 1466–73.

Field, E., S. D'Imperio, A. Miller, M. VanEngelen, R. Gerlach, B. Lee, W. Apel, and B. Peyton. 2010. "Application of Molecular Techniques To Elucidate the Influence of Cellulosic Waste on the Bacterial Community Structure at a Simulated Low-Level-Radioactive-Waste Site." *Appl. Environ. Microbiol.*, 76(10): 3106–3115.*

Francis, A.J. 1998. "Biotransformation of Uranium and Other Actinides in Radioactive Wastes." *Journal of Alloys and Compounds*, vol. 271–273: 78–84.

Francis, A.J., and J.B. Gillow. 1994. *Effects of Microbial Processes on Gas Generation Under Expected Waste Isolation Pilot Plant Repository Conditions. Progress Report through 1992*. SAND93-7036. WPO 26555. Albuquerque, NM: Sandia National Laboratories.

Francis, A.J., C.J. Dodge, and J. B. Gillow. 2008. "Reductive Dissolution of Pu(IV) by Costridium sp. under Anaerobic Conditions." *Environmental Science and Technology*, vol. 42: 2355–60.

Francis, A.J., C.J. Dodge, J.B. Gillow, and H.W. Papenguth. 2000. "Biotransformation of Uranium Compounds in High Ionic Strength Brine by a Halophilic Bacterium under Denitrifying Conditions." *Environmental Science and Technology*, vol. 34: 2311.

Francis, A.J., J.B. Gillow, and M.R. Giles. 1997. *Microbial gas generation under expected Waste Isolation Pilot Plant repository conditions*. SAND96-2582 Report. Albuquerque, NM: Sandia National Laboratories.*

Francis, A.J., J.B. Gillow, C.J. Dodge, R. Harris, T.J. Beveridge, and H.W. Papenguth. 2004. "Uranium Association with Halophilic and non-Halophilic Bacteria and Archaea." *Radiochimica Acta*, vol. 92: 481–88.*

Fredrickson, J.K., J.M. Zachara, D.W. Kennedy, M.C. Duff, Y.A. Gorby, S.W. Li, and K.M. Krupka. 2000. "Reduction of U(VI) in Goethite (α-FeOOH) Suspensions by a Dissimilatory Metal-Reducing Bacteria." *Geochimica et. Cosmochimica Acta*, vol. 64: 3085–98.

Garner, J.W. 1996. *Radioisotopes to be Used in the 1996 CCA Calculation*s. ERMS 540572. Carlsbad, NM: Sandia National Laboratories.

Garner, J.W., and C. Leigh. 2005. *Analysis Package for PANEL: CRA-2004 Performance Assessment Baseline Calculation* (Revision 0). ERMS 540572. Albuquerque, NM: Sandia National Laboratories.

Gayer, K.H., and H. Leider. 1957. "The Solubility of Uranium (IV) Hydroxide in Solutions of Sodium Hydroxide and Perchloric Acid at 25°C." *Canadian Journal of Chemistry*, vol. 35: 5–7.

Giambalvo, E.R. 2002a. Memorandum to L.H. Brush (Subject: *Recommended Parameter Values for Modeling An(III) Solubility in WIPP Brines*). 25 July 2002. ERMS 522982. Carlsbad, NM: Sandia National Laboratories.

Giambalvo, E.R. 2002b. Memorandum to L.H. Brush (Subject: *Recommended Parameter Values for Modeling An(IV) Solubility in WIPP Brines*). 26 July 2002. ERMS 522986. Carlsbad, NM: Sandia National Laboratories.

Giambalvo, E.R. 2002c. Memorandum to L.H. Brush (Subject: *Recommended Parameter Values for Modeling An(V) Solubility in WIPP Brines*). 26 July 2002. ERMS 522990. Carlsbad, NM: Sandia National Laboratories.

Gillow, J.B., M. Dunn, A.J. Francis, D. A. Lucero, and H.W. Papenguth. 2000. "The Potential of Subterranean Microbes in Facilitating Actinide Migration at the Grimsel Test Site and Waste Isolation Pilot Plant." *Radiochimica Acta*, vol. 88: 769–74.

Gillow J.B.,and A.J. Francis. 2006. *Microbial gas generation under expected Waste Isolation Pilot Plant Repository Conditions: Final Report*. Report BNL-96148-2011-IR. Albuquerque, NM: Sandia National Laboratories.*

Grambow, B., E. Smailos, H. Geckeis, R. Muller, and H. Hentschel. 1996. "Sorption and Reduction of Uranium (VI) on Iron Corrosion Products under Reducing Saline Conditions." *Radiochimica Acta*, vol. 74: 149–54.

Grenthe, I., D. Ferri, F. Salvatore, and G. Riccio. 1984. "Studies on Metal Carbonate Equilibria. Part 10. A Solubility Study of the Complex Formation in the Uranium (VI)-Water-Carbon Dioxide (g) System at 25ºC." *Journal of Chemical Society*, Dalton Trans.: 2439–43.

Griffith, J., S. Wilcox, D. Powers, R. Nelson, and B. Baxter. 2008. "Discovery of Abundant Cellulose Microfibers Encased in 250 Ma Permian Halite: A Macromolecular Target in the Search for Life on Other Planet." *Astrobiology*, 8(2): 215-228.*

Gu, B., L. Liang, M.J. Dickey, X. Yin, and S. Dai. 1998. "Reductive Precipitation of Uranium (VI) by Zero-Valent Iron." *Environmental Science and Technology*, vol. 32: 3366–73.

Guillaumont, R., T. Fanghänel, J. Fuger, I. Grenthe, V. Neck, D.A. Palmer, and M.H. Rand. 2003. "Update on the Chemical Thermodynamics of Uranium, Neptunium, Plutonium, Americium and Technetium." F.I. Mompean, M. Illemassene, C. Domenech-Orti, and K. Ben Said, eds. *Chemical Thermodynamics*. Vol. 5. Amsterdam: Elsevier.

Gunde-Cimerman , N., J. Ramos, and A. Plemenitas. 2009. "Halotolerant and Halophilic Fungi." *Mycological Research*, 113: 1231-1241.*

Harvie, C.E., N. Møller, and J.H. Weare. 1984. "The Prediction of Mineral Solubilities in Natural Waters, The Na-K-Mg-Ca-H-Cl-SO$_4$-OH-HCO$_3$-CO$_2$-H$_2$O System to High Ionic Strengths at 25°C." *Geochimica et Cosmochimica Acta*, vol. 48: 723–51.

Haschke, J.M., and T.E. Ricketts. 1995. *Plutonium Dioxide Storage: Conditions for Preparing and Handling*. LA-12999. Los Alamos, NM: Los Alamos National Laboratory.

Haschke, J.M., T.H. Allen, and L.A. Morales. 2000. "Reaction of Plutonium Dioxide with Water: Formation and Properties of PuO$_{2+x}$." *Science*, vol. 287: 285–87.

Hobart, D.E. 1990. *Actinides in the Environment*. Proceedings of the Robert A. Welch Foundation Conference on Chemical Research, No. XXXIV: 50 Years With Transuranium Elements (pp. 378–436). Houston, TX: Robert A. Welch Foundation.

Hobart, D.E., and R.C. Moore. 1996. *Analysis of Uranium (VI) Solubility Data for WIPP Performance Assessment.* (May 28, 1996). AP-028. Unpublished report. Albuquerque, NM: Sandia National Laboratories.

Hobart, D.E., K. Samhoun, and J. R. Peterson. 1982. "Spectroelectrochemical Studies of the Actinides: Stabilization of Americium (IV) in Aqueous Carbonate Solution." *Radiochimica Acta*, vol. 31: 139–45.

Holm, T.R., and C.D. Curtiss. 1989. "A Comparison of Oxidation-Reduction Potentials Calculated from the As(V)/As(III) and Fe(III)/Fe(II) Couples with Measured Platinum-Electrode Potentials in Groundwater." *Journal of Contaminant Hydrology*, vol. 5: 67-81.*

Huang, F.Y C., P.V. Brady, E.R. Lindgren, and P. Guerra. 1998. "Biodegradation of Uranium-Citrate Complexes: Implications for Extraction of Uranium from Soils." *Environmental Science and Technology*, vol. 32: 379.

Icopini, G.A., J. Boukhalfa, and M.P. Neu. 2007. "Biological Reduction of Np(V) and Np(V) Citrate by Metal-Reducing Bacteria." *Environmental, Science, & Technology*, vol. 41: 2764–69.

Ilton, E.S., J.S. Lezama Pacheco, J.R. Bargar, Z. Shi, J. Liu, L. Kovarik, M.H. Engelhard, and A.R. Felmy. 2012. "Reduction of U(VI) Incorporated in the Structure of Hematite." *Environmental Science & Technology*, vol.46: 9428-36.*

Ionova, G., C. Madic, and R. Guillamount. 1998. "About the Existence of Th(III) in Aqueous Solution." *Polyhedron*, vol. 17: 1991–95.

Ismail, A.E. 2007 Memorandum to File (Subject: *Revised Porosity Estimates for the DRZ*). 10 April 2007. ERMS 545755. Carlsbad NM: Sandia National Laboratories.

Itagaki, H., S. Nakayama, S. Tanaka, and M. Yamawaki. 1992. "Effect of Ionic Strength on the Solubility of Neptunium(V) Hydroxide." *Radiochimica Acta*, vol. 58/59: 61–66.

Katz, J.J., G.T. Seaborg, and L.R. Morss. 1986. *The Chemistry of the Actinide Elements*. 2nd ed. New York: Chapman and Hall.

Keller, C. 1971. *The Chemistry of Transuranium Elements*. Weinheim, Germany: Verlag Chemie.

Kelm, M., I. Pashalidis, and J.I. Kim. 1999. "Spectroscopic Investigation on the Formation of Hypochlorite by Alpha Radiolysis in Concentrated NaCl Solutions." *Applied Radiation and Isotopes*, vol. 51: 637–42.

Kerber Schütz, M., N. Lopes, A. Cenci, R. Ligabue, J. Dullius, S. Einloft, and J.M. Ketzer. 2011. "Effect of Time on the Carbonation Reaction of Saline Aquifers with Controlled pH." *Energy Procedia*, vol.4 :4546-51.*

Kerisit, S., A.R. Felmy, and E.S. Ilton. 2011. "Influence of Magnetite Stoichiometry on $U^{VI}$ Reduction." *Environmental Science & Technology*, vol.45: 2770-76.*

Khasanova, A.B., N.S. Shcherbina, S.N. Kalmykov, Yu.A. Teterin, and A.P. Novikov. 2007. "Sorption of Np(V), Pu(V), and Pu(VI) on Colloids of Fe(III) Oxides and Hydrous Oxides and $MnO_2$." *Radiochemistry*, vol. 49: 419–25.

Kicker, D.C. and T. Zeitler. 2013. *Radionuclide Inventory Screening Analysis for the 2014 Compliance Recertification Application Performance Assessment (CRA-2014 PA)*. ERMS 559257. Carlsbad, NM: Sandia National Laboratories.*

Kim, J.I., Ch. Apostolidis, G. Buckau, K. Buppelmann, B. Kanellakopulos, Ch. Lierse, S. Magirius, R. Stumpe, I. Hedler, Ch. Rahner, and W. Stoewer. 1985. *Chemisches Verhalten von Np, Pu und Am in verschiedenen konzentrierten Salzloesunger = Chemical Behaviour of Np, Pu, and Am in Various Brine Solutions*. RCM 01085. Munich, Germany: Institut für Radiochemie der Technische Universitaet Muenchen. (Available from National Technical Information Service, 555 Port Royal Road, Springfield, VA 22161, 703/487-4650 as DE857 2334.)

Kim, J.I., M. Bernkopf, Ch. Lierse, and F. Koppold. 1984. *Hydrolysis Reactions of Am(III) and Pu(VI) Ions in Near-Neutral Solutions*. Geochemical Behavior of Disposed Radioactive Waste (pp. 115–34). G.S. Barney, J.D. Navratill, and W.W. Schultz, eds. ACS Symposium Series No. 246. Washington, DC: American Chemical Society.

Kim, S. 2013a. *Analysis Package for Salado Transport Calculations: CRA-2014 Performance Assessment*. ERMS 560174. Carlsbad, NM: Sandia National Laboratories.*

Kim, S. 2013b. *Analysis Package for PANEL: CRA-2014 Performance Assessment*. ERMS 560056. Carlsbad, NM: Sandia National Laboratories.*

Kim, S.S., M.H. Baik, J.W. Choi, H.S. Shin, and J.I. Yun. 2010. "The dissolution of $ThO_2(cr)$ in carbonate solutions and a granitic groundwater." *J. Radioanal. Nucl. Chem.*, 286: 91-97.

Kim, W.H., K.C. Choi, K.K. Park, and T.Y. Eom. 1994. "Effects of Hypochlorite Ion on the Solubility of Amorphous Schoepite at 25°C in Neutral to Alkaline Aqueous Solutions." *Radiochimica Acta*, vol. 66/67: 45–49.

Klapötke, T.M., and A. Schulz. 1997. "The First Observation of a $Th^{3+}$ ion in Aqueous Solution." *Polyhedron*, vol. 16: 989–91.

Korpusov, G.V., E.N. Patrusheva, and M.S. Dolidze. 1975. "The Study of Extraction Systems and the Method of Separation of Trivalent Transuranium Elements Cm, Bk, and Cf." *Soviet Radiochemistry*, vol. 17: 230–36.

Kramer-Schnabel, U., H. Bischoff, R.H. Xi, and G. Marx. 1992. "Solubility Products and Complex Formation Equilibria in the Systems Uranyl Hydroxide and Uranyl Carbonate at 25°C and I=0.1M." *Radiochimica Acta*, vol. 56: 183–88.

Langmuir, D., and J.S. Herman. 1980. "Mobility of Thorium in Natural Waters at Low Temperatures." *Geochimica et. Cosmochimica Acta*, vol. 44: 1753–66.

Latta, D.E., C.A. Gorski, M.I. Boyanov, E.J. O'Loughlin, K.M. Kemner, and M.M. Scherer. 2012. "Influence of Magnetite Stoichiometry on $U^{VI}$ Reduction." *Environmental Science & Technology*, vol.46: 778-86.*

LaVerne, J.A., and L. Tandon. 2002. "$H_2$ Production in the Radiolysis of Water on $CeO_2$ and $ZrO_2$." *Journal of Physical Chemistry B*, vol. 106: 380–86.

Leigh, C., J. Kanney, L. Brush, J. Garner, R. Kirkes, T. Lowry, M. Nemer, J. Stein, E. Vugrin, S. Wagner, and T. Kirchner. 2005. *2004 Compliance Recertification Application Performance Assessment Baseline Calculation* (Revision 0). ERMS 541521. Carlsbad, NM: Sandia National Laboratories.

Lemire, R.J., J. Fuger, H. Nitsche, P. Potter, M.H. Rand, J. Rydberg, K. Spahiu, J.C. Sullivan, W.J. Ullman, P. Vitorge, and H. Wanner. 2001. *Chemical Thermodynamics of Neptunium and Plutonium*. Amsterdam: Elsevier.

Lin, M.R., P. Paviet-Hartmann, Y. Xu, and W.H. Runde. 1998. *Uranyl Compounds in NaCl Solutions: Structure, Solubility and Thermodynamics*. 216th ACS National Meeting: Preprints of Extended Abstracts, vol. 38: 208. Abstract for the National Meeting of the American Chemical Society, Division of Environmental Chemistry, Boston: 23-27 August.

Lloyd JR, and L.E. Macaskie. 2002. *Biochemical basis of microbe-radionuclide interactions*. In: Keith-Roach MJ, Livens FR, editors. Interactions of Microorganisms with Radionuclides. London: Elsevier Science Ltd. pp. 313-342.*

Lloyd, J.R., P. Yong, and L.E. Macaskie. 2000. "Biological Reduction and Removal of Np(V) by Two Microorganisms." *Environmental Science and Technology*, vol. 34: 1297–1301.

Lovley, D.R., E.E. Roden, E.J.P. Phillips, and J.C. Woodward. 1993. "Enzymatic Iron and Uranium Reduction by Sulfate-Reducing Bacteria." *Marine Geology*, vol. 113: 41.

Lovley, D.R., E.J.P. Phillips, Y.A. Gorbi, and E.R. Landa. 1991. "Microbial Reduction of Uranium." *Nature*, vol. 350: 413.

Lucchini, J.-F., H. Khaing, M. Borkowski, M.K. Richmann, and D.T. Reed. 2010a. *Actinide (VI) Solubility in Carbonate-free WIPP Brine: Data Summary and Recommendations*. LCO-ACP-10, LANL\ACRSP Report. LA-UR 10-00497. Los Alamos, NM: Los Alamos National Laboratory.*

Lucchini J.F., H. Khaing, and D.T. Reed. 2010b. *Uranium (VI) Solubility in Carbonate-free ERDA-6 Brine*. Scientific Basis for Nuclear Waste Management XXXIV, edited by K.L. Smith, S. Kroeker, B. Uberuaga, K.R. Whittle, Material Research Society Symposium Proceedings, vol.1265: 21-26.*

Lucchini, J.-F., M.K. Richmann, and M. Borkowski. 2013a. *Uranium (VI) Solubility in WIPP Brine*. LCO-ACP-14, LANL\ACRSP Report. LA-UR 13-20786. Los Alamos, NM: Los Alamos National Laboratory.*

Lucchini, J.-F., M. Borkowski, M.K. Richmann, and D.T. Reed. 2013b. "Uranium(VI) Solubility in carbonate-free WIPP Brine." *Radiochim. Acta*, 101, 391-398.*

Lucchini, J.-F., M. Borkowski, H. Khaing, M.K. Richmann, J. Swanson, K. Simmons, and D.T. Reed. 2013c. *WIPP Actinide-Relevant Brine Chemistry*. LCO-ACP-15, LANL\ACRSP Report. LA-UR 13-20620. Los Alamos, NM: Los Alamos National Laboratory.*

Lucchini, J.-F., M. Borkowski, M.K. Richmann, S. Ballard, and D.T. Reed. 2007. "Solubility of $Nd^{3+}$ and $UO_2^{2+}$ in WIPP Brine as Oxidation-State Invariant Analogs for Plutonium." *Journal of Alloys and Compounds*, vol. 444/445: 506–11.

Lynd, L., P. Weimer, W. van Zyl, and I. Pretorius. 2002. "Microbial Cellulose Utilization : Fundamentals and Biotechnology." *Microbiology and Molecular Biology Reviews*, 66(3): p. 506-577.*

Magirius, S., W.T. Carnall, and J.I. Kim. 1985. "Radiolytic Oxidation of Am(III) to Am(V) in NaCl Solution." *Radiochimical Acta*, vol. 38: 29–32.

Martinot, L., and J. Fuger. 1985. "The Actinides." *Standard Potentials in Aqueous Solution* (pp. 631–674). A.J. Bard, R. Parsons, and J. Jordan, eds. New York: Dekker.

Masue-Slowey, Y., B.D. Kocar, S.A.B. Jofré, K.U. Mayer, and S. Fendorf. 2011. "Transport Implications Resulting from Internal Redistribution of Arsenic and Iron within Constructed Soil Aggregates." *Environmental Science and Technology*, vol. 45(2): 582-588.*

McCabe, A. 1990. "The Potential Significance of Microbial Activity in Radioactive Waste Disposal." *Experientia*, 46: p. 779-787.*

Meinrath, G., and J.I. Kim. 1991. "The Carbonate Complexation of the Am(III) Ion." *Radiochimica Acta*, vol. 52/53: 29–34.

Meyer, D., S. Fouchard, E. Simoni, and C. DenAuwer. 2002. "Selective Dissolution of Am in Basic Media in the Presence of Ferricyanide Ions: a Mechanistic and Structural Study on Am(V) and Am(VI) Compounds." *Radiochimica Acta*, vol. 90: 253–58.

Moriyama, H., T. Sasaki, T. Kobayashi, and I. Takagi. 2005. "Systemics of Hydrolysis Constants of Tetravalent Actinide Ions." *Journal of Nuclear Science and Technology*, vol. 42-7: 626–35.

Mormile, M., M. Biesen, M. Gutierrez, A. Ventosa, J. Pavlovich, T. Onstott, and J. Fredrickson. 2003. "Isolation of Halobacterium Salinarum Retrieved Directly from Halite Brine Inclusions." *Env. Microbiol.*, 5(11): 1094-1102.*

Morss, L.R., N. Edelstein, and J. Fuger. 2006. *The Chemistry of the Actinide and Transactinide Elements*. 3rd ed. New York: Springer.

Moulin, C., B. Amekraza, S. Hubert, and V. Moulin. 2001. "Study of Thorium Hydrolysis Species by Electrospray-Ionization Mass Spectrometry." *Analytica Chimica Acta*, vol. 441: 269–79.

Myllykylä, E., and K. Ollila. 2011. *Reduction of Uranyl Carbonate and Hydroxide Complexes by Ferrous Ions in Aqueous Solution under Anaerobic Conditions*. Abstract PA4-3, 13th International Conference on the Chemistry and Migration Behaviour of Actinides and Fission Products in the Geosphere Migration, Beijing, China, September 18-23, 2011.*

Nakata, K., S. Nagasaki, S. Tanaka, Y. Sakamoto, T. Tanaka, and H. Ogawa. 2004. "Reduction Rate of Neptunium(V) in Heterogeneous Solution with Magnetite." *Radiochimica Acta*, vol. 92: 145–49.

National Institute of Standards and Technology (NIST). 2004. *Critical Stability Constants.Standard Reference Database 46 (Version 8.0)*.

1    Neck, V., and J.I. Kim.  2001.  "Solubility and Hydrolysis of Tetravalent Actinides."
2    *Radiochimica Acta*, vol. 89: 1–16.

3    Neck, V., J.I. Kim, and B. Kanellakopulos.  1992.  "Solubility and Hydrolysis Behavior of
4    Neptunium (V)."  *Radiochimica Acta*, vol. 56:, 25–30.

5    Neck, V., M. Altmaier, and Th. Fanghänel.  2006.  "Ion Interaction (SIT) Coefficients for the
6    $Th^{4+}$ Ion and Trace Activity Coefficients in $NaClO_4$, $NaNO_3$ and NaCl Solution Determined by
7    Solvent Extraction with TBP."  *Radiochimica Acta*, vol. 94: 501–07.

8    Neck, V., M. Altmaier, R. Müller, A. Bauer, Th. Fanghänel, and J.I. Kim.  2003.  "Solubility of
9    Crystalline Thorium Dioxide."  *Radiochimica Acta*, vol. 91: 253–62.

10   Neck, V., M. Altmaier, T. Rabung, J. Lützenkirchen, and Th. Fänghanel.  2009.
11   "Thermodynamics of Trivalent Actinides and Neodymium in NaCl, $MgCl_2$, and $CaCl_2$ Solutions:
12   Solubility, Hydrolysis and Ternary Ca-M(III)-OH Complexes."  *Pure and Applied Chemistry*,
13   vol. 81(9), 1555-1568.

14   Neck, V., R. Müller., M. Bouby, M. Altmaier, J. Rothe, M.A. Denecke, and J.I. Kim.  2002.
15   "Solubility of Amorphous Th(IV) Hydroxide: Application of LIBD to Determine the Solubility
16   Product and EXAFS for Aqueous Speciation."  *Radiochimica Acta*, vol. 90: 485–94.

17   Neck, V., W. Runde, and J.I. Kim.  1995.  "Solid-Liquid Equilibria of Np(V) in Carbonate
18   Solutions at Different Ionic Strengths: II."  *Journal of Alloys and Compounds*, vol. 225: 295–
19   302.

20   Nemer, M., Y. Xiong, A.E. Ismail, and J. Jang.  2011.  "Solubility of $Fe_2(OH)_3Cl$ (pure-iron end-
21   member of hibbingite) in NaCl and $Na_2SO_4$ brines."  *Chemical Geology*, v. 280, no. 1-2, 26-32.*

22   Neretnieks, I.  1982.  *The Movement of a Redox Front Downstream From a Repository for
23   Nuclear Waste.*  KBS Report TR 82-16.  Stockholm: Svensk Kärnbränsleforsorjning AB.

24   Neu, M.P., C.E. Ruggiero, and A.J. Francis.  2002.  *Bioinorganic Chemistry of Plutonium and
25   Interactions of Plutonium with Microorganisms in Plants*.  Advances in Plutonium Chemistry
26   (pp. 1967-2000).  La Grange Park, IL: American Nuclear Society.

27   Nitsche, H., K. Roberts, K. Becraft, T. Prussin, D. Keeney, S. Carpenter, and D. Hobart.  1995.
28   *Solubility and Speciation Results from Over- and Under-saturation Experiments on Neptunium,
29   Plutonium and Americium in water from Yucca Mountain Region Well UE-25p#1*.  Report LA-
30   13017-MS.  Los Alamos, NM: Los Alamos National Laboratory.

31   Nitsche, H., K. Roberts, R. Xi, T. Prussin, K. Becraft, I. Al Mahamid, H.B. Silber, S.A.
32   Carpenter, R.C. Gatti, and C.F. Novak.  1994.  "Long-Term Plutonium Solubility and Speciation
33   Studies in a Synthetic Brine."  *Radiochimica Acta*, vol. 66/67: 3.

1  Nitsche, H., K. Roberts, R.C. Gatti, T. Prussin, K. Becraft, S.C. Leung, S.A. Carpenter, and C.F.
2  Novak. 1992. *Plutonium Solubility and Speciation Studies in a Simulant of Air Intake Shaft*
3  *Water from the Culebra Dolomite at the Waste Isolation Pilot Plant*. SAND92-0659. WPO
4  23480. Albuquerque, NM: Sandia National Laboratories.

5  Norton, C., and W. Grant. 1988. "Survival of Halobacteria Within Fluid Inclusions in Salt
6  Crystals." *J. General Microbiology*, 134: 1365-1373.*

7  O'Loughlin, E.J., S.D. Kelly, R.E. Cook, R. Csencsits, and K.M. Kemner. 2003. "Reduction of
8  Uranium (VI) by Mixed Iron (II)/ Iron (III) Hydroxide (Green Rust): Formation of $UO_2$
9  Nanoparticles." *Environmental Science and Technology*, vol. 37: 721–27.

10  Okajima, S., and D.T. Reed. 1993. "Initial Hydrolysis of Pu(VI)." *Radiochimica Acta*, vol. 60:
11  173–84.

12  Okamoto, Y., Y. Mochizuki, and S. Tsushim. 2003. "Theoretical Study of Hydrolysis Reactions
13  of Tetravalent Thorium Ion." *Chemical Physics Letters*, vol. 373: 213–17.

14  Oren, A. 1999. "Bioenergetic Aspects of Halphilism." *Microbiology and Molecular Biology*
15  *Reviews*, 63(2): 334-348.*

16  Oren, A. 2006. *Life at high salt concentrations*. In: Falkow S, Rosenberg E, Schleifer K-H,
17  Stackebrandt E, Dworkin M, editors. The Prokaryotes. New York: Springer. pp. 263-282.*

18  Oren, A. 2008. "Microbial life at high salt concentrations: phylogenetic and metabolic
19  diversity." *Saline Systems*, vol. 4:2. DOI: 10.1186/1746-1448-4-2.*

20  Oren, A. 2011. "Thermodynamic limits to microbial life at high salt concentrations."
21  *Environmental Microbiology*, vol. 13: 1908-1923.*

22  Orlandini, J.A., W.R. Penrose, and D.M. Nelson. 1986. "Pu(V) as the Stable form of Oxidized
23  Plutonium in Natural Waters." *Marine Chemistry*, vol. 18: 49–57.

24  Östhols, E., J. Bruno, and I. Grenthe. 1994. "On the Influence of Carbonate on Mineral
25  Dissolution: III: The Solubility of Microcrystalline $ThO_2$ in $CO_2$-$H_2O$ Media." *Geochimica et.*
26  *Cosmochimica Acta*, vol. 58: 613–623.

27  Oversby, V.M. 2000. *Plutonium Chemistry under Conditions Relevant for WIPP Performance*
28  *Assessment: Review of Experimental Results and Recommendations for Future Work*
29  (September). EEG-77. Albuquerque, NM: Environmental Evaluation Group.

30  Papenguth, H.W. 1996a. Letter to Christine T. Stockman (Subject: *Parameter Record Package*
31  *for Colloidal Actinide Source Term Parameters, Attachment A: Rationale for Definition of*
32  *Parameter Values for Microbes*). 7 May 1996. ERMS 235856. Carlsbad, NM: Sandia National
33  Laboratories.

1   Papenguth, H.W.  1996b.  Letter to Christine T. Stockman (Subject: *Parameter Record Package*
2   *for Colloidal Actinide Source Term Parameters, Attachment A: Rationale for Definition of*
3   *Parameter Values for Humic Substances*).  7 May 1996.  ERMS 235855.  Carlsbad, NM: Sandia
4   National Laboratories.

5   Papenguth, H.W.  1996c.  Letter to Christine T. Stockman (Subject: *Parameter Record Package*
6   *for Colloidal Actinide Source Term Parameters, Attachment A: Rationale for Definition of*
7   *Parameter Values for Mineral Fragment Type Colloids*).  7 May 1996.  ERMS 235850.
8   Carlsbad, NM: Sandia National Laboratories.

9   Papenguth, H.W., and Y.K. Behl.  1996.  *Test Plan for Evaluation of Colloid-Facilitated*
10  *Actinide Transport at the Waste Isolation Pilot Plant* (16 January).  TP 96-01.  ERMS 417319.
11  Carlsbad, NM: Sandia National Laboratories.

12  Pashalidis, I., J.I. Kim, Ch. Lierse, and J.C. Sullivan.  1993.  "The Chemistry of Pu in
13  Concentrated Aqueous NaCl Solution: Effects of Alpha Self-Radiolysis and the Interaction
14  Between Hypochlorite and Dioxoplutonium (VI)."  *Radiochimica Acta*, vol. 60: 99.

15  Pazukhin, E.M., and S.M. Kochergin.  1989.  "Stability Constants of Hydrolyzed Forms of
16  Americium(III) and Solubility Product of its Hydroxide."  *Soviet Radiochemistry,* vol. 31: 430–
17  36.

18  Pedersen, K.  2002.  *Microbial processes in the disposal of high level radioactive waste 500m*
19  *underground in Fennoscandian shield rocks*.  In: Keith-Roach MJ, Livens, FR, editors.
20  Interactions of Microorganisms with Radionuclides.  London: Elsevier Science Ltd.  pp. 279-
21  311.*

22  Pitzer, K.S.  1973.  "Thermodynamics of Electrolytes. I. Theoretical Basis and General
23  Equations."  *The Journal of Physical Chemistry*, vol. 77(2): 268-277.*

24  Popielak, R.S., R.L. Beauheim, S.R. Black, W.E. Coons, C.T. Ellingson, and R.L. Olsen.  1983.
25  *Brine Reservoirs in the Castile Formation, Waste Isolation Pilot Plant Project, Southeastern*
26  *New Mexico*.  TME 3153.  Carlsbad, NM: U.S. Department of Energy.

27  Porter, D., A.N. Roychoudhury, and D. Cowan.  2007.  "Dissimilatory Sulfate Reduction in
28  Hypersaline Coastal Pans: Activity Across a Salinity Gradient."  *Geochimica et Cosmochimica*
29  *Acta*, 71: 5102-5116.*

30  Powers, D.W., S.J. Lambert, S.E. Shaffer, I.R. Hill, and W.D. Weart, eds.  1978.  *Geological*
31  *Characterization Report, Waste Isolation Pilot Plant (WIPP) Site, Southeastern New Mexico*.
32  SAND78-1596.  2 vols.  ERMS 205448.  Albuquerque, NM: Sandia National Laboratories.

33  Pryke, D.C., and J.H. Rees.  1986.  "Understanding the Behaviour of the Actinides Under
34  Disposal Conditions: A Comparison between Calculated and Experimental Solubilities."
35  *Radiochimica Acta*, vol. 40: 27–32.

1  Qui, S.R., C. Amrhein, M.L. Hunt, R. Pfeffer, B. Yakshinskiy, L. Zhang, T.E. Madey, and J.A.
2  Yarmoff. 2001. "Characterization of Uranium Oxide Thin Films Grown from Solution onto Fe
3  Surfaces." *Applied Surface Science*, vol. 181: 211–34.

4  Rabindra, N.R., K.M. Vogel, C.E. Good, W.B. Davis, L.N. Roy, D.A. Johnson, A.R. Felmy, and
5  K.S. Pitzer. 1992. "Activity Coefficients in Electrolyte Mixtures: HCl + ThCl$_4$ + H$_2$O for 5–55
6  °C." *Journal of Physical Chemistry*, vol. 96: 11,065–072.

7  Rai, D., A.R. Felmy, and J.L. Ryan. 1990. "Uranium (VI) Hydrolysis Constants and Solubility
8  Products of UO$_2$.xH$_2$O (am)." *Inorganic Chemistry*, vol. 29: 260–64.

9  Rai, D., A.R. Felmy, and R.W. Fulton. 1995. "Nd$^{3+}$ and Am$^{3+}$ Ion Interaction with Sulfate Ion
10  and Their Influence on NdPO$_4$(c) Solubility." *Journal of Solution Chemistry*, vol. 24: 879–95.

11  Rai, D., A.R. Felmy, N.J. Hess, and D.A. Moore. 1998. "A Thermodynamic Model for the
12  Solubility of UO$_2$(am) in the Aqueous K$^+$-Na$^+$-HCO$_3^-$-CO$_3^{2-}$-OH$^-$-H2O System." *Radiochimica*
13  *Acta*, vol. 82: 17–25.

14  Rai, D., A.R. Felmy, S.M. Sterner, D.A. Moore, M.J. Mason, and C.F. Novak. 1997. "The
15  Solubility of Th(IV) and U(IV) Hydrous Oxides in Concentrated NaCl and MgCl$_2$ Solutions."
16  *Radiochimica Acta*, vol. 79: 239–47.

17  Rai, D., and J.L. Ryan. 1982. "Crystallinity and Solubility of Pu(IV) Oxide and Hydrous Oxide
18  in Aged Aqueous Suspensions." *Radiochimica Acta*, vol. 30: 213–16.

19  Rai, D., and J.L. Ryan. 1985. "Neptunium (IV) Hydrous Oxide Solubility under Reducing and
20  Carbonate Conditions." *Inorganic Chemistry*, vol. 24: 247–51.

21  Rai, D., D.A. Moore, C.S. Oakes, and M. Yui. 2000. "Thermodynamic Model for the Solubility
22  of Thorium Dioxide in the Na$^+$-Cl$^-$-OH$^-$-H$_2$O System at 23 °C and 90°C." *Radiochimica Acta*,
23  vol. 88: 297–306.

24  Rai, D., J.L. Ryan, D.A. Moore, and R.G. Strickert. 1983. "Am(III) Hydrolysis Constants and
25  Solubility of Am(III) Hydroxide." *Radiochimica Acta*, vol. 33: 201–06.

26  Rai, D., R.G. Strickert, and G.L. McVay. 1982. "Neptunium Concentrations in Solutions
27  Contacting Actinide-Doped Glass." *Nuclear Technology*, vol. 58: 69–76.

28  Rao, L., D. Rai, A.R. Felmy, R.W. Fulton, and C.F. Novak. 1996. "Solubility of
29  NaNd(CO$_3$)$_2$·6H$_2$O(c) in Concentrated NaCO$_3$ and NaHCO$_3$ Solutions." *Radiochimica Acta*, vol.
30  75: 141–47.

31  Reed, D.T., and D.R. Wygmans. 1997. *Actinide Stability/Solubility in Simulated WIPP Brines*
32  (March 21). WPO44625. Argonne, IL: Argonne National Laboratory, Actinide Speciation and
33  Chemistry Group, Chemical Technology Group.

1   Reed, D.T., J.-F. Lucchini, M. Borkowski, and M.K. Richmann.  2009.  *Reduction of Higher*
2   *Valent Plutonium by Iron under Waste Isolation Pilot Plant (WIPP)- Relevant Conditions: Data*
3   *Summary and Recommendations.*  LCO-ACP-09, LANL\ACRSP Report.  Los Alamos, NM: Los
4   Alamos National Laboratory.

5   Reed, D.T., J.-F. Lucchini, S.B. Aase, and A.J. Kropf.  2006.  "Reduction of Plutonium (VI) in
6   Brine under Subsurface Conditions." *Radiochimica Acta*, vol. 94: 591–97.

7   Reed, D.T., J.S. Swanson, J-F. Lucchini, and M.K. Richmann.  2013. I*ntrinsic, Mineral, and*
8   *Microbial Colloid Enhancement Parameters for the WIPP Actinide Source Term.*  Report LCO-
9   ACP-18, LA-UR 13-20858.  Carlsbad, NM: Los Alamos National Laboratory.*

10  Reed, D.T., R. Deo, and B.E. Rittmann.  2010.  *Subsurface Interactions of Actinide Species and*
11  *Microorganisms*.  In The Chemistry of the Actinide and Transactinide Elements by L.R. Morss,
12  N.M. Edelstein and J. Fuger eds., Chapter 33.  Netherlands: Springer Press, 2010.*

13  Reed, D.T., S. Okajima, and M.K. Richmann.  1994.  "Stability and Speciation of Plutonium(VI)
14  in WIPP Brine." *Radiochimica Acta*, vol. 66/67: 95–101.

15  Reed, D.T., S. Okajima, L.H. Brush, and M.A. Molecke.  1993.  *Radiolytically Induced Gas*
16  *Production in Plutonium-Spiked WIPP Brine.*  Materials Research Society Symposium
17  Proceedings (pp. 431–38). Vol. 294. Warrendale, PA: Materials Research Society.

18  Reed, D.T., S.B. Aase, D. Wygmans, and J. E. Banaszak.  1998.  "The Reduction of Np(VI) and
19  Pu(VI) by Organic Chelating Agents." *Radiochimica Acta*, vol. 82: 109-14.

20  Reed, D.T., S.E. Pepper, M.K. Richmann, G. Smith, R. Deo, and B.E. Rittmann.  2007.
21  "Subsurface Bio-Mediated Reduction of Higher-Valent Uranium and Plutonium." *Journal of*
22  *Alloys and Compounds*, vol. 444/445: 376–82.

23  Refait, Ph., and J.-M.R. Génin.  1994.  "The Transformation of Chloride-Containing Green Rust
24  One into Sulphated Green Rust Two by Oxidation in Mixed $Cl^-$ and $SO_4^{2-}$ Aqueous Media."
25  *Corrosion Science*, vol. 36, no. 1: 55–65.

26  Richmann, M.K.  2008.  Letter report to D. Reed (Subject: *Eh/pH Diagrams for Am(III), Th(IV)*
27  *and Np(V) Based on the FMT Database and Current PA Assumptions*).  21 November 2008.
28  Carlsbad, NM: Los Alamos National Laboratory.

29  Rittmann, B.E., J.E. Banaszak, and D.T. Reed.  2002.  "Reduction of Np(V) and Precipitation of
30  Np(IV) by an Anaerobic Microbial Consortium." *Biodegradation*, vol. 13: 329–42.

31  Rohban, R., M. Amoozegar, and A. Ventosa.  2009.  "Screening and Isolation of Halophilic
32  Bacteria Producing Extracellular Hydrolysis from Howz Soltan Lake, Iran." *J. Ind. Microbiol.*
33  *Biotechnol.*, 36: 333-340.*

34  Roselle, G.T.  2009.  *Iron and Lead Corrosion in WIPP-Relevant Conditions: Six Month Results.*
35  Milestone Report, October 7, 2009.  ERMS 546084.  Carlsbad, NM: Sandia National
36  Laboratories.*

Roselle, G.T.  2010.  *Iron and Lead Corrosion in WIPP-Relevant Conditions: 12 Month Results*. Milestone report, October 14, 2010.  ERMS 554383.  Carlsbad, NM: Sandia National Laboratories.*

Roselle, G.T.  2011a.  *Iron and Lead Corrosion in WIPP-Relevant Conditions: 18 Month Results*.  Milestone report, January 5, 2011.  ERMS 554715.  Carlsbad, NM: Sandia National Laboratories.*

Roselle, G.T.  2011b.  *Iron and Lead Corrosion in WIPP-Relevant Conditions: 24 Month Results*.  Milestone report, May 3, 2011.  ERMS 555246.  Carlsbad, NM: Sandia National Laboratories.*

Roselle, G.T.  2013.  *Determination of Corrosion Rates from Iron/Lead Corrosion Experiments to be Used for Gas Generation Calculations, Revision 1*.  Analysis report, January 23, 2013. ERMS 559077.  Carlsbad, NM: Sandia National Laboratories.*

Runde, W.  2000.  "The Chemical Interactions of Actinides in the Environment." *Los Alamos Science*, vol. 26: 330.

Runde, W., and J.I. Kim.  1994.  *Untersuchungen der Übertragbarkeit von Labordaten natürliche Verhältnisse. Chemisches Verhalten von drei- und fünfwertigem Americium in salinen NaCl-Lösungen*.  Report RCM-01094, Munich: Institut für Radiochemie, Technische Universität München.  (Available from National Technical Information Service, 555 Port Royal Road, Springfield, VA, 22161, 703/487-4650 as DE 95752244.)

Runde, W., and M. Neu.  2010.  *Actinide Environmental Chemistry*.  In The Chemistry of the Actinide and Transactinide Elements by L.R. Morss, N.M. Edelstein and J. Fuger eds., Chapter 32.  Netherlands: Springer Press, 2010.*

Runde, W., S.D. Conradson, D.W. Efurd, N. Lu, D.E. VanPelt, and C.D. Tait.  2002.  "Solubility and Sorption of Redox-Sensitive Radionuclides (Np,Pu) in j-13 Water from the Yucca Mountain Site: Comparison Between Experiment and Theory." *Applied Geochemistry*, vol. 17: 837–53.

Ryan, J.L., and D. Rai.  1983.  "The Solubility of Uranium (IV) Hydrous Oxide in Sodium Hydroxide Solutions under Reducing Conditions." *Polyhedron*, vol. 2: 947–52.

Sanchez, A.L., J.W. Murray, and T.H. Sibley.  1985.  "The Adsorption of Plutonium IV and V on Geothite." *Geochimica Cosmochimica Acta*, vol. 49: 2297.

Sanchez, L.C., and H.R. Trellue.  1996.  Memorandum to T. Hicks (Subject: *Estimation of Maximum RH-TRU Thermal Heat Load for WIPP*).  17 January 1996.  WPO 31165. Albuquerque, NM: Sandia National Laboratories.

Schubert, B., T. Lowenstein, and M. Timofeeff.  2009.  "Microscipic Identification of Prokaryotes in Modern and Ancient Halite, Saline Valley and Death Valley, California." *Astrobiology* 9(5): 467-482.*

1   Schubert, B., M. Timofeeff, T. Lowenstein, and J. Polle.  2010.  "Dunaliella Cells in Fluid
2   Incusions in Halite:  Signficance for Long-term Survival of Prokaryotes." *Geomicrobiology*
3   *Journal*, 27: 61-75.*

4   Schweitzer, G.K., and L.L. Pesterfield.  2010.  Chapter 7: *The Boron Group*.  <u>The Aqueous</u>
5   <u>Chemistry of the Elements</u>.  (pp. 150-154)  Oxford, USA: Oxford University Press.*

6   Shannon, R.D.  1976.  "Revised Effective Ionic Radii and Systematic Studies of Interatomic
7   Distances in Halides and Chalcogenides." *Acta Cryst*, vol. A32: 751–67.

8   Siekierski, S.  1988.  "Comparison of Yttrium, Lanthanides and Actinides in Respect to Unit Cell
9   Volumes of Isostructural Compounds and Thermodynamic Functions of Complex Formation."
10  *Journal of Radioanalytical Nuclear Chemistry*, vol. 122: 279–84.

11  Silva, R.J., G. Bidoglio, M.H. Rand, P.B. Robouch, H. Wanner, and I. Puigdomenech.  1995.
12  *Chemical Thermodynamics of Americium*.  Chemical Thermodynamics Series 2.  New York
13  Elsevier.

14  Simankova, M.V., and G.A. Zavarzin.  1992.  "Anaerobic Degradation of Cellulose from Lake
15  Sivash and Hypersaline Lagoons of the Arabat Spit." *Microbiologiya*, vol. 61: 288-292.*

16  Simankova, M.V., N. Chernych, G. Osipov and G. Zavarzin.  1993.  "Halocella celluloytica gen.
17  nov., sp. nov., a New Obligately Anaerobic, Halophilic, Cellulolytic bacterium." *System. Appl.*
18  *Microbio.*, 16:  385-389.*

19  Singer, D.M., S.M. Chatman, E.S. Ilton, K.M. Rosso, J.F. Banfield, and G.A. Waychunas.
20  2012a.  "Identification of Simultaneous U(VI) Sorption Complexes and U(VI) Nanoprecipitates
21  on the Magnetite (111) Surface." *Environmental Science & Technology*, vol.46: 3811-20.*

22  Singer, D.M., S.M. Chatman, E.S. Ilton, K.M. Rosso, J.F. Banfield, and G.A. Waychunas.
23  2012b.  "U(VI) Sorption and Reduction Kinetics on the Magnetite (111) Surface."
24  *Environmental Science & Technology*, vol.46: 3821-30.*

25  Skokan, C.K., M.C. Pfeifer, G.V. Keller, and H.T. Anderses.  1987.  *Studies of Electrical and*
26  *Electromagnetic Methods for Characterizing Salt Properties at the WIPP Site, New Mexico*.
27  SAND87-7174.  Carlsbad NM: Sandia National Laboratories.

28  Snider, A.C.  2003a.  *Verification of the Definition of Generic Weep Brine and the Development*
29  *of a Recipe for This Brine*.  ERMS 527505.  Carlsbad, NM: Sandia National Laboratories.

30  Snider, A.C.  2003b.  <u>Hydration of Magnesium Oxide in the Waste Isolation Pilot Plant</u>.
31  Materials Research Society Symposium Proceedings (pp. 665–70).  Vol. 757.  Warrendale, PA:
32  Materials Research Society.

33  Sørensen, K., K. Reháková, E. Zapomělová, and A. Oren.  2009.  "Distribution of Benthic
34  Phototrophs, Sulfate Reducers, and Methanogens in Two Adjacent Saltern Evaporation Ponds in
35  Eilat, Israel." *Aquatic Microbial Ecology*, vol. 56: 275-284.*

1     Sorokin D., and G. Muyzer. 2010. "Bacterial Dissimilatory $MnO_2$ Reduction at Extremely
2     Haloalkaline Conditions." *Extremophiles*, 14:41-46.*

3     Spinks, J.W.T., and R.J. Woods. 1990. *Radiation Sources: The Interaction of Radiation with*
4     *Matter*. Introduction to Radiation Chemistry (pp. 243–313). New York: Wiley.

5     Stadler, S., and J.I. Kim. 1988. "Hydrolysis reactions of Am(III) and Am(V)." *Radiochim.*
6     *Acta*, 44/45: 39–44.

7     Stein, J.S. 2005. Memorandum to L.H. Brush (Subject: *Estimate of Volume of Brine in*
8     *Repository that Leads to a Brine Release*). 13 April 2005. ERMS 539372. Carlsbad, NM:
9     Sandia National Laboratories.

10    Stoelzel, D.M., and D.G. O'Brien. 1996. *Analysis Package for the BRAGFLO Direct Release*
11    *Calculations (Task 4) of the Performance Assessment Analyses Supporting the Compliance*
12    *Certification Application*. AP-029. ERMS 240520. Albuquerque, NM: Sandia National
13    Laboratories.

14    Suzuki, Y., S.D. Kelly, K.M. Kemner, and J.F. Banfield. 2003. "Microbial populations
15    stimulated for hexavalent uranium reduction in uranium mine sediment." *Applied and*
16    *Environmental Microbiology*, 69:1337-46.*

17    Swanson, J.S., and K.A. Simmons. 2013. *Update on Microbial Characterization of WIPP*
18    *Groundwaters*. Report LCO-ACP-20, LA-UR 13-20623. Carlsbad, NM: Los Alamos National
19    Laboratory.*

20    Swanson, J.S., D.M. Norden, H. Khaing, and D.T. Reed. 2013a. "Degradation of Organic
21    Complexing Agents by Halophilic Microorganisms in Brines." *Geomicrobiology Journal*, 30:
22    189-98.*

23    Swanson, J.S., K.A. Simmons, D.M. Norden, and H. Khaing. 2013b. *Biodegradation of*
24    *Organic Complexing Agents by WIPP-indigenous Halophilic Microorganisms in Brines*. Report
25    LCO-ACP-19, LA-UR 13-20616. Carlsbad, NM: Los Alamos National Laboratory.*

26    Swanson, J.S., D.T. Reed, D.A. Ams, D.M. Norden, and K.A. Simmons. 2012. *Status Report on*
27    *the Microbial Characterization of Halite and Groundwater Samples from the WIPP*. Report
28    LCO-ACP-12, LA-UR 12-22824. Carlsbad, NM: Los Alamos National Laboratory.*

29    Telander, M.R., and R.E. Westerman. 1993. *Hydrogen Generation by Metal Corrosion in*
30    *Simulated Waste Isolation Pilot Plant Environments: Progress Report for the Period November*
31    *1989 Through December 1992*. SAND92-7347. ERMS 223456. Albuquerque, NM: Sandia
32    National Laboratories.

33    Telander, M.R., and R.E. Westerman. 1997. *Hydrogen Generation by Metal Corrosion in*
34    *Simulated Waste Isolation Pilot Plant Environments*. SAND96-2538. Albuquerque, NM:
35    Sandia National Laboratories.

Torrero, M.E., I. Casas, J. de Pablo, M.C.A. Sandino, and B.A. Grambow. 1994. "Comparison Between Unirradiated $UO_2$(s) and Schoepite Solubilities in 1 M NaCl Medium." *Radiochimica Acta*, vol. 66/67: 29–35.

Torretto, P., K. Becraft, T. Prussin, K. Roberts, S. Carpenter, D. Hobart, and H. Nitsche. 1995. *Solubility and Speciation Results from Oversaturation Experiments on Neptunium, Plutonium and Americium in a Neutral Electrolyte with a Total Carbonate Similar to Water from Yucca Mountain Region Well UE-25p#1*. Report LA-13018-MS. Los Alamos, NM: Los Alamos National Laboratory.

Trolard, F., J.M.R. Genin, M. Abdelmoula, G. Bourrie, B. Humbert, and A. Herbillon. 1997. "Identification of a Green Rust mineral in a Reductomorphic Soil by Mossbauer and Raman Spectroscopies." *Geochimica Cosmochimica Acta*, vol. 63: 1107–11.

U.S. Department of Energy (DOE). 1996. *Title 40 CFR Part 191 Compliance Certification Application for the Waste Isolation Pilot Plant* (October). 21 vols. DOE/CAO-1996-2184. Carlsbad, NM: Carlsbad Field Office.

U.S. Department of Energy (DOE). 2004. *Title 40 CFR Part 191 Compliance Recertification Application for the Waste Isolation Pilot Plant* (March). 10 vols. DOE/WIPP 2004-3231. Carlsbad, NM: Carlsbad Field Office.

U.S. Department of Energy (DOE). 2009. *Title 40 CFR Part 191 Subparts B and C Compliance Recertification Application 2009, Appendix PA, Attachment SOTERM*. Carlsbad, NM: Carlsbad Field Office.*

U.S. Department of Energy (DOE). 2011. *Waste Isolation Pilot Plant Annual Site Environmental Report for 2010*. DOE/WIPP-11-2225. Carlsbad, NM: Carlsbad Field Office.*

U.S. Environmental Protection Agency (EPA). 1993. "40 CFR Part 191: Environmental Radiation Protection Standards for the Management and Disposal of Spent Nuclear Fuel, High-Level and Transuranic Radioactive Wastes; Final Rule." *Federal Register*, vol. 58 (December 20, 1993): 66398–416.

U.S. Environmental Protection Agency (EPA). 2005. Teleconference with U.S. Department of Energy (DOE), Sandia National Laboratories (SNL), and Los Alamos National Laboratory (LANL) (Subject: *Change in U(VI) Solubility Assumption to a Concentration to 1 mM*). 2 March 2005.

U.S. Environmental Protection Agency (EPA). 2006. *Technical Support Document for Section 194.24: Evaluation of the Compliance Recertification Actinide Source Term and Culebra Dolomite Distribution Coefficient Values* (March). Washington, DC: Office of Radiation and Indoor Air.

Van Loon, L.R., M.A. Glaus, S. Stallone, and A. Laube. 1997. *Alkaline Degradation of Cellulose: Estimation of the Concentration of Isosaccharinic Acid in Cement Pore Water*. Mat. Res. Soc. Symp. Proc. 506, 1009-1010.*

1   Van Luik, A.E., M.J. Apted, W.J. Bailey, J.H. Haberman, J.S. Shade, R.E. Guenther, R.J. Serne,
2   E.R. Gilbert, R. Peters, and R.E. Williford. 1987. *Spent Nuclear Fuel as a Waste Form for*
3   *Geologic Disposal: Assessment and Recommendations on Data and Modeling Needs*. PNL-
4   6329. Richland, WA: Pacific Northwest Laboratories.

5   Van Soest, G. 2012. *Performance Assessment Inventory Report – 2012* (PAIR 2012). INV-PA-
6   12, LANL-CO\Inventory Report, Los Alamos, NM: Los Alamos National Laboratory.*

7   Vandenborre, J., B. Grambov, and A. Abdlouas. 2010. "Discrepancies in Thorium Oxide
8   Solubility Values: Study of Attachment/Detachment Processes at the Solid/Solution Interface."
9   *Inorg. Chem.*, 49, 8736-8748.*

10  Villareal, R., J.M. Bergquist, and S.L. Leonard. 2001. *The Actinide Source-Term Waste Test*
11  *Program (STTP): Final Report*. 3 vols. LA-UR-01-6822, LA-UR-01-6912, and LA-UR-01-
12  6913. Los Alamos, NM: Los Alamos National Laboratory.

13  Vreeland R.H., A.F. Piselli Jr., S. McDonnough, and S.S. Meyers. 1998. "Distribution and
14  diversity of halophilic bacteria in a subsurface salt formation." *Extremophiles* 2: 321-331.*

15  Wall, N.A., and S.A. Mathews. 2005. "Sustainability of Humic Acids in the Presence of
16  Magnesium Oxide." *Applied Geochemistry*, vol. 20: 1704–13.

17  Walther, C. 2003. "Comparison of Colloid Investigations by Single Particle Analytical
18  Techniques: A Case Study on Thorium-Oxyhydroxides." *Colloids and Surfaces A:*
19  *Physicochemical Engineering Aspects*, vol. 217: 81–92.

20  Wang Y., and A.J. Francis. 2005. "Evaluation of microbial activity for long-term performance
21  assessments of deep geologic nuclear waste repositories." *Journal of Nuclear and*
22  *Radiochemical Science* 6: 43-50.*

23  Wang, Y., and L.H. Brush. 1996. Memorandum to M.S. Tierney (Subject: *Estimates of Gas-*
24  *Generation Parameters for the Long-Term WIPP Performance Assessment*). 26 January 1996.
25  ERMS 231943. Carlsbad, NM: Sandia National Laboratories.

26  Wang, Z., RC. Moore, A.R. Felmy, M.J. Mason, and R.K. Kukkadapu. 2001. "A study of the
27  corrosion products of mild steel in high ionic strength brines." *Waste Management* 21:335-341.*

28  Warwick, P., N. Evans, and S.Vines. 2006. "Studies on some divalent metal α-isosaccharinic
29  acid complexes." *Radiochim. Acta* 94, 363-368.*

30  Weiner, R. 1996. Technical memorandum to SWCF-A: Records Center (Subject:
31  *Documentation Package For: Oxidation State Distribution of Actinides in the Repository*). 27
32  March 1996. ERMS 235194. Albuquerque, NM: Sandia National Laboratories.

33  White, A.F., A. Yee, and S. Flexser. 1985. "Surface Oxidation-Reduction Kinetics Associated
34  with Experimental Basalt-Water Reactions at 25 °C." *Chemical Geology*, vol. 49: 73.

1    Wilson D.  2011.  "Microbial Diversity of Cellulose Hydrolysis." *Current Opinion in*
2    *Microbiology* (Ecology and Industrial Microbiology), 14: 259-263.*

3    Wolery, T.J.  1992.  *EQ3/6, A Software Package for Geochemical Modeling of Aqueous Systems:*
4    *Package Overview and Installation Guide* (Version 7.0).  UCRL-MA-110662 PT 1.  Livermore,
5    CA: Lawrence Livermore National Laboratory.

6    Wolery, T.J.  2008.  *Analysis Plan for EQ3/6 Analytical Studies.*  AP-140, Rev. 0., 15 May 2008.
7    ERMS 548930.  Carlsbad, NM: Sandia National Laboratories.*

8    Wolery, T.J., and R.L. Jarek.  2003.  *Software User's Manual: EQ3/6, Version 8.0.*  Software
9    Document No. 10813-UM-8.0-00.  Albuquerque, NM: Sandia National Laboratories.*

10   Wolery, T.J., and S.A. Daveler.  1992.  *EQ3/6, A Computer Program for Reaction Path*
11   *Modeling of Aqueous Geochemical Systems: Theoretical Manual, User's Guide, and Related*
12   *Documentation* (Version 7.0).  UCRL-MA-110662-Pt. 4.  Livermore, CA: Lawrence Livermore
13   National Laboratory.

14   Wolery, T.J., Y.-L. Xiong, and J.J. Long.  2010.  *Verification and Validation Plan/Validation*
15   *Document for EQ3/6 Version 8.0a for Actinide Chemistry, Document Version 8.10.*  ERMS
16   550239.  Carlsbad, NM: Sandia National Laboratories.*

17   Xiong, Y.-L.  2011a.  E-mail to Jennifer Long (Subject: *Release of EQ3/6 Database*
18   *DATA0.FM1*).  9 March 2011.  ERMS 555152.  Carlsbad, NM: Sandia National Laboratories.*

19   Xiong, Y.-L.  2011b.  *WIPP Verification and Validation Plan/Validation Document for EQ3/6*
20   *Version 8.0a for Actinide Chemistry, Revision 1*. *Supersedes ERMS 550239.*  ERMS 555358.
21   Carlsbad, NM: Sandia National Laboratories.*

22   Xiong, Y.-L., and A.S. Lord.  2008.  "Experimental Investigations of the Reaction Path in the
23   MgO-CO$_2$-H$_2$O System in Solution with Various Ionic Strengths, and Their Applications to
24   Nuclear Waste Isolation." *Applied Geochemistry*, vol. 23: 1634–59.

25   Yajima, T., Y. Kawamura, and S. Ueta.  1995.  *Uranium(IV) Solubility and Hydrolysis Constants*
26   *Under Reduced Conditions*.  Materials Research Society Symposium Proceedings, (pp. 1137–
27   42).  Vol. 353.  Warrendale, PA: Materials Research Society.

28   Yamamura, T., A. Kitamura, A. Fukui, S. Nishikawa, T. Yamamoto, and H. Moriyama.  1998.
29   "Solubility of U(VI) in Highly Basic Solutions." *Radiochimica Acta*, vol. 83: 139–146.

30   Yamazaki, H., B. Lagerman, V. Symeopoulos, and G.R. Choppin.  1992.  "Solubility of Uranyl
31   in Brine." *Radioactive Waste Management*, vol. 1992: 1607–11.

32   Zitomer, D.H., and R.E. Speece.  1993.  "Sequential Environments for Enhanced
33   Biotransformation of Aqueous Contaminants." *Environmental Science and Technology*, vol. 27:
34   227.